ENCOUNTERS WITH NEIGHBOURS

CURRENT DEVELOPMENTS OF CONCEPTS BASED ON RECURRENCE PLOTS AND THEIR APPLICATIONS

DISSERTATION
ZUR ERLANGUNG DES AKADEMISCHEN GRADES
DOKTOR DER NATURWISSENSCHAFTEN (DR. RER. NAT.)
IN DER WISSENSCHAFTSDISZIPLIN THEORETISCHE PHYSIK

NORBERT MARWAN

INSTITUT FÜR PHYSIK
FAKULTÄT MATHEMATIK UND NATURWISSENSCHAFTEN
UNIVERSITÄT POTSDAM

Mai 2003

Abstract

In this work, different aspects and applications of the *recurrence plot* analysis are presented. First, a comprehensive overview of recurrence plots and their quantification possibilities is given. New measures of complexity are defined by using geometrical structures of recurrence plots. These measures are capable to find chaos-chaos transitions in processes. Furthermore, a bivariate extension to *cross recurrence plots* is studied. Cross recurrence plots exhibit characteristic structures which can be used for the study of differences between two processes or for the alignment and search for matching sequences of two data series. The selected applications of the introduced techniques to various kind of data demonstrate their ability. Analysis of recurrence plots can be adopted to the specific problem and thus opens a wide field of potential applications.

Regarding the quantification of recurrence plots, chaos-chaos transitions can be found in heart rate variability data before the onset of life threatening cardiac arrhythmias. This may be of importance for the therapy of such cardiac arrhythmias. The quantification of recurrence plots allows to study transitions in brain during cognitive experiments on the base of single trials. Traditionally, for the finding of these transitions the averaging of a collection of single trials is needed.

Using cross recurrence plots, the existence of an El Niño/ Southern Oscillation-like oscillation is traced in northwestern Argentina 34 000 yrs. ago. In further applications to geological data, cross recurrence plots are used for time scale alignment of different borehole data and for dating a geological profile with a reference data set. Additional examples from molecular biology and speech recognition emphasize the suitability of cross recurrence plots.

Kurzfassung

Diese Arbeit beschäftigt sich mit verschiedenen Aspekten und Anwendungen von *Recurrence Plots*. Nach einer Übersicht über Methoden, die auf Recurrence Plots basieren, werden neue Komplexitätsmaße eingeführt, die geometrische Strukturen in den Recurrence Plots beschreiben. Diese neuen Maße erlauben die Identifikation von Chaos-Chaos-Übergängen in dynamischen Prozessen. In einem weiteren Schritt werden *Cross Recurrence Plots* eingeführt, mit denen zwei verschiedene Prozesse untersucht werden. Diese bivariate Analyse ermöglicht die Bewertung von Unterschieden zwischen zwei Prozessen oder das Anpassen der Zeitskalen von zwei Zeitreihen. Diese Technik kann auch genutzt werden, um ähnliche Abschnitte in zwei verschiedenen Datenreihen zu finden. Im Anschluß werden diese neuen Entwicklungen auf Daten verschiedener Art angewendet. Methoden, die auf Recurrence Plots basieren, können an die speziellen Probleme angepaßt werden, so daß viele weitere Anwendungen möglich sind.

Durch die Anwendung der neu eingeführten Komplexitätsmaße können Chaos-Chaos-Übergänge in Herzschlagdaten vor dem Auftreten einer lebensbedrohlichen Herzrhythmusstörung festgestellt werden, was für die Entwicklung neuer Therapien dieser Herzrhythmusstörungen von Bedeutung sein könnte. In einem weiteren Beispiel, in dem EEG-Daten aus einem kognitiv orientierten Experiment untersucht werden, ermöglichen diese Komplexitätsmaße das Erkennen von spezifischen Reaktionen im Gehirn bereits in Einzeltests. Normalerweise können diese Reaktionen erst durch die Auswertung von vielen Einzeltests erkannt werden.

Mit der Hilfe von Cross Recurrence Plots wird die Existenz einer klimatischen Zirkulation, die der heutigen El Niño/ Southern Oscillation sehr ähnlich ist, im Nordwesten Argentiniens vor etwa 34 000 Jahren nachgewiesen. Außerdem können mit Cross Recurrence Plots die Zeitskalen verschiedener Bohrlochdaten aufeinander abgeglichen werden. Diese Methode kann auch dazu genutzt werden, ein geologisches Profil mit Hilfe eines Referenzprofiles mit bekannter Zeitskala zu datieren. Weitere Beispiele aus den Gebieten der Molekularbiologie und der Spracherkennung unterstreichen das Potential dieser Methode.

Contents

1 Introduction **1**

2 Data Analysis Basing on Recurrence Plots **3**

2.1 Phase Space Trajectories 3

2.2 Recurrence Plots 8

2.2.1 Review of Recurrence Plots 8

2.2.2 Structures in Recurrence Plots 18

2.2.3 The Quantitative Analysis of Recurrence Plots 22

2.2.4 New Measures of Complexity: Laminarity and Trapping Time 26

2.2.5 Further Possibilities of Quantification 33

2.3 Cross Recurrence Plots 34

2.3.1 Measures for Similarities Between Two Observed Processes 37

2.3.2 Time Scale Alignment of Time Series 39

2.4 Current Developments of Recurrence Plots 43

2.5 Software and Applications 43

2.5.1 Free Software for Recurrence Plot Based Analysis 43

2.5.2 Cross Recurrence Plot Toolbox 44

2.5.3 Application Potentials 45

3 Applications **48**

3.1 Laminarity and Trapping Time 48

3.1.1 Analysis of VT Heart Rate Intervals 48

3.1.2 Analysis of ERP Data 50

3.2 Similarities Found with Cross Recurrence Plots 55

3.2.1 Finding of Nonlinear Interrelations 55

3.2.2 Investigation of ENSO in the Past 56

3.3 Time Scale Alignment Based on Cross Recurrence Plots 59

3.3.1 Time Scale Alignment of Borehole Data 60

3.3.2 Search for an Appropriate Sequence in Reference Data . 62

4 Conclusion **69**
4.1 Methodical Development 69
4.1.1 New Quantification Measures for Recurrence Plots . . . 69
4.1.2 Extension to Cross Recurrence Plots 70
4.2 Applications 70
4.2.1 Heart Rate Variability Data 70
4.2.2 EEG Data During Stimulus Presentation 71
4.2.3 ENSO-like Influence on Pleistocene Precipitation 71
4.2.4 Time Scale Alignment of Marine Geophysical Data . . . 71
4.2.5 Examples for the Search of Matching Sequences 71
4.3 Perspectives 72

Acknowledgement **73**

Bibliography **74**

Index **87**

Appendix

A Recurrence Plot Based Measures of Complexity and their Application to Heart Rate Variability Data

B Extended Recurrence Plot Analysis and its application to ERP data

C Nonlinear Analysis of Bivariate Data with Cross Recurrence Plots

D Comparing modern and Pleistocene ENSO-like influences in NW Argentina using nonlinear time series analysis methods

E Cross Recurrence Plot Based Synchronization of Time Series

List of Abbreviations and Notations

Abbreviations

ACF	autocorrelation function
AR(p)	autoregressive process of order p
BP	before present (taken conventionally to be before 1950)
CRP	cross recurrence plot
FAN	fixed amount of nearest neighbours (neighbourhood criterion)
FNN	false nearest neighbour
kyr	thousand years
ICA	independent component analysis
L_p-norm	vector norm, e.g. the Euclidean norm (L_2-norm), Maximum norm (L_∞-norm)
LOI	line of identity (the main diagonal line in a RP, $\mathbf{R}_{i,i} = 1$)
LOS	line of synchronization (the distorted main diagonal line in a CRP)
Myr	million years
RP	recurrence plot
RQA	recurrence quantification analysis
SVD	singular value decomposition

Notations

$\langle \cdot \rangle$	average
$\lvert \cdot \rvert$	absolut value
$\lVert \cdot \rVert$	norm
$\{\cdot\}$	set
$\delta(\cdot)$	delta function ($\delta(x) = \{1 \lvert\, x = 0;\ 0 \lvert\, x \neq 0\}$)
$\partial_t(\cdot)$	derivative with respect to time ($\dot{\vec{x}} = \frac{d}{dt}$)

ε	small distance in the phase space in general; threshold value (neighbourhood radius) for the construction of a recurrence plot
σ	standard deviation
$\Theta(\cdot)$	Heaviside function ($\Theta(x) = \{1 \mid x > 0;\ 0 \mid x \leq 0\}$)
τ	time delay (index-based units)
ξ	random numbers
$\mathbf{C}$	covariance matrix
$C^{m,\varepsilon}$	correlation sum for a system of dimension m and by using a threshold ε
$\mathbf{CR}^{m,\varepsilon}$	cross recurrence matrix between two m-dimensional phase space trajectories and a neighbourhood radius ε
$\mathbf{D}^m$	distance matrix between vectors in an m-dimensional phase space
DET	measure for recurrence quantification: determinism
DET_*	measure for recurrence quantification: determinism of a certain diagonal in the RP
DIV	measure for recurrence quantification: divergence
$ENTR$	measure for recurrence quantification: entropy
L	measure for recurrence quantification: average line length of diagonal lines
L_*	measure for recurrence quantification: average line length of diagonal lines of a certain diagonal in the RP
L_{max}	measure for recurrence quantification: length of the longest diagonal line
LAM	measure for recurrence quantification: laminarity
$\mathfrak{m}$	slope of a line in an RP
N	length of a data series
$\mathbb{N}$	set of natural numbers
$p(\cdot)$	probability distribution
$P(\cdot)$	histogram or frequency distribution
$P_c(\cdot)$	cumulative histogram or frequency distribution
$\mathbb{R}$	set of real numbers
$\mathbf{R}^{m,\varepsilon}$	recurrence matrix of an m-dimensional phase space trajectory and a neighbourhood radius ε
RR, REC	measure for recurrence quantification: recurrence rate (percent recurrence)
RR_*	measure for recurrence quantification: recurrence rate of a certain diagonal in the RP
$TREND$	measure for recurrence quantification: trend
TT	measure for recurrence quantification: trapping time
V_{max}	measure for recurrence quantification: length of the longest vertical line

Chapter 1

Introduction

Mankind has to arrange itself with the phenomena in nature. Scientists observe various complex processes in nature, e.g. by measuring temperatures, magnitudes of earthquakes, fluxes of solar radiation, heart rate variability etc. and try to predict them. Especially since the discussions about greenhouse effect, global warming and natural hazards the understanding of the relationships in nature have become more important. The investigation of complex systems in nature and engineering (e.g. turbulence, laser) has revealed that the underlying nonlinear processes have also to be taken into account in order to understand and model these systems. In the last decades data analysis using classical (linear) methods were further improved and enriched with new methods which were derived from chaos theory. Many analysts have tried to estimate nonlinear measures and properties e.g. scaling laws or fractal dimensions of natural processes. However, most methods of nonlinear data analysis (Kantz and Schreiber, 1997) need rather long or stationary data series – both are not typical features of data series which are gained from nature. Furthermore, it was shown that these methods work very well for appropriate prototypical model systems; however, the nature cannot be described in a Laplacian sense – too many coincidences cover the interrelations, which e.g. overwhelm the estimation of the dimension of natural processes. Thus, the results of data analysis should be considered with a healthy portion of scepticism. This fact challenges to develop new techniques of nonlinear data analysis.

In the last decade a new method based on nonlinear data analysis has become popular: recurrence plots (Eckmann et al., 1987). Recurrence is a fundamental property of dissipative dynamical systems. Although small disturbations of such a system cause exponentially divergence of its state, after some time the system will come back to a state that is arbitrary close to a former state and pass through a similar evolution. Recurrence plots visualize

such recurrent behaviour of dynamical systems. Although they are not completely understood, practitioners of this method claim its relevance for short and nonstationary data. These features are indeed the crucial advantage of recurrence plots. Zbilut and Webber Jr. (1992) have made an important further step by introducing a quantification analysis based on recurrence plots, which became well known in the analysis especially of physiological data. Hundreds of works and publications using this quantification analysis can be found in literature. It seems that the reason for this amazing growth in the popularity of recurrence plots is not only the technical aspect. Recurrence plots can be very decorative and attract attention.

In this PhD thesis I will present new extensions of recurrence plots and some applications especially in geology and physiology. A methodical overview over recurrence plots and cross recurrence plots will be given in the second chapter. The classical quantification analysis will be extended by introducing new measures of complexity, which can be also used to find chaos-chaos transitions. Then the concept of cross recurrence plots will be introduced, which allows to find similar epochs in different systems. The third chapter is assigned to the applications. In the first part, the new recurrence plot based measures will be used to study physiological data. Analysis of heart rate variability data will reveal early signs of life threatening cardiac arrhythmias. Regarding event related physiological data (brain potentials), the introduced measures will allow to study characteristic processes in the brain during unexpected stimulation even using single trials. Then, cross recurrence plots will be applied to geological data. Application to data of modern and past climate will give indications for the existence of the El Niño phenomenon in the past. Other applications will present the usage of cross recurrence plots in the geological context for time scale alignment of borehole data and for dating geological profiles. Finally, cross recurrence plots will be applied to further data from molecular biology and speech recognition in order to present its ability for the search of matching sequences. In the appendix my publications which were published or submitted during my PhD are compiled. Moreover, a comprehensive bibliography of publications regarding to recurrence plots and our Matlab toolbox developed for application of recurrence and cross recurrence plots are provided through the WorldWideWeb (`http://tocsy.agnld.uni-potsdam.de`).

Chapter 2

Data Analysis Basing on Recurrence Plots

The analysis of phase space trajectories is a basic concept of nonlinear data analysis. This chapter begins with an introduction of the concept of phase space reconstruction. Then, a technical and historical review on recurrence plots is given and the new quantification techniques are presented. This part is followed by the generalization to cross recurrence plots with their potentials for application. Finally, rather promising current developments of recurrence plots will be briefly mentioned.

2.1 Phase Space Trajectories

The states of systems in nature or engineering typically change in time. The investigation of these mostly complex processes is an important task in numerous scientific disciplines that helps to understand and describe these changes (e.g. for forecasts). The aim is usually to find mathematical models which can be adapted to the real processes and used for solving the given problems. The measuring of a state (which leads to observations of the state but not to the state itself) and subsequent data analysis are the first steps toward the understanding of a process. Well known and approved methods for data analysis are those based on linear concepts as estimations of moments, correlations, power spectra or principle components analyses etc. In the last two decades this zoo of analysis methods has been enriched with methods of the theory of nonlinear dynamics. Some of these new methods base on a metric or topological analysis of the phase space of the underlying dynamics or on an appropriate reconstruction of it (Kantz and Schreiber, 1997; Takens, 1981). This section will focus on the reconstruction of a phase space.

The state of a system can be described by its state variables

$$x^1(t),\ x^2(t), \ldots,\ x^d(t), \tag{2.1}$$

for example the both state variables temperature and pressure for a thermodynamic system. Note that the superscript number is used here as an index of the component and not as an exponent. The d state variables at time t form a vector $\vec{x}(t)$ in a d-dimensional space which is called phase space. This vector moves in time and in the direction that is specified by its velocity vector

$$\dot{\vec{x}}(t) = \partial_t \vec{x}(t) = \vec{F}(x). \tag{2.2}$$

The temporary succession of the phase space vectors forms a trajectory (phase space trajectory, orbit). The velocity field $\vec{F}(x)$ is tangent to this trajectory. For autonomous systems the trajectory must not cross itself. The time evolution of the trajectory explains the dynamics of the system, i. e. the attractor of the system. If $\vec{F}(x)$ is known, the state at a given time can be determined by integrating the equation system (2.2). However, a graphical visualization of the trajectory enables the determination of a state without integrating the equations. The shape of the trajectory gives hints about the system; periodic or chaotic systems have characteristic phase space portraits.

The observation of a real process usually does not yield all possible state variables. Either not all state variables are known or not all of them can be measured. Most often only one observation $u(t)$ is available. Since measurements result in discrete time series, the observations will be written in the following as u_i, where $t = i\,\Delta t$ and Δt is the sampling rate of the measurement. The sampling rate may be constant, resulting in a time series with equidistant sampling points. However, a constant sampling rate is not always available, which often leads to problems in applying standard methods of data analysis, because they require equidistant time series. In general, variables with a subscribed index are in this work time discrete (e.g. $\vec{x}_i$, $\mathbf{R}_{i,j}$), whereas a braced t denotes continuous variables (e.g. $\vec{x}(t)$, $\mathbf{R}(t_1, t_2)$).

Couplings between the system's components imply that each single component contains essential information about the dynamics of the whole system. Therefore, an equivalent phase space trajectory, which preserves the topological structures of the original phase space trajectory, can be reconstructed by using only one observation or time series, respectively (Packard et al., 1980; Takens, 1981). A method frequently used for reconstructing such a trajectory $\hat{\vec{x}}(t)$ is the time delay method: $\hat{\vec{x}}_i = (u_i,\ u_{i+\tau},\ \ldots, u_{i+(m-1)\tau})^T$, where m is the embedding dimension and τ is the time delay (index based; the real time delay is $\tau\,\Delta t$). The preservation of the topological structures of the original trajectory

is guaranteed if $m \geq 2d + 1$, where d is the dimension of the attractor (Takens, 1981).

Both embedding parameters, the dimension m and the delay τ, have to be chosen appropriately. Different approaches are applicable for the determination of the smallest sufficient embedding dimension (Cao, 1997; Kantz and Schreiber, 1997):

1. The first approach may be the computation of some invariant measure on the reconstructed attractor, which will change if the current embedding dimension is too small, but which will persist if it is large enough. This method, however, is rather subjective and usually requires lengthy data sets.

2. The investigation of the changes in the neighbourhood of phase space points under changes of the embedding dimension may be applied. Inappropriate embedding dimensions cause an increasing amount of false nearest neighbours.

3. The single value decomposition of an initial set of reconstructed phase space vectors reveals the smallest number of uncorrelated directions in the phase space, which can be used as an embedding dimension.

At this point, we will only focus on methods which use false nearest neighbours.

There are various methods that use false nearest neighbours in order to determine the embedding dimension. The basic idea is that by decreasing the dimension an increasing amount of phase space points will be projected into the neighbourhood of any phase space point, even if they are not real neighbours (Fig. 2.1). Such points are called *false nearest neighbours (FNNs)*. The simplest method uses the amount of these FNNs as a function of the embedding dimension in order to find the minimal embedding dimension (Kantz and Schreiber, 1997). Such a dimension has to be taken where the FNNs vanish. Other methods use the ratios of the distances between the same neighbouring points for different dimensions (Kennel et al., 1992; Cao, 1997).

There are further methods for the determination of attractor dimensions, e.g. the correlation sum (Grassberger and Procaccia, 1983).

Random errors and low measurement precision can lead to a linear dependence between the subsequent vectors $\vec{x}_i$. Hence, the delay has to be chosen in such a way that such dependences vanishes. One possible means of determining the delay is by using the *autocovariance function* $C(\tau) = \langle u_i \, u_{i-\tau} \rangle$ (using the assumption $\langle u_i \rangle = 0$).

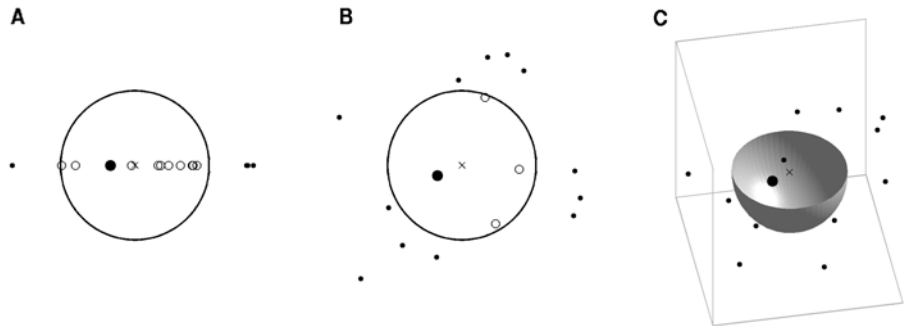

Figure 2.1: Decreasing the embedding dimension causes an increase of false nearest neighbours (small circles) which fall into the neighbourhood (the circle or the sliced ball) of a phase space point (the cross); the real nearest neighbours are the larger black dots; (A) $m = 1$, (B) $m = 2$ and (C) $m = 3$. The neighbourhood in (C) seems to be smaller than in the other two plots, but this is the result of downscaling.

A delay may be appropriate when the autocovariance approaches zero. This minimizes the linear correlation between the components but does not have to mean they are independent. However, the converse is true: if two variables are independent they will be uncorrelated. Therefore, another well established possibility for determining the delay is the *mutual information* (Fraser and Swinney, 1986)

$$I(\tau) = -\sum_{\varphi,\psi} p_{\varphi,\psi}(\tau) \log \frac{p_{\varphi,\psi}(\tau)}{p_\varphi\, p_\psi} = \left\langle \log \frac{p_{u_i,u_{i+\tau}}}{p_{u_i}\, p_{u_{i+\tau}}} \right\rangle . \tag{2.3}$$

Here $p_{\varphi,\psi}(\tau)$ is the joint probability that $u_i = \varphi$ and $u_{i+\tau} = \psi$. p_φ and p_ψ are the probabilities that u_i has the value φ and ψ, respectively. In order to simplify the notations, we use $p_{u_i} = p_\varphi$, $p_{u_{i+\tau}} = p_\psi$ and $p_{u_i,u_{i+\tau}} = p_{\varphi,\psi}(\tau)$. The mutual information is not a function of the variables φ and ψ but of the joint probability $p_{\varphi,\psi}(\tau)$. It is the average of the information about a value after a delay τ, which can be yielded from the knowledge of the current value. The best choice for the delay is where $I(\tau)$ has its smallest local minimum. The advantage of the mutual information vs. the autocovariance function is that it finds the nonlinear interrelations and, hence, determines such a delay which fulfils the criterion of independence.

Some further methods for the reconstruction of the attractor should also be mentioned. Broomhead and King (1986) have suggested the method of *singular value decomposition (SVD)*. First, a set $\mathbf{X} = (\vec{x}_1, \vec{x}_2, \ldots, \vec{x}_N)$ of embedding vectors for a sufficient large dimension m and with a delay of $\tau = 1$ is formed (note that $\tau = 1$ means that the real delay corresponds to the time resolution of

the data). Then, the eigenvalues and eigenvectors from the covariance matrix

$$\mathbf{C} = \frac{1}{N}\mathbf{X}^T\mathbf{X}$$

are computed. The amount of non-zero eigenvalues (rank of $\mathbf{C}$) is the value of the smallest sufficient embedding dimension, and the corresponding eigenvectors are the components of the searched phase space reconstruction. The advantage is that it is not necessary to determine a delay. However, the SVD minimizes only the linear correlation between the components, which – as mentioned above – does not mean independence in general (vanishing linear correlation corresponds to independence only for Gaussian distributed data). An alternative way for such decomposition is the *independent component analysis (ICA)* (Hyvärinen et al., 2001). This decomposition method separates the signals in nonlinearly uncorrelated (i. e. independent) components, avoiding the disadvantage of the SVD whereby the components are still dependent. Although this approach cannot be found in any publication, the development of an embedding method based on ICA seems promising.

Another alternative for a phase space reconstruction is based on mutual information. Fraser (1989) has generalized the mutual information (2.3) for higher dimensional joint distributions $p_{u_i, u_{i+\tau}, \ldots, u_{i+(m-1)\tau}}$ (definition corresponding to (2.3)) by definition of the *redundancy*

$$R^m(\tau) = \left\langle \log \frac{p_{u_i, u_{i+\tau}, \ldots, u_{i+(m-1)\tau}}}{p_{u_i}\, p_{u_{i+\tau}} \cdots p_{u_{i+(m-1)\tau}}} \right\rangle \tag{2.4}$$

and the marginal redundancy

$$\tilde{R}^m(\tau) = R^{m+1}(\tau) - R^m(\tau). \tag{2.5}$$

First, a dimension m must be chosen, which maximizes $\tilde{R}^m(\tau)$. Then, the delay τ should be selected to maximize the information about the original phase space that is provided by the reconstructed phase space vectors. This information can be estimated with a further measure defined by Fraser (1989). Fraser has compared his method to that based on SVD and has found that the redundancy approach revealed better reconstructions. This method maximizes the "number of distinguishable predictions about the state" while the method based on SVD minimizes only the linear correlation.

For the reconstruction of low-dimensional phase spaces the differential phase space embedding is suitable, for example $\hat{\vec{x}}_i = (u_i, \partial_t(u_i), \partial_t^2(u_i))^T$, where the partial derivatives ∂_t can be estimated from the differences of the successive values u_i (Mindlin and Gilmore, 1992). The advantage is that the topological

properties of the attractor (e. g. relative rotation, linking properties) can be determined from this embedding. In addition to it the components of this phase space are natural variables which are used to model the dynamics.

Especially for the application of recurrence plots, Zbilut et al. (2002) suggest a heuristic approach for the determination of the embedding dimension. First create a recurrence plot (RP) with a high embedding dimension ($m = 20 \ldots 25$). Then decrease progressively the dimension until a significant change in the RP results. Since this change is due to a topological change of the phase space trajectory caused by the occurrence of FNNs, the current dimension plus a few dimensions should be sufficient for the embedding. This procedure is analogous to the statement of Atay and Altıntaş (1999) that such an embedding would be sufficient, where the RP is cleaned from single points and linear structures dominate. However, this criterion has to be considered with the utmost caution because with a high embedding dimension ($m = 10$ would be enough) it is possible to create an RP with a large amount of diagonal lines from random data (e. g. Gaussian noise). In an early work, Zbilut and Webber Jr. (1992) have tried to use a quantification of RPs in order to find the optimal embedding parameters. However, this approach fails in the case of nonstationarity (Trulla et al., 1996; Marwan, 1999).

A phase space reconstruction can be used in order to estimate characteristic properties of the dynamical system. For reviews on corresponding methods see for example Eckmann and Ruelle (1985), Abarbanel et al. (1993) or Ott (1993). Besides, the phase space reconstruction is the starting point for the construction of a recurrence plot.

2.2 Recurrence Plots

In this section an overview about recurrence plots, recurrence quantification analysis and their history will be given.

2.2.1 Review of Recurrence Plots

Natural processes can have a distinct recurrent behaviour, e.g. periodicities (as seasonal or Milanković cycles), but also irregular cyclicities (as El Niño Southern Oscillation). Moreover, the recurrence of states, in the meaning that states are arbitrary close after some time, is a fundamental property of deterministic dynamical systems and is typical for nonlinear or chaotic systems (e.g. Ott, 1993; Argyris et al., 1994). The recurrence of states in nature has been known for a long time and has also been discussed in early publications (e.g. recur-

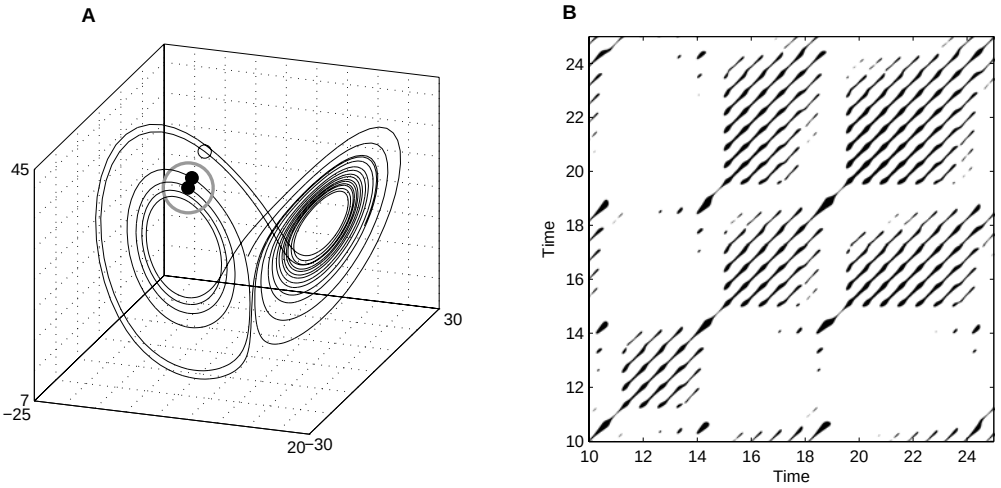

Figure 2.2: (A) Segment of the phase space trajectory of the Lorenz system (for standard parameters $r = 28$, $\sigma = 10$, $b = \frac{8}{3}$; Lorenz, 1963) by using its three components and (B) its corresponding recurrence plot. A point of the trajectory at j which falls into the neighbourhood (gray circle in (A)) of a given point at i is considered as a recurrence point (black point on the trajectory in (A)). This is marked with a black point in the RP at the location (i, j). A point outside the neighbourhood (small circle in (A)) causes a white point in the RP. The radius of the neighbourhood for the RP is $\varepsilon = 5$.

rence phenomena in cosmic-ray intensity, Monk and Compton, 1939).

Eckmann et al. (1987) have introduced a tool which can visualize the recurrence of states $\vec{x}_i$ in a phase space. Usually, a phase space does not have a dimension (two or three) which allows it to be pictured. Higher dimensional phase spaces can only be visualized by projection into the two or three dimensional sub-spaces. However, Eckmann's tool enables us to investigate the m-dimensional phase space trajectory through a two-dimensional representation of its recurrences (Fig. 2.2). Such recurrence of a state at time i at a different time j is pictured within a two-dimensional squared matrix with black and white dots, where black dots mark a recurrence, and both axes are time axes. This representation is called *recurrence plot (RP)*. Such an RP can be mathematically expressed as

$$\mathbf{R}_{i,j}^{m,\varepsilon_i} = \Theta\left(\varepsilon_i - \left\|\vec{x}_i - \vec{x}_j\right\|\right), \quad \vec{x}_i \in \mathbb{R}^m, \quad i, j = 1 \ldots N, \tag{2.6}$$

where N is the number of considered states x_i; ε_i is a threshold distance, $\|\cdot\|$ a norm and $\Theta(\cdot)$ the Heaviside function.

Since $\mathbf{R}_{i,i} = 1$ $(i = 1 \ldots N)$ by definition, the RP has a black main diagonal line, the *line of identity (LOI)*, with an angle of $\pi/4$. It has to be noted that a sin-

gle recurrence point at (i, j) does not contain any information about the current states at the times i and j. However, from the totality of all recurrence points it is possible to reconstruct the properties of the data. McGuire et al. (1997) have shown the preservation of the dynamical properties for the distance matrix (2.11). However, the phase space trajectory can also be reconstructed from the binary RP, where the information about the absolute length of the phase space vectors is lost. The RP provides information for reordering the indices of the phase space vectors so that the vectors are sorted by their norm. If the cumulative distribution of the lengths of the phase space vectors is known, the restored phase space trajectory will recover its amplitude by equating the sorted indices with this distribution (Thiel, 2003).

In practice it is not useful and largely impossible to find complete recurrences in the sense $\vec{x}_i \equiv \vec{x}_j$ (e. g. the state of a chaotic system would not recur exactly to the initial state but approaches the initial state arbitrarily close). Therefore, a recurrence is defined as a state $\vec{x}_j$ is sufficiently close to $\vec{x}_i$. This means that those states $\vec{x}_j$ that fall into an m-dimensional neighbourhood (e.g. a ball for the L_2-norm or a box for the L_∞-norm) with a radius ε_i centered at $\vec{x}_i$ are recurrent. These $\vec{x}_j$ are called *recurrence points*. In (2.6), this is simply expressed by the Heaviside function and its argument ε_i.

In the original definition of the RPs, the neighbourhood is a ball (i. e. L_2-norm is used) and its radius is chosen in such a way that it contains a fixed amount of states $\vec{x}_j$ (Eckmann et al., 1987). With such a neighbourhood, the radius ε_i changes for each $\vec{x}_i$ ($i = 1 \dots N$) and $\mathbf{R}_{i,j} \neq \mathbf{R}_{j,i}$ because the neighbourhood of $\vec{x}_i$ does not have to be the same as that of $\vec{x}_j$. This property leads to an asymmetric RP, but all columns of the RP have the same recurrence density (Fig. 2.5D). Using this neighbourhood criterion we will use the parameter ε for the predefinition of the recurrence density. This means that with a given $\varepsilon = 0.15$ the real, locally chosen ε_i is adjusted in such a way that the neighbourhood covers 15% of all phase space vectors, and thus the recurrence density is 0.15. We denote this neighbourhood as *fixed amount of nearest neighbours (FAN)*. However, the most commonly used neighbourhood is that with a fixed radius $\varepsilon_i = \varepsilon, \forall i$. For RPs this neighbourhood was firstly used by Zbilut et al. (1991). A fixed radius means that $\mathbf{R}_{i,j} = \mathbf{R}_{j,i}$ resulting in a symmetric RP. The type of neighbourhood that should be used depends on the application. Especially in applications of the later introduced cross recurrence plots, the neighbourhood with a FAN will play an important role.

In order to compute an RP, a norm has to be chosen. The most known norms are the L_1-norm, the L_2-norm (Euclidean norm) and the L_∞-norm (Maximum or Supremum norm). The neighbourhoods of these norms have differ-

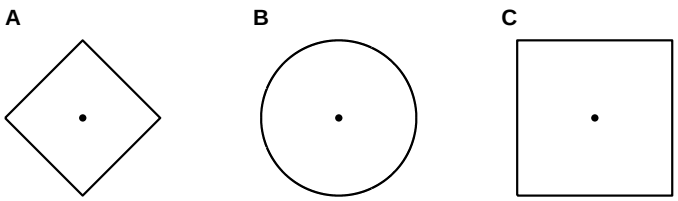

Figure 2.3: Three commonly used norms for the neighbourhood with the same radius around a point (black dot) exemplarily shown for the two-dimensional phase space: (A) L_1-norm, (B) L_2-norm and (C) L_∞-norm.

ent shapes (Fig. 2.3). Considering a fixed ε, the L_∞-norm finds the most, the L_1-norm the fewest and the L_2-norm an intermediate amount of neighbours. For computing the RPs, the L_∞-norm is most commonly applied (Fig. 2.5A), because it is independent of the phase space dimension and easier to compute than any other norm. The independence from the dimension will become relevant if in the same analysis different embeddings of a time series have to be used. Since other norms depend on the dimension, RPs of different embedding dimensions cannot be compared without a rescaling. But such rescaling is not necessary for the maximum norm, and the RPs of different embeddings can be compared directly. Finally, this norm allows to study the RPs theoretically, because the analytical expressions can be solved in a much simpler way than those gained by using other norms (Faure and Korn, 1998; Thiel et al., 2002). The application of the L_1-norm has been presented in the publication by Zbilut et al. (1991). The authors mentioned that by using this norm "an increase in recurrences becomes more robust in its significance" (Fig. 2.5B).

Special attention has to be turned to the choice of the threshold ε. It is desirable that the smallest threshold possible is chosen. However, the influence of noise can necessitate a larger threshold, because noise would distort any existing structure in the RP. Higher threshold may preserve these structures. Suggestions from literature show that this threshold should be a few per cent of the maximum phase space diameter (Mindlin and Gilmore, 1992) and should not exceed 10% of the mean or the maximum phase space diameter (Zbilut and Webber Jr., 1992; Koebbe and Mayer-Kress, 1992). Using the recurrence point density of the RP, the threshold can be chosen from the analysis of this measure in respect to a changing threshold (Zbilut et al., 2002). The threshold can then be found by looking for a scaling region in the recurrence point density. However, this may not work for nonstationary data. For this case Zbilut et al. (2002) have suggested to choose ε so that the recurrence point density is approximately 1%. For noisy periodic processes, Matassini et al.

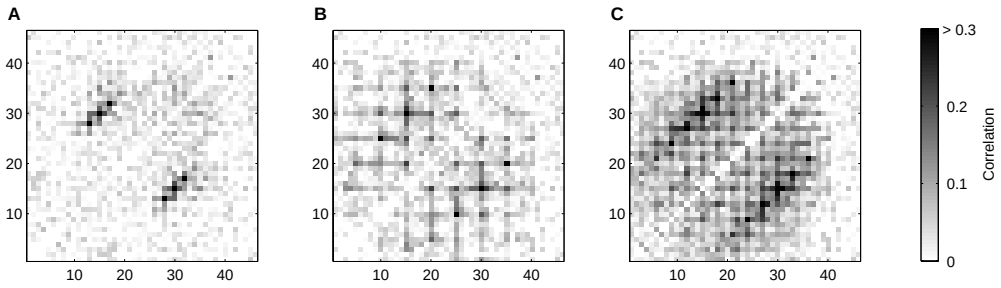

Figure 2.4: Correlation between the recurrence point at $(15, 30)$ and the other recurrence points in an RP of realizations of the AR(1) process $x_{i+1} = 0.6\, x_i + 0.3\, \xi$. The embedding parameters are (A) $m = 3$, $\tau = 2$, $\varepsilon = 0.3$, (B) $m = 3$, $\tau = 5$, $\varepsilon = 0.35$ and (C) $m = 5$, $\tau = 2$, $\varepsilon = 0.5$, which preserve an approximately constant recurrence rate (0.2). The delay $\tau = 2$ corresponds to the correlation time of x_i (when its ACF falls below $1/\mathrm{e}$). The redundancy increases with rising embedding dimension. The correlation coefficients are gained from 1 000 realizations of the underlying process.

(2002) have suggested to use the diagonal structures within the RP in order to determine an optimal threshold. Their criterion minimizes the fragmentation and thickness of the diagonal lines in respect to the threshold. Recent studies about RPs in our group have revealed a more exact criterion for choosing this threshold. This criterion takes into account that a measurement of a process is a composition of the real signal and some observational noise with standard deviation. In order to get similar results by using RPs, a threshold has to be chosen which is five times larger than the standard deviation of the observational noise (Thiel et al., 2002). This criterion holds for a wide class of processes.

Since the RP is a representation of multiple tests, it is obvious that an RP contains an amount of redundancy. This redundancy increases when the embedding dimension increases (Fig. 2.4). This effect can yield distinct diagonal oriented structures in an RP of a time series of uncorrelated values if the embedding is high, although such diagonal structures are expected only for correlation. The increase of the embedding dimension always cleans up the RP from single recurrence points (representatives for the uncorrelated states) and emphasizes the diagonal structures as diagonal lines (representatives for the correlated states). Therefore, if embedding is used, this effect has to be taken into account. The embedding has to be chosen so that the dynamics of the system will be well presented by its phase space trajectory. An overembedding has to be avoided because a large amount of diagonal lines may be considered

as artifacts.

Some authors exclude the LOI from the RP. This may be useful for the quantification of RPs, which we will discuss later. It can also be motivated by the definition of the Grassberger-Procaccia correlation sum (Grassberger and Procaccia, 1983) which was introduced for the determination of the correlation dimension D_2 and is closely related to RPs:

$$\mathbf{C}^{m,\varepsilon} = \frac{1}{N^2} \sum_{\substack{i,j=1 \\ i \neq j}}^{N} \Theta\left(\varepsilon - \left\|\vec{x}_i - \vec{x}_j\right\|\right). \tag{2.7}$$

The correlation integral excludes the tests of $\vec{x}_i$ with itself. Nevertheless, since the threshold value ε is finite (and normally about 10% of the mean phase space radius), further long diagonal lines can occur directly below and above the LOI for smooth or high resolution data. Therefore, the diagonal lines in a small corridor around the LOI correspond to the *tangential motion* of the phase space trajectory, but not to different orbits. Thus, for the estimation of invariants it is better to exclude this entire predefined corridor and not only the LOI. This step corresponds with suggestions to exclude the tangential motion as it is done for the computation of the correlation dimension (known as Theiler correction or Theiler window; Theiler, 1986) or for the alternative estimators of Lyapunov exponents (Gao and Zheng, 1994) in which only those phase space points are considered that fulfil the constraint $|j - i| \geq w$. Theiler (1986) has suggested using the autocorrelation time as an appropriate value for w, and Gao and Zheng (1994) state that $w = (m-1)\tau$ would be a sufficient approach. However, in a representation of an RP it is better to keep the LOI. Later, this LOI will gain more importance when extensions of the recurrence plot strategies will be discussed.

In the literature further variations of the recurrence plots can be found:

- Iwanski and Bradley (1998) have defined a variation of an RP with a corridor threshold $[\varepsilon_{in}, \varepsilon_{out}]$ (Fig. 2.5E),

$$\mathbf{R}_{i,j}^{m,[\varepsilon_{in},\varepsilon_{out}]} = \Theta\left(\left\|\vec{x}_i - \vec{x}_j\right\| - \varepsilon_{in}\right) \cdot \Theta\left(\varepsilon_{out} - \left\|\vec{x}_i - \vec{x}_j\right\|\right). \tag{2.8}$$

  Those points $\vec{x}_j$ are considered to be recurrent that fall into the shell with the inner radius ε_{in} and the outer radius ε_{out}. The authors have suggested to use this kind of RPs in order to study "interesting structures" in the RP. An advantage of such a *corridor thresholded recurrence plot* is its increased robustness against recurrence points coming from the tangential motion. However, the threshold corridor removes the inner points in broad diagonal lines, which results in two lines instead of one. These

RPs are, therefore, not suitable for a quantification analysis. The usage of a shell as a neighbourhood can be found in an algorithm for computing Lyapunov exponents from experimental time series (Eckmann et al., 1986).

- Choi et al. (1999) have introduced the *perpendicular recurrence plot* (Fig. 2.5F)

$$\mathbf{R}_{i,j}^{m,\varepsilon} = \Theta\left(\varepsilon - \left\|\vec{x}_i - \vec{x}_j\right\|\right) \cdot \delta\left(\dot{\vec{x}}_i \cdot (\vec{x}_i - \vec{x}_j)\right). \tag{2.9}$$

  Here, δ is the Delta function. This recurrence plot contains only those points $\vec{x}_j$ that fall into the neigbourhood of $\vec{x}_i$ and lie in the $(m-1)$-dimensional subspace of $\mathbb{R}^m$ that is perpendicular to the phasespace trajectory at $\vec{x}_i$. These points correspond locally to those lying on a Poincaré section. This criterion cleans up the RP more from recurrence points based on the tangential motion than the previous corridor thresholded RPs. The authors have shown the increased efficiency of the perpendicular RPs for their application on estimation of the largest Lyapunov exponent. Using this kind of an RP, the finding of unstable periodic orbits (if they exist) is more robust.

- The RP contains, finally, tests of all states with each other, which results in N^2 tests for N considered states. Still, it is also possible to test each state with a predefined amount k of subsequent states (Zbilut et al., 1991; Koebbe and Mayer-Kress, 1992; Atay and Altıntaş, 1999)

$$\mathbf{R}_{i,j}^{m,\varepsilon} = \Theta\left(\varepsilon - \left\|\vec{x}_i - \vec{x}_{i+i_0+j-1}\right\|\right), \quad i = 1 \ldots N-k, j = 1 \ldots k. \tag{2.10}$$

  This reveals an $(N-k) \times k$-matrix which does not have to be square (Fig. 2.5H). The y-axis represents the time distances to the following recurrence points but not their absolute time. All diagonal oriented structures in the common RP are now projected to the horizontal orientation. For $i_0 = 0$, the LOI, which was the diagonal line in the common RP, is now the horizontal line on the x-axis. With non-zero i_0 the RP contains recurrences of a certain state only in the predefined time interval after time i_0 (Koebbe and Mayer-Kress, 1992).

  This representation of recurrences may be more intuitive than the RPs usually are because the consecutive states are not oriented diagonally. However, such an RP represents only the first $(N-k)$ states. Mindlin and Gilmore (1992) have proposed the *close returns plot* which is, in fact, such an RP exactly for one dimension. Using this kind of RP, a first quantification approach of RPs (or "close returns plots") can be found ("close

returns histogram", recurrence times). It has been used for the investigation of periodic orbits and topological properties of strange attractors (Lathrop and Kostelich, 1989; Tufillaro et al., 1990; Mindlin and Gilmore, 1992).

- Instead plotting the recurrences with black points, the distances

$$\mathbf{D}^{m}_{i,j} = \|\vec{x}_i - \vec{x}_j\| \tag{2.11}$$

between the states $\vec{x}_i$ and $\vec{x}_j$ can be plotted (Fig. 2.5G). Although this is not a real recurrence plot, it is sometimes called *global recurrence plot* (Webber Jr., 2003) or *unthresholded recurrence plot* (Iwanski and Bradley, 1998). However, it should be termed *distance plot*. This representation can also help in studying phase space trajectory. Moreover, it may help to find an appropriate threshold value ε.

- The *windowed* and *meta recurrence plots* have been suggested as means of investigating an external force or the nonstationarity in a system (Manuca and Savit, 1996; Casdagli, 1997). The first ones are obtained by covering an RP with $w \times w$-sized squares (windows) and by averaging the recurrence points that are contained in these windows (Casdagli, 1997). Consequently, a windowed recurrence plot is an $N_w \times N_w$-matrix, where N_w is the floor-rounded N/w, and consists of values which are not limited to zero and one (this suggests a colour-encoded representation). These values correspond with the *cross correlation sum*

$$\mathbf{C}^{m,\varepsilon}_{I,J} = \frac{1}{w^2} \sum_{i,j=1}^{w} \mathbf{R}^{m,\varepsilon}_{i+(I-1)w,j+(J-1)w}, \quad I,J = 1 \ldots \frac{N}{w} \tag{2.12}$$

between sections in $\vec{x}$ with length w and starting at $(I-1)w+1$ and $(J-1)w+1$ (for cross-correlation integral cf. Kantz, 1994). The *meta recurrence plot* as it has been defined by Casdagli (1997) is a distance matrix derived from the cross correlation sum (2.12),

$$\mathbf{D}^{m,\varepsilon}_{I,J} = \frac{1}{\varepsilon^m} \left(\mathbf{C}^{m,\varepsilon}_{I,I} + \mathbf{C}^{m,\varepsilon}_{J,J} - 2\,\mathbf{C}^{m,\varepsilon}_{I,J} \right). \tag{2.13}$$

By applying a further threshold value to $\mathbf{D}^{m,\varepsilon}_{I,J}$ (analogous to Eq. (2.6)), a black-white dotted representation is also possible.

Manuca and Savit (1996) have gone one step further. They have used quotients from the cross correlation sum to form a *meta phase space*. From this meta phase space a recurrence or non-recurrence plot is created, which can be used to characterize the nonstationarity in time series. For

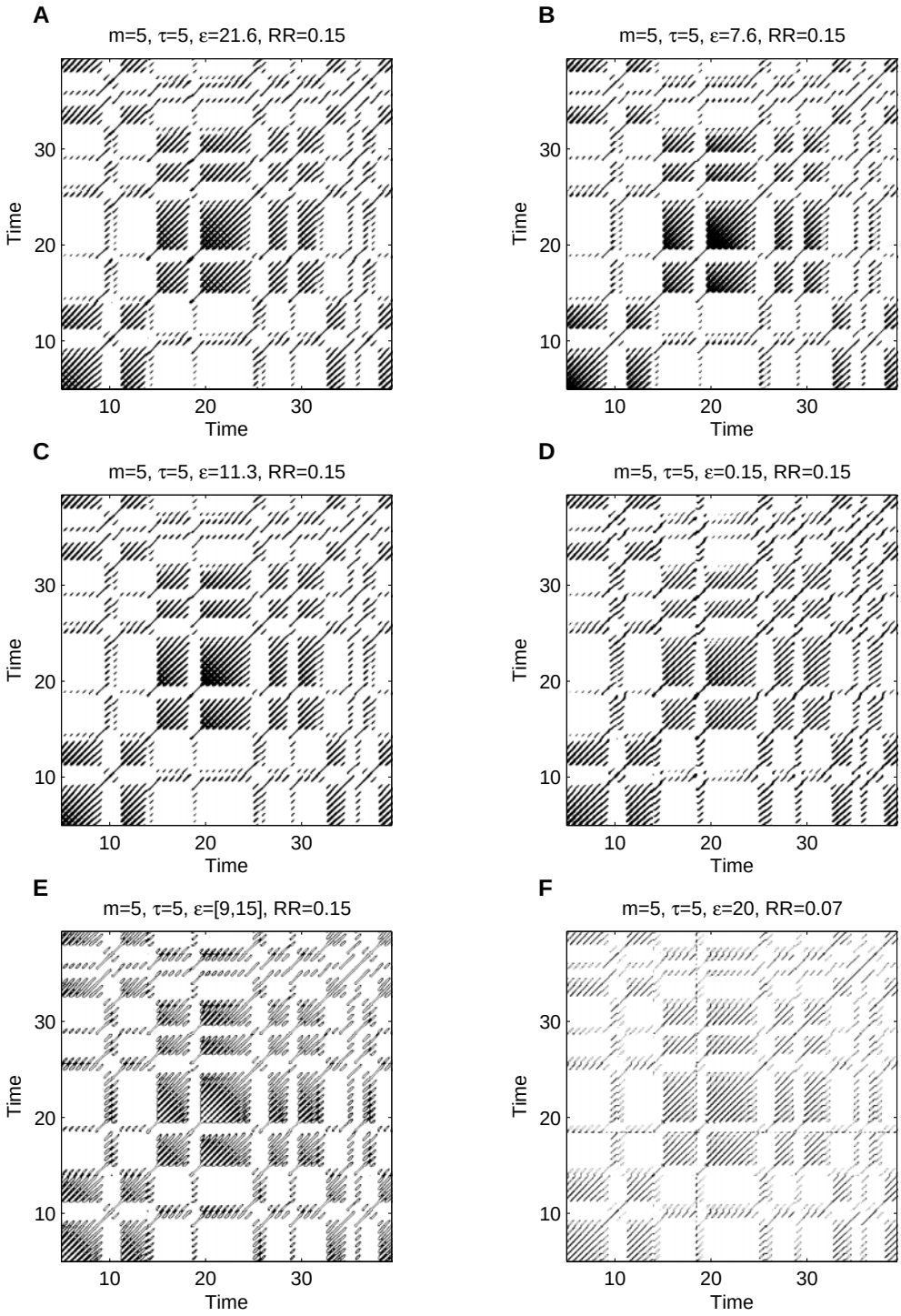

Figure 2.5: Continuous on p. 17.

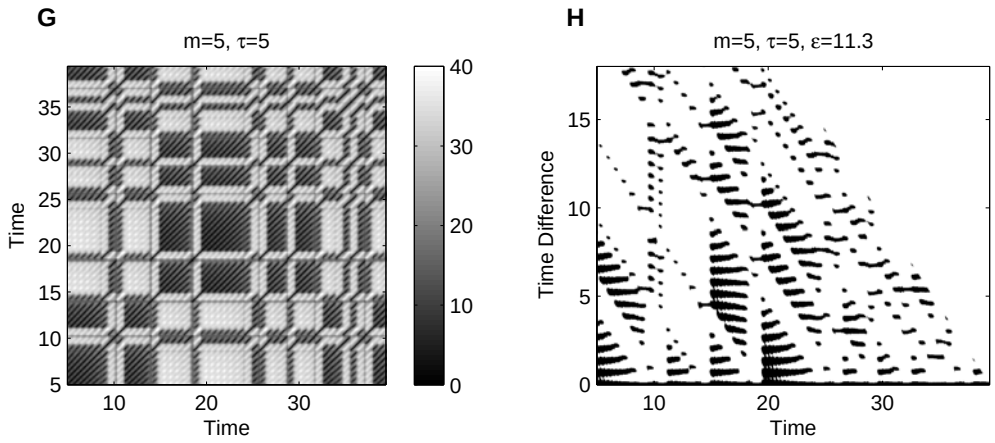

Figure 2.5: Examples of various defined RPs for a section of the x-component of the Lorenz system (sampling time $\Delta t = 0.03$): (A) RP computed by using the L_∞-norm, (B) RP computed by using the L_1-norm, (C) RP computed by using the L_2-norm, (D) RP computed by using a fixed amount of nearest neighbours (FAN), (E) RP computed by using a threshold corridor $[\varepsilon_{in}, \varepsilon_{out}]$, (F) perpendicular RP ($L_2$-norm), (G) distance plot (unthresholded RP, L_2-norm) and (H) RP where the y-axis represents the relative time distances to the next recurrence points but not their absolute time ("close returns plot", L_2-norm). Except for (F) and (G), the parameter ε is chosen in such a way that the recurrence point density (RR) is approximately the same. The embedding parameters ($m = 5$ and $\tau = 5$) correspond to an appropriate time delay embedding.

a sufficient explanation the work of Manuca and Savit (1996) is recommended.

Furthermore, the term *recurrent plots* can be found for RPs in the literature (e.g. Balasubramaniam et al., 2000). However, this term should not be used for RPs (it seems that it is sometimes used for return time plots). Finally, it should be mentioned that the term *recurrence plots* is sometimes used for another representation not related to RPs (e.g. Huang and Sobolev, 2002).

The selection of a specific variant from this variety of RPs depends on the problem and on the kind of data. Perpendicular RPs are highly recommended for the quantification analysis based on diagonal structures, whereas corridor thresholded RPs are not suitable for this task. Windowed RPs are appropriate for the visualization of the long range behaviour of rather long data sets. If the recurrence behaviour for the states $\vec{x}_i$ within a predefined section $\{\vec{x}_{i+i_0}, \ldots, \vec{x}_{i+i_0+k}\}$ of the phase space trajectory is of special interest, an RP with a horizontal LOI will be practical. We will use the standard RP (2.6)

according to Eckmann et al. (1987) in this work.

It should be emphasized again that the recurrence of states is an important feature. Beside the recurrence plots, there are some other methods that use recurrences. For example, the recurrence in the phase space is used for the recurrence time statistics (Kac, 1947; Gao, 1999; Balakrishnan et al., 2000), first return map (Lathrop and Kostelich, 1989), space time separation plot (Provenzale et al., 1997) or as a measure for nonstationarity (Kennel, 1997; Rieke et al., 2002, closely related to the recurrence time statistics).

2.2.2 Structures in Recurrence Plots

The initial purpose of RPs is the visual inspection of higher dimensional phase space trajectories. The view on RPs gives hints about the time evolution of these trajectories. The advantage of RPs is that they can also be applied to rather short and even nonstationary data.

The RPs exhibit characteristic large scale and small scale patterns. The first patterns were denoted by Eckmann et al. (1987) as *typology* and the latter as *texture*. The typology offers a global impression which can be characterized as *homogeneous*, *periodic*, *drift* and *disrupted*.

- *Homogeneous* RPs are typical of stationary and autonomous systems in which relaxation times are short in comparison with the time spanned by the RP. An example of such an RP is that of a random time series (Fig. 2.6A).

- Oscillating systems have RPs with diagonal oriented, *periodic* recurrent structures (diagonal lines, checkerboard structures). The illustration in Fig. 2.6B is a rather clear periodic system with two frequencies and a frequency ratio of four (the main diagonal lines are divided by four crossing short lines; irrational frequency ratios cause more complex periodic recurrent structures). However, even for those oscillating systems whose oscillations are not easily recognizable, the RPs can be used in order to find their oscillations (an example can be found in Eckmann et al., 1987, cp. unstable periodic orbits).

- The *drift* is caused by systems with slowly varying parameters. Such slow (adiabatic) change brightens the RP's upper-left and lower-right corners (Fig. 2.6C).

- Abrupt changes in the dynamics as well as extreme events cause *white areas or bands* in the RP (Fig. 2.6D). RPs offer an easy possibility to find

and to assess extreme and rare events by using the frequency of their recurrences.

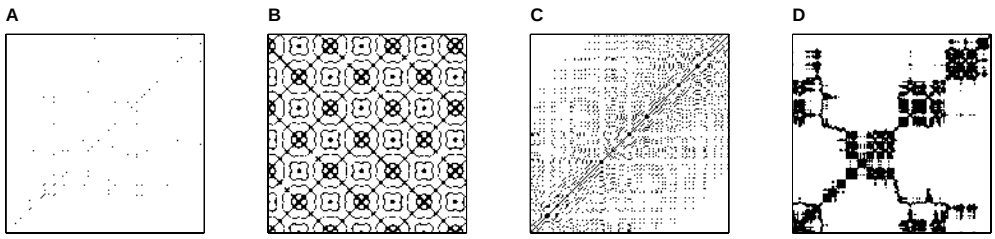

Figure 2.6: Characteristic typology of recurrence plots: (A) homogeneous (uniformly distributed noise), (B) periodic (super-positioned harmonic oscillations), (C) drift (logistic map $x_{i+1} = 4x_i(1 - x_i)$ corrupted with a linearly increasing term, cp. Fig. 2.9D) and (D) disrupted (Brownian motion). These examples illustrate how different RPs can be. The used data have the length 400 (A, B, D) and 150 (C), respectively; no embeddings are used; the thresholds are $\varepsilon = 0.2$ (A, C, D) and $\varepsilon = 0.4$ (B).

The closer inspection of the RPs reveals small scale structures (the texture) which are *single dots*, *diagonal lines* as well as *vertical* and *horizontal lines* (the combination of vertical and horizontal lines obviously forms rectangular clusters of recurrence points).

- *Single, isolated recurrence points* can occur if states are rare, if they do not persist for any time or if they fluctuate heavily. However, they are not a unique sign of chance or noise (for example in maps).

- A *diagonal line* $\mathbf{R}_{i+k,j+k} = 1$ (for $k = 1 \ldots l$, where l is the length of the diagonal line) occurs when a segment of the trajectory runs parallel to another segment, i. e. the trajectory visits the same region of the phase space at different times. The length of this diagonal line is determined by the duration of such similar local evolution of the trajectory segments. The direction of these diagonal structures can differ. Diagonal lines parallel to the LOI (angle $\pi/4$) represent the parallel running of trajectories for the same time evolution. The diagonal structures perpendicular to the LOI represent the parallel running with contrary times (mirrored segments; this is often a hint for an inappropriate embedding). Since the definition of the Lyapunov exponent uses the time of the parallel running of trajectories, the relationship between the diagonal lines and the Lyapunov exponent is obvious (further explanation in Subsec. 2.2.3).

- A *vertical (horizontal) line* $\mathbf{R}_{i,j+k} = 1$ (for $k = 1 \dots v$, with v the length of the vertical line) marks a time length in which a state does not change or changes very slowly. It seems, that the state is trapped for some time. This is a typical behaviour of laminar states (intermittency).

These small scale structures are the base of a quantitative analysis of the RPs.

The examples in Fig. 2.6 illustrate how different the small scale patterns can be. A large amount of single points and the vanishing amount of lines are caused by heavy fluctuation, which is characteristic for uncorrelated noise (Fig. 2.6A). The relationship between periodically recurrent structures and oscillators is obvious (Fig. 2.6B). The exact recurrent dynamics cause long diagonal lines separated by a fixed distance. The nonregular occurrence of short as well as of long diagonal lines is characteristic for chaotic processes (Fig. 2.6C), whereas the nonregular occurrence of extended black clusters and extended white areas corresponds with a nonregular behaviour in the system, which could be, for example, correlated noise (Fig. 2.6D).

In a more general sense the line structures in an RP exhibit locally the time relationship between the current trajectory segments. A line structure in an RP of length l corresponds to the closeness of the segment $f(T_1(t))$ to another segment $f(T_2(t))$, where $T_1(t)$ and $T_2(t)$ are the local time scales (or transformations of an imaginary absolute time scale t) which preserve that $f(T_1(t)) \approx f(T_2(t))$ for some time $t = 1 \dots l$. Under some assumptions (e. g. piecewise existence of an inverse of the transformation $T(t)$) the local slope $\mathfrak{m}(t)$ of a line in an RP represents the local time derivative of the product of the inverse second time scale $T_2^{-1}(t)$ and the first time scale $T_2(t)$

$$\mathfrak{m}(t) = \partial_t T_2^{-1}\left(T_1(t)\right). \tag{2.14}$$

We will consider here an illustrative example. A further explanation of the relationship between the slope of the lines and the trajectories is given in the Subsec. about cross recurrence plots (2.3.2). Let us consider a function $f(T) = T(t)$ with a section of a monotonical, linear increase $T_{lin} = t$ and another (hyperbolic) section which follows $T_{hyp} = -\sqrt{r^2 - t^2}$ (Fig. 2.7A) and both sections visit the same area in the phase space. Since the inverse of the hyperbolic section is $T_{hyp}^{-1} = \sqrt{r^2 - t^2}$, the derivative

$$\mathfrak{m} = \partial_t T_{lin}^{-1}\left(T_{hyp}(t)\right) = \frac{t}{\sqrt{r^2 - t^2}} \tag{2.15}$$

corresponds to the derivative of a circle line with a radius r, a bowed line structure with the form of a circle occurs in the RP (Fig. 2.7C).

Summarizing the last mentioned points we can establish the following list of observations and give the corresponding qualitative interpretation:

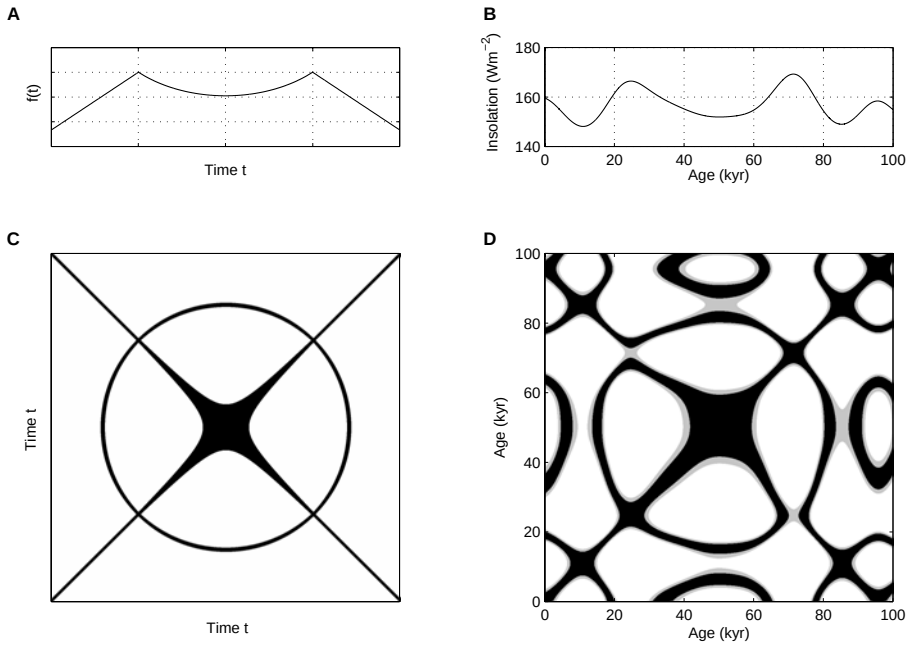

Figure 2.7: (A, C) Illustrative example of the relationship between the slope of lines in an RP and the local derivatives of the involved trajectory segments. Since the local derivative of the transformation the time scales of the linear and the hyperbolic sections corresponds to the derivative of a circle line, a circle occurs in the RP. (B, D) A corresponding structure found in nature: the solar insolation on the latitude 44°N for the last 100 kyr (data from Berger and Loutre, 1991). RPs created without embedding.

1. Homogeneity → the process is obviously stationary
2. Fading to the upper left and lower right corners → nonstationarity; the process contains a trend or drift
3. Disruptions (white bands) occur → nonstationarity; some states are rare or far from the normal; transitions may have occurred
4. Periodic patterns → cyclicities in the process; the time distance between periodic patterns (e. g. lines) corresponds to the period
5. Single isolated points → heavy fluctuation in the process; if only single isolated points occur, the process may be a random process
6. Diagonal lines (parallel to the LOI) → the evolution of states is similar at different times; the process could be deterministic; if these diagonal lines occur beside single isolated points, the process can be from chaos

(if, in addition, these diagonal lines are periodic, the considered system contains unstable periodic orbits)

7. Diagonal lines (orthogonal to the LOI) → the evolution of states is similar at different times but with inverse time; sometimes this is a sign for an insufficient embedding

8. Vertical and horizontal lines/ clusters → some states do not change or change slowly for some time (laminar states)

The visual interpretation of RPs requires some experience. The study of RPs from paradigmatic systems gives a good introduction into characteristic typology and texture. However, their quantification offers a more objective way for the investigation of the considered system. With this quantification, the RPs have become more and more popular within a growing group of scientists who use RPs and their quantification techniques for data analysis (a search with the Scirus search engine reveals over 200 journal published works and approximately 700 web published works about RPs).

2.2.3 The Quantitative Analysis of Recurrence Plots

Zbilut and Webber have developed a tool which quantifies the mentioned structures in the RPs, the *recurrence quantification analysis (RQA)* (Zbilut and Webber Jr., 1992; Webber Jr. and Zbilut, 1994). They define measures of complexity using the recurrence point density and diagonal structures in the recurrence plot: the *recurrence rate* (or per cent recurrences), the *determinism* (or per cent determinism), the *divergence* (the inverse of the maximal length of diagonal structures), the *entropy* and the *trend* (or drift). A computation of these measures in small windows (sub-matrices) of the RP moving along the LOI yields the time dependent behaviour of these variables. Some studies based on these RQA measures show that these measures are able to find bifurcation points, especially chaos-order transitions (Trulla et al., 1996). The RQA is based on RPs gained by using a fixed threshold ε, hence the RPs are symmetric. In the following, these RQA measures are introduced. In the Subsec. 2.2.4 we will adopt this concept in order to quantify the vertical structures in the RP.

The first measure of the RQA is the *recurrence rate* or *per cent recurrences (REC)*

$$RR = \frac{1}{N^2} \sum_{i,j=1}^{N} \mathbf{R}_{i,j}^{m,\varepsilon}, \tag{2.16}$$

which simply counts the black dots in the RP. It is a measure of the density of recurrence points and corresponds to the definition of the correlation sum (2.7)

except that the LOI is included. Nevertheless, the constraint for the correlation sum, that a large amount of data points are needed, also applies to the RR when used as an estimation of the correlation sum. In the limit

$$P_\bullet = \lim_{N\to\infty} \frac{1}{N^2} \sum_{i,j=1}^{N} \mathbf{R}_{i,j}^{m,\varepsilon}, \tag{2.17}$$

this measure becomes the probability of finding a recurrence point in the RP (probability that a state will recur). With the knowledge of the probability $\rho(x)$ of the states where dimension $m = 1$ (or the maximum norm) the recurrence rate can be analytically computed by using the convolution (Thiel et al., 2003a)

$$P_\bullet^\varepsilon = \int_{-\varepsilon}^{\varepsilon} \rho(x) * \rho(x)\, dx. \tag{2.18}$$

This probability $P_\bullet^\varepsilon$ can be used to analytically describe the RQA measures for some systems (Thiel et al., 2002, 2003a).

The next measures consider the diagonal lines. The frequency distribution of the lengths l of the diagonal structures in the RP is $P^\varepsilon(l) = \{l_i;\ i = 1 \ldots N_l\}$, where N_l is the absolute number of diagonal lines (each line is counted only once in contrast to the cumulative distribution[1]). Processes with stochastic behaviour cause none or very short diagonals, whereas deterministic processes cause longer diagonals and less single, isolated recurrence points. Therefore, the ratio of recurrence points that form diagonal structures to all recurrence points

$$DET = \frac{\sum_{l=l_{min}}^{N} l\, P^\varepsilon(l)}{\sum_{i,j}^{N} \mathbf{R}_{i,j}^{m,\varepsilon}}, \tag{2.19}$$

is introduced as a measure for the *determinism* (or predictability) in the system. However, this measure does not have the real meaning of the determinism of a process. The threshold l_{min} excludes the diagonal lines which are formed by the tangential motion of the phase space trajectory. For $l_{min} = 1$ the determinism is equal to the recurrence rate. The choice of l_{min} could be made in a similar way as the choice of the size for the Theiler window (cf. remark on p. 13), but one has to take into account that a too large l_{min} can worsen the histogram $P(l)$ and thus the reliability of the measure DET.

[1]The cumulative distribution for the line length

$$P_c^\varepsilon(l) = \sum_{i=1}^{N_l} (i - l + 1)\, P^\varepsilon(i)$$

counts each diagonal line several times, in the sense that a line of length l contains l lines of length one, $(l-1)$ lines of length two, $(l-2)$ lines of length three ... one line of length l.

Diagonal structures show the range in which a segment of the trajectory is rather close to another segment of the trajectory at a different time; thus these lines give a hint about the divergence of the trajectory segments. The *average diagonal line length*

$$L = \frac{\sum_{l=l_{min}}^{N} l\, P^{\varepsilon}(l)}{\sum_{l=l_{min}}^{N} P^{\varepsilon}(l)} \tag{2.20}$$

is the average time that two segments of the trajectory are close to each other, and can be interpreted as the mean prediction time. Instead of this average the RQA uses the *maximum length* of the diagonal structures or its inverse, the *divergence*,

$$L_{max} = \max\left(\{l_i;\ i = 1 \ldots N_l\}\right) \quad \text{respective} \quad DIV = \frac{1}{L_{max}}. \tag{2.21}$$

Eckmann has stated that "the length of the diagonal lines is related to the largest positive Lyapunov exponent" if there is one in the considered system (Eckmann et al., 1987). Different approaches have been suggested in order to use these lengths for the estimation of the largest positive Lyapunov exponent as DIV (Trulla et al., 1996) or the average of the inverse of the half lengths of the diagonals (Choi et al., 1999, they have defined this measure for perpendicular RPs).

The measure *entropy* refers to the Shannon entropy of the frequency distribution of the diagonal line lengths

$$ENTR = -\sum_{l=l_{min}}^{N} p(l) \ln p(l) \quad \text{with} \quad p(l) = \frac{P^{\varepsilon}(l)}{\sum_{l=l_{min}}^{N} P^{\varepsilon}(l)} \tag{2.22}$$

and reflects the complexity of the deterministic structure in the system. However, this entropy depends sensitively on the bin number and, thus, may differ for different realizations of the same process, as well as for different data preparations.

The measures introduced up to now, RR, DET, L etc. can also be computed separately for each diagonal parallel to the LOI. The representation of these diagonalwise computed measures, $RR_*(t)$, $DET_*(t)$ and $L_*(t)$, over the time distance t from the LOI hints at the determination of the already mentioned Theiler window (cf. Subsec. 2.2.1). Henceforth, measures with a subscribed asterisk or index denote diagonalwise computed measures. This diagonalwise determination of the RQA measures will receive more importance in the analysis of CRPs (the definition of the diagonalwise computed measures can be found in Subsec. 2.3.1, which can be adopted for the RPs). Furthermore, the measure RR_* is closely related to the *close returns histogram* introduced

by Lathrop and Kostelich (1989). This can be used to find periodic orbits in low-dimensional chaotic systems (Lathrop and Kostelich, 1989; Mindlin and Gilmore, 1992; Gilmore, 1998). Since periodic orbits are more closely related to the occurrence of longer diagonal structures, the measures DET_* and L_* are more suitable candidates for this kind of study. The measure RR_* have been already used by Eckmann et al. (1987) for the study of nonstationarity in the data.

The last RQA measure is the *trend*, which is a linear regression coefficient over the recurrence point density RR_* of the diagonals parallel to the LOI (for definition see Eq. (2.34) in Subsec. 2.3.1) as a function of the time distance between these diagonals and the LOI

$$TREND = \frac{\sum_{i=1}^{\tilde{N}} (i - \tilde{N}/2)(RR_i - \langle RR_i \rangle)}{\sum_{i=1}^{\tilde{N}} (i - \tilde{N}/2)^2}. \tag{2.23}$$

The trend gives information about a nonstationarity in the process, especially a drift. The computation excludes the edges of the RP ($\tilde{N} < N$) because the statistic lacks by reason of less recurrence points. The choice of $\tilde{N}$ depends on the studied process. Whereas $N - \tilde{N} > 10$ should be sufficient for noise, this difference should be much larger for a process with some autocorrelation (ten times the order of magnitude of the autocorrelation time should always be enough). It should be noted that if the time dependent RQA (measures are computed in shifted windows) is used, $TREND$ will depend strongly on the size of the windows and may reveal contrary results for different window sizes.

In some publications a further measure, the *ratio*, can be found. It is defined as the ratio between DET and RR (Webber Jr. and Zbilut, 1994) and can be computed from the frequency distributions of the lengths of the diagonal lines

$$RATIO = N^2 \, \frac{\sum_{l=l_{min}}^{N} l \, P^{\varepsilon}(l)}{\left(\sum_{l=1}^{N} l \, P^{\varepsilon}(l)\right)^2}. \tag{2.24}$$

A heuristic study of physiological systems has revealed that this ratio can be used in order to discover transitions, because it was found that during certain types of transitions the RR can decrease, whereas DET does not change at the same time (Webber Jr. and Zbilut, 1994).

Currently, a satisfying theory about the statistics of these measures of complexity has not been developed. Therefore, a reliable statement about the significance of these measures cannot be made. Nevertheless, a possibility for assessing the significance of these measures lies in applying a sufficient surrogate test (but this works only for stationary processes).

In a more theoretical study, Thiel et al. (2003b) have revealed analytical solutions for the RQA measures of stochastic systems and maps. Gao and Cai (2000) have studied the relationship between the RQA measures and a divergence exponent which is closely related to the largest Lyapunov exponent. Furthermore, the clear relationship between the cumulative distribution (cf. footnote on p. 23) $P_c(l)$ and the second order Rényi entropy K_2 has been found (Faure and Korn, 1998; Thiel et al., 2003a). Referring to their studies Thiel et al. (2003a), have stated that the distribution $P_c(l)$ is related rather to K_2 than to the largest positive Lyapunov exponent.

An appropriate embedding of time series is motivated by the desire to avoid false nearest neighbours. However, in an RP false nearest neighbours will occur as black dots, rather short black lines or (for a specific embedding) as black lines perpendicular to the LOI (i. e. with an angle of $-\pi/4$). Whereas the estimation of some invariants of the RP (like K_2) are independent from the embedding (and consequently does not need any embedding), the estimation of the measures RR, DET, L etc. depends on the embedding and needs a sufficient choice (Thiel et al., 2003a).

All these RQA measures are based largely on the distribution of the length of the diagonal structures in the RP. Additional information about further geometrical structures as vertical and horizontal elements is not included. In the following, I will extend this quantitative view to vertical structures and propose new measures of complexity based on the distribution of the vertical line length. Since we are using symmetric RPs, we will only consider the vertical structures in the following.

2.2.4 New Measures of Complexity: Laminarity and Trapping Time

Let us consider a point $\vec{x}_i$ of the trajectory and the set of its associated recurrence points $\mathcal{R}_i$

$$\mathcal{R}_i = \left\{ \vec{x}_j : \mathbf{R}_{i,j} = 1 \,;\; j \in [1 \dots N] \right\}. \tag{2.25}$$

Let us denote subsets of these recurrence points

$$\mathcal{V}_{i,j} = \left\{ j+1 \dots j+v_j : \vec{x}_j \notin \mathcal{R}_i;\; \vec{x}_{j+1} \dots \vec{x}_{j+v_j} \in \mathcal{R}_i;\; \vec{x}_{j+v_j+1} \notin \mathcal{R}_i \right\} \tag{2.26}$$

which form connected vertical structures of the length v_j. In continuous time systems with high time resolution and with an adequately large threshold ε a large part of these subsets $\mathcal{V}_{i,j}$ usually corresponds to the tangential motion of the phase space trajectory (cp. Subsec. 2.2.1 on p. 13), i. e. to the sojourn points described by Gao (1999). However, not all elements of these sets are real sojourn points. Although sojourn points do not occur in maps, the subsets $\mathcal{V}_{i,j}$

are not necessarily empty because of laminar states. Furthermore, the finite size of the threshold ε can pretend a tangential motion, although there are rather small cycles instead of a tangential motion (e. g. Shilnikov chaos).

Next, we determine the length $v_j = \left|\mathcal{V}_{i,j}\right|$ of all subsets $\mathcal{V}_{i,j}$. $\mathcal{P}_i(v) = \{v_j\,;\ j = 1 \ldots N_v\}$ denotes the set of all occurring subset lengths in $\mathcal{V}_i$ (N_v is the absolute number of the vertical lines), and from $\bigcup_{i=1}^{N} \mathcal{P}_i(v)$ we determine the distribution of the vertical line lengths $P^{\varepsilon}(v)$ in the entire RP.

Analogous to the definition of the determinism (2.19), we compute the ratio between the recurrence points forming the vertical structures and the entire set of recurrence points

$$LAM = \frac{\sum_{v=v_{min}}^{N} v P^{\varepsilon}(v)}{\sum_{v=1}^{N} v P^{\varepsilon}(v)}, \tag{2.27}$$

and call it *laminarity* LAM. The computation of LAM is realized for those v that exceed a minimal length v_{min} in order to decrease the influence of sojourn points. For maps we use $v_{min} = 2$. LAM is the measure of the amount of vertical structures in the whole RP and represents the occurrence of laminar states in the system without, however, describing the length of these laminar phases. LAM will decrease if the RP consists of more single recurrence points than vertical structures.

We define the average length of vertical structures (cp. (2.20))

$$TT = \frac{\sum_{v=v_{min}}^{N} v P^{\varepsilon}(v)}{\sum_{v=v_{min}}^{N} P^{\varepsilon}(v)}, \tag{2.28}$$

which we call *trapping time* TT. The computation also uses the minimal length v_{min} as in LAM (2.27). The measure TT contains information about the amount and the length of the vertical structures in the RP. It measures the mean time that the system will abide at a specific state (how long the state will be trapped).

Finally, we use the *maximal length of the vertical structures* in the RP

$$V_{max} = \max\left(\{v_l\,;\ l = 1 \ldots L\}\right) \tag{2.29}$$

as a measure which is the analogue to the standard measure L_{max} (2.21).

In contrast to the known RQA measures, these new measures are able to find chaos-chaos transitions (Marwan et al., 2002b). Hence, these measures make the investigation of intermittency possible, even if they are only represented by rather short and nonstationary data series. Since for periodic dynamics these measures are zero, chaos-order transitions can also be identified.

An application to the logistic map $x_{n+1} = a\,x_n\,(1 - x_n)$ illustrates the potentials of LAM, TT and V_{max}. We generate for each control parameter $a \in [3.5, 4]$, $\Delta a = 0.0005$ a separate time series (Fig. 2.8). In the analyzed range

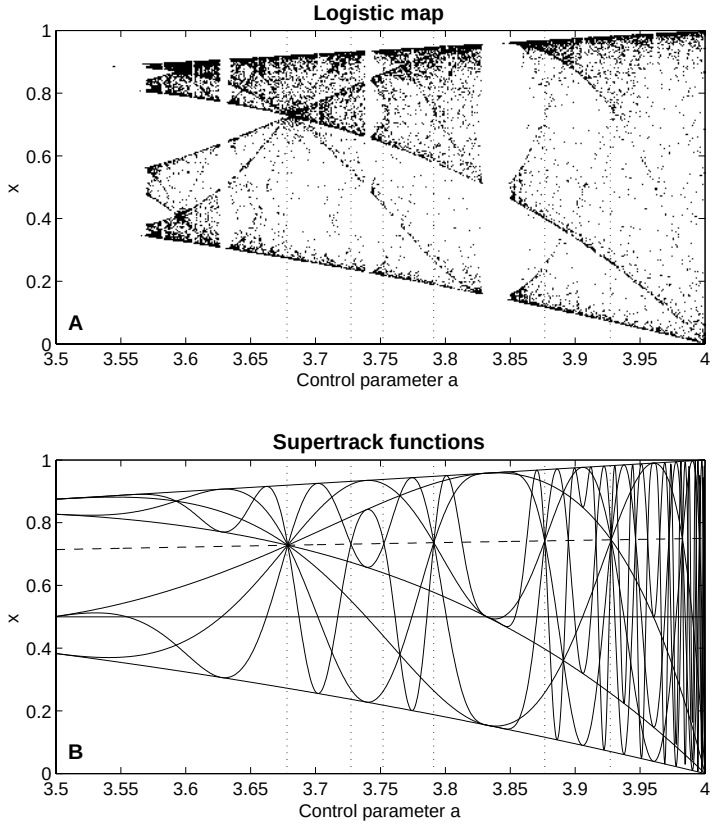

Figure 2.8: (A) Bifurcation diagram of the logistic map. (B) Low ordered supertrack functions $s_i(a)$ ($i = 1 \ldots 10$) and the fixed point of the logistic map $1 - 1/a$ (dashed). Their intersections represent periodic windows, band merging and laminar states. The dotted lines show a choosing of points of band merging and laminar phases ($a = 3.678, 3.727, 3.752, 3.791, 3.877, 3.927$).

of a, various regimes and transitions between them occur, e. g. accumulation points, periodic and chaotic states, band merging points, period doublings, inner and outer crises (Collet and Eckmann, 1980).

Useful tools for studying the chaotic behavior of the logistic map are the *supertrack functions*, which are recursively generated from

$$s_{i+1}(a) = a\, s_i(a)\big(1 - s_i(a)\big), \quad s_0(a) = \frac{1}{2}, \quad i = 1, 2, \ldots \tag{2.30}$$

Supertrack functions $s_i(a)$ represent the functional dependence of stable states at a given iteration number i on the control parameter a (Oblow, 1988). The intersection of $s_i(a)$ with $s_{i+j}(a)$ indicates the occurrence of a j-period cycle and the intersection of $s_i(a)$ with the fixed-point $(1 - 1/a)$ of the logistic map indicates the point of an unstable singularity, i. e. laminar behavior (Fig. 2.8, intersection points are marked with dotted lines).

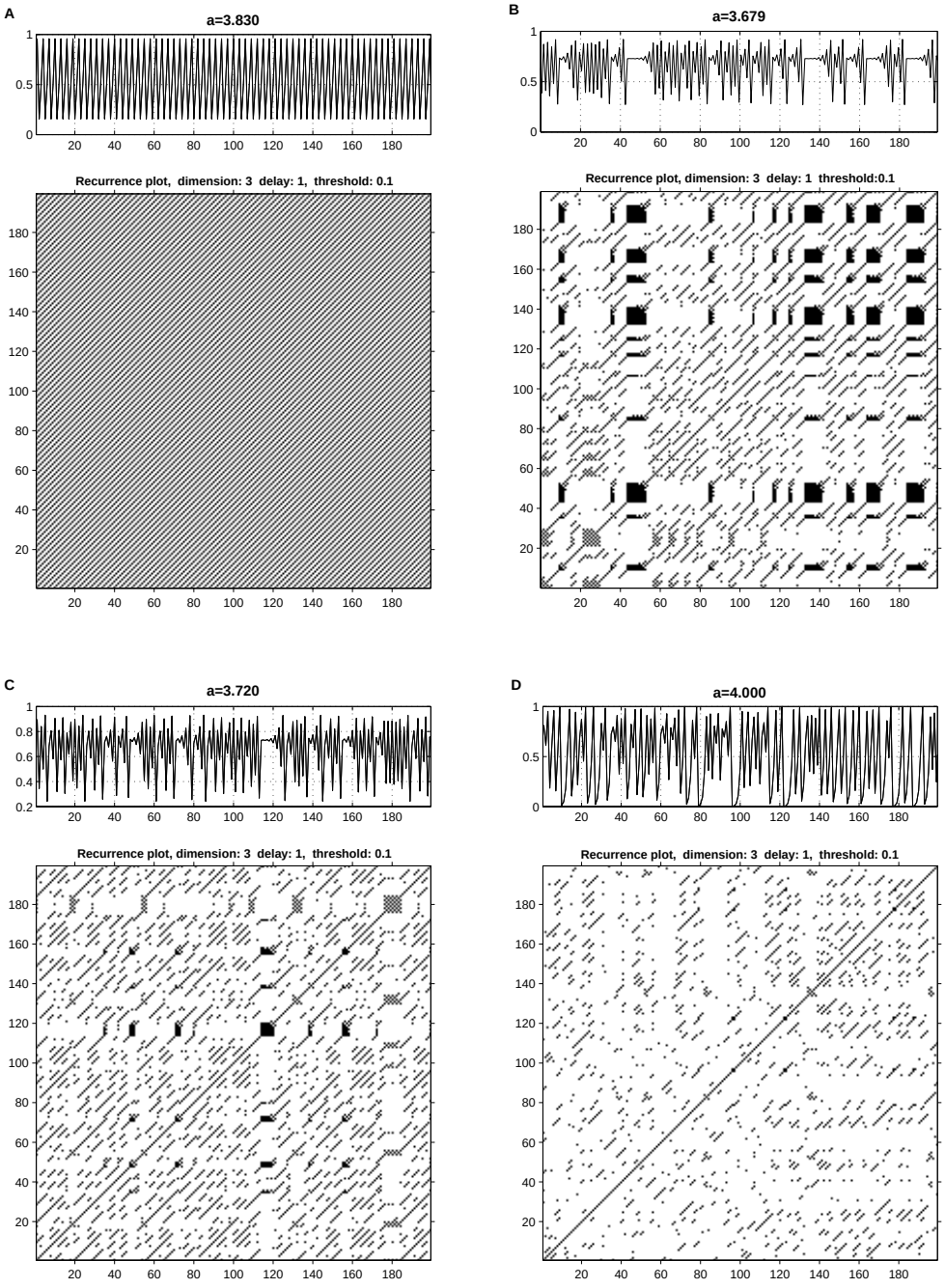

Figure 2.9: Recurrence Plots (RP) of the logistic map for various control parameters a, near different qualitative changes: periodic-3-window $a = 3.830$ (A), band merging $a = 3.679$ (B), supertrack intersection $a = 3.720$ (C) and chaos (exterior crisis) $a = 4$ (D); with embedding dimension $m = 3$, time delay $\tau = 1$ and distance cutoff $\varepsilon = 0.1\sigma$.

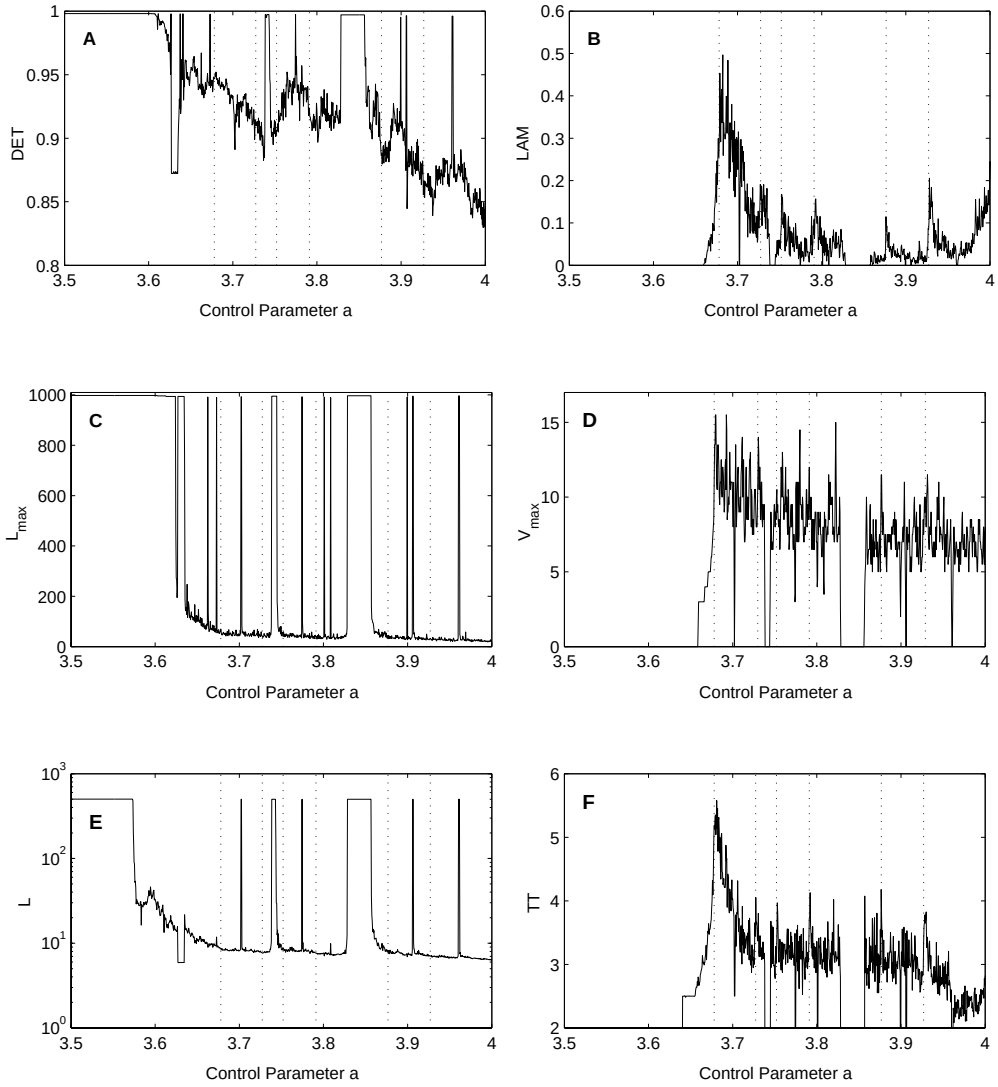

Figure 2.10: Selected RQA measures DET, L_{max} and L and the measures LAM, V_{max} and TT. The vertical dotted lines show some of the points of band merging and laminar behavior (cf. Fig. 2.8), whereby not all of them have been marked. Whereas DET (A), L_{max} (C) and L (E) show periodic-chaotic/ chaotic-periodic transitions (maxima), LAM (B), V_{max} (D) and TT (F) exhibit in addition to those transitions (minima) chaotic-chaotic transitions (maxima). The differences between LAM and V_{max} are caused by the fact that LAM measures only the amount of laminar states, whereas V_{max} measures the maximal duration of the laminar states. Although some peaks of V_{max} and TT are not at the dotted lines, they correspond with laminar states (not all can be marked).

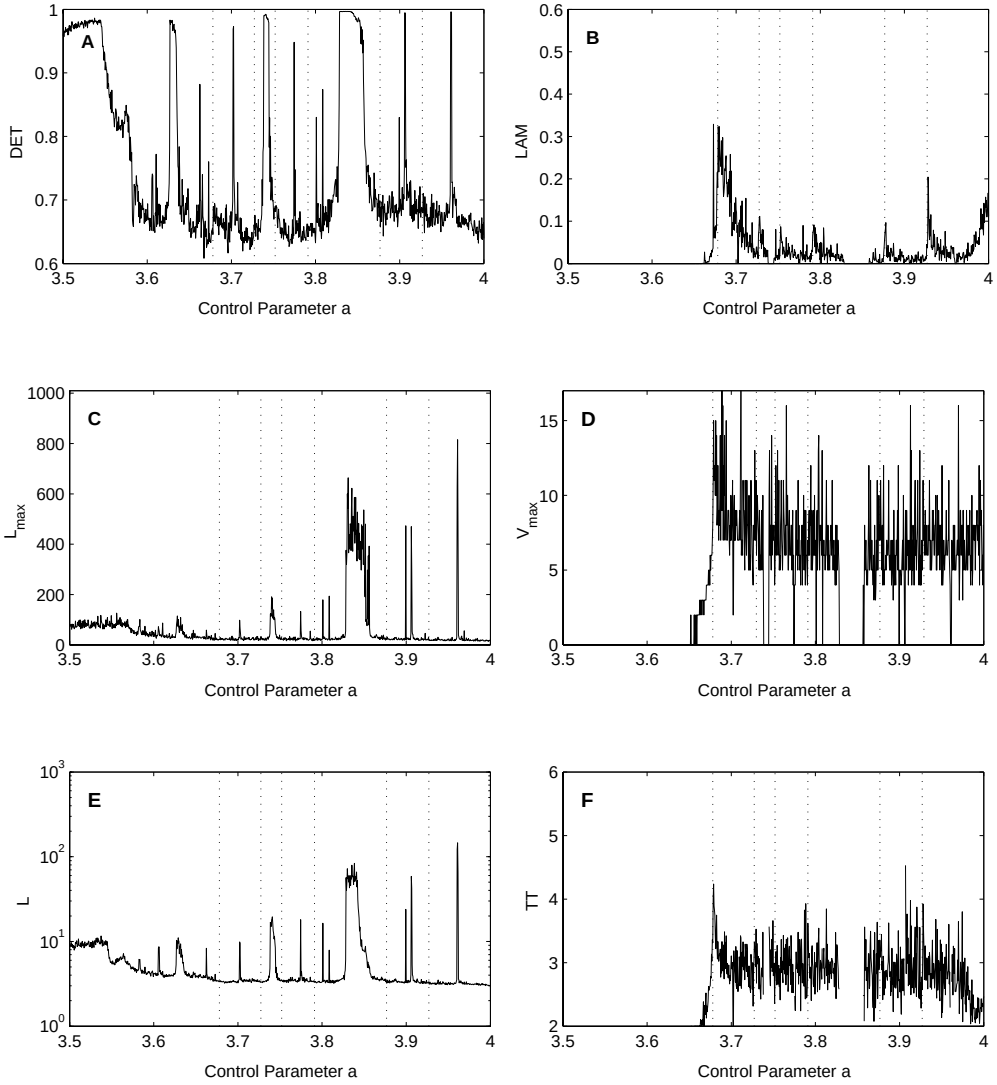

Figure 2.11: The same RQA parameters as shown in Fig. 2.10 under the influence of additive noise (Gaussian white noise with standard deviation $\sigma = 0.01$). All measures show distortions and different levels of decrease due to the additive noise. LAM, V_{max} and TT still reveal the transitions, whereby V_{max} and TT are less distinct.

We compute the RPs of at least 1 000 data points and with a cut-off distance $\varepsilon = 0.1$ (in units of the standard deviation σ). Although an embedding is not necessary for maps (i. e. $m = 1$), we use here an embedding of $m = 3$ and $\tau = 1$ according to Trulla et al. (1996). The cut-off distance ε is selected to be 10% of the diameter of the phase space. Smaller values would lead to a better distinction of small variations (e. g. the range before the accumulation point consists of small variations), but the recurrence point density decreases in the same way and thus the statistics of continuous structures in the RP becomes soon insufficient.

For various values of the control parameter a the RPs exhibit specific characteristics (Fig. 2.9). Periodic states cause continuous and periodic diagonal lines in the RP, but no vertical or horizontal lines. Band merging points inner crises and regions of intermittency represent states with short laminar behaviour and cause vertically and horizontally spread black areas in the RP. Moreover, diagonal lines occur. Fully developed chaotic states ($a = 4$) cause a rather homogeneous RP with numerous single points and rare, short, diagonal or vertical lines. Vertical (and horizontal) lines occur much more frequently at supertrack crossing points (band merging points included) than in other chaotic regimes (Fig. 2.8).

We indeed find that the measures LAM, TT and V_{max}, which are based on these vertical structures, enable the identification of the chaos-chaos transitions to the laminar states (Fig. 2.10 B, C). The measures show distinct maxima or peaks at these transitions. Besides, the measures fall to zero within the period windows, hence, the chaos-order transitions can also be identified. Since vertical lines occur much more frequently at inner crisis, band merging points and in regions of intermittency (i. e. laminar states) than in other chaotic regimes, TT and V_{max} grow up significantly at those points. This can also be seen by looking at the supertrack functions (Fig. 2.8). Although LAM also reveals laminar states, it is quite different from the other two measures because it does not increase at inner crises.

Although noise would influence the analysis, for small noise levels most of these transitions can be identified (Fig. 2.11). LAM is more robust against noise than TT and V_{max}. With increasing noise LAM, TT and V_{max} decrease, narrow periodic windows are blurred and local maxima at the regions of intermittency become progressively irrecognisable.

The behaviour of these measures regarding the control parameter a is similar to some of formerly proposed measures of complexity (Saparin et al., 1994; Wackerbauer et al., 1994). The Rényi dimension D_q of order $q < 0$, the fluctuation complexity as well as the normalized entropy exhibit local maxima at re-

gions of intermittency, rapid increase at inner crises and a rapid decrease and increase at the transitions between chaos and periodic windows. The difference between the formerly proposed measures and LAM, TT and V_{max} is the amount of data points needed. Where Saparin et al. (1994) and Wackerbauer et al. (1994) have used more than 100 000 data points in order parameterize the mentioned regions of interest, 1 000 would be enough for the measures based on RPs.

In the Subsec. 3.1 further illustrations will be presented.

2.2.5 Further Possibilities of Quantification

As already mentioned in the subsection 2.2.3, further measures of complexity can be defined by using RPs. Faure and Korn (1998) have suggested an estimator for the Kolmogorov-Sinai entropy K, which is based on a scaling law over the cumulative distribution of the diagonal line lengths. Thiel et al. (2003a) have proposed three further measures of complexity, which are estimators for the second order Rényi entropy K_2, the correlation dimension D_2 and the generalized mutual information I. These measures are invariants of the RP and do not need any embedding. The generalized mutual information can be resolved by the intersection (multiplication) of the RPs and by computing the RR of this intersection. For some chaotic oscillatory systems, they have found two scaling regions in the cumulative distribution of the diagonal line lengths. The second corresponds to K_2, whereas the first one applies to short time scales. This first scaling region cannot be resolved with the Grassberger-Procaccia algorithm.

Gao (1999) has used the time distance of recurrence points in the vertical direction and calls it recurrence time. He has distinguished between recurrence times of first type T^1 and second type T^2:

$$T_j^1 = \left|\left\{i, j : \vec{x}_i, \vec{x}_j \in \mathcal{R}_i\right\}\right| \tag{2.31}$$

and

$$T_j^2 = \left|\left\{i, j : \vec{x}_i, \vec{x}_j \in \mathcal{R}_i;\ \vec{x}_{j-1} \notin \mathcal{R}_i\right\}\right| \tag{2.32}$$

where $\mathcal{R}_i$ are the recurrence points which belong to the state $\vec{x}_i$ (2.25). These times are the time distances between the state at time i and its recurrences at time j. In an RP these time distances are expressed as vertical distances of the recurrence points in a column from the LOI. According to Gao (1999) the sojourn times have to be removed which leads to the recurrence time of the second type. However, following the given definition (2.32), all points forming vertical structures are removed except the first point of these structures, hence, laminar states are also excluded. If the recurrence times are determined by

using a perpendicular RP, the effect of the tangential motion will vanish, and consequently $T^1 \approx T^2$, although the vertical structures based on the laminar states still occur. The power law of $\langle T^1 \rangle$ respective $\langle T^2 \rangle$ over the threshold ε corresponds with the information dimension D_I (Gao, 1999). This procedure is called recurrence time statistics and goes back to the middle of the last century (Kac, 1947).

Likewise, the vertical distribution of the recurrence points is used for the study of unstable periodic orbits. Lathrop and Kostelich (1989) have introduced a histogram of recurrence points in respect to their time distance to a reference point (vertical distance to the LOI). This histogram corresponds to the histogram of T^1 as well as to the diagonalwise computed recurrence rate RR_* (cp. Eq. (2.34) in Subsec. 2.3.1, which defines RR_* for CRPs, but it holds also for RPs) and has been denoted as "close returns histogram" by these authors. However, they have not used an embedding for this approach, hence, a lot of false recurrences as well as the effect of the tangential motion will distort the "close returns histogram". This is not a real problem for prototypical model systems, but it complicates the determination of periodic orbits in real data (for example, the application to economic data does not manifest satisfying results; Gilmore, 1993, 2001). The analysis of the measures based on the diagonal structures DET_* and L_*, the embedding of the data as well as the usage of perpendicular RPs would significantly improve this technique for finding unstable periodic orbits.

Using the set of recurrence points $\mathcal{R}_i$ (2.25) associated to the state at i and using a linear approach (dynamics is locally linear), Lathrop and Kostelich (1989) have estimated Lyapunov exponents from the recurrence information. Additionally, once the Lyapunov exponents are found, they can be used for an estimation of the information dimension D_I (Lathrop and Kostelich, 1989).

The RPs test the distance between all points of the same phase space trajectory. However, why should not it be possible to test each point of one trajectory with each point of another trajectory in the same phase space? This leads us to the concept of *cross recurrence plots (CRP)*, which we will focus on in the next section.

2.3 Cross Recurrence Plots

Starting with the concept of RPs we regard a phase space with one trajectory $\vec{x}_i$ of length N_x. Now we add a second trajectory $\vec{y}_j$ with the length N_y into the same phase space (Fig. 2.12). The test between all points of the first trajectory

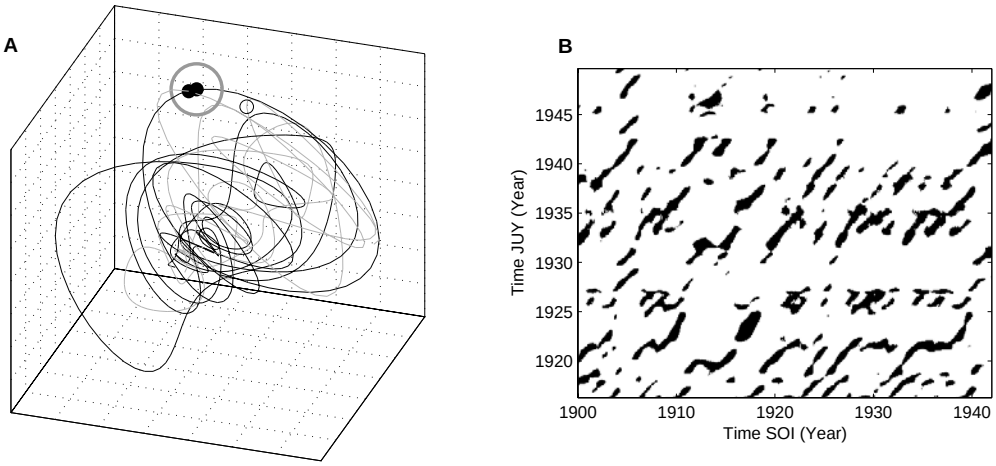

Figure 2.12: (A) Segments of the phase space trajectories of the El Niño Southern Oscillation Index (SOI, black line) and a precipitation time series of San Salvador de Jujuy (Argentina, gray line) by using time delay embedding (smoothed, monthly data; $\tau = 7$ months). In (B) the corresponding cross recurrence plot is shown. If a point of the precipitation trajectory at j (black point on the gray line in (A)) falls into the neighbourhood (gray circle in (A)) of a point of the SOI trajectory at i, in the CRP at the location (i, j), a black point will be marked. A point outside the neighbourhood (small circle in (A)) is marked as a white point in the CRP. For creating this CRP the FAN criterion with $\varepsilon = 0.15$ is used.

with all points of the second trajectory leads to the *cross recurrence plot (CRP)*

$$\mathbf{CR}_{i,j}^{m,\varepsilon_i} = \Theta\left(\varepsilon_i - \left\|\vec{x}_i - \vec{y}_j\right\|\right), \quad \vec{x}_i, \vec{y}_j \in \mathbb{R}^m, \\ i = 1 \ldots N_x, \; j = 1 \ldots N_y. \tag{2.33}$$

The notation is analogous to the definition of RPs (2.6). If in the second trajectory a state at time j is close to a state on the first trajectory at time i, a black dot will be assigned to the matrix **CR** at location (i, j). This occurrence of neighbours in both trajectories is not a "recurrence" of states, hence, the matrix (2.33) does not represent recurrences but the conjunctures of states of both systems. Therefore, this representation is not really a "cross recurrence plot". Nevertheless we call it "cross recurrence plot" in order to follow the way of a generalization of RPs and because of the occurrence of the term "cross recurrence quantification" in the literature for the parallel concept of the generalization of the RQA (Zbilut et al., 1998). The vectors $\vec{x}$ and $\vec{y}$ do not need to have the same length, hence the matrix **CR** is not necessarily square. This extension of RPs was first used by Zbilut et al. (1998) for the *cross recurrence quantification*. Inde-

pendently of their work, the concept of cross recurrence plots also surfaces in Marwan (1999).

Both trajectories for the creation of a CRP have to represent the same dynamical system with equal state variables because they are in the same phase space. This must be taken into account if time series of different measurements (e. g. temperature and pressure) are involved. For the embedding and the following CRP analysis the time series can be taken from different measurements if they are components or state variables of the same system. A precedent data normalization solves the problem of different units. However, the application of CRPs to absolutely different measurements, which are not observations of the same dynamical system (e. g. a stocks index and the precession of the Earth's rotation), is not possible. For such different kinds of data the presently developed concept of intersected RPs can be used (cf. Subsec. 2.4).

Assuming that both trajectories come from the same process but different absolute values, the CRP will not become the expected RP if a fixed threshold ε is chosen. Therefore, it is necessary to adapt both trajectories to the same range of values, e. g. by using a normalization to the standard deviation. However, the application of a fixed amount of nearest neighbours (FAN), i. e. ε_i changes for each state x_i, solves this problem automatically, and a modification of the amplitudes is not necessary. The latter choice of a neighbourhood has the additional advantage of working well for slowly changing trajectories (e. g. drift).

Since the values of $\mathbf{CR}_{i,i}$ $(i = 1 \ldots N)$ are not necessarily one, the black main diagonal usually vanishes. As we will discuss in Subsec. 2.3.2, the line of identity (LOI) can be replaced by the *line of synchronization (LOS)* and may ultimately not have the angle $\pi/4$. Apart from that, the statements given in the subsection about the structures in RPs (Subsec. 2.2.2) hold also for the CRPs. However, the lines which are more or less diagonally orientated are here of major interest too. They represent segments on the both trajectories, which run parallel for some time. The frequency and lengths of these lines are obviously related to a certain similarity between the dynamics of both systems.

An additional time dilatation or time compression of one of the trajectories causes a distortion of the main diagonal line (cp. remarks about the relationship between the slope of RP lines and the local derivatives of the trajectories in Subsec. 2.2.2). This case will be discussed in subsection 2.3.2. In the following subsection we presume that both systems have the same time scale (equal length N and sample time Δt), hence, the CRP is a $N \times N$ array.

2.3.1 Measures for Similarities Between Two Observed Processes

The long diagonal structures in the CRP reveal similar time evolution of the trajectories of both processes. It is obvious that a progressively increased similarity between both processes causes an increase of the recurrence point density along the main diagonal $\mathbf{CR}_{i,i}$ $(i = 1 \dots N)$ until a black straight main diagonal line occurs (which would be in fact the LOI, and the CRP becomes an RP). Thus, the occurrence of diagonal lines in a CRP can be used in order to benchmark the similarity between the considered processes.

In order to quantify this similarity some quantitative measures have to be defined. Since we use the occurrence of the more or less discontinuous diagonal lines, the RQA measures (cf. Subsec. 2.2.3) should be suitable for this purpose after some modifications. Especially, they have to be modified in such a way that they can be used as a diagonalwise criterion for the vanishing diagonal lines (Marwan and Kurths, 2002).

Let us consider a diagonal $\mathbf{CR}_{i,j}$ $(j - i = k = \text{const.})$ which is parallel to the main diagonal and has a time distance $t = k\,\Delta t$ from the main diagonal. The recurrence points in this diagonal correspond with tests between the time delayed trajectories (delay t). In the following, some RQA measures will be redefined for these diagonals. Hence, these measures will be functions of the distance k from the main diagonal. Using this approach it is possible to assess the similarity in the dynamics depending on a certain time delay.

Following this procedure we need to define the frequency distributions of the diagonal line lengths $P_k^\varepsilon(l) = \{l_i;\ i = 1 \dots N_l\}$ (N_l is the absolute number of diagonal lines) for each diagonal parallel to the main diagonal $\mathbf{CR}_{i,j}^{m,\varepsilon}$ $(j - i = k)$. For $k = 0$ this line is the LOI, $k > 0$ diagonals above and $k < 0$ diagonals below the LOI, which represent positive and negative time delays, respectively.

The recurrence rate RR is now modified to

$$RR_k = RR_*(t) = \frac{1}{N-k} \sum_{j-i=k} \mathbf{CR}_{i,j}^{m,\varepsilon} = \frac{1}{N-k} \sum_{l=1}^{N-k} l\, P_k^\varepsilon(l) \tag{2.34}$$

and reveals the probability of the occurrence of similar states in both systems with a certain delay $t = k\,\Delta t$. A high density of recurrence points in a diagonal results in a high value of RR_*. This is the case for the systems whose trajectories often visit the same phase space regions.

Analogous to the RQA the determinism

$$DET_k = \frac{\sum_{l=l_{min}}^{N-k} l\, P_k^\varepsilon(l)}{\sum_{l=1}^{N-k} l\, P_k^\varepsilon(l)} \tag{2.35}$$

is the proportion of recurrence points forming long diagonal structures to all recurrence points, but here it is constrained to the considered diagonal. Smooth trajectories with long autocorrelation times will result in a CRP with long diagonal structures, even if the trajectories are not linked to each other (this effect corresponds to the tangential motion of one trajectory). In order to avoid the counting of such "false" diagonals, the lower limit for the diagonal line length l_{min} should be of the order of the autocorrelation time.

Stochastic as well as heavily fluctuating processes cause none or only short diagonals, whereas deterministic processes cause longer diagonals. If two deterministic processes have the same or similar time evolution, i. e. parts of the phase space trajectories meet the same phase space regions for certain times, the amount of longer diagonals increases and the amount of shorter diagonals decreases. The average diagonal line length

$$L_k = \frac{\sum_{l=l_{min}}^{N-k} l\, P_k^{\varepsilon}(l)}{\sum_{l=l_{min}}^{N-k} P_k^{\varepsilon}(l)} \tag{2.36}$$

quantifies the duration of such a similarity in the dynamics. A high coincidence of both trajectories increases the length of these diagonals. Besides, the entropy of the probability $P_k^{\varepsilon}(l)$ can also be defined. Still, we focus here on the first three measures.

High values of RR_* represent high probabilities of the occurrence of the same state in both processes, high values of DET_* and L_* represent a long time span of the occurrence of a similar dynamics in both processes. Whereas DET_* and L_* are sensitive to fast and highly fluctuating data, RR_* measures the probabilities of the occurrence of the same states in spite of these high fluctuations (noisy data). It is important to emphasize that these parameters are statistical measures and that their validity increases with the size of the CRP, i. e. with the observation length.

An additional CRP

$$\mathbf{CR}_{i,j}^{-} = \Theta\left(\varepsilon_i - \left\|\vec{x}_i + \vec{y}_j\right\|\right) \tag{2.37}$$

with opposite signed second trajectory $-\vec{y}_j$ allows to distinguish positive and negative relations between the considered trajectories (Marwan and Kurths, 2002). In order to recognize the measures for both possible CRPs, we add the superscript index $+$ to the measures for the positive linkage and the superscript index $-$ for the negative linkage, e. g. RR_k^+ and RR_k^-.

Another approach used to study the positive and negative relations between the considered trajectories involves using the composited measures for

the recurrence rate

$$RR_k^c = \frac{1}{N-k} \sum_{j-i=k} \left(\mathbf{CR}_{i,j}^+ - \mathbf{CR}_{i,j}^- \right), \tag{2.38}$$

the determinism

$$DET_k^c = DET_k^+ - DET_k^-, \tag{2.39}$$

and the average diagonal length

$$L_k^c = L_k^+ - L_k^-, \tag{2.40}$$

where $P_k^{\pm}(l)$ is the histogram of the diagonal line lengths in $\mathbf{CR}_{i,j}^{\pm}$ $(j-i=k)$, as it is used in Marwan et al. (2003) and in the example in Subsec. 3.2.2. This representation is similar to those of the cross correlation function and is more intuitive than the separate representation of RR_*^+, RR_*^- etc. However, for the investigation of interrelations based on even functions, these composited measures are not suitable.

A further substantial advantage of this method is its capability of also finding nonlinear similarities in short and nonstationary time series with high noise levels as they typically occur, e. g., in biology or earth sciences (examples in Subsec. 3.2.1).

However, the shortness and nonstationarity of data limit this method as well. As mentioned, one way to reduce problems accompanying nonstationary data is the alternative choice of a neighbourhood with a fixed amount of neighbours.

2.3.2 Time Scale Alignment of Time Series

In data analysis one is often faced with time series measured on varying time scales. These could be, for example, sets from borehole or core data in geophysics or tree rings in dendrochronology. Sediment cores might have undergone a number of coring disturbances such as compression or stretching. Moreover, cores from different sites with differing sedimentation rates would have different temporal resolutions. All these factors require a method of synchronizing or aligning the time scales.

Regarding the conventional RP (2.6), a black main diagonal line (LOI) can always be found in the plot because of the identity of the (i,i) states. The RP can be considered as a special case of the CRP which usually does not have a main diagonal because the (i,i) states are not identical.

Assuming two identical trajectories, the CRP is the same as the RP of one trajectory and contains an LOI. If we slightly modify the values of the second

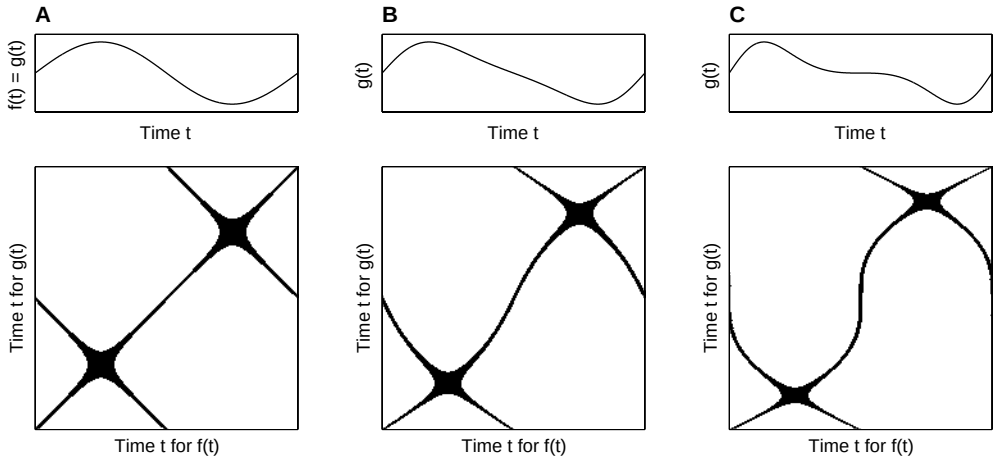

Figure 2.13: Cross recurrence plots of sine functions $f(t) = \sin(\varphi t)$ and $g(t) = \sin(\varphi t + a\sin(\psi t))$, whereas (A) $a = 0$, (B) $a = 0.5$ and (C) $a = 1$. The variation in the time domain leads to a deforming of the synchronization line. The CRPs are computed without embedding.

trajectory, the LOI will become somewhat disrupted. This leads to the situation discussed in Subsec. 2.3.1. However, if we do not modify the amplitudes but stretch or compress the second trajectory slightly, the LOI will be kept continuous but not as a straight line with an angle of $\pi/4$. Rather this line can be bowed (Fig. 2.13). As we have already seen in the Subsec. 2.2.2, the local slope of lines in an RP as well as CRP corresponds to the transformation of the time axes of the two considered trajectories (Eq. (2.14); Marwan et al., 2002a). A time shift between the trajectories causes a dislocation of the LOS. Hence, the LOS may lie rather far from the main diagonal of the CRP.

For illustration, let us consider two sine functions where we rescale the time axis of the second sine function in the following way

$$\sin(\varphi t) \longrightarrow \sin\big(\varphi t + a\sin(\psi t)\big). \tag{2.41}$$

The terms rescaling and synchronization are used here in the meaning of the rescaling of the time scale. The rescaling of the second sine function with different parameters a results in a deformation of the main diagonal (Fig. 2.13). The distorted line contains the information on the rescaling, which we need in order to re-synchronize the two functions. Therefore, this distorted diagonal is called *line of synchronization (LOS)*.

In the following, we present a toy model in order to explain the relation between the time series $f(t_1)$, $g(t_2)$ and the LOS $t_2 = \phi(t_1)$. In a one dimensional

situation, the CRP is simply

$$\mathbf{CR}(t_1, t_2) = \Theta\big(\varepsilon - \|f(t_1) - g(t_2)\|\big). \tag{2.42}$$

Provided that we set $\varepsilon = 0$ to simplify the condition, (2.42) will deliver a recurrence point if

$$f(t_1) \equiv g(t_2). \tag{2.43}$$

In general, this is an implicit condition that links the variable t_1 to t_2. Considering the physical examples above it can be assumed that the time series are essentially the same; that means that $f \equiv g$, up to a rescaling function of time. So we can state

$$f(t_1) \equiv f\big(\phi(t_1)\big). \tag{2.44}$$

In some special cases (2.44) can be resolved with respect to t_1. An example of such a special case is a system of two sine functions with different frequencies

$$f(t) = \sin(\varphi \cdot t + \alpha), \quad g(t) = \sin(\psi \cdot t + \beta) \tag{2.45}$$

Using (2.43) and (2.44) we find

$$\sin(\varphi\, t_1 + \alpha) - \sin(\psi\, t_2 + \beta) = 0, \tag{2.46}$$

and one explicit solution of this equation is

$$\Rightarrow \quad t_2 = \phi(t_1) = \left(\frac{\varphi}{\psi} t_1 + \gamma\right) \tag{2.47}$$

with $\gamma = \frac{\alpha - \beta}{\psi}$. In this special case the slope $\mathfrak{m}$ of the main line in the corresponding cross recurrence plot represents the frequency ratio, and the distance between the origin of the axes and the intersection of the LOS with the ordinate reveals the phase difference. Considering the time transformation functions $T_1 = \varphi \cdot t + \alpha$ and $T_2 = \psi \cdot t + \beta$ whithin the equations (2.45) and the inverse $T_2^{-1} = \frac{t-\beta}{\psi}$, we get the same result for the slope of the LOS by using the derivative (2.14)

$$\mathfrak{m} = \partial_t T_2^{-1}\left(T_2(t)\right) = \frac{\varphi}{\psi}. \tag{2.48}$$

The function $t_2 = \phi(t_1)$ is the transfer or rescaling function which allows to rescale the second system to the first system. If the rescaling function is not linear, the LOS will also be curved.

If the functions $f(\cdot)$ and $g(\cdot)$ are not identical, our method will in general not be capable of deciding whether the difference in the time series is due to different dynamics ($f(\cdot) \neq g(\cdot)$) or to simple rescaling. So the assumption is essential that the dynamics remain equal up to a rescaling in time (the

underlying systems must be the same). Nevertheless, for some cases where $f \neq g$, the method can be applied in the same way. If we consider the functions $f(\cdot) = a \cdot \bar{f}(\cdot) + b$ and $g(\cdot) = \bar{g}(\cdot)$, whereby $f(\cdot) \neq g(\cdot)$ are the observations and $\bar{f}(\cdot) = \bar{g}(\cdot)$ are the states, normalization, with respect to the mean and the standard deviation, will allow to use our method,

$$f(\cdot) = a \cdot \bar{f}(\cdot) + b \longrightarrow \tilde{f}(\cdot) = \frac{f(\cdot) - \langle f(\cdot) \rangle}{\sigma\left(f(\cdot)\right)} \tag{2.49}$$

$$\tilde{g}(\cdot) = \frac{g(\cdot) - \langle g(\cdot) \rangle}{\sigma\left(g(\cdot)\right)}. \tag{2.50}$$

With $\bar{g}(\cdot) = \bar{f}(\cdot)$ the functions $\tilde{f}(\cdot)$ and $\tilde{g}(\cdot)$ are the same after the normalization, hence, our method can be applied without any further modification.

For application one has to determine the LOS – usually non-parametrically – and then rescale one of the time series by using this function (for an illustration cf. Subsec. 3.3.1). This connection between the local slope of the LOS and the relation between the segments of the trajectories also applies to the other line structures in CRPs as well as RPs (cp. Fig. 2.7 on p. 21).

This technique can also be used in order to find the closest matching segments in two data series. For example, in the geological framework there could be a long reference data series which has a time scale and a second but short profile with the same physical measurement. The task lies in finding the section in the reference data which matches to the second profile in order to yield the corresponding time scale for the profile. This section can be found by looking for a more or less continuous black line in the CRP (the dislocated LOS). An example is given in Subsec. 3.3.2.

The CRP based alignment of time series has conspicuous similarities with the method of sequence slotting described by Thompson and Clark (1989). The first step in their method is the calculation of a distance matrix (2.11), which allows the use of multivariate data sets. Thompson and Clark (1989) referred to the distance measure as dissimilarity. It is used to determine the alignment function in such a way that the sum of the dissimilarities along a path in the distance matrix is minimized. This approach is based on dynamic programming methods which were mainly developed for speech pattern recognition in the 1970's (e. g. Sakoe and Chiba, 1978). In contrast, RPs were developed to visualize the phase space behaviour of dynamical systems. Therefore, a threshold was introduced to make recurrent states visible. The involvement of a FAN in the phase space and the possibility of increasing the embedding dimensions distinguish my approach from the sequence slotting method.

2.4 Current Developments of Recurrence Plots

During the last five years, a rather promising development of recurrence plots has been in progress. These new findings work toward a better understanding of the structures found in RPs. As already explained in the subsection about the RQA (Subsec. 2.2.3), an RP can be used in order to obtain some properties of dynamical systems, such as the Rényi entropy, the correlation dimension or the information dimension (Faure and Korn, 1998; Gao, 1999; Thiel et al., 2003a). The most recent development in our group proposes intersections of RPs and time shifted RPs

$$\mathbf{R}_{i,j}^{m,\hat{\varepsilon}} \cdot \mathbf{R}_{i+\tau,j+\tau}^{m,\tilde{\varepsilon}} \tag{2.51}$$

which can be used for the estimation of the generalized mutual information (Thiel et al., 2003a). Furthermore, this approach can also be applied to different phase space trajectories, which leads to a completely new concept of cross recurrence plots (Romano et al., 2003, this kind of cross recurrence plot is denoted as XRP). Based on this new approach, the cross mutual information and Rényi entropy can be estimated. In addition, the XRP can be used to study phase synchronization. The XRP can be applied to measurements of different systems whose observations cannot be considered as state variables of the same system. XRPs are not restricted to only two systems; it is a multivariate analysis tool. In contrast to CRPs, XRPs can only be applied to time series of equal time scale, length and sample resolution.

The development of RP based methods is not yet concluded. The last three years in particular have shown that large potential lies in the analysis of RPs.

2.5 Software and Applications

Since RPs are especially suitable for the analysis of short and nonstationary data, their application to real measurements in numerous scientific fields is obvious. Moreover, a representation of an RP displays amazing structures and can be rather decorative. Therefore, RPs and their quantification analysis have become increasingly present in the scientific community.

2.5.1 Free Software for Recurrence Plot Based Analysis

Free available software for the creation of RPs and their quantitative analysis facilitates the spread of their application (no requirement on completeness):

- *RQA Software 7.1* (by Charles Webber Jr.)
  allows for the creation of RPs as well as CRPs and their quantification,

only for DOS, commandline based
`http://homepages.luc.edu/~cwebber`

- *Visual Recurrence Analysis 4.2* (by Eugene Kononov)
  creation of RPs and computing the RQA measures, only for MS Windows, graphical user interface
  `http://home.netcom.com/~eugenek`

- *CRP Toolbox 4.3* (by Norbert Marwan)
  allows for the creation of RPs as well as CRPs, quantification analysis of RPs and CRPs includes the new measures of complexity proposed in this work, time scale alignment tool based on CRPs and further useful tools and methods of nonlinear time series analysis and data preparation are provided, platform independent (for Matlab), both usage of graphical user interface as well as commandline call is possible
  `http://tocsy.agnld.uni-potsdam.de`

A comparison between some of these programmes can be found in (Belaire-Franch and Contreras, 2002).

2.5.2 Cross Recurrence Plot Toolbox

During my study with recurrence plots, I have developed a comprehensive Matlab toolbox. This toolbox contains various algorithms for creating RPs and CRPs by providing several norms, criteria of neighbourhoods and various types of RPs and CRPs. The tool for quantification of RPs and CRPs includes the measures of complexity proposed in this work (LAM, TT, V_{max}) as well as the known RQA measures (RR, DET, L, $ENTR$, $TREND$ etc.). These measures can be computed for shifted windows as well as for diagonals of the RPs and CRPs. An alignment tool enables the search of a non-parametric LOS in CRPs. Further useful tools for data preparation and nonlinear data analysis are included, like tools for normalization of data, aligning the length of two time series, computation of multi-dimensional histograms, multi-dimensional mutual information, entropies, 2D and 3D phase space representation, estimation of AR coefficients etc.

This toolbox is available through the WorldWideWeb. An online and printable manual with illustrative examples as well as an extensive bibliography of applications of RPs can also be found there. The current address is

`http://tocsy.agnld.uni-potsdam.de`.

Several scientists from Canada, China, Germany, Italy, Poland, United Kingdom, USA and others are applying this toolbox for the analysis of data from, for example, economics, climate, solar physics, cardiology or hardware analysis.

2.5.3 Application Potentials

The search for applications via search engines in the World Wide Web reveals numerous workings which have used RPs (at present, the Scirus search engine finds over 200 journal published articles and approximately 700 web published works). RPs and the RQA are most popular in physiology. However, first applications in economy, ecology, astrophysics and geology can also be found. In the following, a small selection of applications of RPs and the classical RQA gives an overview about the applicability of the method. In the next chapter some special applications of the new proposed RP measures as well as of the CRPs are presented.

One of the first applications of RPs has been the analysis of heart beat intervals (Zbilut et al., 1991). This study has revealed typical RPs for cardiac transplant patients and cardiomyopathy patients who underwent volume loading. Applying the RPs, the authors have inferred that the dimensionality and entropy of the heart beat variations decrease during a significant cardiac event like myocardial infarction or ventricular tachycardia.

In further physiology research RPs as well as RQA have been applied to, for example, electromyographic data (Webber Jr. et al., 1995), measurements based on eye movements (optokinetic nystagmus, Shelhamer, 1997), data of postural fluctuations (Riley et al., 1999), EEG data (Babloyantz, 1991; Thomasson et al., 2001) or neuronal signals (Faure and Korn, 2001), in order to study the interacting physiological processes.

The RPs have been used for research in economics. For example, RPs have been inspected visually in order to find chaos in economics time series (Gilmore, 1993, 2001). Whereas these visual inspections could not find chaos in the considered economic time series (e. g. unemployment rate, private domestic investment, exchange rate), a combined "close returns" and surrogate test seems to reveal nonlinear dependences among data of exchange rates. Other studies of exchange data have used the RQA and have also found significant correlations between various currencies (Strozzi et al., 2002). In contrast to the results of Gilmore (2001) the research of others who used the RQA has revealed chaos in exchange data (Hołyst et al., 2001; Belaire-Franch et al., 2002).

An astrophysical application of RPs has used the radiocarbon data of the

last 7 000 years (Kurths et al., 1994). The atmospheric radiocarbon is influenced by the variation of solar activity and exhibits century-scale variations of chaotic nature. The main findings based on the RP analysis and a surrogate test reveal that these variations are indeed different from linear processes and that there are different types of large events affecting their tendency to recur (e. g. the Maunder Minimum seems to be unique, whereas the Oort and Dalton Minima as well as the Medieval Maximum tend to recur). Moreover, the authors have found that the present day data are similar to the Medieval Maximum.

An RQA has applied to a DNA sequence of the genome *Caenorhabditis elegans* (Frontali and Pizzi, 1999). *Caenorhabditis elegans* is a small (approximately 1 mm long) soil nematode found in temperate regions. This analysis has revealed long-range correlations in the introns and intergenic regions, which are caused by the frequent recurrence of oligonucleotides (a short sequence of some hundreds of nucleotides) in these regions. The recurrence of the oligonucleotides has been discovered by computing the recurrence rate for overlapping windows which cover the DNA sequence.

Elwakil and Soliman (1999) have applied RPs to time series generated by models of the Twin-T, Wien-bridge and other chaos generating electronic oscillator circuits. Through visual inspection of the RPs, the chaotic behaviour of the model results has been confirmed. RPs have been used to estimate optimal embedding parameters and vicinity threshold which are used for a noise reduction scheme in human speech signals (Matassini and Manfredi, 2002).

An analysis based on RPs has been used to study monopole giant resonances in atomic nuclei (Vretenar et al., 1999). Due to the fact that a nucleus consists of protons and neutrons, the oscillations can be divided into two modes: (1) the densities of protons and neutrons oscillates in phase (isoscalar mode) and (2) the two densities have opposite phases (isovector mode). Both of these modes exhibit significantly different RPs. Where the oscillation of the isoscalar mode has an RP typical for regular oscillations, the RP for the isovector mode uncovers nonstationary and chaotic dynamics.

Further applications can be found in chemistry. Rustici et al. (1999) have applied the RQA to the Belousov-Zhabotinsky reaction and have studied the transitions during its chemical evolution in an unstirred batch reactor. Using the RQA measures, the transitions between periodic, quasiperiodic and chaotic states could be observed. Other applications in chemistry / molecular biology concern the dynamics of chemical processes, for example in molecular dynamics simulations of polypeptides (Giuliani and Manetti, 1996; Manetti

et al., 2001). Applying the RQA to glycoproteins of the paramyxovirus[2] has uncovered the interaction between specific glycoprotein partners (Giuliani and Tomasi, 2002).

There are many examples of further research which uses RPs and RQA. A more extensive bibliography can be found on the web site of the CRP toolbox (`http://tocsy.agnld.uni-potsdam.de`) or on the recurrence plot web site (`http://www.recurrence-plot.tk`).

[2]The family of *Paramyxoviridae* contains viruses that induce a wide range of distinct clinical illnesses in humans, for example the measles virus, mumps virus and the parainfluenza viruses (Source: `http://web.uct.ac.za/depts/mmi/stannard/paramyx.html`).

Chapter 3

Applications

The high potential for the analysis based on recurrence plots arises with their applicability. Hundreds of applications of recurrence plots and recurrence quantification analysis, especially to physiological data, represent the increasing importance of these methods. In this chapter selected applications of the newest strategies based on recurrence plots to geological and physiological data are presented. Methods of linear and nonlinear data analysis mostly fail in these applications because of the rather short length of the time series and their nonstationarity. Except for the examples in the Subsec. 3.3.2 all results of these applications are already published or in press. The corresponding articles are attached in the Appendix.

3.1 Laminarity and Trapping Time

Recent studies suggest also including the vertical structures of RPs into the RQA. In order to quantify them, the new measures laminarity and trapping time were introduced (definitions in Subsec. 2.2.4). The analysis of the vertical structures in RPs with these measures enables a detection of chaos-chaos transitions as they occur as laminar states. The suitability of these measures is presented in the following two applications.

3.1.1 Analysis of VT Heart Rate Intervals

A major challenge in physiology is the analysis of cardiac time series. Heart rate variability (HRV) typically shows a complex behaviour, and it is difficult to identify disease specific patterns (Fig. 3.1). Implantable cardioverter defibrillators (ICD) are a safe and effective treatment of ventricular tachycardia or fibrillation (VT). These fatal cardiac arrhythmias are the main factors triggering sudden cardiac death. A fundamental challenge in cardiology is detecting

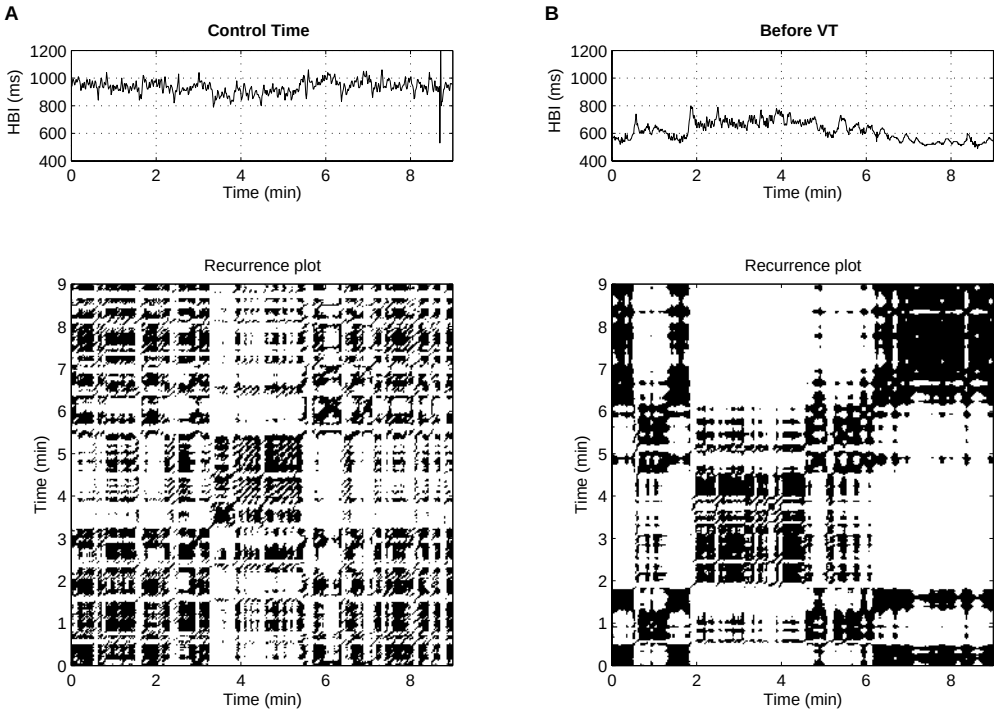

Figure 3.1: Recurrence plots of the heart beat interval (HBI) time series at a control time (A) and before a VT (B) with $m = 6$ and $\varepsilon = 170$. The RP before a life-threatening arrhythmia is characterized by big black rectangles whereas the RP from the control series shows only small rectangles.

of early signs of VT in patients with an ICD based on HRV data (e. g. Diaz et al., 2001). Recent studies have applied standard methods, methods based on symbolic dynamics as well as finite time growth rates to the HRV parameters of time and frequency domain (Diaz et al., 2001; Kurths et al., 1995; Voss et al., 1996; Wessel et al., 2000). One of the first applications of RPs has been in the study of heart beat intervals (Zbilut et al., 1991). The authors of this early application have supposed that the RPs may be useful for the study of heart rate variability in patients at risk for cardiac arrhythmia.

The defibrillators used in this study are able to store at least 1000 heart beat intervals (HBIs) prior to the onset of VT (10 ms resolution), corresponding to approximately 9–15 minutes. 24 ICD stored HBIs of 17 ICD patients at the Franz-Volhard-Hospital with severe congestive heart failure are available. We have studied their HBIs before the onset of VT episodes and at control intervals without VT.

The RP before a life threatening arrhythmia is characterized by large black rectangles, whereas the RP from the control series shows only small rectangles

Table 3.1: Results of maximal diagonal and vertical line length shortly before VT and at control time, nonparametric Mann-Whitney U-test, p – significance; * – $p < 0.05$; ** – $p < 0.01$; n. s. – not significant $p \geq 0.05$)

m	ε	VT	Control	p
Maximal diagonal line length L_{max}				
3	77	396.6±253.8	261.5±156.6	n. s.
6	110	447.6±269.1	285.5±160.4	*
9	150	504.6±265.9	311.6±157.2	*
12	170	520.7±268.8	324.7±180.2	*
Maximal vertical line length V_{max}				
3	77	261.4±193.5	169.2±135.9	*
6	110	283.7±190.4	179.5±134.1	**
9	150	342.4±193.6	216.1±137.1	**
12	170	353.5±221.4	215.1±138.6	**

(Fig. 3.1). All standard RQA measures described in Webber Jr. and Zbilut (1994) as well as the new measures LAM, TT and V_{max} for different embedding dimensions m and vicinity threshold radii ε are calculated for these data (fixed ε and Euclidean norm are used). By using a rank test (Mann-Whitney U-test), significant differences between both groups of data for several of the measures mentioned above can be found. However, the most significant measures for rather large radii are V_{max} and L_{max} (Tab. 3.1). The vertical line length V_{max} is more powerful in significantly discriminating between both groups than the diagonal line length L_{max}, as can be recognized by the higher significance for V_{max} (p-values in Tab. 3.1).

The application of the newly introduced measures to heart rate variability data has shown that they are able to detect and quantify laminar phases before a life threatening cardiac arrhythmia and, thus, predict its occurrence (cp. App. A, Marwan et al., 2002b; Wessel et al., 2001). These findings may be of importance for the therapy of malignant cardiac arrhythmias.

3.1.2 Analysis of ERP Data

Neurons are known to be nonlinear devices because they become activated when their somatic membrane potential crosses a certain threshold (Kandel et al., 1995). This nonlinearity is one of the essentials in neural modelling as described by the sigmoidal activation functions in neural networks (Amit, 1989). The activity of large formations of neurons is macroscopically measurable in the electroencephalogram (EEG) of the human scalp, which results from a spa-

tial integration of postsynaptic potentials. However, it is debated whether the EEG should be treated as a time series stemming from a linear or a nonlinear dynamical system. Applying nonlinear techniques of data analysis to EEG measurements has a long tradition. Most of these attempts involved estimating of the correlation dimension of spontaneous EEG (e. g. Babloyantz et al., 1985; Rapp et al., 1986; Gallez and Babloyantz, 1991; Lutzenberger et al., 1992; Pritchard and Duke, 1992). Theiler et al. (1992) have applied the technique of surrogate data to correlation dimensions of EEG and reported that there is no evidence of low dimensional chaos but of significance for nonlinearity in the data. While correlation dimensions are only well defined for stationary time series generated by a low dimensional dynamical system moving around an attractor, these measures fail in investigating event related brain potentials (ERPs) because they are nonstationary by definition (Sutton et al., 1965). Event related potentials are characteristic changes in the EEG of a subject during and short after a stimulus (surprising moment).

Traditionally, ERP waveforms are determined by computing an ensemble average of a large collection of EEG trials that are stimulus time locked. This is based on the following assumptions: (1) the presentation of stimuli of the same kind is followed by the same sequence of processing steps, (2) these processing steps always lead to activation of the same brain structures, (3) this activation always elicits the same pattern of electrophysiological activity, which can be measured at the scalp (Rösler, 1982) and (4) spontaneous activity is stationary and ergodic.

By averaging the data points, which are time locked to the stimulus presentation (cf. Oddball experiment), it is possible to filter out some signal (ERP) of the noise (spontaneous activity). This way, the P300 component of the ERP was the first potential discovered to vary in dependence on subject internal factors, like attention and expectation, instead on physical characteristics (Sutton et al., 1965). The amplitude of the P300 component is highly sensitive to the novelty of an event and its relevance (surprising moment), so this component is assumed to reflect the updating of the environmental model of the information processing system (context updating, Donchin, 1981; Donchin and Coles, 1988). The disadvantage of the averaging method is the high number of trials needed to reduce the signal-to-noise-ratio. This disadvantage is crucial for example in clinical studies, studies with children and studies in which repeating a task would influence the performance. Moreover, several high frequency structures are filtered out by using the averaging method. It is, therefore, desirable to find new ways of analyzing event related activity on a single trial basis. Applying the concepts of the RQA to electrophysiological data could be

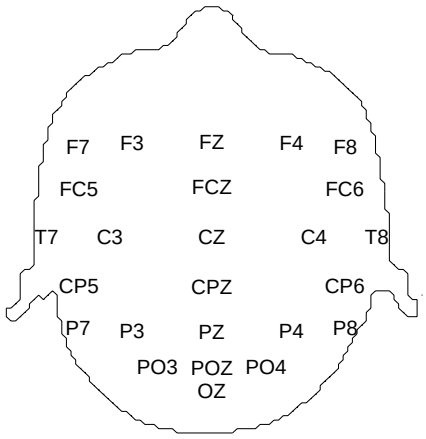

Figure 3.2: Localization of the electrodes on the head.

Table 3.2: Notation of the electrodes and their numbering as it is used in the figures.

#	Electr.	#	Electr.	#	Electr.	#	Electr.	#	Electr.
1	F7	2	FC5	3	F3	4	FZ	5	F4
6	FC6	7	F8	8	T7	9	CP5	10	C3
11	FCZ	12	C4	13	CP6	14	T8	15	P7
16	PZ	17	P3	18	CZ	19	P4	20	P8

one way of dealing with this problem.

For this study, we analyze measurements of an Oddball experiment. The Oddball experiment studies brain potentials during a stimulus presentation (acoustic stimulii were used here). For the experimental description and settings see (cp. App. B, Marwan and Meinke, 2004). In the analysis of a set of 40 trials of ERP data for an event frequency of 90% (ERP90) and a second set of 31 trials for an event frequency of 10% (ERP10), the RQA measures DET and L, and the newly introduced measures LAM and TT are computed (Marwan and Meinke, 2004). The ERPs were measured at 25 electrodes (Fig. 3.2 and Tab. 3.2). The classical method of studying such ERP data is averaging them over many trials. Our aim is to study the single trials in order to find transitions in the brain processes during unexpected stimulation. Due to the N100 and the P300 components in the data, the RPs show varying structures changing in time (Fig. 3.3). Diagonal structures and clusters of black points occur. The nonstationarity of the data around the N100 and P300 causes extended white bands along these times in the RPs. However, the clustered black points around 300 ms occur in almost all RPs of the ERP10 data set. The application of the measures of complexity to these ERP data discriminates the single trials

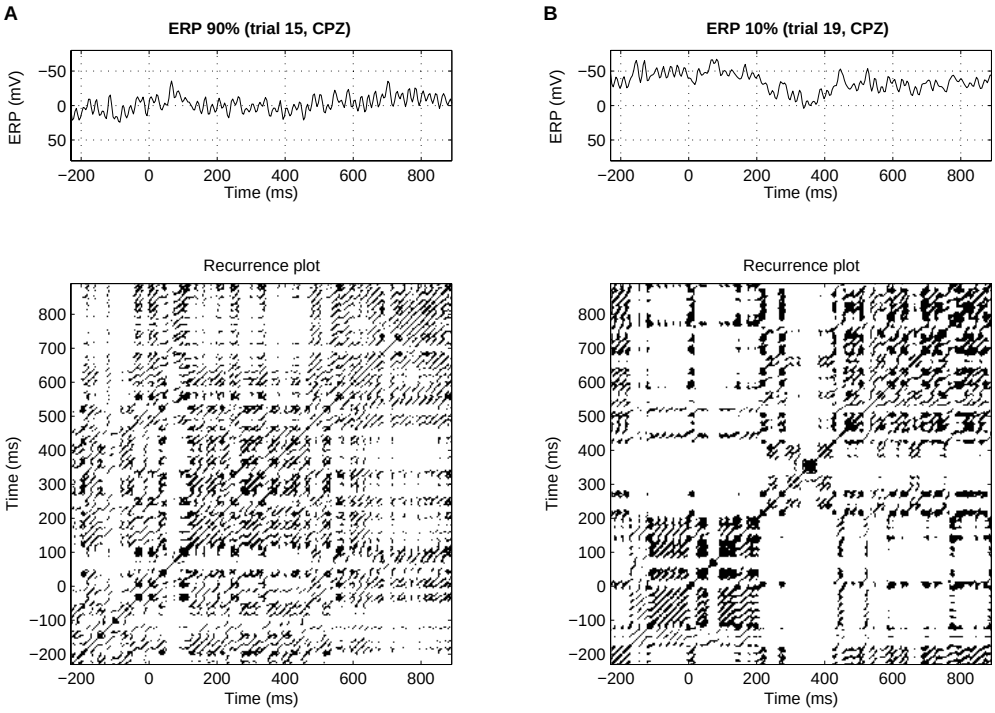

Figure 3.3: ERP data for event frequencies of 90% (A) and 10% (B), and their corresponding recurrence plots. For the lower event frequency (B) more cluster of recurrence points occur at 100ms and 300ms and a white band marks some transition in the process.

with a distinct P300 component resulting from a low surprise moment (high frequent events) in favour of such trials with a high surprise moment (less frequent events). The LAM is the most distinct parameter in this analysis. In the ERP data the LAM reveals transitions from less laminar states to more laminar states after the occurrence of the event and a transition from more laminar states to less laminar states after approximately 400 ms. These transitions occur around bounded brain areas (parietal to frontal along the central axis). The comparable measures DET and LAM as well as L and TT are quite different in their amplitudes. There are also differences in time and brain location of the found transitions.

These results show that the measures based on vertical RP structures make the identification of transitions possible, which are not found by the classical RQA measures. These newly proposed measures indicate transitions in the brain processes into laminar states due to the surprising moment of observed events.

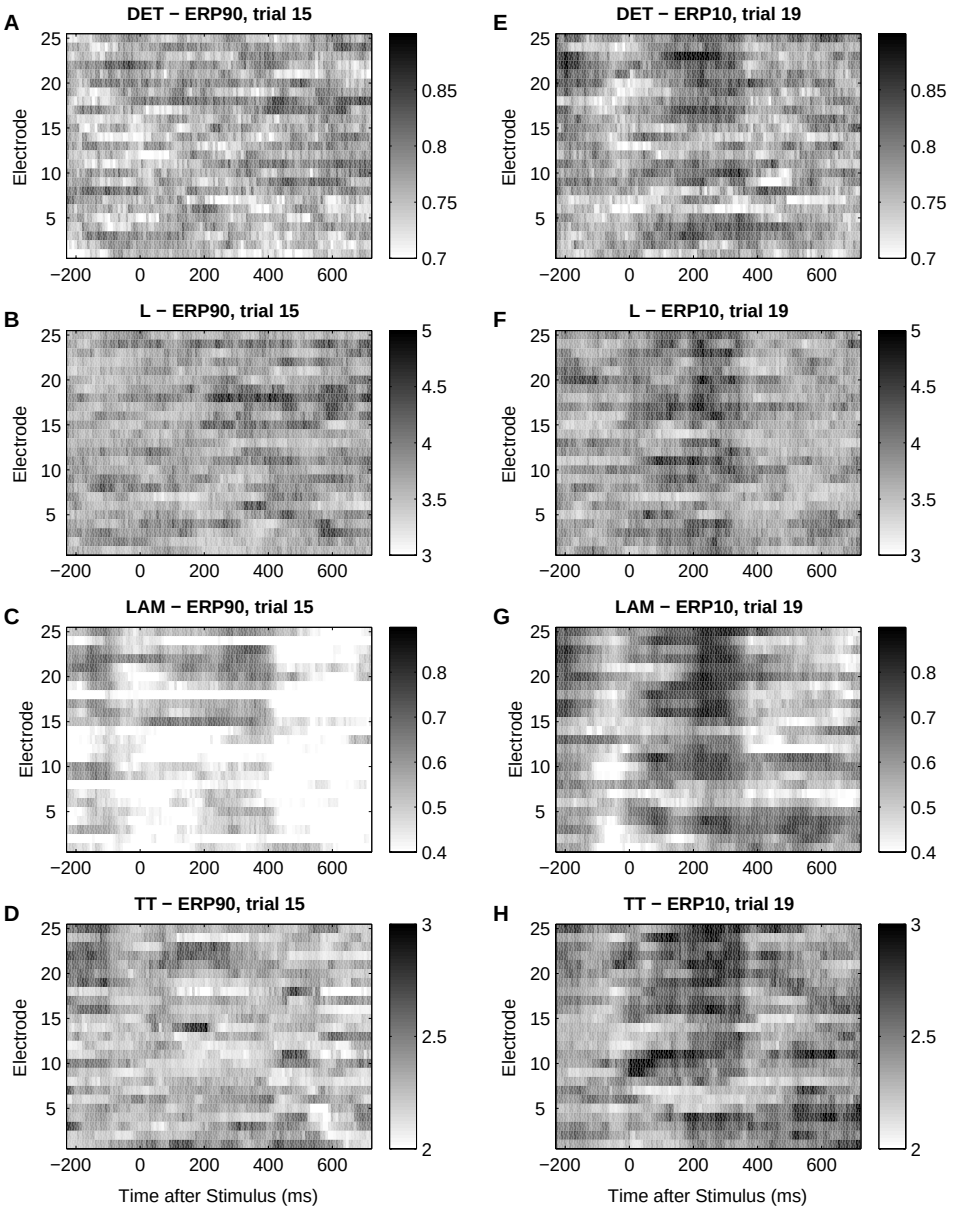

Figure 3.4: RQA measures for selected trials for event frequencies of 90% (A–D) and 10% (E–H). The P300 component reflects the surprising moment and can be detected in single trials by the measures LAM (G) and TT (H), which base on the vertical structures in the RP. The measures based on diagonal structures, DET and L, are less apparent.

3.2 Similarities Found with Cross Recurrence Plots

Cross recurrence plots can be used to study a similar time evolution of phase space trajectories and hence to assess the similarity or interrelation between the underlying processes. The following examples illustrate the functioning of this technique on prototypical model systems as well as on natural data.

3.2.1 Finding of Nonlinear Interrelations

This application shows the ability to find nonlinear interrelations between two processes (cp. App. C, Marwan and Kurths, 2002), where linear tests are not able to find them. We demonstrate this on a paradigmatic system from stochastic processes and nonlinear dynamics. We consider linear correlated noise (autoregressive process) which is nonlinearly coupled with the x-component of the Lorenz system $x(t)$ which is solved with an ODE solver for the standard parameters $\sigma = 10$, $r = 28$, $b = 8/3$ and a time resolution of $\Delta t = 0.01$ (Lorenz, 1963; Argyris et al., 1994). We use an autoregressive process y_i of first order and force it with the squared x-component of the Lorenz system,

$$y_i = 0.86\, y_{i-1} + 0.500\, \xi_i + \kappa\, x_i^2, \tag{3.1}$$

where ξ is Gaussian white noise and x_n ($x(t) \to x_i$, $t = i\,\Delta t$) is normalized to standard deviation. The data length is 8 000 points. The coupling κ is realized without any lag.

As expected, due to the nonlinear linkage the cross correlation analysis of x and y does not reveal a significant linear correlation between these data series (Fig. 3.5 A). However, the mutual information shows a strong dependence between x and y at a delay of 0.05 (Fig. 3.5 B). The CRP based measures RR_* and L_* exhibit maxima at a lag of about 0.05 for RR^+ / L^+ and RR_*^- / L_*^- and additionally at 0.45 and -0.32 for RR_*^- / L_*^- (Fig. 3.5 C, D). The maxima around 0.05 for the $+$ and $-$ measures are a clear sign of the nonlinear linkage between the data. The delay of approximately 0.05 stems from the autocorrelation of y and approximately corresponds to its correlation time $\Delta t / \ln 0.86 = 0.066$. Since the result is rather independent of the sign of the second data before the embedding, the found interrelation is of the kind of an even function. A significance test for this method has not yet been developed. We use here 500 realizations of the AR model in order to receive the distributions of the measures. The 2σ margins of these distributions can be used to assess the results. Moreover, a surrogate test can be applied in order to estimate the significance of the result. An example for such a surrogate test is presented in the next application.

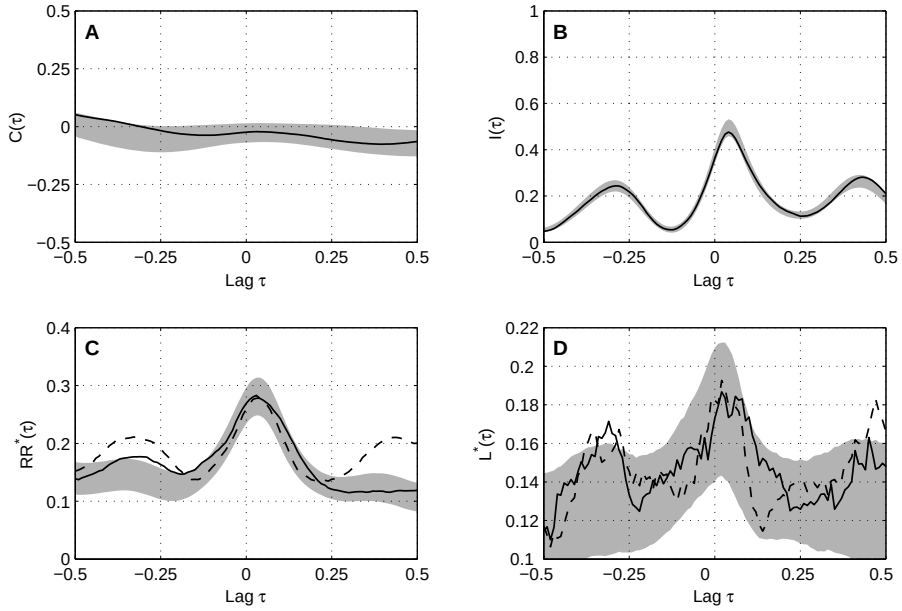

Figure 3.5: (A) Crosscorrelation $C(\tau)$, (B) mutual information $I(\tau)$, (C) recurrence rate RR_* and (D) average line length L_* for the forced autoregressive process and the forcing function; the curves represent the measures for one realization as functions of the delay τ for a coupling $\kappa = 0.2$. In (C) and (D) the solid lines show positive relation; the dashed lines show negative relation. The gray bands mark the 2σ margin of the distributions of the measures gained from 500 realizations. The lag τ and the average line length L_* have units of time.

Due to the rapid fluctuation of y the number of longer diagonal structures is less. Therefore, measures based on these diagonal structures, especially DET_*, do not work well with such heavily fluctuating data. However, we can infer that the measures RR_* as well as L_* (though less significant for rapidly fluctuating data) are suitable for finding the nonlinear relation between the considered data series x and y, where the linear analysis is not able to detect this relation. Furthermore, this technique is applicable to rather short and nonstationary data, often appearing in geology. In the next subsection we will apply this CRP method to palaeoclimatology data.

3.2.2 Investigation of ENSO in the Past

Data from geology are often characterized as short and nonstationary. The unique character of outcrops or drilling cores does not usually allow to repeat or refine a measurement. Therefore, data analysis of geological data is often

confrontated with problems regarding the length, nonstationarity or gaps in the data. In the previous application of CRPs we have seen that this method can be used for this kind of data. Therefore, in this subsection the application of CRPs will be used for the analysis of palaeoclimatology data that are of short length and nonstationarity (cp. App. D, Marwan et al., 2003; Trauth et al., 2003).

Higher variability in rainfall and river discharge could be of major importance in landslide generation in the northwestern Argentine Andes. A potential cause of such variability is the El Niño/ Southern Oscillation (ENSO). Annual layered deposits of a landslide-dammed lake in the Santa Maria Basin (site El Paso, Province Salta, NW Argentina) with an age of 30 000 ^{14}C years provide an archive of precipitation variability during this time. The annual cycle of wet summers and dry winters caused significant changes in the lake's sedimentation. During the rainy season mainly ocher coloured silty sediments were deposited; during the subsequent dry season a thin white layer consisting of the skeletons of silica algae (diatoms) was deposited. Due to its white colour, the diatomaceous layer can be used to identify single years in these sediments. Recurring intense red colouration of the silty part of the annual layers comes from reworked older sediments which are eroded and deposited only during extreme rainfall events. Therefore, the intensity of red colour in the varved deposits can be interpreted as a proxy for precipitation variation in the Santa Maria Basin (Trauth and Strecker, 1999; Trauth et al., 2000). The more intense red colouration is evidence of more precipitation during the rainy season. The estimate of the power spectrum of the red colour intensity reveals significant peaks within the ENSO frequency band of two to four years, suggesting an ENSO-like influence (Trauth et al., 2000). Because of the nonstationarity of these data (the sedimentation process in a lake is not stationary, which results in nonstationary proxy variables for the in-lake processes) linear correlation analysis is unsuitable. Therefore, the CRP analysis is applied to these data.

Our research includes the quantification analysis of CRPs of an index data series of the ENSO (Southern Oscillation Index, SOI) and the modern as well as palaeoprecipitation data in order to compare the magnitude and causes of rainfall variability in the NW Argentine Andes today and during the time of enhanced landsliding around 30 000 ^{14}C years ago (Marwan et al., 2003; Trauth et al., 2003). For the assessment of the modern ENSO influence on local rainfall in NW Argentina, the monthly precipitation data from the three stations San Salvador de Jujuy (JUY), Salta (SAL) and San Miguel de Tucuman (TUC) are analyzed. These locations are influenced by different local winds; Jujuy and

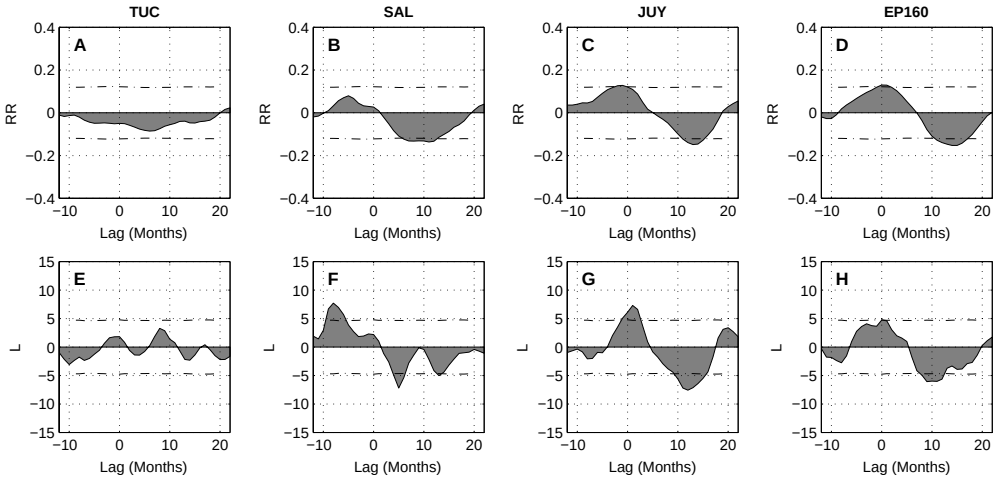

Figure 3.6: RR^c_* and L^c_* measures of the cross recurrence plots between SOI and precipitation in Tucuman (A, E), Salta (B, F), Jujuy (C, G) and palaeoprecipitation (D, H). Extreme values reveal high similarity between the dynamics of the rainfall and the ENSO. The dash-dotted lines are the empirical 2σ-bounds from the distributions of an ensemble of data based on a 5th-order AR-model.

Salta mainly receive northeasterly and easterly moisture-bearing winds during the summer rainy season whereas Tucuman is characterized by southerly and south-westerly winds (Prohaska, 1976). An appended surrogate test provides an evaluation of the results of the CRP analysis.

We find that the parameter RR^c_* of the CRPs between TUC and SOI has small negative values which do not exceed the 2σ-bounds and do not show preferences for a distinct lag. The parameter L^c_* also has small values, but it has rather small maxima and minima at delays of -1, 4 and 8 months. These results indicate that the precipitation in Tucuman is not strongly influenced by ENSO. If there is a weak influence, the rainfall will increase during El Niño (Fig. 3.6 A, E). However, the analysis of JUY and SOI reveals clear positive values around a lag of zero and negative values after 8 – 12 months, which suggests a significant link between Jujuy rainfall and ENSO (Fig. 3.6 C, G). The measures for the analysis of SAL versus SOI show smaller maxima for a delay of about zero and minima after a lag of 8 – 12 months. Therefore, we infer a weaker link between Salta rainfall and ENSO (Fig. 3.6 B, F; the disrupted minima in the L^c_* parameter at around ten months is due to the short data length and a resulting nonstationarity in the CRP). The measures for both SAL and JUY exceed the 2σ-bounds.

The 30 000 ^{14}C year old precipitation data are not simply comparable with present day data, because there is no information available about how to syn-

chronize the rainfall records with modern climate indices. Therefore, we seek the time window in these data showing the highest coincidence in the dynamics using maximum values for RR^c_* and L^c_* as the key criterion. The linear correlation coefficients could be used to find such a sequence, but this results in numerous ambigous possibilities. The complexity measures based on CRP provide a differentiated search that also considers time based features of the signal. This method reveals indeed a clearer result. The measures presented herein are not the only measures used. To maintain clarity, the further measures are not presented in this application, although they are used to find the sequence in the sediment data. Although the observed coincidence is not very high, it yields the time section in the palaeoprecipitation record EP160 which can be in best accordance with modern data. In our palaeoclimate data EP160 we find such a section represented by maximum and minima values for RR^c_* and L^c_* for delays of about zero and ten months, similar to those found for JUY and SAL (Fig. 3.6D, H). The RR^c_* and L^c_* measures also exceed the 2σ-bounds.

The similarities between the time series of the modern rainfall data and the palaeoprecipitation record from the lake sediments suggest that an ENSO-like oscillation was active around 30 000 ^{14}C years ago (roughly corresponding to 34 000 cal. years BP), which corresponds with the results of the investigation of Coccolithophores production (Beaufort et al., 2001). In the semiarid basins of the NW Argentine Andes, the ENSO-like variation could have caused significant fluctuations in local rainfall around 30 000 ^{14}C years ago similar to modern conditions. Together with generally higher moisture levels as indicated by lake balance modeling results (Bookhagen et al., 2001) this mechanism could help explain more frequent landsliding approximately 34 000 years ago in the semiarid basins of the Central Andes. For the comparison of the past and modern climate conditions, the CRP analysis has been used because a linear correlation analysis would reveal ambiguous results.

3.3 Time Scale Alignment Based on Cross Recurrence Plots

The CRP contains information about the time synchronization of data series (in the following the terms synchronization and rescaling refers to the alignment of the time scales). This is revealed by the distorted main diagonal, the LOS. A nonparametric rescaling function is provided by isolating this LOS from the CRP and can be used for the re-alignment of the time scales of the considered time series. I expect that this approach will open a wide range of

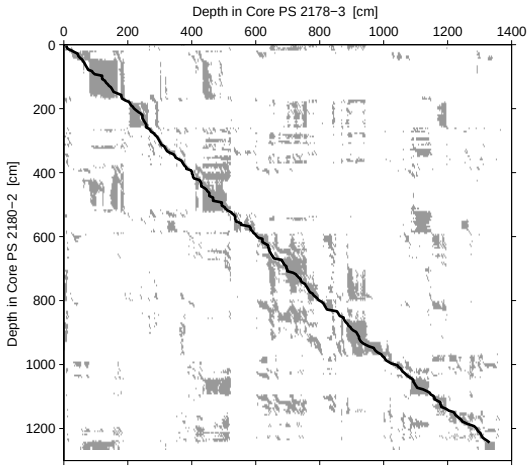

Figure 3.7: Cross recurrence plot (gray) based on six normalized sediment measures and an additional embedding dimension of $m = 3$ ($\tau = 1$, $\varepsilon = 0.05$) and line of synchronization (black line).

applications such as scale alignment and pattern recognition, for example in geology, molecular biology and ecology.

3.3.1 Time Scale Alignment of Borehole Data

In this first application we consider geophysical measurements of two sediment cores from the Makarov Basin, in the central Arctic Ocean, PS 2178-3 and PS 2180-2 (cp. App. E, Marwan et al., 2002a). The task is to align the data of the PS 2178-3 core (data length $N = 436$) with the scale of the PS 2180-2 (data length $N = 251$) in order to get a depth-depth-function which that to synchronize both data sets.

The phase space trajectories are formed by the following normalized six measures: low field magnetic susceptibility (κ_{LF}), anhysteretic remanent magnetization (ARM), ratio of anhysteretic susceptibility to κ_{LF} (κ_{ARM}/κ_{LF}), relative palaeointensity (PJA), median destructive field of ARM (MDF_{ARM}) and inclination (INC). Each measure is used as one component of the phase space vector. However, this embedding can be combined with the time delay method according to Takens (1981) in order to further increase the dimension of the phase-space.

Using an embedding of $m = 3$ (absolute dimension is $3 \times 6 = 18$), $\tau = 1$ and a recurrence criterion of FAN with $\varepsilon = 0.05$, the resulting CRP shows a clear LOS and some clustering of black patches (Fig. 3.7). Black patches arise whenever the variation in the data is smaller than the used vicinity threshold ε

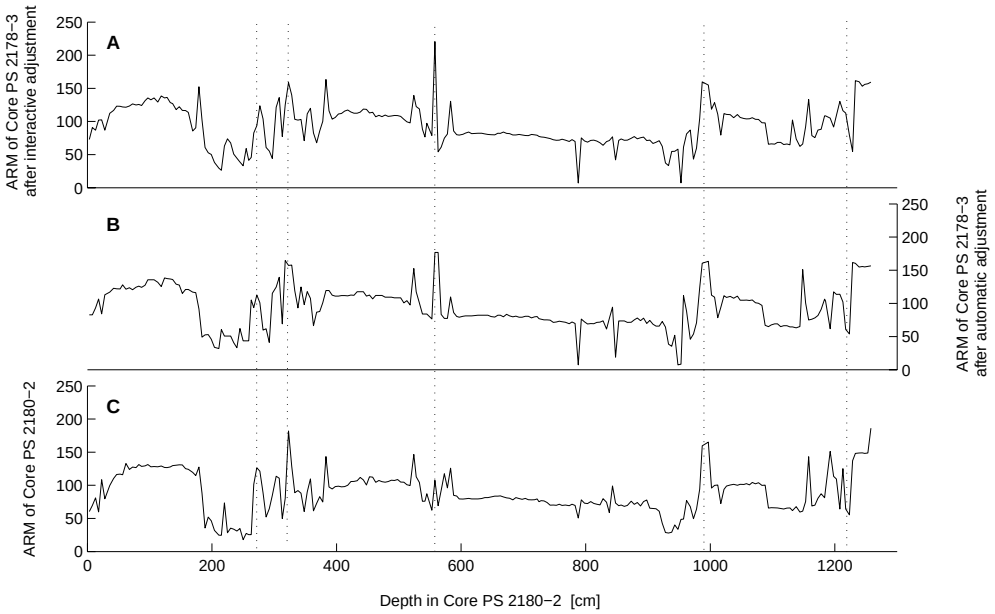

Figure 3.8: The ARM data are exemplary shown after alignment by wiggle matching (A) and by automatic alignment (B) using the LOS from Fig. 3.7. Plot (C) shows the reference data.

for a given time (plateau). The next step is to fit a nonparametric function (the desired depth-depth-curve) to the LOS in this CRP (black curve in Fig. 3.7). Different approaches can be considered for this procedure. However, they could have to be chosen appropriately because they have a large effect on the quality of the found LOS. In our example a two step algorithm is chosen that is able to tend locally towards the direction of the centre of gravity of clustered black points. A full explanation is given in Marwan et al. (2002a). With so determined LOS we are able to align the scale of the PS 2178-3 core to that of PS 2180-2 (Fig. 3.8).

The comparison of the CRP aligned geophysical measurements with the conventional visual matching (wiggle matching) shows an acceptable reliability level of the new method (Marwan et al., 2002a). The advantage is the automatic, objective and multivariate alignment. Moreover, further attempts exist to align geological data automatically. They either use parametrical approaches (minimal cost functions, Fourier series estimation of the mapping function and others; Martinson et al., 1982; Brüggemann, 1992) or they have to fit a large number of parameters and apply trial-and-error algorithms (sequence slotting; Thompson and Clark, 1989).

3.3.2 Search for an Appropriate Sequence in Reference Data

In the following three applications of CRPs the possibility of finding an appropriate sequence in a given data series relating to a reference series (and vice versa, respectively) is presented. For this task the LOS in the CRP must be found.

Dating of a Geological Profile (Magnetostratigraphy)

From a sediment profile (Olguita profile, Patagonia, Argentina; Warkus, 2002) a measurement of the palaeopolarity of the Earth's magnetic field (along with other measurements) is available. The starting point for any geological investigation of such a profile is determining the time at which these sediments were deposited. By applying the magnetostratigraphic approach and a geomagnetic polarity reference with known time scale, the polarity measurements can be used to determine a possible time scale for the profile. Cande and Kent (1995) provide such a geomagnetic polarity reference, which covers the last 83 Myr. The Olguita profile contains seven reversals. The polarity data consist of the values one, for the polarity direction as today, and the values zero, for the inverse polarity. Unfortunately, this data series is too short (only 16 measurements) for a credible analysis. Nevertheless, for our purpose of demonstration we will enlarge this data by interpolation. The Olguita profile is transformed to an equidistant scale of 300 data points and the reference data is transformed to an equidistant scale of 1 200 data points.

A CRP is created from these two data series by using an embedding dimension $m = 4$, a delay of $\tau = 6$ and a neighbourhood criterion of FAN (30% recurrence rate). Varying degrees of continuous lines between 21 and 16 Myr BP and between 12 and 8 Myr BP occur in the CRP, which can be interpreted as the desired LOS (Fig. 3.9). We will analyse six of these possibilities for the LOS. The search for the potential LOS is conducted using the same algorithm described in Marwan et al. (2002a). Moreover, we can evaluate the quality of these potential LOS by introducing a quality factor that takes into consideration the amount of gaps $N_\circ$ and black dots $N_\bullet$ on this line

$$Q = \frac{N_\bullet}{N_\bullet + N_\circ}\, 100\%. \tag{3.2}$$

A larger Q is a better LOS; $Q = 100\%$ stands for an absolute continuous line. Moreover, the obtained LOS can be interpreted as the sedimentation rate (Fig. 3.10). Abrupt changes in the sedimentation rate are not expected, thus, the potential LOS should not change abruptly. As an evaluator for this criterion we can use the averaged second derivative with respect to the time $\langle \partial_t^2 \rangle$.

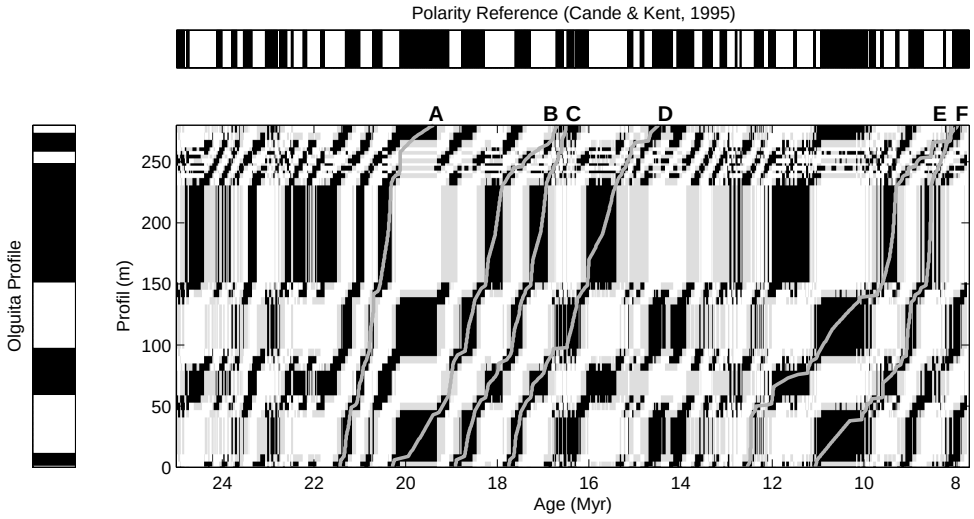

Figure 3.9: CRP between the polarity data of the Olguita profile and the reference data according to Cande and Kent (1995). In the polarity data the white colour marks a polarity of the Earth's magnetic field in the present, whereas the black colour marks a reversal. Six potential LOS are marked with gray lines (A–F, corresponding to the potential LOS given in Fig. 3.10).

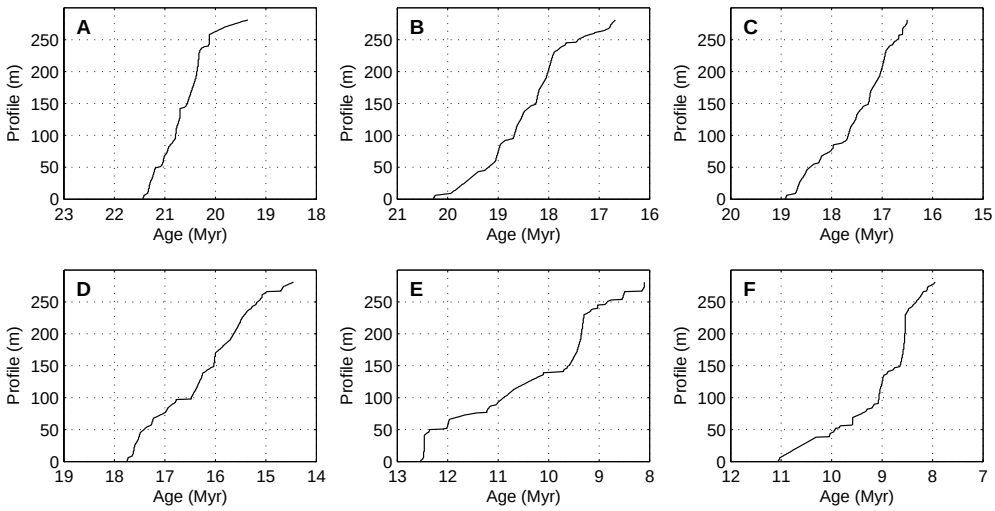

Figure 3.10: Potential LOS of the CRP presented in Fig. 3.9. They correspond to the potential sedimentation rates of the Olguita profile and mark sequences in the polarity reference, which match with the Olguita profile. Due to this matching, the Olguita profile can be dated.

Table 3.3: Possible ages of the Olguita profile, which are based on the found potential LOS (Fig. 3.10) and characteristics of these potential LOS.

Plot	Age (Myr)	$N_\bullet$	$N_\circ$	Q (%)	$\langle \partial_t^2 \rangle$
A	19.4–21.4	345	23	93.8	5.5
B	16.7–20.3	407	43	90.4	12.5
C	16.5–18.9	351	15	95.9	5.0
D	14.4–17.8	392	16	96.1	20
E	8.1–12.6	482	16	96.8	23
F	7.9–11.1	399	13	96.8	18

The potential LOS differs slightly in the Q factor, but more in the occurrence of abrupt changes in their slope (Fig. 3.10 and Tab. 3.3). The LOS in Fig. 3.10C has the smallest $\langle \partial_t^2 \rangle$ and could be, therefore, a good LOS for the dating of the Olguita profile. Regarding this result, the Olguita profile would have an age between 16.5 and 18.9 Myr and an age-depth-relation as it is represented by the possibility of a LOS in Fig. 3.10C. Warkus' investigation reveals the same result (Warkus, 2002), although he also mentioned that the dating based on the polarity data is ambiguous.

I must mention that the stated results are only possible sequences and do not lay claim to absolute correctness. It is rather a question of showing the potentials of CRPs. In general, for such geological tasks as presented in the two previous applications, the distance matrix (Eq. (2.11)) may be more appropriate. Future development would have to to improve the search algorithm for the LOS and to define an appropriate quality factor for the found LOS.

Looking for a Known Gene in a DNA String

Physiological processes are based on the interpretation of specific information stored in the DNA molecules by a definite sequence of the nitrogenous bases adenine (A), thymine (T), cytosine (C) and guanine (G). This information code is called a gene. Three consecutive bases are needed for the coding of one amino acid. A specific sequence of amino acids form a protein. The protein coding sequences of the gene are denoted as *exons*.

The human genome is estimated to contain more than 100 000 genes of various length (3 000 base pairs on average) and three billion base pairs. The genes are distributed over various DNA molecules which form the chromosomes. A DNA molecule does not consist solely of genes. Only around 10% of the human genome consists of genes. Moreover, the genes are usually not contin-

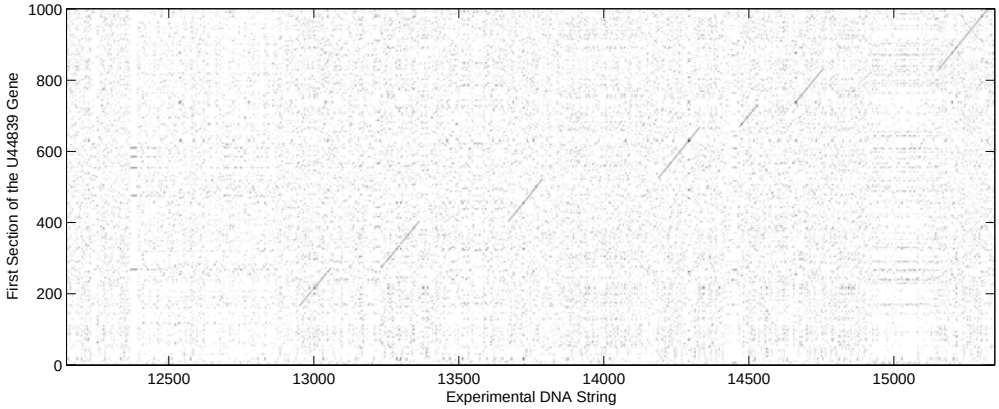

Figure 3.11: A detail of the CRP between the human U44839 gene and a sequence from the X chromosome. The LOS marks the exons and the jumps in the LOS mark the introns.

uous. They are interrupted by sequences that (probably) contain no information. These sequences are called *introns*. Whereas a specific gene is the same for all humans, the introns which fragment this gene differ greatly. These introns as well as the huge length of the DNA sequences (the largest DNA sequence known has more than 350 thousand base pairs) make the search for a specific gene in a given DNA sequence rather difficult if not impossible. However, gene sequencing is the fundamental method for discovering genes (Myers, 1991; Giegerich and Wheeler, 1996). A CRP provides an easy although computing intensive method for finding a specific gene, given e. g. by a database, in an experimental DNA string (similar algorithms can be found in literature, e. g. Vihinen, 1988). The application of RPs to DNA sequences is not new. For example, the RQA was applied to DNA sequences in order to study long-range correlations in introns and intergenic regions (Frontali and Pizzi, 1999) and to protein sequences in order to classify and compare special proteins (Giuliani et al., 2000).

We will try to locate the gene U44839 (ubiquitin C-terminal hydrolase gene) in a DNA sequence from the human X chromosome (genome data from the Human Genome Browser, 2001, `http://genome.cse.ucsc.edu`). The gene U44839 has a length of 3 167, and the used subsequence of the X chromosome has a length of 16 363. Since the gene data are alpha coded, we have to substitute numbers for the letters (e. g. A $\rightarrow$ 0, C $\rightarrow$ 1, G $\rightarrow$ 2, T $\rightarrow$ 3). Taking into account that a triplet of consecutive bases codes an amino acid, we use an embedding dimension of three and an embedding delay of one. In the CRP a shifted and interrupted LOS marks the location of the U44839 gene in the X

chromosome sequence (Fig. 3.11). Each jump in the LOS marks the occurrence of an intron in the DNA sequence.

Since DNA sequences are rather long, the visual inspection of CRPs is not applicable. The computation and visualization of measures based on the diagonal lines within sub-CRPs can reduce the amount of nonsignificant information. This procedure will be used in the next application. High values of, for example, L_{max} mean good matching. The position of the sub-CRP with a high L_{max} is associated with the location of the gene in the DNA sequence.

Speech Recognition

This last application completes the illustrations of the potentials of the CRP analysis. We consider a typical problem of speech analysis, the recognition of some spoken sentences with already present reference data. This reference data can be single sounds or words. A large amount of studies regarding speech recognition exist already (cf. Aubert, 2002; Huckvale and Fang, 2002). Therefore, we will not claim that our method is the ultimate solution. There may be better and faster methods for this task.

We analyze a german sentence which is given in the form of wave-form data of 22.05 kHz and 41 251 data points (Fig. 3.12A). The task is to find a selected word in this sentence. This word is provided as a reference vocabular from another audio record (Fig. 3.12B, 22.05 kHz, 11 000 data points, spoken by the same person). With the reference vocabular and the test sentence, we create a CRP of the both data series by using an overembedding with $m = 20$ and $\tau = 5$ (according to Matassini et al. (2002) this overembedding is used to reduce noise as much as possible; overembedding is suitable here for our task of sequence matching). Wave-form audio data have a distinct periodic nature

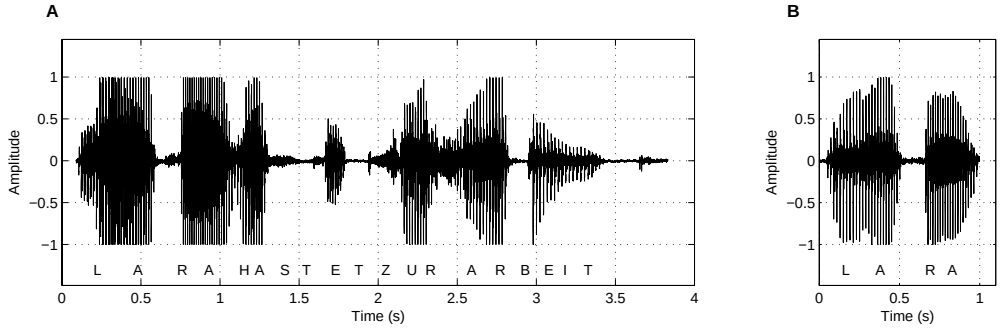

Figure 3.12: Wave data of a german sentence used for this study (A) and a reference pattern (B).

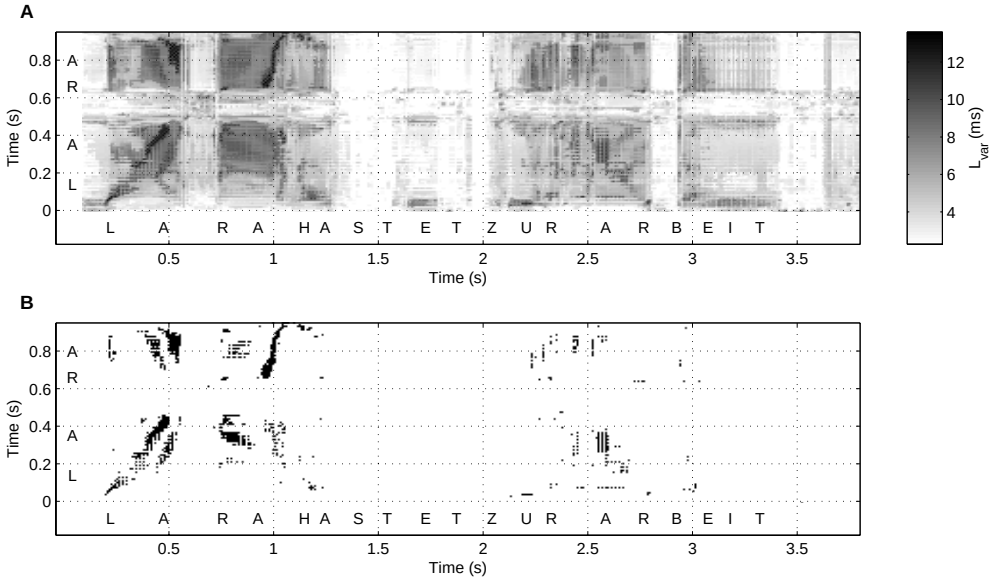

Figure 3.13: (A) Variation L_{var} of the length of the diagonal lines in the CRP of the sentence and the reference vocabular presented in Fig. 3.12. In (B) only the variations with $L_{var} > 9$ ms are presented, which reveal the location of the reference vocabular in the test sentence. Similar to CRPs, large, more or less diagonal structures correspond to high concordance between the considered sequences. The bowed diagonal oriented structure is caused by varying speech tempo.

leading to periodic and pronounced diagonal lines in its RP or CRP. The used high embedding provides a large amount of rather long, more or less diagonal lines. Since speech data contain a large amount of data points, it is impossible to inspect visually such a huge RP or CRP. The CRP of the data used here has the size of $41\,239 \times 10\,988$. Therefore, we divide the CRP into several, overlapping sub-CRPs of the size 400×400 (shifted by 100 steps) and compute the RQA measures for these sub-matrices. These measures can be presented in a time-time plot analogously to the representation of the CRP. The high coincidence of periodic data corresponds with long diagonal lines. Therefore we focus on that RQA measure that measures the maximal line length, L_{max}. This measure exhibits the highest values for the time between 0.2 and 1.1 s in the sentence Fig. 3.13, which corresponds to the searched word in the sentence. Analogous the LOS in a CRP, high coincidence causes line-like structures, which can be diagonal or bowed. The phonemes in the test sentence and in the reference word have been spoken in a different tempo, which causes a distortion of the line-like structures in the plot at about 1 s. Single phonemes,

like "A", can also be recognized by L_{max} at different locations in the word.

Moreover, regions with low values of L_{max} attract the attention. On the one hand, these regions mark the occurrence of short breaks (e. g. "glottis stop") and on the other hand, they mark specific phonemes. These are phonemes which are made in an alveolar[1] and fricative manner, like "s", "c" or "z" (german pronounciation) and cause distortions in the oscillations. This can be seen with a recurrence quantification analysis, especially when we focus on an analysis of the distribution of the length of the diagonal lines. The variation of the line lengths L_{var} as well as the entropy $ENTR$ reveal significantly the locations of these phonemes (Fig. 3.14). Adopting the RQA to the specific manner of speech production, this analysis may help to refer the phonemes of a spoken sentence to a specific class and therefore to simplify appropriate search algorithms for speech recognition.

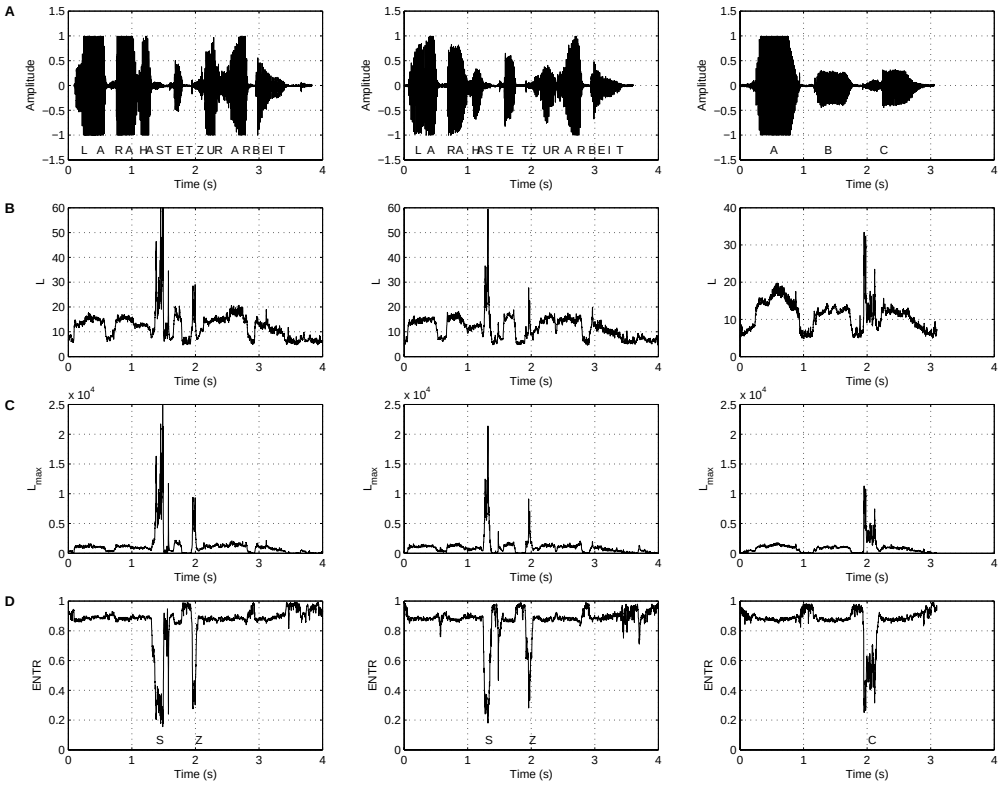

Figure 3.14: RQA measures L (B), L_{max} (C) and $ENTR$ (D) for two versions of a german sentence and the first three letters of the alphabet. These measures reveal the phonemes made in an alveolar and fricative manner. Embedding was $m = 3$, $\tau = 6$ and $\varepsilon = 0.05$ (FAN).

[1]Articulated with the tip or blade of the tongue against the ridge behind the upper teeth (Source: *http://www.xrefer.com*).

Chapter 4

Conclusion

In this study I have shown that recurrence plots (RPs) offer manifold possibilities of application. RP based techniques can be modified and adopted to a specific problem.

In this work different aspects of the application of RPs to time series have been studied. Methodical extensions have been introduced for the univariate and bivariate data analysis. Applications to model and real data have revealed the applicability of these methodical extensions, especially where other methods fail, and have given new insights into the processes behind the considered data. Besides, a comprehensive overview of earlier introduced techniques based on RPs is given.

4.1 Methodical Development

4.1.1 New Quantification Measures for Recurrence Plots

Recurrence plots (RPs) are binary plots which consist of black dots and black diagonal as well as vertical lines. Classical measures of complexity based on RPs use mainly the diagonal structures within an RP. These measures allow to identify transitions between chaos and order. We have introduced new measures of complexity that also use the vertical structures in an RP, the *laminarity*, the *trapping time* and the *maximal vertical line length*.

A vertical line structure occurs when a state does not change or changes rather slowly. It seems that the state is trapped for some time, which is typical for laminar behaviour. The *laminarity* measures the occurrence of such laminar states. The time length of the laminar states is measured by the other two measures where the *trapping time* is defined as the average duration of a laminar state. These new measures of complexity enable also identification of

chaos-chaos transitions.

We have also shown the relations of these new measures to formerly introduced quantification techniques.

4.1.2 Extension to Cross Recurrence Plots

The extension of the concept of recurrence plots to test for interrelations between two different phase space trajectories leads to cross recurrence plots (CRPs). From the point of view of a CRP, an RP can be considered as a special case of a CRP for two identical processes. However, if these two processes become progressively different, typical structures of the RP, like the main diagonal (*line of identity, LOI*), will dissolve. A quantification of these structures can be used in order to assess the variation or similarity between the dynamics of both processes.

The CRP analysis provides another useful application. The orientation of the line structures in the CRP is related to the time relation between the corresponding segments of the phase space trajectories. In the case of two sufficiently similar processes with different time dilatations, the CRP shows a bowed line of identity which is called *line of synchronization (LOS)*. This line corresponds to the transfer function between the time scales of the considered time series. A nonparametrical function fitted to LOS can be used in order to align the two processes to the same time scale.

Considering two processes, where epochs of the second are partly contained in the first, the CRP facilitates finding the location of these epochs in the first process.

4.2 Applications

The applications presented here are from different scientific disciplines and include various types of problems. Using RP based techniques, we have achieved important results, whereas other methods were mostly not sufficient.

4.2.1 Heart Rate Variability Data

The application of the new introduced measures of complexity to heart rate variability data of patients with fatal cardiac arrhythmias has revealed characteristic patterns in the RPs before the onset of a ventricular tachycardia (VT). The new measures of complexity allow to detect early signs of occurrence of a life threatening cardiac arrhythmia. These result may be of importance for the therapy of malignant cardiac arrhythmias.

4.2.2 EEG Data During Stimulus Presentation

In the analysis of data of cognitive experiments (event related EEG data, Oddball experiment) we have found components in the brain potential which are typical for attention and expectation already from a single trial analysis. This is an important progress because traditionally such components can only be found after averaging an ensemble over a collection of EEG trials. This study suggests further chaos-chaos transitions between laminar and non-laminar states during event induced processes in the brain.

4.2.3 ENSO-like Influence on Pleistocene Precipitation

CRPs have been used for the search for an influence of the El Niño/ Southern Oscillation (ENSO) on the climate in northwestern Argentina 34 000 years ago. The CRP analysis of the colour variation of lake sediments as a proxy for the palaeorainfall has uncovered similarities to the modern precipitation which is influenced by the ENSO. From this result we can infer that an ENSO-like oscillation was active at approximately 34 000 years ago.

4.2.4 Time Scale Alignment of Marine Geophysical Data

The characteristic shape of the LOS has been used for the time scale alignment of geophysical borehole data from the central Arctic Ocean. The transfer function has been found by its non-parametrical fit to the LOS. The comparison with the standard method of wiggle matching has shown the reliability of the alignment based on CRPs.

4.2.5 Examples for the Search of Matching Sequences

Sequences of high concordance can be found with the help of CRPs. In a geological frame we have presented this technique in order to date a geological profile with a reference whose time scale is known.

In a second example the CRP has been applied to a DNA sequence and a known gene. The CRP has found and visualized the locations of the gene in the DNA string. Diagonal lines and jumps therein have marked the occurrence of exons and introns.

The last example has shown the applicability of CRPs to speech recognition. We could recognize a single word within a spoken sentence by comparing it with a reference vocabular. Using the RQA, specific phonemes can be classified regarding to their manner and location of production.

4.3 Perspectives

Since recurrence plots offer various possibilities of application and become more popular, numerous applications to different kind of data can be expected.

However, the theoretical background of RPs is not yet completely understood. Promising studies are still under work by Thiel et al. (2003a) and Romano et al. (2003). For example, they evolve a new approach to cross recurrence. The development of a basic theory about the statistics of the quantification measures based on RPs needs further research. This statistics have to consider the embedding as well as the non-normal distribution of the measures and is required to assess the significance of the measures. Since the measures of complexity based on RPs depend on the embedding as well as the construction parameters, future work should further focus on possible pitfalls.

Regarding the theory of RPs, there is a further demand for research of the perpendicular RPs and the RPs created with the criteria of a fixed amount of nearest neighbours. The recurrence points in a perpendicular RP are closely related to Poincaré sections and may be useful for the definition of further invariant measures based on RPs.

There is still an open question in the context of the distribution of the lengths of vertical structures in an RP. The lengths of these vertical structures and thus their corresponding measures depend on the choice of the embedding parameters. Especially if the product of the dimension and delay exceeds the averaged length of vertical structures, these measures decrease abruptly but do not vanish. After further increase of the embedding, these measures may increase again. However, this relation is not yet studied in detail.

Future development considering optimization of the LOS searching algorithm and definition of an improved quality factor of the found LOS is needed in order to get a clear LOS even if the data are non-smooth. Moreover, the influence of dynamical noise to the result needs a further study. Probably, this problem may be bypassed by a suitable LOS searching algorithm too.

A forthcoming study will try to adopt the concepts of RPs to applications of image processing. Moreover, the applicability to the analysis of spatio-temporal data is an important task.

The independent component analysis may offer a further method for the phase space reconstruction. The development of such embedding method seems promising.

Acknowledgement

This work could not be realized without help and support of many people.

First, I wish to express my gratitude to Prof. Jürgen Kurths who has given me the chance for this PhD study, procured the support by the DFG, who offers new contacts with scientists from other disciplines and therefore new possibilities of applications and, of course, has encouraged and inspired me with new ideas and with fruitful discussions.

I am grateful to the members of the Nonlinear Dynamics Group for the talks, discussions, the good and cooperative atmosphere and the countless coffee, tea and cake. In particular I would like to thank Dr. Udo Schwarz who has always found the time to discuss about problems and who has enriched my work with new ideas and suggestions. Further I sincerely thank Mamen Romano and Marco Thiel for the interesting talks and discussions about recurrence plots, for sharing their ideas and for the fruitful co-operation and I wish them success and good luck for their current PhD studies. I gratefully thank Dr. Niels Wessel for his supply of heart rate variability data as well as his cooperation, discussion and support regarding their analysis. I want to thank Jörg-Uwe Tessmer for the technical support and maintenance of the computing power, Birgit Nader and Marita Dörrwand for their advice and support in the concern of organization and finance.

During my PhD study some co-operations with scientists from other disciplines have been arised. The applications in this work base mostly on these cooperations. I gratefully thank Dr. Martin Trauth of the Institute of Geosciences, University of Potsdam. He has generously supported my work since the beginning by presenting me interesting geological tasks, supplying me with different kind of geological and climate data, providing further computing resources, discussions about climate and geology and invitations to geological field trips in Argentina and Kenya. I also thank Frank Warkus of the same institute for other geological data. I thank Dr. Mathias Vuille, Climate System Research Center at the University of Massachusetts, for his friendly support in our study of the climate in South America. The geologists of the Geo-

ForschungsZentrum Potsdam, especially Dr. Norbert Nowaczyk and Dr. Uta Frank, are gratefully acknowledged for co-operation in the context of palaeomagnetism and for providing corresponding data sets. I appreciate the co-operations with Dr. Peter beim Graben and Anja Meinke from the Institute of Linguistics, University of Potsdam. They have provided data from the Oddball experiment and introduced me into the cognitive sciences.

I would like to thank Prof. Joseph Zbilut for encouraging my study on recurrence quantification and acting as a referee for this thesis. During my PhD study, several scientists have been interested in the application of the *CRP toolbox* for Matlab. I am grateful for this interest and the succeeding usage of this toolbox. I have received some help from students in programming the toolbox. I am grateful for this to Michael Pahle, Falko Zetsche, Christian Hönnicke and Christian Guse. I thank Matthew Belcher for proofreading this thesis.

My special thanks go to my parents for their support and sympathies, and, last but not least, I am truly grateful to Lara Subašić for her endless and manifold support and encouragement. I appreciate particularly her patience with me and her help in translations.

This work was partly supported by the Priority Programme 1097, *Geomagnetic Variations, Spatio-temporal structure, processes and effects on system Earth* of the Deutsche Forschungsgemeinschaft.

Bibliography

ABARBANEL, H. D. I., BROWN, R., SIDOROWICH, J. J., TSIMRING, L. S., The analysis of observed chaotic data in physical systems. Review of Modern Physics 65 (4), 1993, 1331–1392. DOI: 10.1103/RevModPhys.65.1331

AMIT, D. J., Modeling Brain Function. The World of Attractor Neural Networks. Cambridge University Press, Cambridge, 1989.

ARGYRIS, J. H., FAUST, G., HAASE, M., An Exploration of Chaos. North Holland, Amsterdam, 1994.

ATAY, F. M., ALTINTAŞ, Y., Recovering smooth dynamics from time series with the aid of recurrence plots. Physical Review E 59 (6), 1999, 6593–6598. DOI: 10.1103/PhysRevE.59.6593

AUBERT, X. L., An overview of decoding techniques for large vocabulary continuous speech recognition. Computer Speech & Language 16 (1), 2002, 89–114. DOI: 10.1006/csla.2001.0185

BABLOYANTZ, A., Evidence for slow brain waves: a dynamical approach. Electroencephalography and Clinical Neurophysiology 78 (5), 1991, 402–405. DOI: 10.1016/0013-4694(91)90101-9

BABLOYANTZ, A., SALAZAR, J. M., NICOLIS, C., Evidence of chaotic dynamics of brain activity during the sleep cycle. Physics Letters A 111 (3), 1985, 152–156. DOI: 10.1016/0375-9601(85)90444-X

BALAKRISHNAN, V., NICOLIS, G., NICOLIS, C., Recurrence time statistics in deterministic and stochastic dynamical systems in continuous time: A comparison. Physical Review E 61 (3), 2000, 2490–2499. DOI: 10.1103/PhysRevE.61.2490

BALASUBRAMANIAM, R., RILEY, M. A., TURVEY, M. T., Specificity of postural sway to the demands of a precision task. Gait & Posture 11 (1), 2000, 12–24. DOI: 10.1016/S0966-6362(99)00051-X

BEAUFORT, L., DE GARIDEL-THORON, T., MIX, A. C., PISIAS, N. G., ENSO-like Forcing on Oceanic Primary Production During the Late Pleistocene. Science 293, 2001, 2440–2444.

BELAIRE-FRANCH, J., CONTRERAS, D., Recurrence Plots in Nonlinear Time Series Analysis: Free Software, 2002.
URL: http://www.jstatsoft.org/index.php?vol=7

BELAIRE-FRANCH, J., CONTRERAS, D., TORDERA-LLEDÓ, L., Assessing nonlinear structures in real exchange rates using recurrence plot strategies. Physica D 171 (4), 2002, 249–264. DOI: 10.1016/S0167-2789(02)00625-5

BERGER, A., LOUTRE, M., Insolation values for the climate of the last 10 million years. Quaternary Science Reviews 10, 1991, 297–317.

BOOKHAGEN, B., HASELTON, K., TRAUTH, M. H., Hydrological modelling of a Pleistocene landslide-dammed lake in the Santa Maria Basin, NW Argentina. Palaeogeography, Palaeoclimatology, Palaeoecology 169, 2001, 113–127. DOI: 10.1016/S0031-0182(01)00221-8

BROOMHEAD, D. S., KING, G. P., Extracting qualitative dynamics from experimental data. Physica D 20 (2–3), 1986, 217–236.
DOI: 10.1016/0167-2789(86)90031-X

BRÜGGEMANN, W., A Minimal Cost Function Method For Optimizing the Age-Depth Relation of Deep-Sea Sediment Cores. Paleoceanography 7 (4), 1992, 467–487.

CANDE, S. C., KENT, D. V., Revised calibration of the geomagnetic polarity timescale for the late Cretaceous and Cenozoic. Journal of Geophysical Research 100, 1995, 6093–6095.

CAO, L., Practical method for determining the minimum embedding dimension of a scalar time series. Physica D 110 (1–2), 1997, 43–50.
DOI: 10.1016/S0167-2789(97)00118-8

CASDAGLI, M. C., Recurrence plots revisited. Physica D 108 (1–2), 1997, 12–44.
DOI: 10.1016/S0167-2789(97)82003-9

CHOI, J. M., BAE, B. H., KIM, S. Y., Divergence in perpendicular recurrence plot; quantification of dynamical divergence from short chaotic time series. Physics Letters A 263 (4–6), 1999, 299–306.
DOI: 10.1016/S0375-9601(99)00751-3

COLLET, P., ECKMANN, J.-P., Iterated maps on the interval as dynamical systems. Birkhäuser, Basel Boston Stuttgart, 1980.

DIAZ, J. O., MAKIKALLIO, T. H., HUIKURI, H. V., LOPERA, G., MITRANI, R. D., CASTELLANOS, A., MYERBURG, R. J., ROZO, P., PAVA, F., MORILLO, C. A., Heart rate dynamics before the spontaneous onset of ventricular tachyarrhythmias in Chagas' heart disease. American Journal of Cardiology 87 (9), 2001, 1123–1125. DOI: 10.1016/S0002-9149(01)01477-1

DONCHIN, E., Surprise! ... Surprise? Psychophysiology 18, 1981, 493–513.

DONCHIN, E., COLES, M. G. H., Is the P300 component a manifestation of context updating? Behavioral and Brain Sciences 11, 1988, 357–374.

ECKMANN, J.-P., KAMPHORST, S. O., RUELLE, D., Recurrence Plots of Dynamical Systems. Europhysics Letters 5, 1987, 973–977.

ECKMANN, J.-P., OLIFFSON KAMPHORST, S., RUELLE, D., CILIBERTO, S., Liapunov exponents from time series. Physical Review A 34 (6), 1986, 4971–4979. DOI: 10.1103/PhysRevA.34.4971

ECKMANN, J.-P., RUELLE, D., Ergodic theory of chaos and strange attractors. Review of Modern Physics 57 (3), 1985, 617–656.
DOI: 10.1103/RevModPhys.57.617

ELWAKIL, A. S., SOLIMAN, A. M., Mathematical Models of the Twin-T, Wienbridgeand Family of Minimum Component Electronic ChaosGenerators with Demonstrative Recurrence Plots. Chaos, Solitons, & Fractals 10 (8), 1999, 1399–1411. DOI: 10.1016/S0960-0779(98)00109-X

FAURE, P., KORN, H., A new method to estimate the Kolmogorov entropy from recurrence plots: its application to neuronal signals. Physica D 122 (1–4), 1998, 265–279. DOI: 10.1016/S0167-2789(98)00177-8

FAURE, P., KORN, H., Is there chaos in the brain? I. Concepts of nonlinear dynamics and methods of investigation. Comptes Rendus de l'Acadmie des Sciences - Series III - Sciences de la Vie 324 (9), 2001, 773–793.

FRASER, A. M., Reconstructing attractors from scalar time series: A comparison of singular system and redundancy criteria. Physica D 34 (3), 1989, 391–404. DOI: 10.1016/0167-2789(89)90263-7

FRASER, A. M., SWINNEY, H. L., Independent coordinates for strange attractors from mutual information. Physical Review A 33 (2), 1986, 1134–1140.
DOI: 10.1103/PhysRevA.33.1134

FRONTALI, C., PIZZI, E., Similarity in oligonucleotide usage in introns and intergenic regions contributes to long-range correlation in the Caenorhabditis elegans genome. Gene 232 (1), 1999, 87–95.
DOI: 10.1016/S0378-1119(99)00111-0

GALLEZ, D., BABLOYANTZ, A., Predictability of human EEG: a dynamical approach. Biological Cybernetics 64, 1991, 381–39.

GAO, J., ZHENG, Z., Direct dynamical test for deterministic chaos and optimal embedding of a chaotic time series. Physical Review E 49, 1994, 3807–3814.
DOI: 10.1103/PhysRevE.49.3807

GAO, J. B., Recurrence Time Statistics for Chaotic Systems and Their Applications. Physical Review Letters 83 (16), 1999, 3178–3181.
DOI: 10.1103/PhysRevLett.83.3178

GAO, J. B., CAI, H. Q., On the structures and quantification of recurrence plots. Physics Letters A 270 (1–2), 2000, 75–87.
DOI: 10.1016/S0375-9601(00)00304-2

GIEGERICH, R., WHEELER, D., Pairwise Sequence Alignment. In: BioComputing Hypertext Coursebook, 1996.
URL:http://www.techfak.uni-bielefeld.de/bcd/Curric/PrwAli

GILMORE, C. G., A new test for chaos. Journal of Economic Behavior & Organization 22 (2), 1993, 209–237. DOI: 10.1016/0167-2681(93)90064-V

GILMORE, C. G., An examination of nonlinear dependence in exchange rates, using recent methods from chaos theory. Global Finance Journal 12 (1), 2001, 139–151. DOI: 10.1016/S1044-0283(01)00018-7

GILMORE, R., Topological analysis of chaotic dynamical systems. Review of Modern Physics 70 (4), 1998, 1455–1529.
DOI: 10.1103/RevModPhys.70.1455

GIULIANI, A., BENIGNI, R., SIRABELLA, P., ZBILUT, J. P., COLOSIMO, A., Nonlinear Methods in the Analysis of Protein Sequences. Biophysical Journal 78 (1), 2000, 136–149.

GIULIANI, A., MANETTI, C., Hidden pecularities in the potential energy time series of a tripeptide highlighted by a recurrence plot analysis: A molecular dynamics simulation,. Physical Review E 53 (6), 1996, 6336–6340.
DOI: 10.1103/PhysRevE.53.6336

GIULIANI, A., TOMASI, M., Recurrence quantification analysis reveals interaction partners in paramyxoviridae envelope glycoproteins. Proteins: Structure, Function, and Genetics 46 (2), 2002, 171–176.
DOI: 10.1002/prot.10044

GRASSBERGER, P., PROCACCIA, I., Measuring the strangeness of strange attractors. Physica D 9 (1–2), 1983, 189–208.
DOI: 10.1016/0167-2789(83)90298-1

HO§YST, J. A., ZEBROWSKA, M., URBANOWICZ, K., Observations of deterministic chaos in financial time series by recurrence plots, can one control chaotic economy? The European Physical Journal B 20 (4), 2001, 531–535.

HUANG, Q., SOBOLEV, G. A., Precursory seismicity changes associated with the Nemuro Peninsula earthquake, January 28, 2000. Journal of Asian Earth Sciences 21 (2), 2002, 135–146. Hat nichts mit RPs zu tun, aber dieser begriff fuer etwas anderes verwendet. DOI: 10.1016/S1367-9120(02)00032-9

HUCKVALE, M., FANG, A. C., Using phonologically-constrained morphological analysis in continuous speech recognition. Computer Speech & Language 16 (2), 2002, 165–181. DOI: 10.1006/csla.2001.0187

HYVÄRINEN, A., KARHUNEN, J., OJA, E., Independent component analysis. John Wiley & Sons Inc., New York, 2001.

IWANSKI, J. S., BRADLEY, E., Recurrence plots of experimental data: To embed or not to embed? Chaos 8 (4), 1998, 861–871. DOI: 10.1063/1.166372

KAC, M., On the notion of recurrence in discrete stochastic processes. Bulletin of the American Mathematical Society 53, 1947, 1002–1010.

KANDEL, E. R., SCHWARTZ, J. H., JESSEL, T. M., Essentials of Neural Science and Behavior. Appleton & Lange, East Norwalk, Connecticut, 1995.

KANTZ, H., Quantifying the closeness of fractal measures. Physical Review E 49 (6), 1994, 5091–5097. DOI: 10.1103/PhysRevE.49.5091

KANTZ, H., SCHREIBER, T., Nonlinear Time Series Analysis. University Press, Cambridge, 1997.

KENNEL, M. B., Statistical test for dynamical nonstationarity in observed time-series data. Physical Review E 56 (1), 1997, 316–321.
DOI: 10.1103/PhysRevE.56.316

KENNEL, M. B., BROWN, R., ABARBANEL, H. D. I., Determining embedding dimension for phase-space reconstruction using a geometrical construction. Physical Review A 45 (6), 1992, 3403–3411.
DOI: 10.1103/PhysRevA.45.3403

KOEBBE, M., MAYER-KRESS, G., Use of Recurrence Plots in the Analysis of Time-Series Data. In: Casdagli, M., Eubank, S. (Eds.), Proceedings of SFI Studies in the Science of Complexity. Vol. XXI. Addison-Wesley, Redwood City, 1992. pp. 361–378.

KURTHS, J., SCHWARZ, U., SONETT, C. P., PARLITZ, U., Testing nonlinearity in radiocarbon data. Nonlinear Processes in Geophysics 1 (1), 1994, 72–75.

KURTHS, J., VOSS, A., WITT, A., SAPARIN, P., KLEINER, H. J., WESSEL, N., Quantitative analysis of heart rate variability. Chaos 5, 1995, 88–94.
DOI: 10.1063/1.166090

LATHROP, D. P., KOSTELICH, E. J., Characterization of an experimental strange attractor by periodic orbits. Physical Review A 40 (7), 1989, 4028–4031. DOI: 10.1103/PhysRevA.40.4028

LORENZ, E. N., Deterministic Nonperiodic Flow. Journal of the Atmospheric Sciences 20, 1963, 120–141.

LUTZENBERGER, W., ELBERT, T., BIRBAUMER, N., RAY, W. J., SCHUPP, H., The scalp distribution of the fractal dimension of the EEG and its variation with mental tasks. Brain Topography 5 (1), 1992, 27–33.

MANETTI, C., GIULIANI, A., CERUSO, M.-A., WEBBER JR., C. L., ZBILUT, J. P., Recurrence analysis of hydration effects on nonlinear protein dynamics: multiplicative scaling and additive processes. Physics Letters A 281 (5–6), 2001, 317–323. DOI: 10.1016/S0375-9601(01)00147-5

MANUCA, R., SAVIT, R., Stationarity and nonstationarity in time series analysis. Physica D 99 (2–3), 1996, 134–161.
DOI: 10.1016/S0167-2789(96)00139-X

MARTINSON, D. G., MENKE, W., STOFFA, P., An Inverse Approach to Signal Correlation. Journal of Geophysical Research 87, 1982, 4807–4818.

MARWAN, N., Untersuchung der Klimavariabilität in NW Argentinien mit Hilfe der quantitativen Analyse von Recurrence Plots. Master's thesis, Dresden University of Technology, Dresden University of Technology, October 1999.

MARWAN, N., KURTHS, J., Nonlinear analysis of bivariate data with cross recurrence plots. Physics Letters A 302 (5–6), 2002, 299–307.
DOI: 10.1016/S0375-9601(02)01170-2

MARWAN, N., MEINKE, A., Extended recurrence plot analysis and its application to ERP data. International Journal of Bifurcation and Chaos "Cognition and Complex Brain Dynamics" 14 (2), 2004.

MARWAN, N., THIEL, M., NOWACZYK, N. R., Cross Recurrence Plot Based Synchronization of Time Series. Nonlinear Processes in Geophysics 9 (3/4), 2002a, 325–331.

MARWAN, N., TRAUTH, M. H., VUILLE, M., KURTHS, J., Comparing modern and Pleistocene ENSO-like influences in NW Argentina using nonlinear time series analysis methods. Climate Dynamics, 2003, in press.
DOI: 10.1007/s00382-003-0335-3

MARWAN, N., WESSEL, N., KURTHS, J., Recurrence Plot Based Measures of Complexity and its Application to Heart Rate Variability Data. Physical Review E 66 (2), 2002b, 026702. DOI: 10.1103/PhysRevE.66.026702

MATASSINI, L., KANTZ, H., YST, J. H., HEGGER, R., Optimizing of recurrence plots for noise reduction. Physical Review E 65 (2), 2002, 021102.
DOI: 10.1103/PhysRevE.65.021102

MATASSINI, L., MANFREDI, C., Software corrections of vocal disorders. Computer Methods and Programs in Biomedicine 68 (2), 2002, 135–145.
DOI: 10.1016/S0169-2607(01)00161-4

MCGUIRE, G., AZAR, N. B., SHELHAMER, M., Recurrence matrices and the preservation of dynamical properties. Physics Letters A 237 (1–2), 1997, 43–47. DOI: 10.1016/S0375-9601(97)00697-X

MINDLIN, G. M., GILMORE, R., Topological analysis and synthesis of chaotic time series. Physica D 58 (1–4), 1992, 229–242.
DOI: 10.1016/0167-2789(92)90111-Y

MONK, A. T., COMPTON, A. H., Recurrence phenomena in cosmic-ray intensity. Review of Modern Physics 11, 1939, 173–179.
DOI: 10.1103/RevModPhys.11.173

MYERS, E. W., An Overview of Sequence Comparison Algorithms in Molecular Biology. Tech. Rep. TR 91-29, University of Arizona, Tucson, Department of Computer Science, Tucson, 1991.

OBLOW, E. M., Supertracks, supertrack functions and chaos in the quadratic map. Physics Letters A 128 (8), 1988, 406.
DOI: 10.1016/0375-9601(88)90119-3

OTT, E., Chaos in Dynamical Systems. University Press, Cambridge, 1993.

PACKARD, N. H., CRUTCHFIELD, J. P., FARMER, J. D., SHAW, R. S., Geometry from a Time Series. Physical Review Letters 45 (9), 1980, 712–716.
DOI: 10.1103/PhysRevLett.45.712

PRITCHARD, W. S., DUKE, D. W., Dimensional analysis of no-task human EEG using the Grassberger-Procaccia method. Psychophysiology 29 (2), 1992, 182–191.

PROHASKA, F. J., The climate of Argentina, Paraguay and Urugay. Vol. 12 of World Survey of Climatlogy. Elsevier, Amsterdam, Oxford, New York, 1976. pp. 13–73.

PROVENZALE, A., SMITH, L. A., VIO, R., MURANTE, G., Distinguishing between low-dimensional dynamics and randomness in measured time series. Physica D 58 (1–4), 1997, 31–49. DOI: 10.1016/0167-2789(92)90100-2

RAPP, P. E., ZIMMERMAN, I. D., ALBANO, A. M., DEGUZMAN, G. C., GREENBAUN, N. N., BASHORE, T. R., Experimental studies of chaotic neural behavior: Cellular activity and electroencephalographic signals. In: Othmer, H. G. (Ed.), Nonlinear Oscillations in Biology and Chemistry. Vol. 66 of Lecture Notes in Biomathematics. Springer, Berlin, 1986. pp. 175–205.

RIEKE, C., STERNICKEL, K., ANDRZEJAK, R. G., ELGER, C. E., DAVID, P., LEHNERTZ, K., Measuring Nonstationarity by Analyzing the Loss of Recurrence in Dynamical Systems. Physical Review Letters 88 (24), 2002, 244102.
DOI: 10.1103/PhysRevLett.88.244102

RILEY, M. A., BALASUBRAMANIAM, R., TURVEY, M. T., Recurrence quantification analysis of postural fluctuations. Gait & Posture 9 (1), 1999, 65–78.
DOI: 10.1016/S0966-6362(98)00044-7

ROMANO, M., THIEL, M., KURTHS, J., A new definition of Cross Recurrence Plots. Physics Letters A (subm.), 2003.

RÖSLER, F., Hirnelektrische Korrelate kognitiver Prozesse. Springer, Berlin, 1982.

RUSTICI, M., CARAVATI, C., PETRETTO, E., BRANCA, M., MARCHETTINI, N., Transition Scenarios during the Evolution of the Belousov-Zhabotinsky Reaction in an Unstirred Batch Reactor. Journal of Physical Chemistry A 103 (33), 1999, 6564–6570. DOI: 10.1021/jp9902708

SAKOE, H., CHIBA, S., Dynamic programming algorithm optimization for spoken word recognition. IEEE Trans. Acoustics, Speech and Signal Proc. 26, 1978, 43–49.

SAPARIN, P., WITT, A., KURTHS, J., ANISHCHENKO, V., The Renormalized Entropy–an Appropriate Complexity Measure? Chaos, Solitons & Fractals 4 (10), 1994, 1907–1916. DOI: 10.1016/0960-0779(94)90006-X

SHELHAMER, M., On the correlation dimension of optokinetic nystagmus eye movements: computational parameters, filtering, nonstationarity, and surrogate data. Biological Cybernetics 76 (4), 1997, 237–250.

STROZZI, F., ZALDÍVAR, J.-M., ZBILUT, J. P., Application of nonlinear time series analysis techniques to high-frequency currency exchange data. Physica A 312 (3–4), 2002, 520–538. DOI: 10.1016/S0378-4371(02)00846-4

SUTTON, S., BRAREN, M., ZUBIN, J., JOHN, E. R., Evoked potential correlates of stimulus uncertainty. Science 150, 1965, 1187–1188.

TAKENS, F., Detecting Strange Attractors in Turbulence. Vol. 898 of Lecture Notes in Mathematics. Springer, Berlin, 1981. pp. 366–381.

THEILER, J., Spurious dimension from correlation algorithms applied to limited time-series data. Physical Review A 34 (3), 1986, 2427–2432. DOI: 10.1103/PhysRevA.34.2427

THEILER, J., EUBANK, S., LONGTIN, A., GALDRIKIAN, B., FARMER, B., Testing for nonlinearity in time series: the method of surrogate data. Physica D 58, 1992, 77–94. DOI: 10.1016/0167-2789(92)90102-S

THIEL, M., private communication, 2003.

THIEL, M., ROMANO, M. C., KURTHS, J., Analytical description of Recurrence Plots of white noise and chaotic processes. Chaos (subm.), 2003a.

THIEL, M., ROMANO, M. C., KURTHS, J., Recurrence Plots for Stochastic and Chaotic Systems. Physics Letters A (subm.), 2003b.

THIEL, M., ROMANO, M. C., KURTHS, J., MEUCCI, R., ALLARIA, E., ARECCHI, F. T., Influence of observational noise on the recurrence quantification

analysis. Physica D 171 (3), 2002, 138–152.
DOI: 10.1016/S0167-2789(02)00586-9

THOMASSON, N., HOEPPNER, T. J., WEBBER JR., C. L., ZBILUT, J. P., Recurrence quantification in epileptic EEGs. Physics Letters A 279 (1–2), 2001, 94–101. DOI: 10.1016/S0375-9601(00)00815-X

THOMPSON, R., CLARK, R. M., Sequence slotting for stratigraphic correlation between cores: theory and practice. Journal of Paleolimnology 2, 1989, 173–184.

TRAUTH, M. H., ALONSO, R. A., HASELTON, K., HERMANNS, R., STRECKER, M. R., Climate change and mass movements in the northwest Argentine Andes. Earth and Planetary Science Letters 179 (2), 2000, 243–256.
DOI: 10.1016/S0012-821X(00)00127-8

TRAUTH, M. H., BOOKHAGEN, B., MARWAN, N., STRECKER, M. R., Multiple landslide clusters record Quaternary climate changes in the northwestern Argentine Andes. Palaeogeography Palaeoclimatology Palaeoecology 194 (1–3), 2003, 109–121. DOI: 10.1016/S0031-0182(03)00273-6

TRAUTH, M. H., STRECKER, M. R., Formation of landslide-dammed lakes during a wet period between 40,000 and 25,000 yr B.P. in northwestern Argentina. Palaeogeography, Palaeoclimatology, Palaeoecology 153 (1–4), 1999, 277–287. DOI: 10.1016/S0031-0182(99)00078-4

TRULLA, L. L., GIULIANI, A., ZBILUT, J. P., WEBBER JR., C. L., Recurrence quantification analysis of the logistic equation with transients. Physics Letters A 223 (4), 1996, 255–260. DOI: 10.1016/S0375-9601(96)00741-4

TUFILLARO, N. B., SOLARI, H. G., GILMORE, R., Relative rotation rates: Fingerprints for strange attractors. Physical Review A 41 (10), 1990, 5717–5720.
DOI: 10.1103/PhysRevA.41.5717

VIHINEN, M., An algorithm for simultaneous comparison of several sequences. Computer applications in the biosciences: CABIOS 4 (1), 1988, 89–92.

VOSS, A., KURTHS, J., KLEINER, H. J., WITT, A., WESSEL, N., SAPARIN, P., OSTERZIEL, K. J., SCHURATH, R., DIETZ, R., The application of methods of non-linear dynamics for the improved and predictive recognition of patients threatened by sudden cardiac death. Cardiovascular Research 31 (3), 1996, 419–433. DOI: 10.1016/0008-6363(96)00008-9

VRETENAR, D., PAAR, N., RING, P., LALAZISSIS, G. A., Nonlinear dynamics of giant resonances in atomic nuclei. Physical Review E 60 (1), 1999, 308–319. DOI: 10.1103/PhysRevE.60.308

WACKERBAUER, R., WITT, A., ATMANSPACHER, H., KURTHS, J., SCHEINGRABER, H., A Comparative Classification of Complexity Measures. Chaos, Solitons & Fractals 4 (4), 1994, 133–173. DOI: 10.1016/0960-0779(94)90023-X

WARKUS, F., Die neogene Hebungsgeschichte der Patagonischen Anden im Kontext der Subduktion eines aktiven Spreizungszentrums. Ph.D. thesis, University of Potsdam, Institute of Earth Sciences, 2002. URL: urn:nbn:de:kobv:517-0000555

WEBBER JR., C. L., Recurrence Quantification Analysis, 2003. URL: http://homepages.luc.edu/~cwebber

WEBBER JR., C. L., SCHMIDT, M. A., WALSH, J. M., Influence of isometric loading on biceps EMG dynamics as assessed by linear and nonlinear tools. Journal of Applied Physiology 78 (3), 1995, 814–822.

WEBBER JR., C. L., ZBILUT, J. P., Dynamical assessment of physiological systems and states using recurrence plot strategies. Journal of Applied Physiology 76 (2), 1994, 965–973.

WESSEL, N., MARWAN, N., MEYERFELDT, U., SCHIRDEWAN, A., KURTHS, J., Recurrence quantification analysis to characterise the heart rate variability before the onset of ventricular tachycardia. Lecture Notes in Computer Science 2199, 2001, 295–301.

WESSEL, N., ZIEHMANN, C., KURTHS, J., MEYERFELDT, U., SCHIRDEWAN, A., VOSS, A., Short-term forecasting of life-threatening cardiac arrhythmias based on symbolic dynamics and finite-time growth rates. Physical Review E 61, 2000, 733–739. DOI: 10.1103/PhysRevE.61.733

ZBILUT, J. P., GIULIANI, A., WEBBER JR., C. L., Detecting deterministic signals in exceptionally noisy environments using cross-recurrence quantification. Physics Letters A 246 (1–2), 1998, 122–128. DOI: 10.1016/S0375-9601(98)00457-5

ZBILUT, J. P., KOEBBE, M., LOEB, H., MAYER-KRESS, G., Use of Recurrence Plots in the Analysis of Heart Beat Intervals. In: Proc. IEEE Conference on Computers in Cardiology Chicago 1990, 1991. pp. 263–266.

ZBILUT, J. P., WEBBER JR., C. L., Embeddings and delays as derived from quantification of recurrence plots. Physics Letters A 171 (3–4), 1992, 199–203.
DOI: 10.1016/0375-9601(92)90426-M

ZBILUT, J. P., ZALDÍVAR-COMENGES, J.-M., STROZZI, F., Recurrence quantification based Liapunov exponents for monitoring divergence in experimental data. Physics Letters A 297 (3–4), 2002, 173–181.
DOI: 10.1016/S0375-9601(02)00436-X

Recurrence Plot Web Site, 2003.
URL: http://www.recurrence-plot.tk

Index

attractor **4**, 5
  reconstruction *see* phase space
autocovariance **5**

close returns
  close returns histogram 15, **24**, **34**, 45
  close returns plot **14**
correlation dimension **13**, 33
correlation sum **13**, 22
  cross correlation sum 15, **15**
cross recurrence plot 10, **34–36**, 55, 58, 60, 62, 65, 67
  application **55–68**
  cross recurrence quantification **35**, 55, 57
  determinism **37**, 56, 58
  diagonal line 36, 37
  diagonal line length **38**, 55, 58
  line of synchronization 36, **39–42**, 60, 62, 65
  neighbourhood *see* recurrence plot
  recurrence quantification 37
  recurrence rate **37**, 55, 58
  slope of lines **40–42**
  software **43–45**
  time scale alignment *see* line of synchronization
cross recurrence quantification *see* cross recurrence plot

determinism *see* recurrence quantification
dimension *see* embedding
distance matrix **10**, 15
distance plot **15**
divergence *see* recurrence quantification
dynamics **4**, 12

embedding **4–8**, 36
  differential phase space embedding **7**
  dimension **4–6**, 12
  independent component analysis **7**
  singular value decomposition **6**
  time delay **4–7**
  time delay embedding **4**

false diagonals *see* tangential motion
false nearest neighbours **5**, 26

information dimension **34**
intermittency *see* state (laminar state), **27**

laminarity *see* recurrence quantification
line of identity *see* recurrence plot
line of synchronization *see* cross recurrence plot
logistic map **27**
Lyapunov exponent 13, 14, 19, **24**, 26

mutual information **6**

norm **10**

observation **3**, 4
orbit **4**

percent determinism *see* recurrence quantification
percent recurrence *see* recurrence quantification
phase space **4**, 9
  embedding *see* embedding
  meta phase space **15**
  reconstruction **3–8**
  tangential motion **13–17**, 23, 26, 34, 38
  trajectory **4**, 9, 18
  vector **4**
Poincaré section **14**

Rényi entropy **26**, 33
ratio *see* recurrence quantification
recurrence 9, **10**, 18
  recurrence point **10**
  recurrence time **33**
  recurrence time statistics 18, **33**
recurrence plot **9**
  application **45–47**
  corridor thresholded recurrence plot **13**
  diagonal line 12, 13, **19**, 23, 36
  disrupted RP **18**
  distribution of diagonal lines **23**, 26
  drift (typology) **18**
  false nearest neighbours **26**
  global recurrence plot **15**
  homogeneous RP **18**
  isolated points **19**
  line of identity **9**, 13, 14, 36
  line of synchronization *see* cross recurrence plot
  meta recurrence plot **15**
  neighbourhood **10**, 36
  pattern **18**
  periodic structures **18**
  perpendicular recurrence plot **14**, 24
  prediction time **24**
  quantification *see* recurrence quantification
  redundancy **12**
  single points **19**
  slope of lines **20**, 40–42
  software **43–45**
  texture **19**
  threshold *see* threshold
  typology **18**
  unthresholded recurrence plot **15**
  vertical line **20**, 26–33, 50, 52
  windowed recurrence plot **15**
recurrence quantification 13, **22–26**
  application **45–47**, 48–53, 68
  determinism **23**
  diagonal line length **24**
  distribution of diagonal lines **23**
  divergence **24**
  entropy **24**
  laminarity **27**, 50, 52
  percent recurrence **22**
  prediction time **24**
  ratio **25**
  recurrence rate **22**
  software **43–45**
  time dependent **22**
  trapping time **27**, 50, 52
  trend **25**
recurrence rate *see* recurrence quan-

tification
RQA *see* recurrence quantification

sampling rate **4**
state **3**
laminar state 20, **27**, 32, 50, 53
recurrence *see* recurrence
state variable **4**, 36
time evolution **4**, 18, 19

tangential motion *see* phase space
threshold **9**
choice **11–12**
corridor threshold **13**
time delay *see* embedding
trajectory *see* phase space
recurrence *see* recurrence
similarity **37–39**, 55–68
tangential motion *see* phase space
time evolution *see* state
transitions 21, **22**, 25
chaos-chaos transitions **27**, 32, 33, 48, 53
chaos-order transitions **22**
trapping time *see* recurrence quantification
trend *see* recurrence quantification

unstable periodic orbits 14, 22, **25**, 34

Appendix A

Recurrence Plot Based Measures of Complexity and their Application to Heart Rate Variability Data

MARWAN, N., WESSEL, N., KURTHS, J., Recurrence Plot Based Measures of Complexity and its Application to Heart Rate Variability Data. Physical Review E 66 (2), 2002, 026702. DOI: 10.1103/PhysRevE.66.026702

Recurrence-plot-based measures of complexity and their application to heart-rate-variability data

Norbert Marwan,[1]* Niels Wessel,[1] Udo Meyerfeldt,[2] Alexander Schirdewan,[2] and Jürgen Kurths[1]
[1]*Nonlinear Dynamics Group, Institute of Physics, University of Potsdam, Potsdam 14415, Germany*
[2]*Franz-Volhard-Hospital, HELIOS Kliniken Berlin, Charité, Humboldt University Berlin, Wiltbergstrasse 50, 13125 Berlin, Germany*
(Received 7 January 2002; published 6 August 2002)

The knowledge of transitions between regular, laminar or chaotic behaviors is essential to understand the underlying mechanisms behind complex systems. While several linear approaches are often insufficient to describe such processes, there are several nonlinear methods that, however, require rather long time observations. To overcome these difficulties, we propose measures of complexity based on vertical structures in recurrence plots and apply them to the logistic map as well as to heart-rate-variability data. For the logistic map these measures enable us not only to detect transitions between chaotic and periodic states, but also to identify laminar states, i.e., chaos-chaos transitions. The traditional recurrence quantification analysis fails to detect the latter transitions. Applying our measures to the heart-rate-variability data, we are able to detect and quantify the laminar phases before a life-threatening cardiac arrhythmia occurs thereby facilitating a prediction of such an event. Our findings could be of importance for the therapy of malignant cardiac arrhythmias.

DOI: 10.1103/PhysRevE.66.026702 PACS number(s): 07.05.Kf, 05.45.Tp, 87.80.Tq, 87.19.Hh

I. INTRODUCTION

Numerous scientific disciplines, such as astrophysics, biology or geosciences, use data analysis techniques to get an insight into the complex processes observed in nature [1–3], which show generally a nonstationary and complex behavior. As these complex systems are characterized by different transitions between regular, laminar, and chaotic behaviors, the knowledge of these transitions is necessary for understanding the process. However, observational data of these systems are typically rather short. Linear approaches of time series analysis are often not sufficient [4,5] and most of the nonlinear techniques (cf. [6,7]), such as fractal dimensions or Lyapunov exponents [7–10], suffer from the curse of dimensionality and require rather long data series. The uncritical application of these methods, especially to natural data, can therefore be very dangerous and it often leads to serious pitfalls.

To overcome these difficulties other measures of complexity have been proposed, such as the Renyi entropies, the effective measure complexity, the ε complexity or the renormalized entropy [11,12]. They are mostly based on symbolic dynamics and are efficient quantities for characterizing measurements of natural systems, such as in cardiology [13–15], cognitive psychology [16] or astrophysics [17–19]. In this paper we focus on another type of measure of complexity, which is based on the method of recurrence plots (RP's). This approach has been introduced for the analysis of nonstationary and rather short data series [20–22]. Moreover, a quantitative analysis of recurrence plots has been proposed to detect typical transitions (e.g., bifurcation points) occurring in complex systems [23–25]. However, the quantities introduced so far are not able to detect more complex transitions, especially chaos-chaos transitions, which are also typical in nonlinear dynamical systems. Therefore in this paper we introduce measures of complexity based on recurrence plots, which allow us to identify laminar states and their transitions to regular as well as other chaotic regimes in complex systems. These measures make the investigation of intermittency of processes possible, even if they are only represented by short and nonstationary data series.

The paper is organized as follows. After a short review of the technique of recurrence plots and some measures, we introduce other measures of complexity based on recurrence plots. After that we apply this approach to the logistic equation and demonstrate the ability to detect chaos-chaos transitions. Finally, we apply this technique to heart-rate-variability data [26]. We demonstrate that by applying our proposed methods we are able to detect laminar phases before the onset of a life-threatening cardiac arrhythmia.

II. RECURRENCE PLOTS AND THEIR QUANTIFICATION

The method of RP was first introduced to visualize the time dependent behavior of the dynamics of systems, which can be pictured as a trajectory $\vec{x}_i \in \mathcal{R}^n$ $(i=1,\ldots,N)$ in the n-dimensional phase space [21]. It represents the recurrence of the phase space trajectory to a certain state, which is a fundamental property of deterministic dynamical systems [27,28]. The main step of this visualization is the calculation of the $N \times N$ matrix,

$$\mathbf{R}_{i,j} := \Theta(\varepsilon_i - \|\vec{x}_i - \vec{x}_j\|), \quad i,j=1,\ldots,N, \tag{1}$$

where ε_i is a cutoff distance, $\|\cdot\|$ is a norm (e.g., the Euclidean norm), and $\Theta(x)$ is the Heaviside function. The phase space vectors for one-dimensional time series u_i from observations can be reconstructed by using the Taken's time delay method, $\vec{x}_i=(u_i, u_{i+\tau}, \ldots, u_{i+(m-1)\tau})$ [7]. The dimension m can be estimated with the method of false nearest neighbors (theoretically, $m=2n+1$) [7,27]. The cutoff distance ε_i defines a sphere centered at $\vec{x}_i$. If $\vec{x}_j$ falls within this sphere, the state will be close to $\vec{x}_i$ and thus $\mathbf{R}_{i,j}=1$. These ε_i can be either constant for all $\vec{x}_i$ [22] or they can vary in such a way

*Electronic address: marwan@agnld.uni-potsdam.de

that the sphere contains a predefined number of close states [21]. In this paper a fixed ε_i and the Euclidean norm are used, resulting in a symmetric RP. The binary values in $R_{i,j}$ can be simply visualized by a matrix plot with the colors black (1) and white (0).

The recurrence plot exhibits characteristic large-scale and small-scale patterns that are caused by typical dynamical behavior [21,24], e.g., diagonals (similar local evolution of different parts of the trajectory) or horizontal and vertical black lines (state does not change for some time).

Zbilut and Webber have recently developed the recurrence quantification analysis (RQA) to quantify an RP [23–25]. They define measures using the recurrence point density and the diagonal structures in the recurrence plot, the *recurrence rate*, the *determinism*, the *maximal length of diagonal structures*, the *entropy*, and the *trend*. A computation of these measures in small windows moving along the main diagonal of the RP yields the time dependent behavior of these variables and, thus, makes the identification of transitions in the time series possible [23].

The RQA measures are mostly based on the distribution of the length of the diagonal structures in the RP. Additional information about further geometrical structures such as vertical and horizontal elements are not included. Gao has therefore recently introduced a recurrence time statistics that corresponds to vertical structures in an RP [29,30]. In the following, we extend this view on the vertical structures and define measures of complexity based on the distribution of the vertical line length. Since we are using symmetric RPs here, we will only consider the vertical structures.

III. MEASURES OF COMPLEXITY

We consider a point $\vec{x}_i$ of the trajectory and the set of its associated recurrence points $S_i := \{\vec{x}_k : \mathbf{R}_{i,k} = 1;\ k \in [1, \ldots, N-1]\}$. Denote a subset of these recurrence points $s_i := \{\vec{x}_l \in S_i : (\mathbf{R}_{i,l} \cdot \mathbf{R}_{i,l+1}) + (\mathbf{R}_{i,l} \cdot \mathbf{R}_{i,l-1}) > 0;\ l \in [1, \ldots, N],\ \mathbf{R}_{i,0} = \mathbf{R}_{i,N+1} := 0\}$, which contains the recurrence points forming the vertical structures in the RP at column *i*. In continuous time systems with high time resolution and with a not too small threshold ε, a large part of this set s_i usually corresponds to the sojourn points described in Refs. [29,30]. Although sojourn points do not occur in maps, the subset s_i is not necessarily empty. Next, we determine the length v of all connected subsets $\{\vec{x}_j \notin s_i; \vec{x}_{j+1}, \ldots, \vec{x}_{j+v} \in s_i; \vec{x}_{j+v+1} \notin s_i\}$ in s_i. $P_i(v) = \{v_l;\ l = 1,2, \ldots, L\}$ denotes the set of all occurring subset lengths in s_i and from $\cup_{i=1}^{N} P_i(v)$ we determine the distribution of the vertical line lengths $P(v)$ in the entire RP.

Analogous to the definition of the determinism [24,31], we compute the ratio between the recurrence points forming the vertical structures and the entire set of recurrence points,

$$\Lambda := \frac{\sum_{v=v_{min}}^{N} v P(v)}{\sum_{v=1}^{N} v P(v)}, \tag{2}$$

and call it *laminarity* Λ. The computation of Λ is realized for v that exceeds a minimal length v_{min}. For maps we use $v_{min} = 2$. Λ is the measure of the amount of vertical structures in the whole RP and represents the occurrence of laminar states in the system, without, however, describing the length of these laminar phases. It will decrease if the RP consists of more single recurrence points than vertical structures,

$$T := \frac{\sum_{v=v_{min}}^{N} v P(v)}{\sum_{v=v_{min}}^{N} P(v)}, \tag{3}$$

and call it as *trapping time T*. The computation also uses the minimal length v_{min} as in Λ. The measure T contains information about the amount and the length of the vertical structures in the RP.

Finally, we use the maximal length of the vertical structures in the RP,

$$V_{max} = \max(\{v_l;\ l = 1,2, \ldots, L\}), \tag{4}$$

as a measure that is the analogue to the standard RQA measure L_{max} [24].

Although the distribution of the diagonal line lengths also contains information about the vertical line lengths, the two distributions are significantly different. In order to compare the measures proposed with the standard RQA measures, we apply them to the logistic map.

IV. APPLICATION TO THE LOGISTIC MAP

In order to investigate the potentials of Λ, T, and V_{max}, we first analyze the logistic map

$$x_{n+1} = a x_n (1 - x_n), \tag{5}$$

especially the interesting range of the control parameter $a \in [3.5,4]$ with a step width of $\Delta a = 0.0005$. Starting with the idea of Trulla *et al.* [23] to look for vertical structures, we are especially interested in finding the laminar states in chaos-chaos transitions. Therefore we generate for each control parameter a a separate time series. In the analyzed range of $a \in [3.5,4]$ various regimes and transitions between them occur, e.g., accumulation points, periodic, and chaotic states, band merging points, period doublings, and inner and outer crises [27,32,33].

A useful tool for studying the chaotic behavior is the recursively formed *supertrack functions*

$$s_{i+1}(a) = a s_i(a)[1 - s_i(a)], \quad s_0(a) = \frac{1}{2}, \tag{6}$$

which represent the functional dependence of stable states [33]. The intersection of $s_i(a)$ with $s_{i+j}(a)$ indicates the occurrence of a *j*-period cycle and the intersection of $s_i(a)$ with the fixed point $(1 - 1/a)$ of Eq. (5) indicates the point of an unstable singularity, i.e., laminar behavior (Fig. 1, inter-

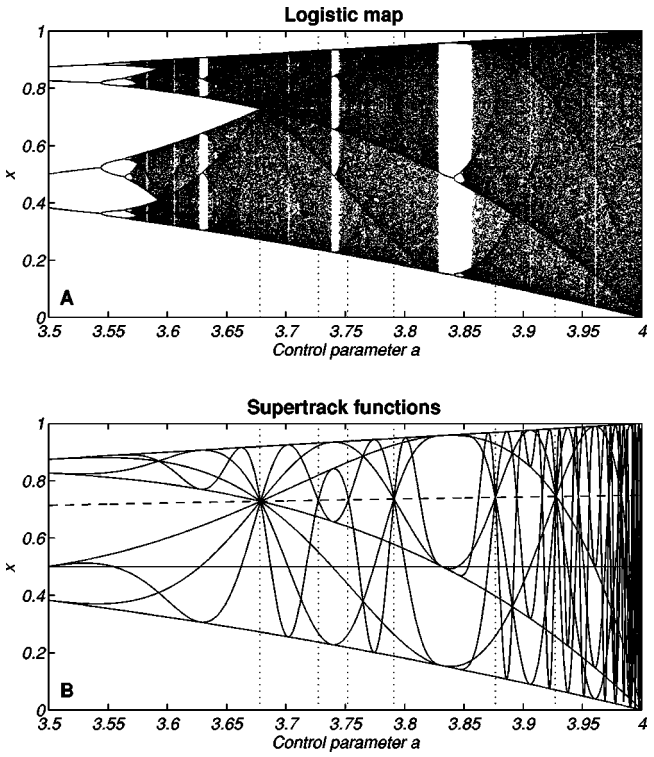

FIG. 1. (a) Bifurcation diagram of the logistic map. (b) Low ordered supertrack functions $s_i(a)(i=1,\ldots,10)$ and the fixed point of the logistic map $1-1/a$ (dashed). Their intersections represent periodic windows, band merging, and laminar states. The vertical dotted lines show a choosing of points of band merging and laminar behavior ($a=3.678$, 3.727, 3.752, 3.791, 3.877, 3.927).

section points are marked with dotted lines). For each a we compute a time series of the length $N=2000$. In order to exclude transient responses we use the last 1000 values of these data series in the following analysis.

We compute the RP after embedding the time series with a dimension of $m=1$, a delay of $\tau=1$, and a cutoff distance of $\varepsilon=0.1$ (in units of the standard deviation σ). Since the considered example is a one-dimensional map, $m=1$ is sufficient. In general, a too small embedding leads to false recurrences, that are expressed in numerous vertical structures and diagonals from the upper left corner to the lower right corner [30]. In contrast, an overembedding should theoretically not distort the reconstructed phase trajectory. Whereas false recurrences and overembedding do not strongly influence the measures based on diagonal structures [30], the measures based on vertical structures are, in general, much more sensitive to the embedding. This is due to the fact that the embedding method causes higher-order correlations in the phase-space trajectory, which will be of course visible in the RP. A theoretical and more detailed explanation of this effect within the analysis of RPs is in preparation and beyond the scope of this paper. For the logistic map, however, an increasing of m slightly amplifies the peaks of the vertical based complexity measures (up to $m=3$), but it does not change the result significantly. The cutoff distance ε is selected to be 10% of the diameter of the reconstructed phase space. Smaller values would lead to a better distinction of small variations (e.g., the range before the accumulation point consists of small variations). However, the recurrence point density decreases in the same way and thus the statistics of continuous structures in the RP soon becomes insufficient. Larger values cause a higher recurrence point density, but a lower sensitivity to small variations.

A. Recurrence plots of the logistic map

For various values of the control parameter a we obtain RPs that already exhibit specific features (Fig. 2). Periodic states (e.g., in the periodic window of length 3 at $a=3.830$) cause continuous and periodic diagonal lines in the RP of width of 1. There are no vertical or horizontal lines [Fig. 2(a)]. Band merging points and other cross points of supertrack functions [e.g., $a=3.720$, Fig. 2(c)] represent states with short laminar behavior and cause vertically and horizontally spread black areas in the RP. The band merging at $a=3.679$ causes frequent laminar states and therefore a lot of vertically and horizontally spread black areas in the RP [Fig. 2(b)]. Fully developed chaotic states ($a=4$) cause a rather homogeneous RP with numerous single points and rare short diagonal or vertical lines [Fig. 2(d)].

B. Complexity measures of the logistic map

Now we compute the known RQA measures Δ, L_{max}, and in addition $\langle L\rangle$ (average length of diagonal lines) and our measures Λ, V_{max}, and T for the entire RP of each control parameter a. As expected, the known RQA measures Δ, L_{max}, and $\langle L\rangle$ clearly detect the transitions from chaotic to periodic sequences and vice versa [Figs. 3(a), 3(c), and 3(e)] [23]. However, it seems that one cannot get more information than the periodic-chaotic/ chaotic-periodic transitions. Near the supertrack crossing points (band merging points included), e.g., $a=3.678$, 3.791, 3.927, there are no significant indications in these RQA measures. They clearly identify the bifurcation points (periodic-chaotic/chaotic-periodic transitions), without, however, finding the chaos-chaos transitions and the laminar states.

Calculating the vertical based measures Λ and T, we are able to find the periodic-chaotic/ chaotic-periodic transitions and the laminar states [Figs. 3(b) and 3(f)]. The occurrence of vertical lines starts shortly before the band merging from two to one band at $a=3.678\ldots$.

For smaller a values the consecutive points jump between the two bands and it is therefore impossible to obtain a laminar behavior. A longer persistence of states is not possible until all bands are merged. However, due to the finite range of neighborhood searching in the phase space, vertical lines occur before this point.

Vertical lines occur much more frequently at supertrack crossing points (band merging points included) than in other chaotic regimes, which is revealed by Λ [cf. Fig. 3(b), again, supertrack crossing points are marked with dotted lines]. As in the states before the merging from two to one band, vertical lines are not found within periodic windows, e.g., $a=3.848$. The mean of the distribution of v is the introduced measure T [Fig. 3(f)]. It will vanish if a is smaller than the point of merging from two to one band. T increases at those

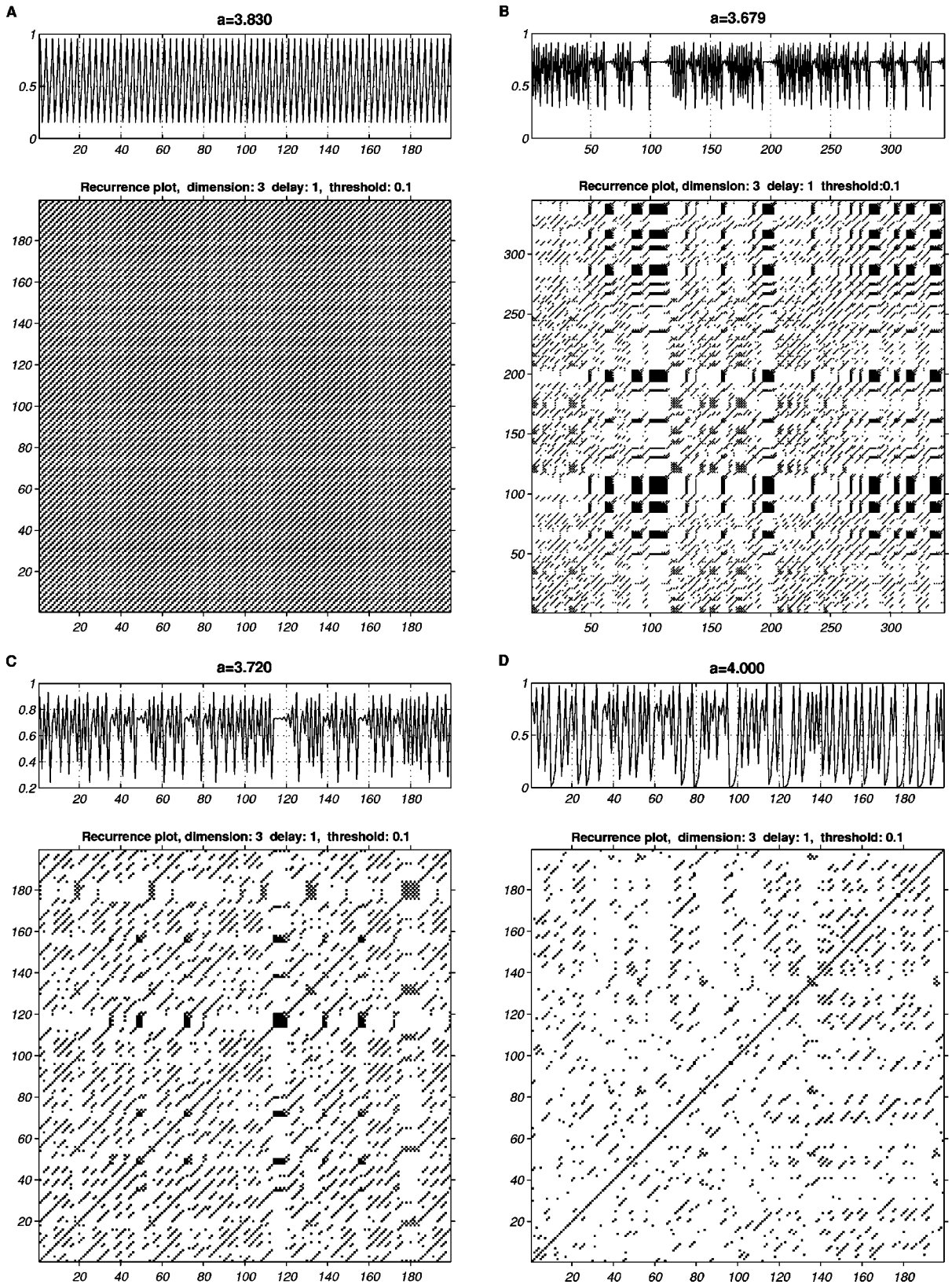

FIG. 2. Recurrence plots (RPs) of the logistic map for various control parameters a, near different qualitative changes: 3-period window $a=3.830$ (a); band merging $a=3.679$ (b); supertrack intersection $a=3.720$ (c); and chaos (exterior crisis) $a=4$ (d), with embedding dimension $m=1$, time delay $\tau=1$, and distance cutoff $\varepsilon=0.1\sigma$.

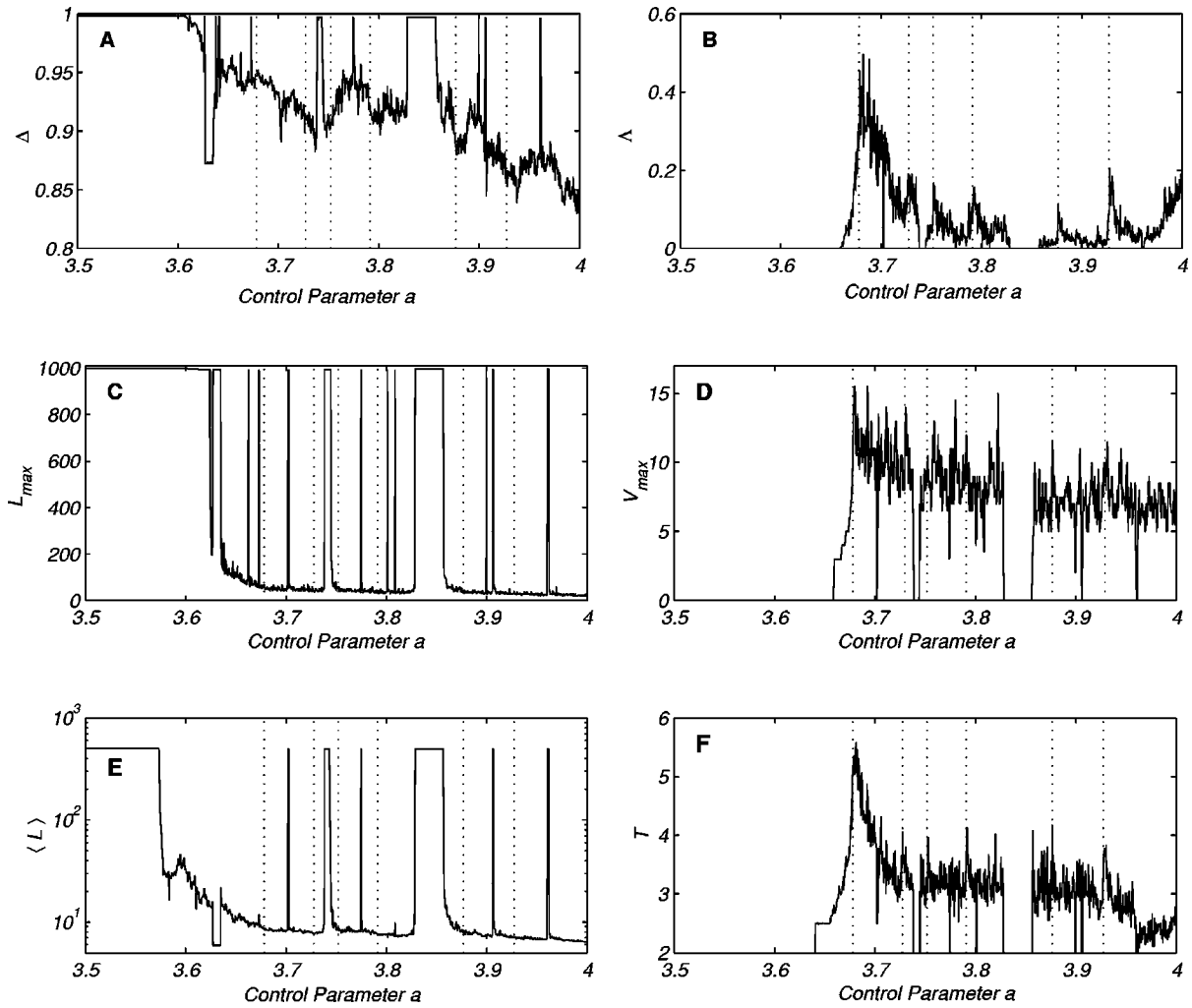

FIG. 3. Selected RQA parameters Δ, L_{max}, and $\langle L \rangle$ and the measures Λ, V_{max}, and T. The vertical dotted lines show some of the points of band merging and laminar behavior (cf. Fig. 1), whereby not all of them have been marked. Whereas Δ (a), L_{max} (c), and $\langle L \rangle$ (e) show periodic-chaotic/ chaotic-periodic transitions (maxima), Λ (b), V_{max} (d), and T (f) exhibit in addition to those transitions (minima) chaotic-chaotic transitions (maxima). The differences between Λ and V_{max} are caused by the fact that Λ measures only the amount of laminar states, whereas V_{max} measures the maximal duration of the laminar states. Although some peaks of V_{max} and T are not at the dotted lines, they correspond to laminar states (not all can be marked).

points where more low ordered supertrack functions are crossing [Fig. 3(f)]. This corresponds to the occurrence of laminar states. Although V_{max} also reveals laminar states, it is quite different from the other two measures, because it gives the maximum of all of the durations of the laminar states. However, periodic states are also associated with vanishing T and V_{max}. Hence, the vertical length based measures yield periodic-chaotic/chaotic-periodic as well as chaos-chaos transitions (laminar states).

We have also computed Λ, V_{max}, and T for the logistic map with transients using the same approach as described in [23]. The qualitative statement of the measures is the same as above.

V. APPLICATION TO HEART-RATE-VARIABILITY DATA

Heart-rate variability (HRV) typically shows a complex behavior and it is difficult to identify disease specific patterns [34]. A fundamental challenge in cardiology is to find early signs of ventricular tachyarrhythmias (VT) in patients with an implanted cardioverter-defibrillator (ICD) based on HRV data [26,35–37]. Therefore standard HRV parameters from time and frequency domains [38], parameters from symbolic dynamics [13,14] as well as the finite-time growth rates [39] were applied to the data of a clinical pilot study [26]. Using two nonlinear approaches, we have recently found significant differences between control and VT time series based mainly on laminar phases in the data before a VT. Therefore the aim of this investigation is to test whether our RP approach is suitable to identify and quantify these laminar phases.

The defibrillators used in the study cited (PCD 7220/ 7221, Medtronic) are able to store at least 1000 beat-to-beat intervals prior to the onset of VT (10-ms resolution), corresponding to approximately 9–15 min. We reanalyze these intervals from 17 chronic heart failure ICD patients just before the onset of a VT and at a control time, i.e., without a following arrhythmic event. Time series including more than

TABLE I. Results of maximal diagonal and vertical line length shortly before VT and at control time, and nonparametric Mann-Whitney *U*-test: *p* represents significance; * is for $p<0.05$; ** for $p<0.01$; ns for not significant, $p\geqslant 0.05$.

m	ε	VT	Control	p
		Maximal diagonal line length L_{max}		
3	77	396.6±253.8	261.5±156.6	ns
6	110	447.6±269.1	285.5±160.4	*
9	150	504.6±265.9	311.6±157.2	*
12	170	520.7±268.8	324.7±180.2	*
		Maximal vertical line length V_{max}		
3	77	261.4±193.5	169.2±135.9	*
6	110	283.7±190.4	179.5±134.1	**
9	150	342.4±193.6	216.1±137.1	**
12	170	353.5±221.4	215.1±138.6	**

one nonsustained VT, with induced VTs, pacemaker activity or more than 10% of ventricular premature beats are not considered in this analysis. Some patients had several VTs; we finally had 24 time series with a subsequent VT and the respective 24 control series without a life-threatening arrhythmia. In order to analyze only the dynamics occurring just before a VT, the beat-to-beat intervals of the VT itself at the end of the time series are removed from the tachograms.

We calculate all standard RQA parameters described in Ref. [24] as well as the measures laminarity Λ, trapping time T, and maximal vertical line length V_{max} (similar to the maximal diagonal line length L_{max}) for different embedding dimensions m and nearest neighboring radii ε. We find differences between both groups of data for several of the parameters mentioned above. However, the most significant parameters are V_{max} and L_{max} for rather large radii (Table I). The vertical line length V_{max} is more powerful in discriminating both groups than the diagonal line length L_{max}, as can be recognized by the higher p values for V_{max} (Table I). Figure 4 gives a typical example of the recurrence plots before a VT and at a control time with an embedding of 6 and a radius of 110. The RP before a life-threatening arrhythmia is characterized by large black rectangles ($V_{max}=242$ here), whereas the RP from the control series shows only small rectangles ($V_{max}=117$).

VI. SUMMARY

We have introduced three more RPs based measures of complexity, the laminarity Λ, the trapping time T, and the maximal length of vertical structures in the RP, V_{max}. These

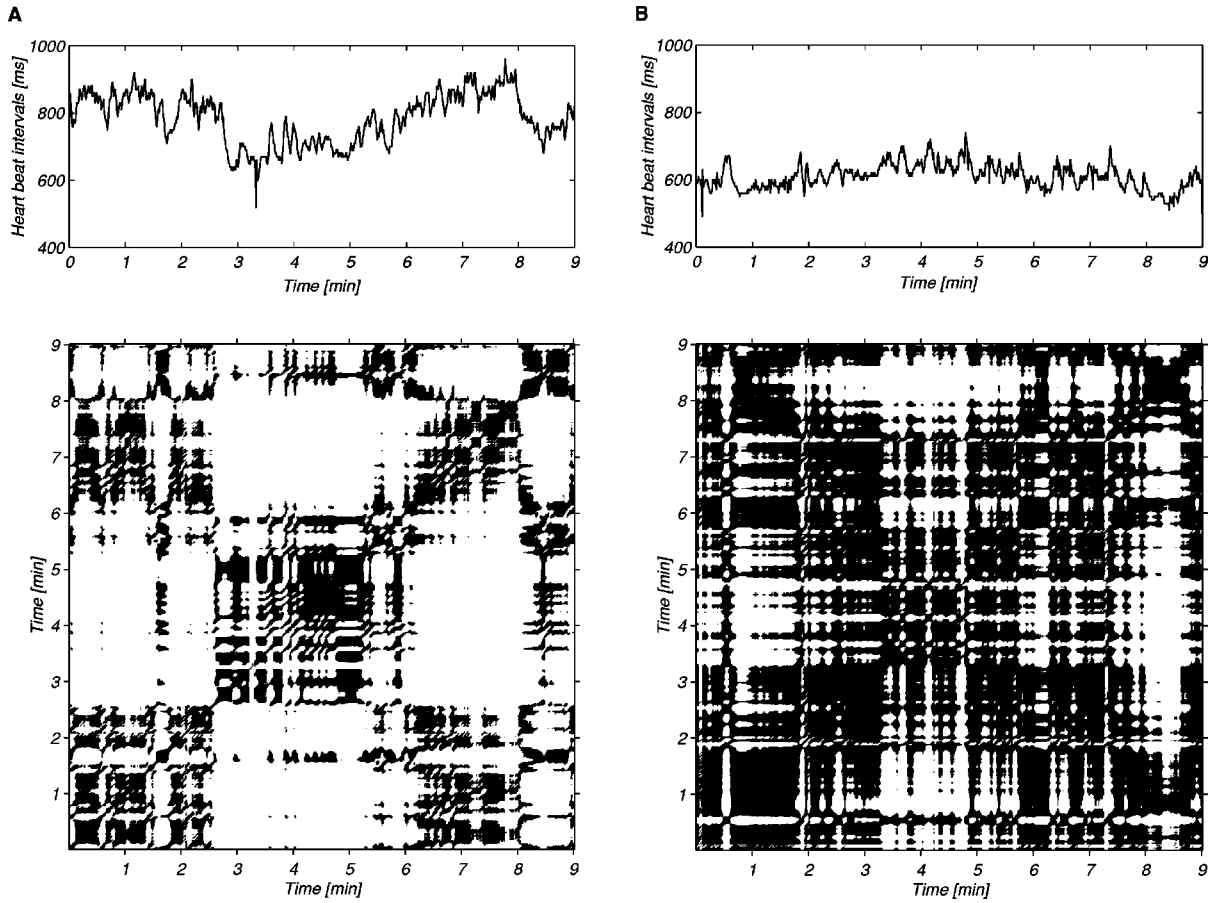

FIG. 4. Recurrence plots of the heart beat interval time series at a control time (a) and before a VT (b) with an embedding of 6 and a radius of 110. The RP before a life-threatening arrhythmia is characterized by big black rectangles, whereas the RP from the control series shows only small rectangles.

measures of complexity have been applied to the logistic map and heart-rate-variability data. In contrast to the known RQA measures [23,25], that are able to detect transitions between chaotic and periodic states (and vice versa), our measures enable us to identify laminar states too, i.e., chaos-chaos transitions. These measures are provided by the vertical lines in recurrence plots. The occurrence of vertical (and horizontal) structures is directly related to the occurrence of laminar states.

The laminarity Λ enables us generally to detect laminar states in a dynamical system. The trapping time T contains information about the frequency of the laminar states and their lengths. The maximal length V_{max} reveals information about the time duration of the laminar states thus making the investigation of intermittency possible.

If the embedding of the data is too small, it will lead to false recurrences, which is expressed in numerous vertical structures and diagonals perpendicular to the main diagonal. Whereas false recurrences do not influence the measures based on diagonal structures, the measures based on vertical structures are sensitive to it.

The application of these measures to the logistic equation for a range of various control parameters has revealed points of laminar states without any additional knowledge about the characteristic parameters or dynamical behavior of the specific systems. Nevertheless, Λ, V_{max}, and T are different in their magnitudes. Further investigations are necessary to understand all relations between the magnitudes of V_{max} and the recognized chaos-chaos transitions.

The application of these complexity measures to the ICD stored heart-rate data before the onset of a life-threatening arrhythmia seems to be very successful for the detection of laminar phases thus making a prediction of such VT possible. The differences between the VT and the control series are more significant than in Ref. [26]. However, two limitations of this study are the relatively small number of time series and the reduced statistical analysis (no subdivisions concerning age, sex, and heart disease). For this reason, our results should to be validated on a larger database. Furthermore, this investigation could be enhanced for tachograms including more than 10% ventricular premature beats. In conclusion, this study has demonstrated that the RQA based complexity measures could play an important role in the prediction of VT events even in short term HRV time series.

Many biological data contain epochs of laminar states, which can be detected and quantified by the RP based measures. We have demonstrated differences between the measures based on the vertical and the diagonal structures and therefore we suggest the use of the method proposed in this paper in addition to the traditional measures.

A download of the Matlab implementation is available at www.agnld.uni-potsdam.de/~ marwan

ACKNOWLEDGMENTS

This work was partly supported by the priority program SPP 1097 of the German Science Foundation (DFG). We gratefully acknowledge M. Romano, M. Thiel, and U. Schwarz for fruitful discussions.

[1] L. Glass, Nature (London) **410**, 277 (2001).
[2] B. Blasius, A. Huppert, and L. Stone, Nature (London) **399**, 354 (1999).
[3] K. B. Marvel, Nature (London) **411**, 252 (2001).
[4] A. L. Goldberger, D. R. Rigney, J. Mietus, E. M. Antman, and S. Greenwald, Experientia **44**, 983 (1988).
[5] L. Glass and D. Kaplan, Med. Prog. Technol. **19**, 115 (1993).
[6] H. D. I. Abarbanel, R. Brown, J. J. Sidorowich, and L. S. Tsimring, Rev. Mod. Phys. **65**, 1331 (1993).
[7] H. Kantz and T. Schreiber, *Nonlinear Time Series Analysis* (Cambridge University Press, Cambridge, England, 1997).
[8] J. Kurths and H. Herzel, Physica D **25**, 165 (1987).
[9] B. B. Mandelbrot, *The Fractal Geometry of Nature* (Freeman, San Francisco, 1982).
[10] A. Wolf, J. B. Swift, H. L. Swinney, and J. A. Vastano, Physica D **16**, 285 (1985).
[11] R. Wackerbauer, A. Witt, H. Atmanspacher, J. Kurths, and H. Scheingraber, Chaos, Solitons Fractals **4**, 133 (1994).
[12] P. E. Rapp, C. J. Cellucci, K. E. Korslund, T. A. Watanabe, and M. A. Jimenez-Montano, Phys. Rev. E **64**, 016209 (2001).
[13] J. Kurths, A. Voss, A. Witt, P. Saparin, H. J. Kleiner, and N. Wessel, Chaos **5**, 88 (1995).
[14] A. Voss, J. Kurths, H. J. Kleiner, A. Witt, N. Wessel, P. Saparin, K. J. Osterziel, R. Schurath, and R. Dietz, Cardiovasc. Res. **31**, 419 (1996).
[15] N. Wessel, A. Voss, J. Kurths, A. Schirdewan, K. Hnatkova, and M. Malik, Med. Biol. Eng. Comput. **38**, 680 (2000).
[16] R. Engbert, M. S. C. Scheffczyk, J. Kurths, R. Krampe, R. Kliegl, and F. Drepper, Nonlin. Anal. Theor. Meth. Appl. **30**, 973 (1997).
[17] A. Hempelmann and J. Kurths, Astron. Astrophys. **232**, 356 (1990).
[18] U. Schwarz, A. O. Benz, J. Kurths, and A. Witt, Astron. Astrophys. **277**, 215 (1993).
[19] A. Witt, J. Kurths, F. Krause, and K. Fischer, Geophys. Astrophys. Fluid Dyn. **77**, 79 (1994).
[20] M. C. Casdagli, Physica D **108**, 12 (1997).
[21] J.-P. Eckmann, S. O. Kamphorst, and D. Ruelle, Europhys. Lett. **5**, 973 (1987).
[22] M. Koebbe and G. Mayer-Kress, in *Proceedings of SFI Studies in the Science of Complexity. Nonlinear Modeling and Forecasting*, edited by M. Casdagli and S. Eubank (Addison-Wesley, Redwood City, CA, 1992), Vol. XXI, pp. 361–378.
[23] L. L. Trulla, A. Giuliani, J. P. Zbilut, and C. L. Webber, Jr., Phys. Lett. A **223**, 255 (1996).
[24] C. L. Webber, Jr., and J. P. Zbilut, J. Appl. Physiol. **76**, 965 (1994).
[25] J. P. Zbilut and C. L. Webber Jr., Phys. Lett. A **171**, 199 (1992).
[26] N. Wessel, C. Ziehmann, J. Kurths, U. Meyerfeldt, A. Schirdewan, and A. Voss, Phys. Rev. E **61**, 733 (2000).

[27] J. H. Argyris, G. Faust, and M. Haase, *An Exploration of Chaos* (North-Holland, Amsterdam, 1994).
[28] E. Ott, *Chaos in Dynamical Systems* (Cambridge University Press, Cambridge, 1993).
[29] J. B. Gao, Phys. Rev. A **83**, 3178 (1999).
[30] J. B. Gao and H. Q. Cai, Phys. Lett. A **270**, 75 (2000).
[31] N. Marwan, Master's thesis, Dresden University of Technology, Dresden, 1999.
[32] P. Collet and J.-P. Eckmann, *Iterated Maps on the Interval as Dynamical Systems* (Birkhäuser, Basel, 1980).
[33] E. M. Oblow, Phys. Lett. A **128**, 406 (1988).
[34] A. Schumann, N. Wessel, A. Schirdewan, K. J. Osterziel, and A. Voss, Stat. Med. (to be published).
[35] J. O. Diaz, T. H. Makikallio, H. V. Huikuri, G. Lopera, R. D. Mitrani, A. Castellanos, R. J. Myerburg, L. P. Rozo, F. Pava, and C. A. Morillo, Am. J. Cardiol. **87**, 1123 (2001).
[36] H. V. Huikuri and T. H. Makikallio, Auton. Neurosci. **90**, 95 (2001).
[37] S. Guzzetti, R. Magatelli, E. Borroni, and S. Mezzetti, Auton. Neurosci. **90**, 102 (2001).
[38] Task Force of the European Society of Cardiology and the North American Society of Pacing and Electrophysiology, Circulation **93**, 1043 (1996).
[39] J. M. Nese, Physica D **35**, 237 (1989).

Appendix B

Extended Recurrence Plot Analysis and its Application to ERP Data

MARWAN, N., MEINKE, A., Extended recurrence plot analysis and its application to ERP data. International Journal of Bifurcation and Chaos "Cognition and Complex Brain Dynamics" 14 (2), 2004, in press.

Extended Recurrence Plot Analysis and its Application to ERP Data

Norbert Marwan[1,*], Anja Meinke[2]

[1] Nonlinear Dynamics Group, Institute of Physics,
University of Potsdam, Potsdam 14415, Germany
[2] Institute of Linguistics,
University of Potsdam, Potsdam 14415, Germany

September 18, 2002

Abstract

We present new measures of complexity and their application to event related potential data. The new measures base on structures of recurrence plots and makes the identification of chaos-chaos transitions possible. The application of these measures to data from single-trials of the Oddball experiment can identify laminar states therein. This offers a new way of analyzing event-related activity on a single-trial basis.

1 Introduction

Neurons are known to be nonlinear devices because they become activated when their somatic membrane potential crosses a certain threshold [Kandel et al., 1995]. This nonlinearity is one of the essentials in neural modelling which leads to the sigmoidal activation functions of neural networks [Amit, 1989]. The activity of large formations of neurons is macroscopically measurable as the electroencephalogram (EEG) at the human scalp which results from a spatial integration of postsynaptic potentials [Nunez, 1981]. However, it is an unsolved problem whether the EEG should be treated as a time series stemming from a linear or a nonlinear dynamical system. Applying nonlinear techniques of data analysis to EEG measurements has a long tradition. Most of these efforts have been done by computing the correlation dimension of spontaneous EEG [e. g. Babloyantz et al., 1985; Rapp et al., 1986; Gallez and Babloyantz, 1991; Lutzenberger et al., 1992; Pritchard and Duke, 1992]. Theiler et al. [1992] applied the technique of surrogate data to correlation dimensions of EEG and reported that there is no evidence of low-dimensional chaos but of significance for nonlinearity in the data.

*email: marwan@agnld.uni-potsdam.de

While correlation dimensions are only well defined for stationary time series generated by a low-dimensional dynamical system moving around an attractor, these measures fail in investigating event-related brain potentials [ERPs, Sutton et al., 1965] since they are nonstationary by definition. Traditionally, ERP waveforms are determined by computing an ensemble average over a collection of stimulus time locked EEG trials. This is based on the following assumptions: (1) the presentation of stimuli of the same kind is followed by the same sequence of processing steps, (2) these processing steps always lead to activation of the same brain structures, (3) this activation always elicits the same pattern of electrophysiological activity, which can be measured at the scalp [Rösler, 1982] and (4) spontaneous activity is stationary and ergodic [beim Graben et al., 2000].

By averaging the data-points time-locked to the stimulus presentation (cf. Oddball experiment) it is possible to filter out the signal (ERP) of the noise (spontaneous activity). In the next step the functional significance of a component is assessed. Antecedent conditions of the occurrence of a component and variables, which influence its parameters are defined. Now the commonalities of these factors are identified. The generalization of all empirically found influencing factors leads to a more abstract cognitive theory of the functional meaning of a event-related potential component and makes it usable for the validation of models of cognitive processes.

The disadvantage of the averaging method is the high number of trials needed to reduce the signal-to-noise-ratio [Kutas and Petten, 1994]. This is crucial for example for clinical studies, for studies with children and for studies, in which repeating a task would influence the performance. So it is desirable to find new ways of analyzing event-related activity on a single-trial basis. Applying nonlinear methods to electrophysiological data could be one way of dealing with this problem.

To compute dimensions of ERPs, Molnár et al. [1995] used the pointwise dimensions and reported a drop of the pointwise dimension as a function of time corresponding to the P300 component observed in the Oddball experiment. Recently, concepts of information theory have been introduced to analyse ERPs. On one hand this is the wavelet entropy of Quiroga et al. [2001] and on the other hand symbolic dynamics of EEG and ERP [beim Graben et al., 2000; Frisch et al., 2002; Steuer, 2002; Schack, 2002].

A further promising approach is the recurrence quantification analysis (RQA), which is based on the quantification of the diagonal oriented structures in recurrence plots [RPs, Webber Jr. and Zbilut, 1994; Zbilut and Webber Jr., 1992]. The RQA was broadly applied in a wide field of the analysis of physiological data [e. g. Casdagli, 1997; Faure and Korn, 1998; Thomasson et al., 2001; Marwan et al., 2002]. The important advantage of methods based on the quantification of RPs is that the required data length can be relatively short. However, the measures of the classical RQA are only able to recognize transitions between periods and chaos and vice versa [Trulla et al., 1996]. In this work, we will use recently introduced additional measures based on RPs in order to find chaos-chaos transitions in physiological data. These new measures use the vertical structures in the RP and are able to identify laminar states [Marwan et al., 2002].

In the first section we will give a short introduction into RPs and their quantification analysis. In the next section we will introduce the new measures and finally we will apply them to event related potential data gained from the Oddball experiment.

2 Recurrence Plots and Their Quantification

The method of recurrence plots (RP) was introduced to visualize the time dependent behavior of the dynamics of systems, which can be pictured as a trajectory in the phase space [Eckmann et al., 1987]. It represents the recurrence of the m-dimensional phase space trajectory $\vec{x}_i \in \mathcal{R}^m$ ($i = 1, \ldots, N$, time discrete) to a certain state. The main step of this visualization is the calculation of the $N \times N$-matrix

$$\mathbf{R}_{i,\,j} := \Theta(\varepsilon_i - \|\vec{x}_i - \vec{x}_j\|), \quad i, j = 1 \ldots N, \tag{1}$$

where ε_i is a state dependent cut-off distance, $\|\cdot\|$ is the norm of vectors, Θ is the Heaviside function and N is the number of states. The phase space vectors for one-dimensional time series u_i from observations can be reconstructed with the Taken's time delay method $\vec{x}_i = (u_i, u_{i+\tau}, \ldots, u_{i+(m-1)\,\tau})$ with dimension m and delay τ [Kantz and Schreiber, 1997]. The recurrence plot exhibits characteristic large-scale and small-scale patterns which are caused by typical dynamical behavior [Eckmann et al., 1987; Webber Jr. and Zbilut, 1994], e. g. diagonals (similar local time evolution of different parts of the trajectory) or horizontal and vertical black lines (state does not change for some time).

Zbilut and Webber have developed the recurrence quantification analysis (RQA) to quantify an RP [Webber Jr. and Zbilut, 1994; Zbilut and Webber Jr., 1992]. They defined measures using the recurrence point density and *diagonal* structures in the recurrence plot, the recurrence rate RR (density of recurrence points), the determinism DET (ratio of recurrence points forming diagonal structures to all recurrence points), the maximal length of diagonal structures L_{max} (or their averaged length L), the Shannon entropy ENT of the distribution of the diagonal lengths and the trend $TREND$ (paling in the RP). The computation of these measures in shifted windows along the main diagonal of the RP enables one to find characteristic excursions of the trajectory in the phase space of the considered systems.

Trulla et al. have applied these measures in order to find transitions in dynamical systems [Trulla et al., 1996]. They have showed, that the RQA is able to find transitions between chaos and order (periodical states). But they could not find the chaos-chaos transitions.

3 Laminarity and Trapping Time

We have recently introduced two additional measures which are based on the *vertical* structures in the RP [Marwan et al., 2002]. We define these

measures analogous to the definition of DET and L, but we consider the distribution $P(v)$ of the length of the vertical structures in the RP.

First, the laminarity LAM

$$LAM := \frac{\sum_{v=2}^{N} vP(v)}{\sum_{v=1}^{N} vP(v)}, \tag{2}$$

is the ratio of recurrence points forming vertical structures to all recurrence points and represents the probability of occurrence of laminar states in the system, but it does not describe the length of these laminar phases. It will decrease if the RP consists of more single recurrence points than vertical structures.

Next, the trapping time TT

$$TT := \frac{\sum_{v=2}^{N} vP(v)}{\sum_{v=2}^{N} P(v)}, \tag{3}$$

is the averaged length of the vertical structures. The measure TT contains information about the amount and the length of the laminar phases.

The difference between these measures and the traditional RQA measures is their ability to find transitions between chaos and chaos [Marwan et al., 2002]. For example, such transitions can be found in the logistic map $x_{n+1} = a\, x_n\, (1 - x_n)$ with increasing control parameter $a \in [0, 4]$ and $x_n \in [0, 1] \subset \mathcal{R}$. For such trajectories $x(a)$ which contain laminar states (e. g. $a = 3.678, 3.791, 3.927$), LAM and TT show pronounced maxima (Fig. 1). The application of these measures to heart rate variability data, has shown, that they are able to detect and quantify laminar phases before a life-threatening cardiac arrhythmia and, thus, to enable a prediction of such an event [Marwan et al., 2002]. These findings can be of importance for the therapy of malignant cardiac arrhythmias.

In the next section we will apply this extended RQA to physiological data.

4 Event Related Potentials

4.1 The Oddball experiment

As mentioned in the Introduction, the Oddball experiment studies brain potentials during a stimulus presentation.

The measurement of the EEG was done with 31 electrodes/ channels (Tab. 1). The first 25 electrodes were localized as shown in Figure 2; the others were reference electrodes. The sample interval for the measurements was 4 ms.

Probands were seated in a dimly lit room in front of a monitor and were instructed to count tones of high pitch. Each subject was tested in nine blocks. The blocks varied in the probability of occurrence of the higher tones from 10 to 90 %. Each block contained at least 30 target tones. Response was

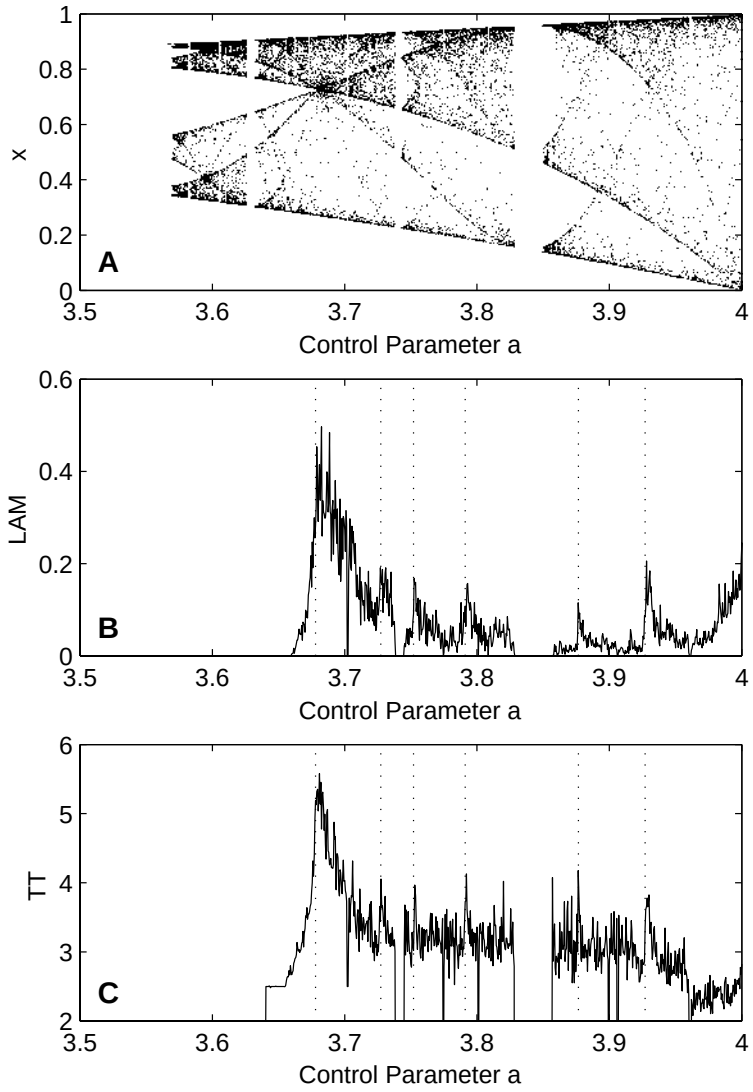

Figure 1: Laminarity (B) and trapping time (C) of time series gained from the logistic map for various control parameters (A). These measures reveal laminar and intermittent states. The vertical dotted lines show a choosing of points of band merging and laminar behaviour ($a = 3.678$, 3.727, 3.752, 3.791, 3.877, 3.927). The length of the data were $N = 1000$ and the embedding parameters were $m = 1$, $\tau = 1$ and $\varepsilon = 0.1$.

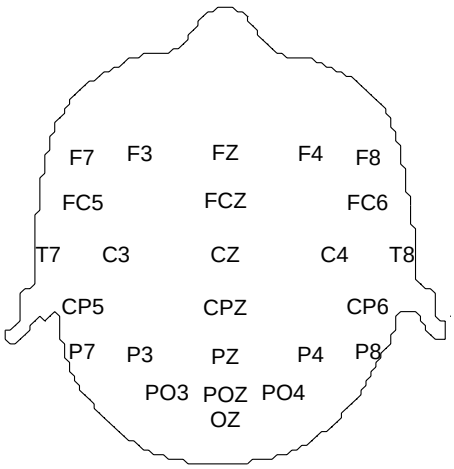

Figure 2: Localization of the electrodes on the head.

Table 1: Notation of the electrodes and their numbering as it is used in the figures (electrodes 26–31 are reference electrodes).

#	Electrode	#	Electrode
1	F7	14	T8
2	FC5	15	P7
3	F3	16	PZ
4	FZ	17	P3
5	F4	18	CZ
6	FC6	19	P4
7	F8	20	P8
8	T7	21	OZ
9	CP5	22	POZ
10	C3	23	PO3
11	FCZ	24	CPZ
12	C4	25	PO4
13	CP6		

given in a three alternative choice (using cursor keys of the keyboard). During the test, the EEG was recorded. The stimuli were computer-generated beeps of 100 ms length. Tones were either high (1400 Hz) or low (1000 Hz). They were presented with an interstimulus interval of 1000 ms.

After computing event-related voltage averages for the experimental manipulations (10 % up to 90 % target probability) one can observe a P300 ERP component whose amplitude is anti-correlated to the probability of the stimuli (surprise ERP, Fig. 3).

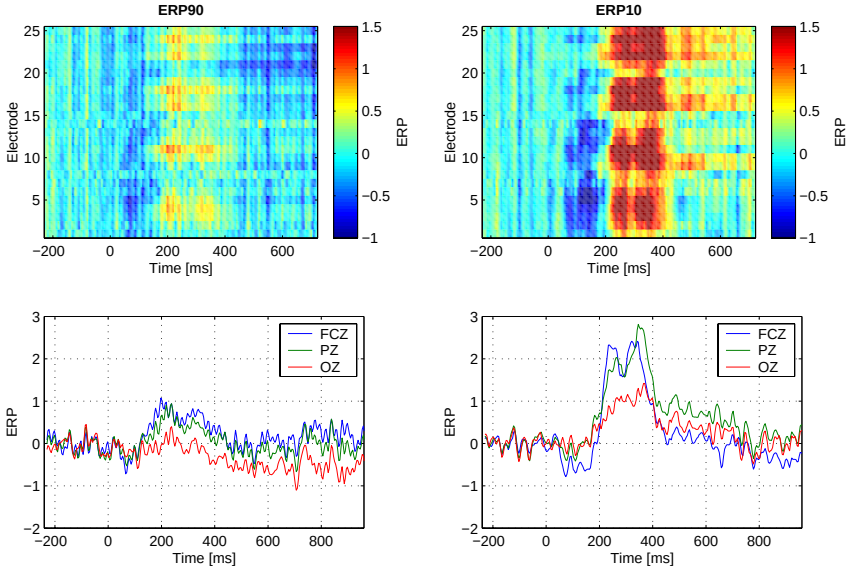

Figure 3: Mean event related potentials for event frequencies of 90 % (left, 40 trials) and 10 % (right, 31 trials). The N100 and P300 components are well pronounced for the frequencies of 10 %. The lower plots show the ERP of selected electrodes. The reference of the electrode numbers is given in Table 1.

The P300 component of the ERP was the first potential discovered to vary in dependence on subject-internal factors like attention and expectation instead of physical characteristics [Sutton et al., 1965]. The amplitude of the P300 component is highly sensitive to novelty of an event and its relevance. So this component is assumed to reflect the updating of the environmental model of the information processing system [context updating, Donchin, 1981; Donchin and Coles, 1988].

4.2 Data analysis

Our focus will be directed to the ERP data of two extreme event probabilities. Henceforth, the time (measured in ms) is denoted as t, the trial number as i and the electrode as e (the allocation of the electrode numbers with their notion, see Fig. 2).

The first set ERP90 contains 40 trials of ERP data for an event frequency of 90 % and the second set ERP10 contains 31 trials for an event frequency of 10 %. Both data sets can be rather well discriminated in the N100 and P300 components by the average over all trials (Fig. 3). As expected, both components have increased for lower event probabilities (ERP10). The maxima of the P300 are located around the central and central-parietal electrodes. However, the single trials do not obtain such a clear result. The P300 component is only well pronounced in 15 trials. When the single trials are observed, then extreme values can also occur in the ERP90 data and vanish in the ERP10 data (Fig. 4). We applied also a statistical variance-based T-test to the single trial ERP data. However, this method could also not clearly distinguish the single trials.

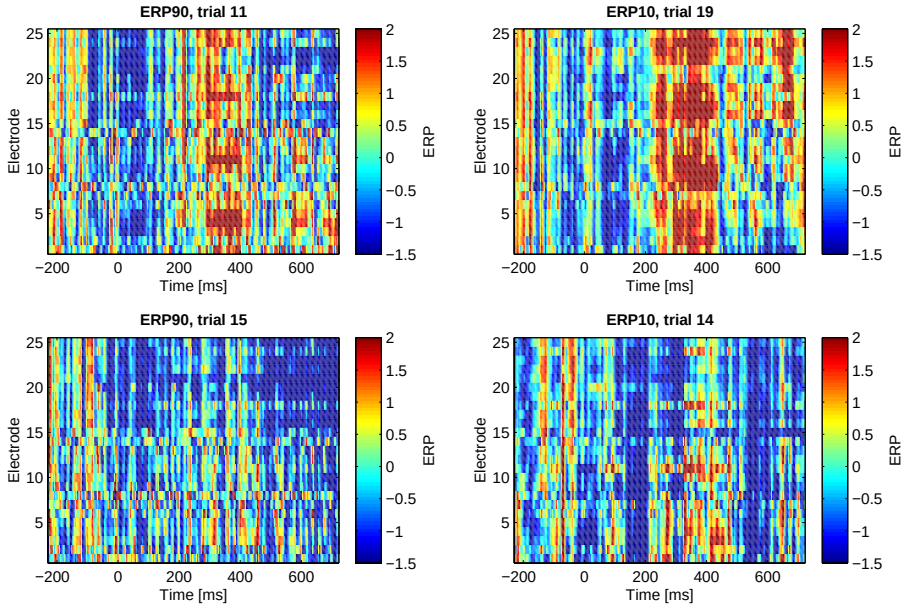

Figure 4: Event related potentials for selected trials of the event frequencies of 90 % (left) and 10 % (right). Both, ERP10 and ERP90 of single trials can be strongly or weakly pronounced, respectively, which makes their discrimination difficult. The reference of the electrode numbers are given in Table 1.

The recurrence quantification analysis (RQA) is based on the structures obtained by recurrence plots (RPs). The RPs were firstly computed for the means of ERP90 and ERP10 over all trials and then for the single trials. This was done with the embedding parameters $m = 3$, $\tau = 3$ and $\varepsilon = 10\,\%$ (fixed amount of nearest neighbours). The embedding parameters were estimated by using the standard methods false nearest neighbours (dimension) and mutual information (delay) [Kantz and Schreiber, 1997]. Due to the N100 and the P300 components in the data, the RPs show varying structures changing in time (Fig. 5). Diagonal structures and clusters of black points occur. The nonstationarity of the data around the N100 and P300 causes extended white bands along these times in the RPs. However,

the clustered black points around 300 ms occur in almost all RPs of the ERP10 data set.

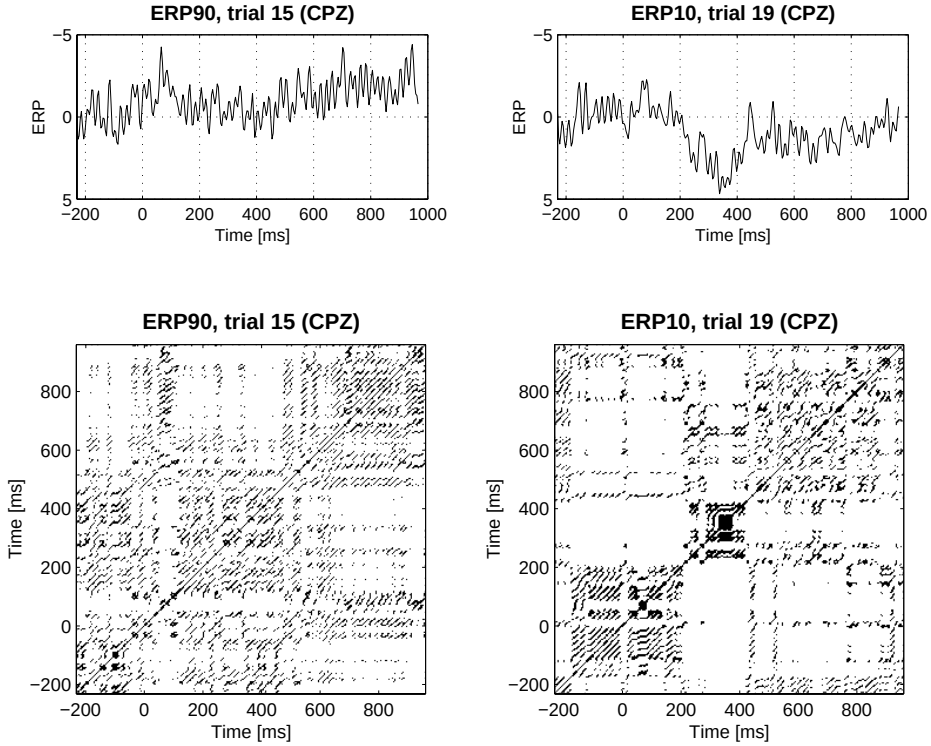

Figure 5: ERP data for event frequencies of 90 % (upper left) and 10 % (upper right), and their corresponding recurrence plots (lower plots). For the lower event frequency, more cluster of recurrence points occur at 100ms and 300ms.

The RQA was computed from the RPs of ERP90 and ERP10 for the single trials, in sliding windows over the RPs (which have the dimension $m = 3$) with a length of 240 ms and with a shifting step of 8 ms. This window length corresponds with a data length of 60 values.

The mean of all RQA variables of ERP10 reveal typical structures in the data (Fig. 6, right column). They indicate the transitions corresponding to the N100 and P300 components around the central electrodes. The RQA variables for the ERP90 do not reveal these transitions (Fig. 6, left column). The onset of the increasing of the parameter is about 120 ms before the event. This is due to the windowed analysis of the RPs (240 ms windows). We have chosen the middle of the RP window for the time, what results in a 120 ms earlier onset of the RQA variables.

The four RQA variables are quite different, especially in their amplitude. For ERP10, LAM and TT are the best pronounced parameter and have two distinct maxima at some electrodes; DET and L reveal these maxima at these electrodes too, but are lesser pronounced (Fig. 6). These maxima occur at the transition around 100 ms and 300 ms after the event and occur at the

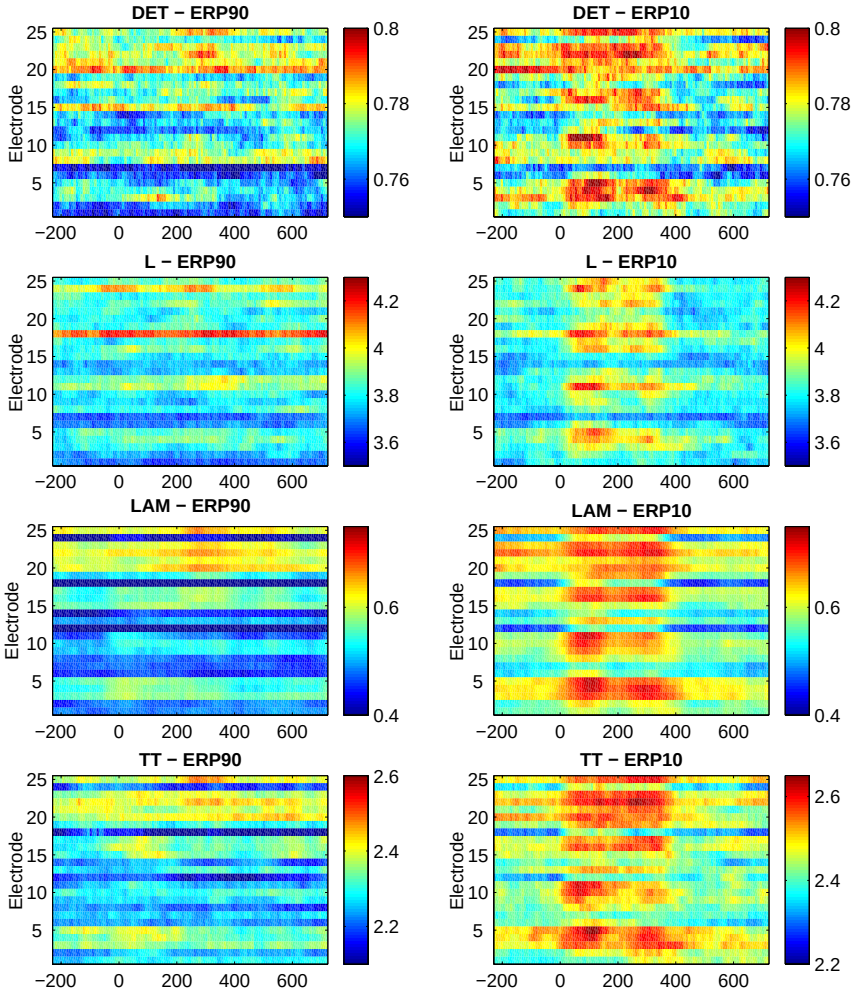

Figure 6: Averaged RQA measures for the ERP data of both event frequencies (averaged over all trials). Whereas the measures do not reveal any transitions in the ERP90 data, they clearly recognize the transitions for the ERP10 data.

electrodes F3, F4, FZ, C3, FCZ, PZ, POZ and PO3. Differences between the various transitions found by these measures also occur in time and brain locations (electrodes). But, the study was not detailed enough in order to give reliable results.

The analysis of the single trials achieves similar results (Figs. 7 and 8 show the results for selected trials). The LAM clearly found the N100 and P300 components for ERP10 in 26 trials (of 31), but not for the ERP90 trials. The other measures have lesser maxima and, thus, are not suitable for such recognition.

This result indicates that our introduced measures of complexity (especially LAM) are able to recognize transitions in brain potentials, which are caused by e. g. stimulative events. These transitions can be found in the single trials, which is an improvement to the classical method of averaging all observations.

5 Summary

We have applied an extended recurrence quantification analysis (RQA) to physiological event related potential data (ERP). The classical RQA consists of measures which are mainly based on diagonal structures in the recurrence plots (RPs), e. g. the determinism (DET), which is the ratio of recurrence points located on connected diagonal structures in the RP, and the averaged diagonal line length (L). We have extended the RQA with two recently introduced measures, the laminarity (LAM) and the trapping time (TT). These measures are analogously defined as DET and L, but provided by the vertical structures in recurrence plots. Whereas the classical RQA enables the identification of period-chaos transitions, the new measures make the identification of chaos-chaos transitions and laminar states possible.

The classical method to study ERP data is to average them over many trials. Our aim was to study the single trials in order to find transitions in the data.

The application of the extended RQA to ERP data has discriminated the single trials with a distinct P300 component due to a high surprise moment (less frequent events) against such trials with a low surprise moment (high frequent events). Considering the raw ERP10 data, the P300 component can only be found in the half of all trials. Also a statistical variance test fails to distinguish cleary the trials. The LAM is the most pronounced parameter in this analysis. It measures the ratio of recurrence points located on connected vertical structures in an RP. This structures correspond with laminarity within the underlying process. In the ERP data, the LAM reveals transitions from less laminar states to higher laminar states after the occurrence of the event and a transition from higher laminar states to less laminar states after about 400 ms. These transitions occur around bounded brain areas (parietal to frontal along the central axis). The comparable measures DET/ LAM and L/ TT are quite different in their am-

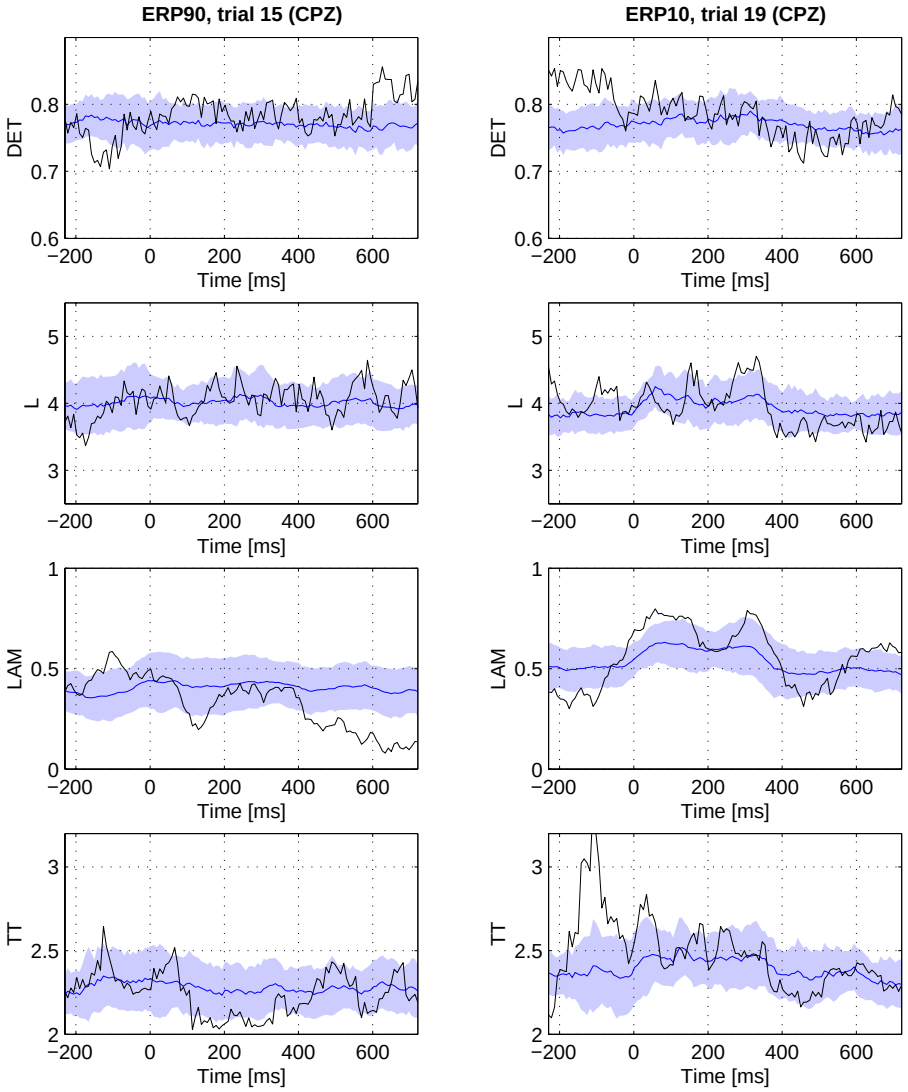

Figure 7: RQA measures for selected single trials and the central-parietal electrode (black). The trial-averaged RQA measures for the same electrode is shown in blue (the light blue band marks the 95 % significance interval).

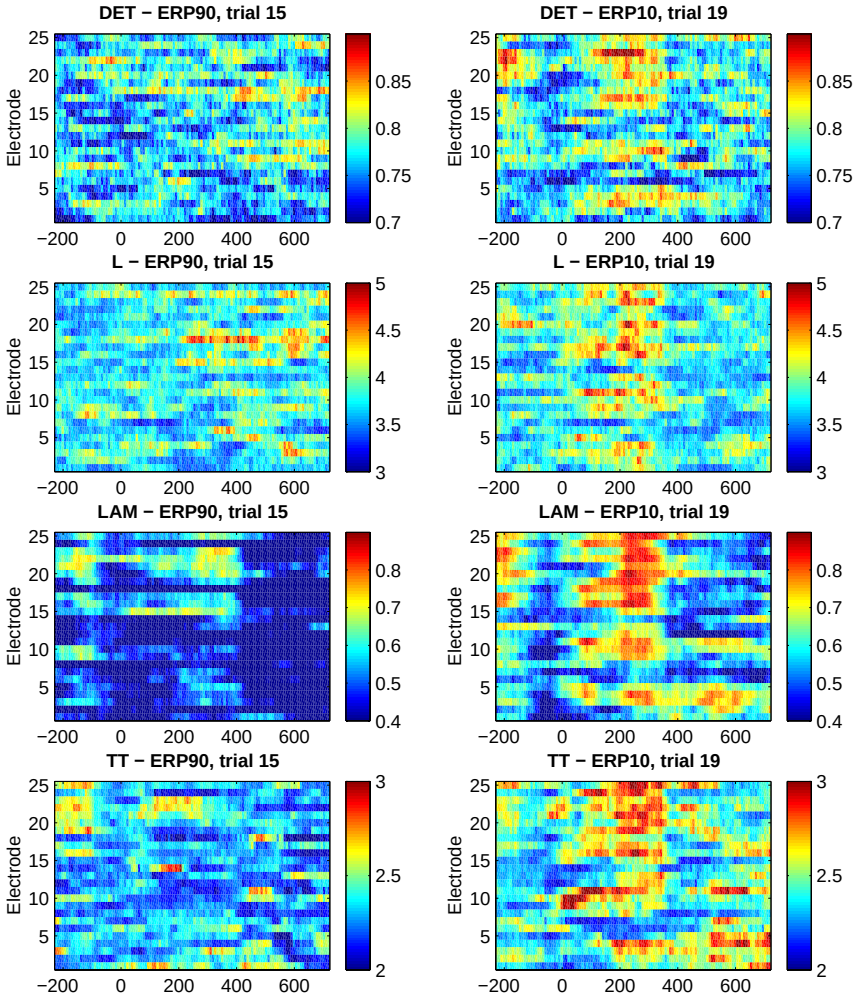

Figure 8: RQA measures for the same trials as in Fig. 7, but shown for all electrodes.

plitude. There should also be differences in time and brain location of the found transitions.

These results show that the measures based on vertical RP structures make the identification of transitions possible, which are not found by the classical RQA measures. They indicate transitions in the brain processes into laminar states due to the surprising moment of observed events.

A future work will be concerned with the development of a statistical evaluation of these results. Furthermore, this investigation has to be extended to ERP data gained from other frequent events and a detailed study of the comparable measures $DET/\,LAM$ and $L/\,TT$ should give hints about the different transitions in the brain processes.

6 Acknowledgments

This work was partly supported by the priority programme SPP 1097 of the German Science Foundation (DFG). We gratefully acknowledge the colleagues of the Nonlinear Dynamics Group Potsdam for useful discussions and support of this work.

References

D. J. Amit. *Modeling Brain Function. The World of Attractor Neural Networks*. Cambridge University Press, Cambridge, 1989.

A. Babloyantz, J. M. Salazar, and C. Nicolis. Evidence of chaotic dynamics of brain activity during the sleep cycle. *Physics Letters A*, 111(3):152–156, 1985.

P. beim Graben, J. D. Saddy, M. Schlesewsky, and J. Kurths. Symbolic dynamics of event-related brain potentials. *Phys. Rev. E*, 62(4):5518–5541, 2000.

M. C. Casdagli. Recurrence plots revisited. *Physica D*, 108:12–44, 1997.

E. Donchin. Surprise! . . . Surprise? *Psychophysiology*, 18:493–513, 1981.

E. Donchin and M. G. H. Coles. Is the P300 component a manifestation of context updating? *Behavioral and Brain Sciences*, 11:357–374, 1988.

J.-P. Eckmann, S. O. Kamphorst, and D. Ruelle. Recurrence Plots of Dynamical Systems. *Europhysics Letters*, 5:973–977, 1987.

P. Faure and H. Korn. A new method to estimate the Kolmogorov entropy from recurrence plots: its application to neuronal signals. *Physica D*, 122: 265–279, 1998.

S. Frisch, P. beim Graben, and M. Schlesewsky. Parallelizing grammatical functions: P600 and P345 reflect different cost of reanalysis. *Int. J. Bifurcation Chaos*, 2002.

D. Gallez and A. Babloyantz. Predictability of human EEG: a dynamical approach. *Biol. Cybern.*, 64:381–39, 1991.

E. R. Kandel, J. H. Schwartz, and T. M. Jessel. *Essentials of Neural Science and Behavior*. Appleton & Lange, East Norwalk, Connecticut, 1995.

H. Kantz and T. Schreiber. *Nonlinear Time Series Analysis*. University Press, Cambridge, 1997.

M. Kutas and C. Van Petten. *Handbook of Psycholinguistics*, chapter Psycholinguistics electrified: Event-related. Academic Press, San Diego, 1994.

W. Lutzenberger, T. Elbert, N. Birbaumer, W. J. Ray, and H. Schupp. he scalp distribution of the fractal dimension of the EEG and its variation with mental tasks. *Brain Topography*, 5(1):27–33, 1992.

N. Marwan, N. Wessel, and J. Kurths. Recurrence Plot Based Measures of Complexity and its Application to Heart Rate Variability Data. *Physical Review E*, 66(2):026702, 2002.

M. Molnár, J. E. Skinner, V. Csépe, I. Winkler, and G. Karmos. Correlation dimension changes accompanying the occurence of the mismatch negativity and the p3 event-related potential component. *Electroenceph. clin. Neurophysiol.*, 95:118–126, 1995.

P. L. Nunez. *Electric Fields of the Brain*. Oxford University Press, New York, 1981.

W. S. Pritchard and D. W. Duke. Dimensional analysis of no-task human EEG using the grassberger-procaccia method. *Psychophysiology*, 29(2): 182–191, 1992.

R. Quian Quiroga, O. A. Rosso, E. Başar, and M. Schürmann. Wavelet entropy in event-related potentials: a new method shows ordering of EEG oscillations. *Biol. Cybern.*, 84:291–299, 2001.

P. E. Rapp, I. D. Zimmerman, A. M. Albano, G. C. deGuzman, N. N. Greenbaun, and T. R. Bashore. Experimental studies of chaotic neural behavior: Cellular activity and electroencephalographic signals. In H. G. Othmer, editor, *Nonlinear Oscillations in Biology and Chemistry*, volume 66 of *Lecture Notes in Biomathematics*, pages 175–205. Springer, Berlin, 1986.

F. Rösler. *Hirnelektrische Korrelate kognitiver Prozesse*. Springer, Berlin, 1982.

B. Schack. How to construct a microstate-based alphabet for evaluating information processing in time. *Int. J. Bifurcation Chaos*, 2002.

R. Steuer. Entropy and complexity analysis of intracranially recorded eeg. *Int. J. Bifurcation Chaos*, 2002.

S. Sutton, M. Braren, J. Zubin, and E. R. John. Evoked potential correlates of stimulus uncertainty. *Science*, 150:1187–1188, 1965.

J. Theiler, S. Eubank, A. Longtin, B. Galdrikian, and B. Farmer. Testing for nonlinearity in time series: the method of surrogate data. *Physica D*, 58: 77–94, 1992.

N. Thomasson, T. J. Hoeppner, C. L. Webber Jr., and J. P. Zbilut. Recurrence quantification in epileptic eegs. *Physics Letters A*, 279:94–101, 2001.

L. L. Trulla, A. Giuliani, J. P. Zbilut, and C. L. Webber Jr. Recurrence quantification analysis of the logistic equation with transients. *Physics Letters A*, 223:255–260, 1996.

C. L. Webber Jr. and J. P. Zbilut. Dynamical assessment of physiological systems and states using recurrence plot strategies. *Journal of Applied Physiology*, 76:965–973, 1994.

J. P. Zbilut and C. L. Webber Jr. Embeddings and delays as derived from quantification of recurrence plots. *Physics Letters A*, 171:199–203, 1992.

Appendix C

Nonlinear Analysis of Bivariate Data with Cross Recurrence Plots

MARWAN, N., KURTHS, J., Nonlinear analysis of bivariate data with cross recurrence plots. Physics Letters A 302 (5–6), 2002, 299–307.
DOI: 10.1016/S0375-9601(02)01170-2


ELSEVIER

Physics Letters A 302 (2002) 299–307

PHYSICS LETTERS A

www.elsevier.com/locate/pla

Nonlinear analysis of bivariate data with cross recurrence plots

Norbert Marwan *, Jürgen Kurths

Department of Physics, University of Potsdam, 14415 Potsdam, Germany

Received 31 January 2002; received in revised form 7 August 2002; accepted 15 August 2002

Communicated by C.R. Doering

Abstract

We use the extension of the method of recurrence plots to cross recurrence plots (CRP) which enables a nonlinear analysis of bivariate data. To quantify CRPs, we develop further three measures of complexity mainly basing on diagonal structures in CRPs. The CRP analysis of prototypical model systems with nonlinear interactions demonstrates that this technique enables to find these nonlinear interrelations from bivariate time series, whereas linear correlation tests do not. Applying the CRP analysis to climatological data, we find a complex relationship between rainfall and El Niño data.

PACS: 05.40; 05.45; 07.05.K

Keywords: Data analysis; Correlation test; Cross recurrence plot; Nonlinear dynamics

1. Introduction

A major task in bi- or multivariate data analysis is to compare or to find interrelations in different time series. Often, these data are gained from natural systems, which show generally nonstationary and complex behaviour. Furthermore, these systems are often observed by very few measurements providing short data series. Linear approaches of time series analysis are often not sufficient to analyze this kind of data. In the last two decades a great variety of nonlinear techniques has been developed to analyze data of complex systems (cf. [1,2]). Most popular are methods to estimate fractal dimensions, Lyapunov exponents or mutual information [2–5]. However, most of these methods need long data series. The uncritical application of these methods especially to natural data often leads to pitfalls.

To overcome the difficulties with nonstationary and rather short data series, the method of *recurrence plots* (RP) has been introduced [6–8]. An additional quantitative analysis of recurrence plots has been developed to detect transitions (e.g., bifurcation points) in complex systems [9–12]. An extension of the method of recurrence plots to cross recurrence plots enables to investigate the time dependent behaviour of two processes which are both recorded in a single time series [13,14]. The basic idea of this approach is to compare the phase space trajectories of two processes in the same phase space. The aim of this Letter is to develop further new measures of complexity, which are

* Corresponding author.
E-mail address: marwan@agnld.uni-potsdam.de (N. Marwan).

0375-9601/02/$ – see front matter
PII: S0375-9601(02)01170-2

based on cross recurrence plots and to evaluate the similarity of the considered systems. This nonlinear approach enables to identify epochs where there are linear and even nonlinear interrelations between both systems.

Firstly, we give an overview about recurrence plots and cross recurrence plots and, than, we develop further new measures of complexity. Lastly, we apply the method to two model systems and to natural data.

2. Recurrence plot

The recurrence plot (RP) is a tool in order to visualize the dynamics of phase space trajectories and was firstly introduced by Eckmann et al. [7]. Following Takens' embedding theorem [15], the dynamics can be appropriately presented by a reconstruction of the phase space trajectory $\vec{x}(t)$ from a time series u_k (with a sampling time Δt) by using an embedding dimension m and a time delay τ

$$\vec{x}(t) = \vec{x}_i = (u_i, u_{i+\tau}, \ldots, u_{i+(m-1)\tau}), \quad t = i\,\Delta t. \tag{1}$$

The choice of m and τ are based on standard methods for detecting these parameters like method of false nearest neighbours (for m) and mutual information (for τ), which ensures the entire covering of all free parameters and avoiding of autocorrelation effects [2].

The recurrence plot is defined as

$$\mathbf{R}_{i,j} = \Theta\big(\varepsilon_i - \big\|\vec{x}_i - \vec{x}_j\big\|\big), \tag{2}$$

where ε_i is a predefined cut-off distance, $\|\cdot\|$ is the norm (e.g., the Euclidean norm) and $\Theta(x)$ is the Heaviside function. The values *one* and *zero* in this matrix can be simply visualized by the colours black and white. Depending on the kind of the application, ε_i can be a fixed value or it can be changed for each i in such a way that in the ball with the radius ε_i a predefined amount of neighbours occurs. The latter will provide a constant density of recurrence points in each column of the RP. Such a RP exhibits characteristic large-scale and small-scale patterns which are caused by typical dynamical behavior [7,10,12], e.g., diagonals (similar local evolution of different parts of the trajectory) or horizontal and vertical black lines (state does not change for some time). A single recurrence point, however, contains no information about the state itself.

As a quantitative extension of the method of recurrence plots, the *recurrence quantification analysis* (RQA) was introduced by Zbilut and Webber [10, 11]. This technique defines several measures mostly based on diagonal oriented lines in the recurrence plot: *recurrence rate*, *determinism*, *maximal length of diagonal structures*, *entropy* and *trend*. The *recurrence rate* is the ratio of all recurrent states (recurrence points) to all possible states and is therefore the probability of the recurrence of a certain state. Stochastic behaviour causes very short diagonals, whereas deterministic behaviour causes longer diagonals. Therefore, the ratio of recurrence points forming diagonal structures to all recurrence points is called the *determinism* (although this measure does not really reflect the determinism of the system). Diagonal structures show the range in which a piece of the trajectory is rather close to another one at different time. The *diagonal length* is the time span they will be close to each other and their mean can be interpreted as the mean prediction time. The inverse of the maximal line length can be interpreted to be directly related with the maximal positive Lyapunov exponent [7,9,16]; in this interpretation it is assumed that the considered system is chaotic and has no stochastic influences. Since real (natural) systems are always affected by noise, we suggest that this measure has to be interpreted in a more statistical way, for instance, as a prediction time. However, if we consider a chaotic system, the maximal positive Lyapunov exponent is much more reflected in the distribution of the line lengths. The *entropy* is defined as the Shannon entropy in the histogram of diagonal line lengths. Stationary systems will deliver rather homogeneous recurrence plots, whereas nonstationary systems cause changes in the distribution of recurrence points in the plot visible by brightened areas. For example, a simple drift in the data causes a paling of the recurrence plot away from the main diagonal to the edges. The parameter *trend* measures this effect by diagonal wise computation of the diagonal recurrence density and its linear relation to the time distance of these diagonals to the main diagonal.

3. Cross recurrence plot

Analogous to Zbilut et al. [13], we will use the recently expanded method of recurrence plots to the method of *cross recurrence plots*, which compares the dynamics represented in two time series. Herein, both time series are simultaneously embedded in the same phase space. The test for closeness of each point of the first trajectory $\vec{x}_i$ $(i = 1, \ldots, N)$ with each point of the second trajectory $\vec{y}_j$ $(j = 1, \ldots, M)$ results in a $N \times M$ array $\mathbf{CR}_{i,j} = \Theta(\varepsilon - \|\vec{x}_i - \vec{y}_j\|)$ called the cross recurrence plot (CRP). Visual inspection of CRPs already reveals valuable information about the relationship between both systems. Long diagonal structures show similar phase space behaviour of both time series. It is obvious, that if the difference of both systems vanishes, the main diagonal line will occur black. An additional time dilatation or compression of one of these similar trajectories causes a distortion of this diagonal line [14]. In the following, we suppose that both systems do not have differences in the time scale and have the same length N, hence, the CRP is a $N \times N$ array and an increasing similarity between both systems causes a raising of the recurrence point density along the main diagonal until a black straight main diagonal line occurs (cf. Fig. 3). Finally, the CRP compares the considered systems and allows us to benchmark their similarity.

4. Complexity measures based on cross recurrence plots

Next, we will define some modified RQA measures for quantifying the similarity between the phase space trajectories. Since we use the occurrence of the more or less discontinuous main diagonal as a measure for similarity, the modified RQA measures will be determined for each diagonal line parallel to the main diagonal, hence, as functions of the distance from the main diagonal. Therefore, it is also possible to assess the similarity in the dynamics depending on a certain delay.

We analyze the distributions of the diagonal line lengths $P_t(l)$ for each diagonal parallel to the main diagonal. The index $t \in [-T, \ldots, T]$ marks the number of the diagonal line, where $t = 0$ marks the main diagonal, $t > 0$ the diagonals above and $t < 0$ the diagonals below the main diagonal, which represent positive and negative time delays, respectively.

The recurrence rate *RR* is now defined as

$$RR(t) = \frac{1}{N-t} \sum_{l=1}^{N-t} l\, P_t(l), \tag{3}$$

and reveals the probability of occurrence of similar states in both systems with a given delay t. A high density of recurrence points in a diagonal results in a high value of *RR*. This is the case for systems whose trajectories often visit the same phase space regions.

Analogous to the RQA the determinism

$$DET(t) = \frac{\sum_{l=l_{\min}}^{N-t} l\, P_t(l)}{\sum_{l=1}^{N-t} l\, P_t(l)}, \tag{4}$$

is the proportion of recurrence points forming long diagonal structures of all recurrence points. Stochastic as well as heavily fluctuating data cause none or only short diagonals, whereas deterministic systems cause longer diagonals. If both deterministic systems have the same or similar phase space behaviour, i.e., parts of the phase space trajectories meet the same phase space regions during certain times, the amount of longer diagonals increases and the amount of smaller diagonals decreases.

The average diagonal line length

$$L(t) = \frac{\sum_{l=l_{\min}}^{N-t} l\, P_t(l)}{\sum_{l=l_{\min}}^{N-t} P_t(l)}, \tag{5}$$

reports the duration of such a similarity in the dynamics. A high coincidence of both systems increases the length of these diagonals.

High values of *RR* represent high probabilities of the occurrence of the same state in both systems, high values of *DET* and *L* represent a long time span of the occurrence of a similar dynamics in both systems. Whereas *DET* and *L* are sensitive to fastly and highly fluctuating data, *RR* measures the probabilities of the occurrence of the same states in spite of these high fluctuations (noisy data). It is important to emphasize that these parameters are statistical measures and that their validity increases with the size of the CRP.

Compared to the other methods, this CRP technique has important advantages. Since all parameters are computed for various time delays, lags can be identified and causal links proposed. An additional analysis with opposite signed second time series allows

us to distinguish positive and negative relations. To recognize the measures for both cases, we add the index '+' to the measures for the positive linkage and the index '−' for the negative linkage, e.g., RR_+ and RR_-. A further substantial advantage of our method is the capability to find also nonlinear similarities in short and nonstationary time series with high noise levels as they typically occur, e.g., in biology or earth sciences. However, the shortness and nonstationarity of data limits this method as well. One way to reduce problems that occur with nonstationary data is the alternative choice of the neighbourhood as a fixed amount of neighbours in the ball with a varying radius ε. A further major aspect is the reliability of the found results. Until a mature statistical test is developed, a first approach could be a surrogate test.

In the next section we apply these measures of complexity to prototypical model systems and to real data.

5. Examples illustrating the CRP

5.1. Noisy periodic data

First, we consider a classical example to check whether our technique is there compatible with linear statistical tools: two sine functions $f(x)$ and $g(x)$ with the same period (2π), whereby the second function $g(x)$ is shifted by $\pi/2$ and strongly corrupted by additive Gaussian white noise $\xi \in [-1, 1]$; the signal to noise ratio is 0.5 (Fig. 1). Both time series have a length of 500 data points with a sampling rate of $2\pi/100$.

We apply our analysis with $m = 3$, $\tau = \pi/2$ and $\varepsilon = 1.5$ (fixed radius, Euclidean distance). The CRP shows diagonal structures separated by gaps (Fig. 2). These gaps are the result of the high fluctuation of the noisy sine function. Due to the periodicity of these functions, the diagonals have a constant distance to each other equal to the value of the period $\lambda = 2\pi$. The interrupted diagonal structures consist of a number of short diagonals. However, these are long enough to achieve significant maxima in the measures *RR*, *DET* and *L*.

As expected, in this example the classical cross-correlation function shows a significant correlation after a lag of $\pi/2$ (Fig. 3A). The *RR*, *DET* and *L*

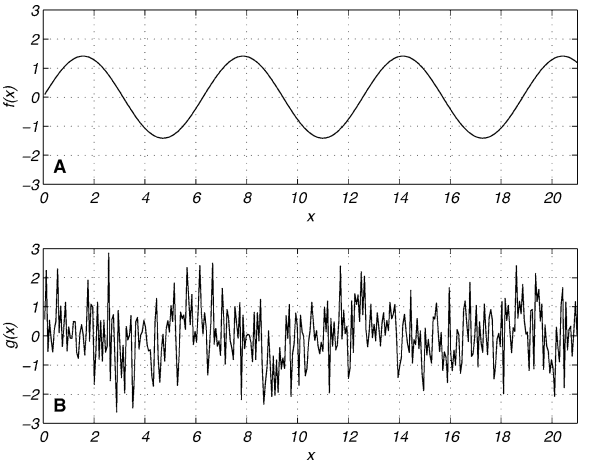

Fig. 1. Two delayed sine functions, one of them corrupted by additive white noise (B).

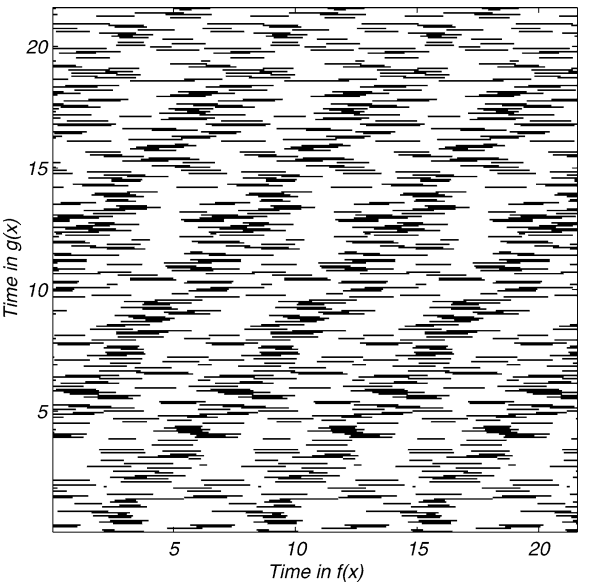

Fig. 2. Cross recurrence plot for two delayed sine functions (Fig. 1) with an embedding of $m = 3$, $\tau = \pi/2$ and $\varepsilon = 1.5$. The diagonal lines in the CRP result from similar phase space behaviour of both functions.

functions also show maxima for positive and negative relation between $f(x)$ and $g(x)$. These maxima occur with the same lags $\pi/2$ like the linear correlation test (Fig. 3B–D). Despite the high noise level, these measures find the correlation. Hence, the result of this CRP analysis agrees with the linear correlation analysis.

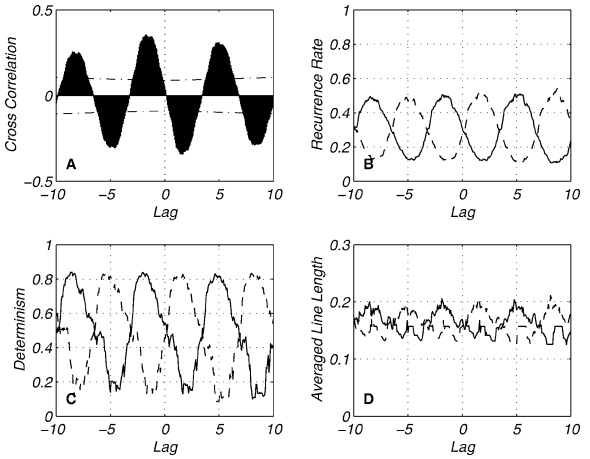

Fig. 3. Cross-correlation (A), *RR* (B), *DET* (C) and *L* (D) for two delayed sine functions. *L* has the unit of time. The solid black lines show positive relation, the dashed lines show negative relation. The dash-dotted line in (A) marks the 5% confidence interval. All functions (A)–(D) detect the correlation after a lag of $\pi/2$.

Due to the noisy data, the trajectories strongly fluctuate in the phase space. Therefore, only short diagonal lines in the CRP occur and the means of the measures *DET* and *L* have (relative) small values.

5.2. System with nonlinear correlations

The next example is concerned to a nonlinear interrelation between systems. We will study this interrelation by using a standard linear method (cross correlation), a standard method from nonlinear data analysis (mutual information, cf. [2]) and the new proposed measures. We consider linear correlated noise (autoregressive process), which is nonlinearly coupled with the x-component of the Lorenz system $x(t)$ (solved with an ODE solver for the standard parameters $\sigma = 10$, $r = 28$, $b = 8/3$ and a time resolution of $\Delta t = 0.01$, [17,18]). We use a first order autoregressive process y_n and force it with the squared x-component

$$y_n = 0.86y_{n-1} + 0.500\xi_n + \kappa x_n^2, \tag{6}$$

where ξ is Gaussian white noise and x_n ($x(t) \to x_n$, $t = n\Delta t$) is normalized to standard deviation $\sigma = 1$ (Fig. 4). The data length is 8000 points. The coupling κ is realized without any lag. In order to study the behaviour of the proposed measures as a function of the coupling strength, we compute the CRPs for

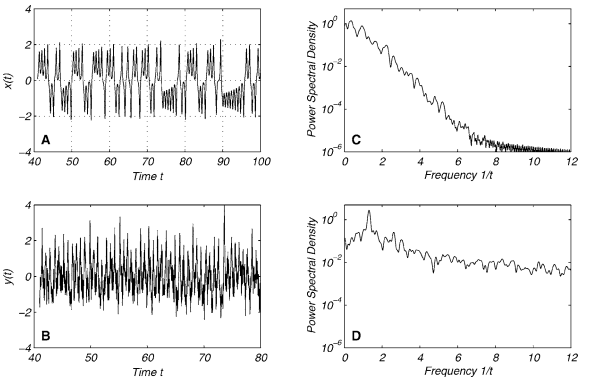

Fig. 4. (B) Time series of a nonlinear related system consisting of a driven first order autoregressive process, forced by the squared (A) x-component of the Lorenz system ($\kappa = 0.2$). The major periods (frequencies) are 2.9 (0.34) and 1.1 (0.94) for x (C) and 0.77 (1.30) and 0.96 (1.05) for y (D).

$\kappa \in [0, 3]$ and for 500 independent realizations. The major periods of the system x are 2.9 and 1.1, whereas the major periods of the selected realization of the system y shown in Fig. 4 are 0.77, 0.96 and 0.59 (ordered from highest to lower).

The cross correlation analysis of x and y do not reveal a significant linear correlation between them (Fig. 6A,B). The linear correlation does not increase for a growing coupling strength κ. However, the mutual information shows a strong dependence between x and y at delays of 0.05, -0.29 and 0.44 (Fig. 6C,D). This measure increases for a growing coupling. Analogous results can also be found with other nonlinear techniques which are designed for the study of interrelations as described in [19,20].

The CRP of the driven AR-process (Eq. (6)) with the x-component of the Lorenz system ($m = 5$, $\tau = 10$, $\varepsilon = 2$) contains a lot of longer diagonal lines, which represent time ranges in which both systems have a similar phase space dynamics (Fig. 5). The results of the quantitative analysis of the CRP is strongly different from those of the linear analysis. It is important to note that the linear correlation analysis is here not able to detect any significant coupling or correlation between both systems (Fig. 6A and B).

Our measures of complexity exhibit the following: RR and L exhibit maxima at a lag of about 0.05 for RR_+/L_+ and RR_-/L_- and additionally at 0.45 and -0.32 for RR_-/L_- (Fig. 7A,E). The delay of about 0.05 stems from the auto correlation of y

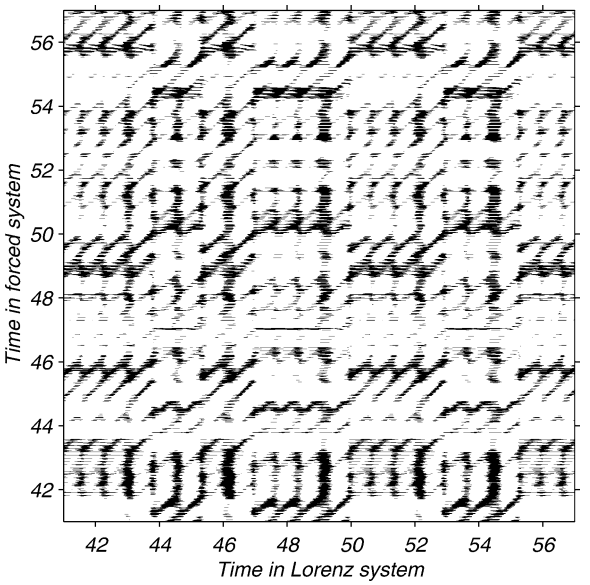

Fig. 5. Cross recurrence plot for the forced autoregressive process y (Fig. 4B) and the forcing function (x-component of the Lorenz system, Fig. 4A) for a coupling strength $\kappa = 0.2$ and an embedding $m = 5$, $\tau = 10$, $\varepsilon = 2$.

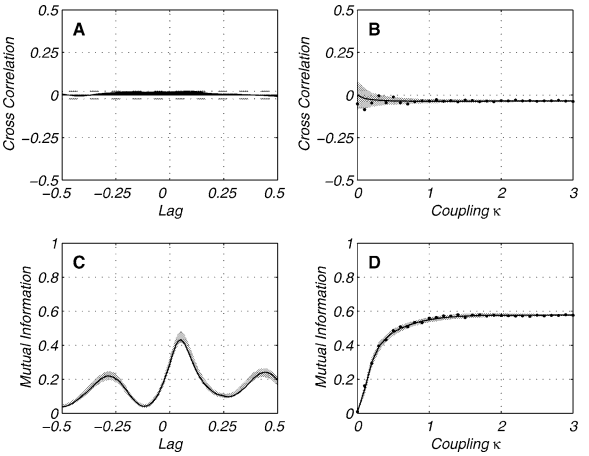

Fig. 6. Cross-correlation (A), (B) and mutual information (C), (D) for the forced autoregressive process and the forcing function; (A) and (C) represents the measures for one realization as functions of the delay and for a coupling $\kappa = 0.2$, (B) and (D) represents the measures for one realization (dots) and averaged (line) as functions of the coupling strength κ (for a delay of zero). The dash-dotted lines in (A) mark the significance level of 5% for the linear correlation between x and y, the gray bands in (B), (C) and (D) mark the 2σ margin of the distributions of the measures gained from the 500 realizations. The cross-correlation function does not find a significant correlation, but the mutual information shows significant interrelations between x and y at delays of 0.05, 0.4 and -0.3. The correlation coefficient does not clearly change for a growing coupling strength (B), however, the mutual information monotonically increases with a growing coupling strength κ up to $\kappa = 1$ and does not change for $\kappa > 1$ (D).

and approximately corresponds to its correlation time $\Delta t / \ln 0.86 = 0.066$. The other both delays are in the sum 0.77 which suggests, that they are due to an interference of the main periods of the systems. DET_+ and DET_- has also maxima at these delays, but these maxima are not significant in the sense that the values exceed the 2σ-level of the *DET* distribution gained from 500 realizations (Fig. 7C). This is due to the rapid fluctuating of y and, thus, the less amount of longer diagonal structures ($l > 3$). The reconstructed phase space trajectories of x and y do not run parallel for some time.

The three measures have a slightly different dependence on the coupling strength κ: whereas *RR* increases rather fast with growing κ, *DET* increases slower and L increases much slower with growing κ (Fig. 7B,D,F). In comparison with the mutual information, the proposed measures have a similar regime, but especially *DET* and L, spread stronger. However, this spread depends on the length of the considered data and decreases for longer data sets.

Finally we can infer, that the measures *RR* and L are suitable in order to find the nonlinear relation between the considered data series, where the linear analysis is not able to detect this relation. In this example, *DET* does not reveal the nonlinear relation, because the rapidly fluctuation in y kicks away the reconstructed phase space trajectory from the parallel running to the trajectory of x. Since the result is rather independent of the sign of the second data before the embedding, the found relation is of the kind of an even function.

5.3. Climatological data

The last example shows the potential of the CRPs in order to find interrelations in natural data. We investigate, whether there is a relation between the precipitation in an Argentinian city and the El Niño/Southern Oscillation (ENSO). Power spectra analysis of local rainfall data found periodicities of 2.3 and 3.6 years within the ENSO frequency band [21].

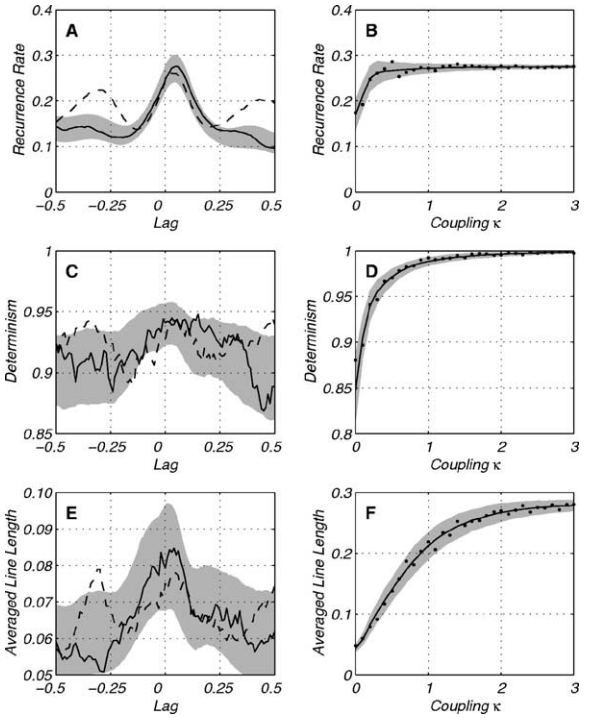

Fig. 7. *RR* (A), (B), *DET* (C), (D) and *L* (E), (F) for the forced autoregressive process and the forcing function (*L* has the unit of time). The solid lines show positive relation, the dashed lines show negative relation. The gray bands mark the 2σ margin of the distributions of the measures gained from the 500 realizations; only the 2σ margins for RR_+, DET_+ and L_+ are shown. RR_+/L_+ and RR_-/L_- have clear maxima for a lag about 0.05, RR_- and L_- have additionally maxima at 0.4 and -0.3, which is the similar behaviour as the mutual information. The dependence from the coupling strength κ is slightly different. Whereas *RR* increases rather fast with growing κ (B), *DET* increases slower (D) and *L* increases much slower (F) with growing κ. Since the maxima occur for RR_+, DET_+ and L_+- as well as for RR_-, DET_- and L_-, the found relation is of the kind of an even function.

For our analysis we use monthly precipitation data from the city San Salvador de Jujuy in NW Argentina for the time span 1908–1987 (data from [22]). The behaviour of the ENSO phenomenon is well represented by the Southern Oscillation Index (SOI), which is a normalized air pressure difference between Tahiti and Darwin (Fig. 8; data from the Climate Server of NOAA, 1999, http://ferret.wrc.noaa.gov). Negative extrema in SOI data mark El Niño events and positive extrema La Niña events. We use the monthly SOI data for the same time span as the rainfall data. Both data sets have lengths of 960 points.

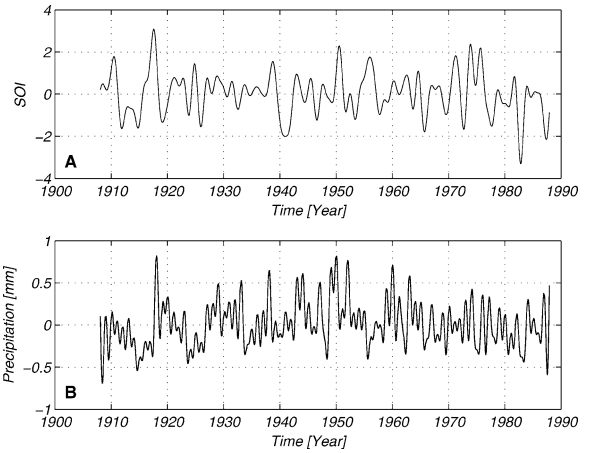

Fig. 8. (A) Southern oscillation index (SOI) and (B) rainfall data of San Salvador de Jujuy.

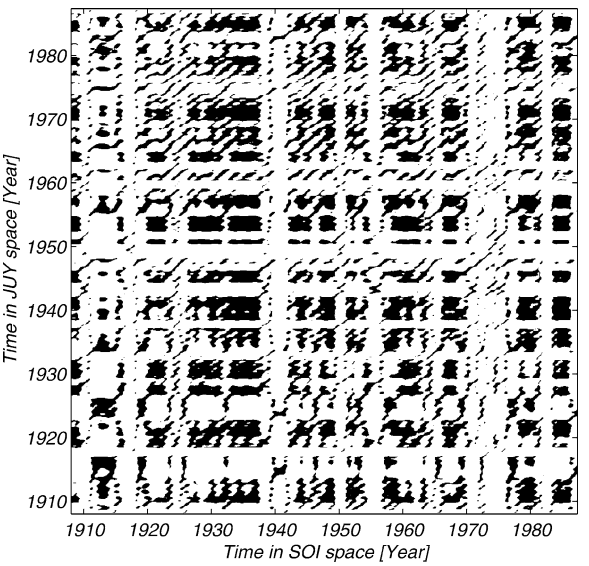

Fig. 9. Cross recurrence plot of SOI vs. precipitation data from the city of San Salvador de Jujuy for an embedding of $m = 3$, $\tau = 4$ and $\varepsilon = 1.3$. The x-axis shows the time along the phase space trajectory of the SOI and the y-axis that of JUY.

The cross correlation function and the mutual information show rather small correlation $\varrho = 0.14$ between both data series with time delays of around 3 and 7 months, respectively (Fig. 10A,B).

After normalization of the data, the CRP with $m = 3$, $\tau = 4$ and $\varepsilon = 1.3$ is calculated and shows several structures (Fig. 9).

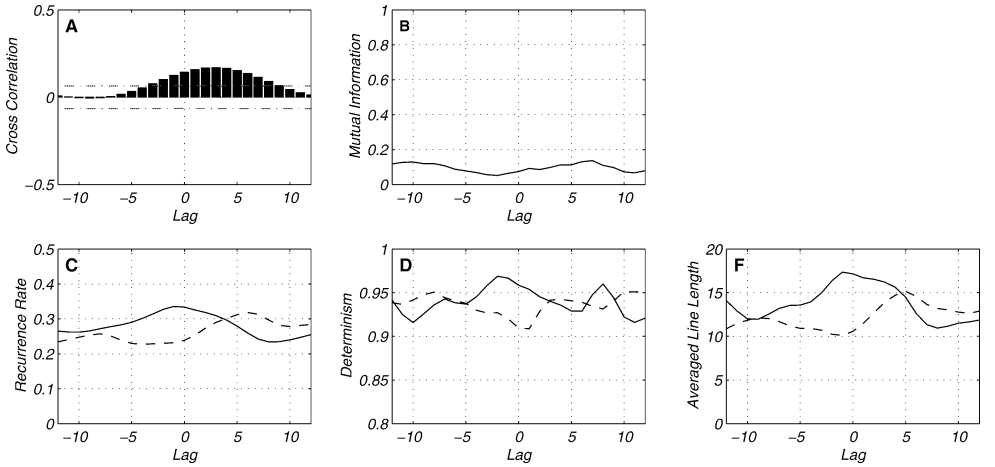

Fig. 10. Cross correlation (A), mutual information (B) and CRP parameters (C)–(E) of SOI vs. precipitation data from the city of San Salvador de Jujuy (JUY). In (C)–(E), the solid lines show positive relation, the dashed lines show negative relation. The dashed-dotted lines in (A) mark the 5% confidence interval. The maxima of the measures reveal an interrelation between the rainfall and the ENSO.

The CRP analysis of local rainfall and SOI is done with a predefined shortest diagonal length $l_{\min} = 6$. The analysis reveals maxima for the complexity measures RR_+, DET_+ and L_+ for correlated behaviour around a delay of zero months, whereas the measures for anti-correlated behaviour RR_-, DET_- and L_- increase after about five months (Fig. 10). This result enables to conclude a positive relation between ENSO and the local rainfall. This gives some indication that the occurrence of an El Niño (extreme negative SOI) at the end of a year causes a decreased rainfall in the rainy season from November to January and the occurrence of a La Niña (extreme positive SOI) causes an increased rainfall during this time of the year. This conclusion extends the results obtained by power spectra analysis, where the similar periodicities in both SOI and local rainfall data were found [21]. These analysis show that a source for inter-annual precipitation variability in NW Argentina is the ENSO [21].

The linear correlation analysis finds the correlation, however, it is scarce above the significance and its mean at a lag of three months. The mutual information does not reveal a clear sign for interrelation between the data. It has small maxima at delays of 7 and -10 months. In contrast, all the complexity measures *RR*, *DET* and *L* show a significant result and decompose the correlation in a positive one with no delay and in a negative one with a delay of about five months, what suggests a more complex interrelation between the ENSO phenomenon and local rainfall in NW Argentina.

6. Conclusions

We have modified the method of cross recurrence plots (CRPs) in order to study the similarity of two different phase space trajectories. Local similar time evolution of the states becomes then visible by long diagonal lines. The distributions of recurrence points and diagonal lines along the main diagonal provides an evaluation of the similarity of the phase space trajectories of both systems. We have introduced three measures of complexity based on these distributions. They enable to quantify a possible similarity and interrelation between both dynamical systems. We have demonstrated the potentials of this approach for typical model systems and natural data. In the case of linear systems, the results with this nonlinear technique agree with the linear correlation test. However, in the case of nonlinear coupled systems, the linear correlation test does not find any correlation, whereas nonlinear techniques, as the mutual information, and the proposed complexity measures clearly reveal this relation. Additionally, the latters determine the kind of coupling as to be an even function. The application to climatological data enables to find a more complex relationship between the El Niño and local rainfall in

NW Argentina than the linear correlation test, the mutual information or the power spectra analysis yielded.

Our quantification analysis of CRPs is able to find nonlinear relations between dynamical systems. It provides more information than a linear correlation analysis and the nonlinear technique of mutual information analysis. The future work is dedicated to the development of a significance test for RPs and the complexity measures which are based on RPs.

Acknowledgements

This work is part of the Special Research Programme *Geomagnetic variations: Spatio-temporal structures, processes and impacts on the system Earth* and the Collaborative Research Center *Deformation Processes in the Andes* supported by the German Research Foundation. We gratefully acknowledge M.H. Trauth and U. Schwarz for useful conversations and discussions and U. Bahr for support of this work. Further we would like to thank the NOAA-CIRES Climate Diagnostics Center for providing COADS data.

References

[1] H.D.I. Abarbanel, R. Brown, J.J. Sidorowich, L.S. Tsimring, Rev. Mod. Phys. 65 (1993) 1331.
[2] H. Kantz, T. Schreiber, Nonlinear Time Series Analysis, Cambridge University Press, Cambridge, 1997.
[3] J. Kurths, H. Herzel, Physica D 25 (1987) 165.
[4] B.B. Mandelbrot, The Fractal Geometry of Nature, Freeman, San Francisco, 1982.
[5] A. Wolf, J.B. Swift, H.L. Swinney, J.A. Vastano, Physica D 16 (1985) 285.
[6] M.C. Casdagli, Physica D 108 (1997) 12.
[7] J.-P. Eckmann, S.O. Kamphorst, D. Ruelle, Europhys. Lett. 5 (1987) 973.
[8] M. Koebbe, G. Mayer-Kress, Use of recurrence plots in the analysis of time-series data, in: M. Casdagli, S. Eubank (Eds.), Proceedings of SFI Studies in the Science of Complexity, Nonlinear Modeling and Forecasting, Vol. XXI, Addison-Wesley, Redwood City, 1992, pp. 361–378.
[9] L.L. Trulla, A. Giuliani, J.P. Zbilut, C.L. Webber Jr., Phys. Lett. A 223 (1996) 255.
[10] C.L. Webber Jr., J.P. Zbilut, J. Appl. Physiol. 76 (1994) 965.
[11] J.P. Zbilut, C.L. Webber Jr., Phys. Lett. A 171 (1992) 199.
[12] N. Marwan, N. Wessel, J. Kurths, Phys. Rev. E 66 (2) (2002) 026702.
[13] J.P. Zbilut, A. Giuliani, C.L. Webber Jr., Phys. Lett. A 246 (1998) 122.
[14] N. Marwan, M. Thiel, N.R. Nowaczyk, Nonlinear Processes Geophys. 9 (3/4) (2002) 325.
[15] F. Takens, Detecting strange attractors in turbulence, in: Lecture Notes in Mathematics, Vol. 898, Springer, Berlin, 1981, pp. 366–381.
[16] J.M. Choi, B.H. Bae, S.Y. Kim, Phys. Lett. A 263 (4-6) (1999) 299.
[17] E.N. Lorenz, J. Atmos. Sci. 20 (1963) 120.
[18] J.H. Argyris, G. Faust, M. Haase, An Exploration of Chaos, North-Holland, Amsterdam, 1994.
[19] T. Schreiber, Phys. Rev. Lett. 85 (2) (2000) 461; http://prola.aps.org/searchabstract/PRL/v85/i2/p461_1.
[20] A. Schmitz, Phys. Rev. E 62 (5) (2000) 7508; http://prola.aps.org/searchabstract/PRE/v62/i5/p7508_1.
[21] M.H. Trauth, R.A. Alonso, K. Haselton, R. Hermanns, M.R. Strecker, Earth Planet. Sci. Lett. 179 (2000) 243.
[22] A.R. Bianchi, C.E. Yañez, Las precipitaciones en el noroeste Argentino, Instituto Nacional de Tecnologia Agropecuaria, Estacion Experimental Agropecuaria Salta, 1992.

Appendix D

Comparing Modern and Pleistocene ENSO-like Influences in NW Argentina Using Nonlinear Time Series Analysis Methods

MARWAN, N., TRAUTH, M. H., VUILLE, M., KURTHS, J., Comparing modern and Pleistocene ENSO-like influences in NW Argentina using nonlinear time series analysis methods. Climate Dynamics, 2003, in press.
DOI: 10.1007/s00382-003-0335-3

Climate Dynamics
(finally accepted: March 28, 2003)

Comparing modern and Pleistocene ENSO-like influences in NW Argentina using nonlinear time series analysis methods

Norbert Marwan[1], **Martin H. Trauth**[2], **Mathias Vuille**[3], **Jürgen Kurths**[1]

[1] Nonlinear Dynamics Group, Institute of Physics, University of Potsdam, Potsdam 14415, Germany
[2] Institute of of Earth Sciences, University of Potsdam, Potsdam 14415, Germany
[3] Climate System Research Center, Department of Geosciences, University of Massachusetts, Amherst, USA

Received: date / Revised version: date

Abstract Higher variability in rainfall and river discharge could be of major importance in landslide generation in the north-western Argentine Andes. Annual layered (varved) deposits of a landslide dammed lake in the Santa Maria Basin (26°S, 66°W) with an age of 30,000 ^{14}C years provide an archive of precipitation variability during this time. The comparison of these data with present-day rainfall observations tests the hypothesis that increased rainfall variability played a major role in landslide generation. A potential cause of such variability is the El Niño/ Southern Oscillation (ENSO). The causal link between ENSO and local rainfall is quantified by using a new method of nonlinear data analysis, the quantitative analysis of cross recurrence plots (CRP). This method seeks similarities in the dynamics of two different processes, such as an ocean-atmosphere oscillation and local rainfall. Our analysis reveals significant similarities in the statistics of both modern and palaeo-precipitation data. The similarities in the data suggest that an ENSO-like influence on local rainfall was present at around 30,000 ^{14}C years ago. Increased rainfall, which was inferred from a lake balance modeling in a previous study, together with ENSO-like cyclicities could help to explain the clustering of landslides at around 30,000 ^{14}C years ago.

1 Introduction

Climate is a major influential factor for mass movements in high mountain regions. Increased humidity (Dethier and Reneau 1996) or increased variability in rainfall (Grosjean et al. 1997; Keefer et al. 1998) can reduce thresholds for catastrophic landsliding. In order to estimate the influence of climate in a given region, the climatic conditions during episodes with enhanced landsliding are compared with periods without important mass movements. The precise definition of climate scenarios at times of high rock avalanche activity helps us to define threshold values for increased landsliding.

About 30,000 ^{14}C years ago, multiple large rock avalanches with volumes in excess of 10^6 m^3 occurred in the arid to semiarid intra-andean basins of north-western Argentina (Strecker and Marret 1999; Hermanns and Strecker 1999; Trauth and Strecker 1999). A potential mechanism that could have caused this enhanced landsliding in such an environment is climate change. Increased humidity and/or higher inter- and intraannual rainfall variability results in higher river discharge and erosion in narrow valleys and therefore increased destabilization of mountain fronts.

The climatic conditions in NW Argentina are not well known for the period at around 30,000 ^{14}C years ago. Marine and terrestrial records from tropical and subtropical South America indeed suggest more humid conditions (the Minchin period between 40,000 and 25,000 ^{14}C years ago, e. g. van der Hammen and Absy 1994; Ledru et al. 1996; Godfrey et al. 1997; Turcq et al. 1997) and a strong El Niño/ Southern Oscillation (ENSO) (e. g. Oberhänsli et al. 1990; Beaufort et al. 2001). Various modeling studies have shown an impact of orbital forcing on ENSO and its weakening during the ice ages (Clement et al. 1999; Liu et al. 2000). Thus El Niño events may be rare around 30,000 ^{14}C years ago (Clement et al. 1999). Beaufort et al. (2001), however, inferred from Coccolithophores production a significant occurence of the ENSO for this period, and Tudhope et al. (2001) based on the analysis of annually banded corals concluded that ENSO has been a persistent component of the climate system over the past 130 ka.

However, the local signal of the climatic changes in NW Argentina is still not well defined. Laminated sediments from a former landslide dammed lake in the Santa Maria Basin (NW Argentina, 26°S 66°W) contain valuable information about the environmental conditions for the period around 30,000 ^{14}C years ago (Trauth and Strecker 1999; Trauth et al. 2000). Hydrologic modeling of this palaeo-lake indeed indicates significantly wetter conditions during this time compared to the present (around 10 to 15 % higher precipitation, Bookhagen et al. 2001). Linear spectral analysis of palaeo-

Correspondence to: Norbert Marwan
e-mail: marwan@agnld.uni-potsdam.de

precipitation data derived from annual layered (varved) lake sediments also suggest an ENSO-like influence on rainfall and consequently increased interannual rainfall variability in river discharge and erosion (Trauth and Strecker 1999; Trauth et al. 2000). However, the results of such linear methods are often ambiguous and not appropriate, since natural processes are complex, exhibit nonstationarities and are mostly recorded as short and noisy time series. In fact, data gained from sedimentation processes (as colour data) are nonstationary by their origin and the relationship between climatic forcing and rainfall is not expected to be linear. Linear methods are usually unsuitable to investigate natural complex data. In addition, these approaches do not provide any information about a change in the climate dynamics, e. g. the sign of precipitation changes related to ENSO-like oscillations.

The aim of our work is to test the hypothesis that an enhanced ENSO-like influence on local rainfall caused a temporal landslide cluster 30,000 ^{14}C years ago. For this purpose, we first try to identify ENSO-like patterns in present-day precipitation data and infer causal links between this ocean-atmosphere oscillation and local rainfall. Secondly, we search for similar influences in palaeo-precipitation data reconstructed from 30,000 ^{14}C year old lake sediments. This comparison is carried out using a new method of nonlinear data analysis, the *cross recurrence plots (CRP)*, which can be applied to short and nonstationary complex data (Marwan and Kurths 2002). This procedure traces similarities and differences in several measures of complexity in both modern and past rainfall data. Significant occurrences of the ENSO-rainfall teleconnection together with increased rainfall could help to explain enhanced landsliding 30,000 ^{14}C years ago in NW Argentina where no major mass movements occur today.

2 Present-day Climatic Conditions

Summertime climate and atmospheric circulation over NW Argentina is largely governed by the South American monsoon system (e. g. Zhou and Lau 1998), featuring heavy precipitation, an upper-air anticyclone (Bolivian High) and a low-level trough (Chaco low). Approximately 80 % of the annual precipitation amount falls within the summer months November – February (Bianchi and Yañez 1992), associated with southward moisture transport to the east of the Andes through the Andean low-level jet (e. g. Nogués-Paegele and Mo 1997). The intra-andean basins and valleys, separated from this low-level moisture flux through the north-south running eastern Andean ridge, are arid and receive less than 200 mm yr^{-1}, whereas the regions to the east of this orographic barrier receive more than 1500 mm yr^{-1} (Bianchi and Yañez 1992).

Due to the seasonal change in the tropospheric temperature gradient between low and mid-latitudes, the subtropical westerly jet extends further north during the winter months, reaching its northernmost position around 27° S. The resulting wintertime mean westerly flow, which prevails over the study region in the mid- and upper troposphere, hinders regional moisture transport over the eastern slopes of the Andes and leads to a typically dry winter climate (less than 50 mm per month).

On interannual time scales, summer precipitation in the Central Andes, is primarily related to changes in meridional baroclinicity between tropical and subtropical latitudes, which in turn is a response to sea surface temperature anomalies in the tropical Pacific (e. g. Vuille et al. 2000; Garreaud and Aceituno 2001; Garreaud et al. in press). The study region therefore shows a significant relationship with ENSO, featuring a weakened westerly flow with a significantly enhanced easterly moisture transport during La Niña summers and strengthened westerly flow with a significantly subdued easterly moisture transport during El Niño summers. As a result, the rainy season is much more active during La Niña episodes and less active during El Niño episodes. These ENSO related atmospheric circulation anomalies are also evident in radiosonde data to the east of the Central Andes over NW Argentina (Salta), featuring enhanced southeasterly (northwesterly) flow and increased (decreased) specific humidity levels in the lower and mid-troposphere during La Niña (El Niño) summers (Vuille 1999). The notion that this ENSO influence indeed extends beyond just the Central Andes is further supported by several recent studies, which indicate that precipitation anomalies in this part of the Andes tend to coincide with anomalies of the same sign over SE Bolivia and NW Argentina (e. g. Aceituno and Montecinos 1997; Garreaud 1999). Bianchi and Yañez (1992) also report a weak but significant tendency toward less rain during El Niño years, based on a high-density network of 380 weather stations. Trauth et al. (2000) provide a detailed statistical analysis on the same data set showing that this tendency is very obvious but spatially and temporally highly variable. As indicated in Fig. 1 for the representative El Niño event 1965/66, precipitation can be decreased up to 80 % with respect to the long-term average in rainfall, with a more significant reduction in the northern part of the study area. A composite analysis of the monthly summer precipitation (DJFM) difference between El Niño and La Niña summers between 1979 and 1999 based on CMAP satellite-derived precipitation data (Xie and Arkin 1997) confirms this notion (Fig. 2). Although weak, the tendency toward less precipitation during El Niño and more precipitation during La Niña episodes is evident even in this low-resolution gridded data. Similar to the pattern in Fig. 1, the ENSO signal is reversed a few degrees further south, where summer precipitation becomes less dominant.

3 Methods

It is difficult to compare rainfall proxies from 30,000 ^{14}C year old lake sediments with present precipitation data. The process recording weather and climate in palaeo-archives is complex and so far not very well understood (Saltzman 1990; Bradley 1999). Because of various signal distortions in both time and frequency domain, the use of linear data analysis

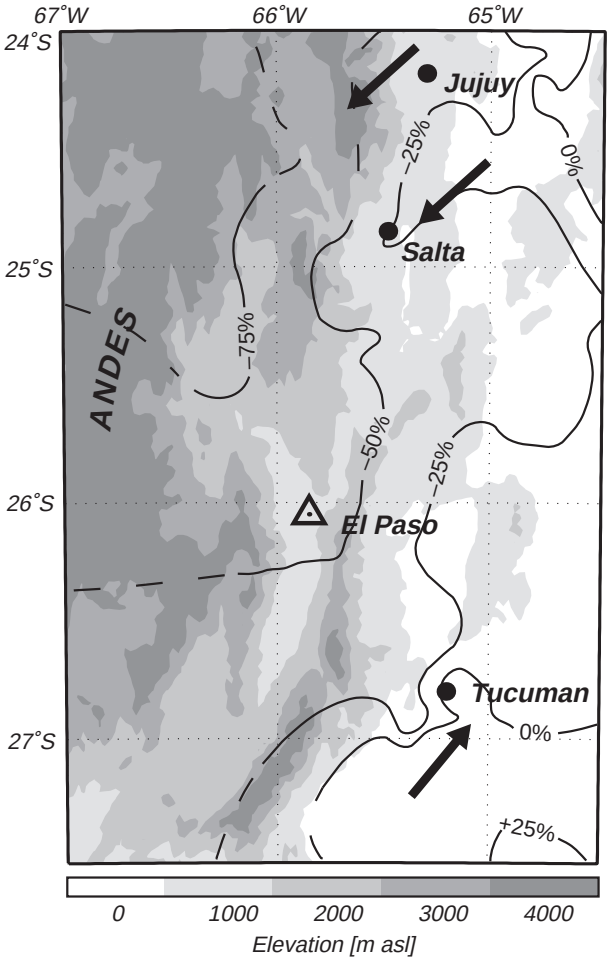

Fig. 1 Study area in the Santa Maria Basin with the locality of annual layered lake deposits in the locality El Paso, the relative precipitation anomaly during the El Niño 1965/66 compared to mean annual precipitation (annual precipitation as a mean from July to June; data from Bianchi and Yañez 1992) and the prevailing wind directions during January (black arrows; wind directions from Prohaska 1976).

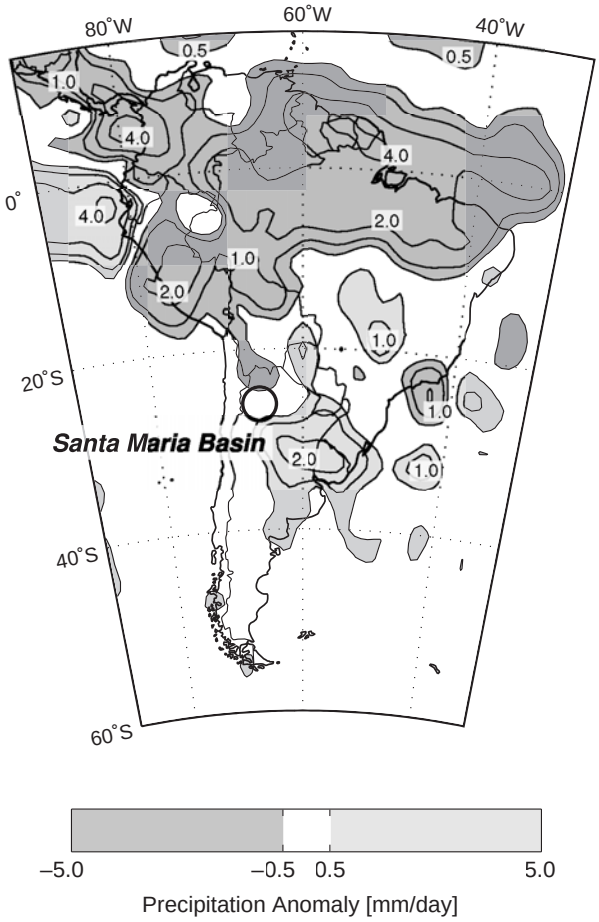

Fig. 2 Difference in precipitation (in mm day^{-1}) between El Niño and La Niña periods (El Niño – La Niña) for December – March based on CPC merged analysis of precipitation (CMAP, Xie and Arkin 1997) between 1979 and 1999. Contour interval is -4, -2, -1, -0.5, 0.5, 1, 2, 4 mm day^{-1}, regions with difference > 0.5 (< -0.5) shaded in light (dark) gray. An El Niño (La Niña) event is defined as a phase of at least six consecutive months in which the 5-month running mean of SSTA in the NINO3.4 region exceeds (or remains below) 0.5°C (-0.5°C). The reference period for the SSTA is 1961-90.

methods reaches its limits. The complexity of natural processes suggests the application of nonlinear methods instead for the analysis and comparison of such complex processes. Most of the nonlinear standard techniques, such as fractal dimensions or Lyapunov exponents, cannot be estimated for such data (Kantz and Schreiber 1997). Therefore, we have tried to quantify cross recurrence plots of present-day and palaeo-data. This reveals a suite of complexity measurements which give hints to identify similar patterns in present-day and palaeo-data. This comparison first tests the hypothesis that the signal extracted from the lake sediments is an appropriate measure for palaeo-precipitation. Secondly, it helps to reconstruct the variability in annual rainfall as compared to the present. Both results can then be used to test the hypothesis that increased interannual variability in climate can explain enhanced landslide activity 30,000 ^{14}C years ago.

3.1 Cross recurrence plots (CRP)

An important aspect of climate changes involves nonlinear interactions among many components of the earth's environmental system (e. g. Palmer 1999). These components include the oceans, land, lakes and continental ice sheets, and involve physical, biological, and chemical processes. Many of the techniques used to diagnose climatic variability such as Fourier analysis, empirical orthogonal functions or singular value decomposition are formulated using methods taken from linear analysis. However, while using these techniques it is difficult to analyze the nonlinear character of the earth's climate system. In the last two decades, a great variety of nonlinear techniques have been developed to analyse data of complex processes. Most popular are methods to estimate fractal dimensions or Lyapunov exponents (e. g. Mandelbrot 1982; Wolf et al. 1985; Kurths and Herzel 1987; Kantz and

Schreiber 1997). However, a number of pitfalls are possible due to the uncritical use of these methods on natural data, which are typically nonstationary and noisy. Furthermore, we cannot expect low dimensions in highly complex natural processes. Therefore, we have modified and applied the nonlinear data analysis method of cross recurrence plots, which was recently introduced by the extension of recurrence plots (Zbilut et al. 1998; Marwan et al. 2002), for detecting similarities and differences in the ENSO influence in present-day and past rainfall data. In order to quantify such similarities by using CRPs, new measures of complexity were introduced. Measures of complexity were developed in order to quantify the complexity of processes; the simplest measure is the entropy, which distinguishs between noisy and periodically processes. Here we use an approach which uses the geometrical structures which are contained in CRPs. This new technique is particularly efficient for the analysis of rather nonstationary, short and noisy data and was successfully applied to prototypical model systems with nonlinear interrelations (Marwan and Kurths 2002). Thus, the CRP is an appropriate method for time series analysis of climate and palaeo-climate data.

The basic idea of this approach is to compare the dynamics of two processes which are both recorded in a single time series. Following Taken's embedding theorem (Takens 1981), the dynamics of a process with $\hat{m}$ state parameters (i.e. $\hat{m}$ differential equations), which is, however, measured by only one time series $u(t) = u_i$ with length N and a sampling time Δt (i.e. $t = i\Delta t$), can be appropriately presented in its reconstructed phase space of a dimension m (theoretically when $m > 2\hat{m}+1$). Such a reconstruction can be formed by using the time delay method (embedding), where for each component of the state vector a value of the time series after a predefined delay τ (time delay) is choosen:

$$\mathbf{x}_i = \left(u_i, u_{i+\tau}, \ldots, u_{i+(m-1)\tau}\right),\ i = 1 \ldots N, \tag{1}$$

The dimension m of such a reconstructed state or phase space is called embedding dimension. The time evolution of the state vectors forms a trajectory $\mathbf{x}_i$, which runs through all possible states at time $t = i\Delta t$ and, thus, present the dynamics of the process.

The similarity in the behaviour of both processes in this reconstructed phase space can be examined by using the CRP, which visualizes the distance between segments of their phase space trajectories $\mathbf{x}_i$ and $\mathbf{y}_i$ of the embedded time series (Marwan and Kurths 2002)

$$\mathbf{CR}^{+}_{i,j} = \Theta(\varepsilon - \|\mathbf{x}_i - \mathbf{y}_j\|), \quad i, j = 1 \ldots N, \tag{2}$$

where ε is a predefined cut-off distance, $\|\cdot\|$ is the norm (e. g. the Euclidean norm) and $\Theta(x)$ is the Heaviside function. Depending on the type of the application, ε can have a fixed value or can vary for each i in such a way that a predefined number of neighbours occur within a certain radius ε (Eckmann et al. 1987; Marwan et al. 2002). This results in a constant density of recurrence points in each column of the CRP and is particularly useful in the analysis of complex processes with differences in the variability of the amplitudes.

The CRP is a two-dimensional $N \times N$ array of points where N is the number of embedding vectors obtained from the delay coordinates of the input signal. The values of the CRP are *one* (black points) if trajectories lie close to each other (recurrence points), whereas values of *zero* (white points) document rather large distances between two trajectories. From the occurrence of lines in the CRP parallel to the diagonal in the recurrence plot it can be seen how fast neighbouring trajectories diverge in the phase space. Recurrent data in a system would create diagonal lines in a distance t from the main diagonal in such a plot comparing both phase-space embeddings with respect to the time delay t. It is important to note that an additional CRP with opposite signed second time series $\mathbf{CR}^{-}_{i,j} = \Theta(\varepsilon - \|\mathbf{x}_i + \mathbf{y}_j\|)$ allows to distinguish positive and negative relations.

Visual inspection of CRPs already reveals valuable information about the relationship between two complex processes. However, a better understanding of causal links between both processes demands a more quantitative examination of the CRPs. Therefore, we introduce the following two statistical measures of complexity (Marwan and Kurths 2002):

the *recurrence rate*,

$$RR(t) = \frac{1}{N-i} \sum_{j=1}^{N-i} \left(\mathbf{CR}^{+}_{j,j+i} - \mathbf{CR}^{-}_{j,j+i}\right), \tag{3}$$

and the *averaged diagonal length*

$$L(t) = \frac{\sum_{l=l_{min}}^{N-i} l\,[P^{+}(l,t) - P^{-}(l,t)]}{\sum_{l=l_{min}}^{N-i} [P^{+}(l,t) - P^{-}(l,t)]}, \tag{4}$$

where l_{min} is a predefined minimal length of a diagonal line segment, $P^{\pm}(l,t)$ is the histogram of the diagonal line lengths in $\mathbf{CR}^{\pm}$ at a distance t from the main diagonal (i. e. the time delay t between the two phase space vectors) and $t = i\Delta t$. The $RR(t)$ is the density of adjacent states, i. e. of the recurrence points in a CRP diagonal. $RR(t)$ therefore measures the probability of similar states in both processes after a delay time t. High densities of recurrence points in a diagonal cause high values of RR, which is typical for processes with a similar behaviour in the phase space.

Strongly fluctuating data cause short or absent diagonals in the CRP, whereas data from deterministic processes produce longer diagonals. If two deterministic processes have the same or similar phase-space behaviour, i. e. the phase-space trajectory reaches the same regions of the phase space during certain times, then the number of longer diagonals will increase and the amount of short diagonals decrease. The average diagonal length L measures the epoch length (i. e. the time span) of significant similarities in the behaviour of both processes. The higher the coincidence of both processes, the larger the length of these diagonals.

Consequently, high values of RR and L correspond to frequent and longer periods of similar behaviour of the processes as recorded in the time series data. Therefore, these parameters are appropriate quantitative measures for the similarities between both processes. However, extrema at longer

delays t do not necessarily correspond with high correlations. Future work will concentrate on the theoretical and more detailed investigation of the interrelations between the structures in CRPs.

We have proposed a statistical evaluation of the quantitative measures of the CRP with an ensemble of a large amount of surrogate data.

The assumption for the surrogate data is that the considered processes are linearly independent and do not have any similar dynamics. These surrogates should reveal some features like in our original data but also features caused by the randomness of a possible correlation (stochastic processes). Linear correlated noise is a paradigmatic example for such processes (Kantz and Schreiber 1997). We calculate a surrogate time series based on this class of processes with the following recursive function, a autoregressive process of order p,

$$x_n = \sum_{i=1}^{p} a_p x_{n-p} + b\xi_n,$$

where ξ is white noise and a_i are coefficients which determine the auto-correlation of the system and allow to adapt this stochastic system to our natural processes. We fit the model to the precipitation series of the station Tucuman. Then we perform the CRP analysis using the SOI data and the ensemble of, e. g. $10,000$ realizations of precipitation series produced by the AR model. Using the distributions of the *RR* and L measures we can estimate their empirical confidence bounds (we will use the 2σ-bounds which approximately correspond with the 95% confidence level).

With these confidence bounds we can evaluate the obtained measures of CRP and the relations of the natural processes. Since the surrogates are from a stationary system and the natural data are nonstationary, we have further applied this kind of evaluation to more stationary segments in the natural data. We got the same results. This kind of surrogates is a special realization, which is prototypical for linear stochastic processes, and there are a lot of other possibilities to construct surrogates.

3.2 Comparison of modern and palaeo-precipitation variability

In order to test the new method on precipitation data, we first compute the CRP for rainfall stations with well established and clear ENSO influence. We use monthly precipitation data from the cities of Buenos Aires (BAI) and Caracas (CAR) from the WMO data set (Hoffmann 1975). For the assessment of the modern ENSO influence on local rainfall in NW Argentina, we analyze monthly precipitation data from three stations: San Salvador de Jujuy (JUY), Salta (SAL) and San Miguel de Tucuman (TUC; Figs. 1 and 3 B). These stations in the capitals of the provinces Jujuy, Salta and Tucuman provide the longest time series from this area and are located on a north-south transect. Moreover, these locations are influenced by different local winds; Jujuy and Salta mainly receive north-easterly and easterly moisture-bearing winds during the summer rainy season, whereas Tucuman is characterized by southerly and south-westerly winds (Prohaska 1976). The Southern Oscillation Index (SOI) is used as a measure for the ENSO variability between the years 1884 and 1990 (Fig. 3 A, based on COADS data). This index is the normalized difference between the sea level air pressure in Tahiti and Darwin. Extreme negative values represent El Niño events and extreme positive values represent La Niña events (Ropelewski and Halpert 1987). In our analysis, we use monthly data, i. e. twelve data points per year in order to avoid loosing valuable intraannual information. Moreover, longer data vectors improve the significance of the CRP measures, thus the use of annual data would significantly reduce the value of our results. The potential distortion of the final result by differences in the causal linkage between ENSO and rainfall over the year, i. e. between dry and wet season, is believed to be of minor importance since the absolute values of precipitation during the dry season are low and hence the contribution to the analysis is small. The rainfall variability during the dry season is not significantly different from white noise and disappears after low-pass filtering preceding the actual time series analysis.

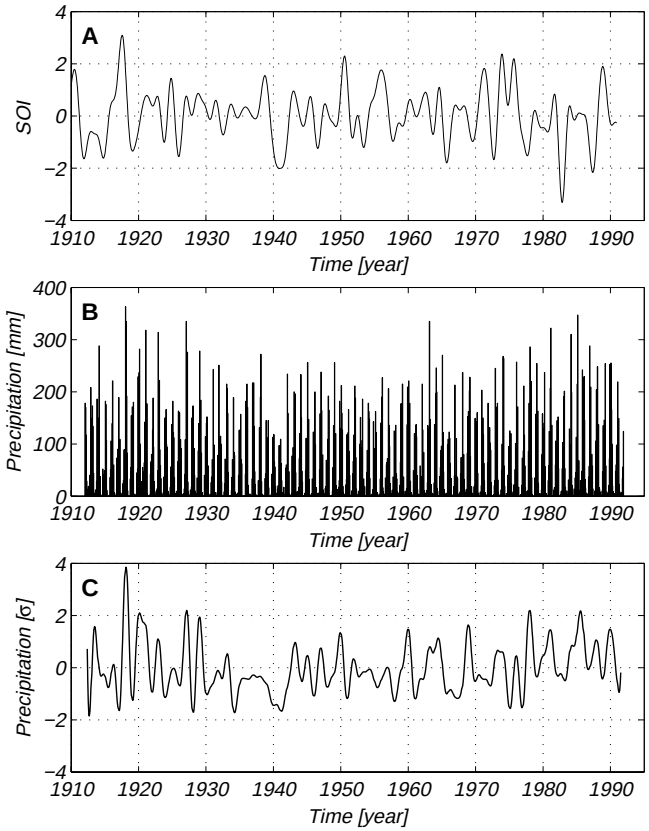

Fig. 3 Smoothed and σ-normalized time series of the Southern Oscillation Index (A), monthly precipitation data of Salta (B) and its smoothed and σ-normalized time series (C). SOI based on COADS data from the NOAA Live Access Server (http://ferret.wrc.noaa.gov).

The CRP analysis of the present-day ENSO and precipitation data reveals characteristic patterns that can now be traced in palaeo-precipitation data. The palaeo-precipitation variability is inferred from varved lake sediments sampled at the location *El Paso* (EP; 26.0°S, 65.8°W) in the Santa Maria Basin in NW Argentina (Figs. 1 and 4). These sediments were deposited in a landslide dammed lake 30,000 ^{14}C years ago (Trauth and Strecker 1999; Hermanns and Strecker 1999). Because of the internal structure of the deposits with intra-varved changing of diatom species and the cyclic recurrence of paired diatomite and clastic layers, these laminations are varves (Trauth and Strecker 1999). The annual cycle with wet summers and dry winters caused significant changes in the lake sedimentation. During the rainy season mainly ocher coloured silty sediments were deposited; during the subsequent dry season a thin white layer consisting of the skeletons of silica algae (diatoms) was deposited. Due to its white colour, the diatomaceous layers can be used to identify single years in these sediments. Recurring intense red colouration of the silty part of the annual layers is sourced from reworked older sediments which are eroded and deposited only during extreme rainfall events. Therefore, the intensity of red colour in the varved deposits can be interpreted as a proxy for precipitation variation at El Paso site (Trauth and Strecker 1999; Trauth et al. 2000). The more intense the red colour the higher was the precipitation during the rainy season.

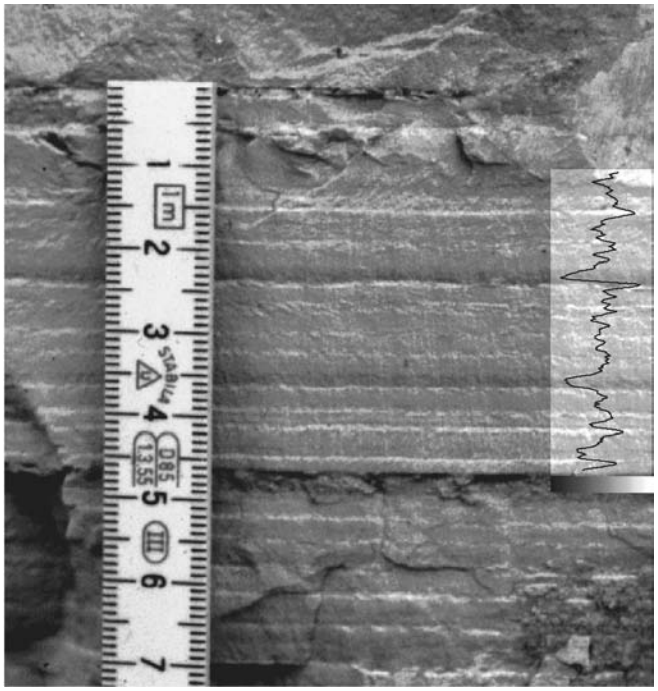

Fig. 4 Detail of varved lake sediments from the El Paso site in the Santa Maria Basin with cyclic occurrence of dark red colourations recording more precipitation and sediment flux with ENSO-like periodicities (Trauth and Strecker 1999). The overlayed curve shows a representative red colour intensity transect of the deposits.

The colour intensity of a section of the sediments profile with a length of 160 varves was gained by scanning high quality photographs. After digital pre-processing, a time series of red intensity values on a length scale was obtained. We transform these data to a time scale assuming an annual recurrence of the diatomaceous layers. Within single varves 12 subannual data points are computed by logarithmic interpolation of the data taking into account the exponential decrease of the sedimentation rate during the annual cycle (Fig. 5). The power spectrum estimate of the red colour intensity reveals significant peaks within the ENSO frequency band of 2 to 4 years, suggesting an ENSO-like influence (Trauth et al. 2000). Because of the nonstationarity of these data (the sedimentation process in a lake is not stationary, resulting in nonstationary proxy parameters for the in-lake processes; mean of the first half of the time series is 0.30, of the second half is -0.32; standard deviation of the first half of the time series is 1.13, of the second half is 0.71), linear correlation analysis is unsuitable. Therefore, we apply the CRP analysis to these data.

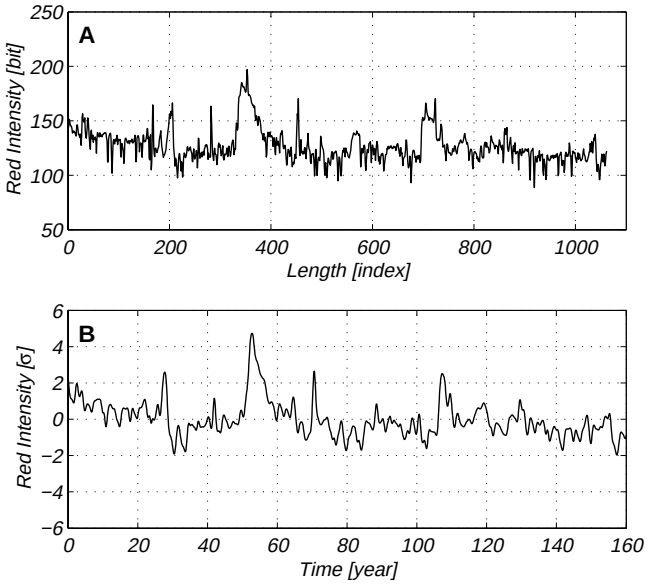

Fig. 5 Red intensity values of the lake sediments of site EP160 on (A) a length scale and on (B) a time scale and after smoothing and normalization; the unit of raw data is one bit, the unit of transformed and smoothed data is the standard deviation σ.

4 Results of Nonlinear Data Analysis

First, all time series are normalized and low-pass filtered using a 7th-order Butterworth filter with a cutoff frequency of 1/18 month^{-1} in order to remove the predominant annual cycle from the data (Figs. 3 C and 5). Butterworth filters are from the infinite-duration impulse response type (IIR filters) and have a monotonically decreasing response with respect to frequency (Elliott 1987).

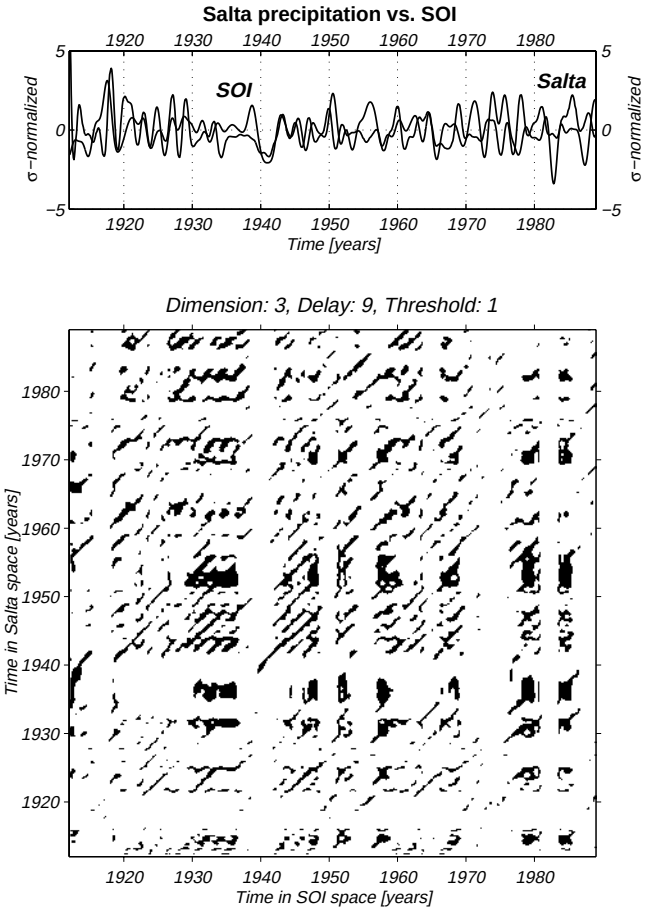

Fig. 6 Cross recurrence plot of SOI vs. precipitation data from the city of Salta (SAL). The *x*-axis shows the time along the phase space trajectory of the SOI and the *y*-axis that of SAL. Black points represent the occurrence of similar states in both processes. Diagonal lines correspond with epochs of similar dynamics in both processes. The amount and length of these lines can be used as measures of the similarity of both processes.

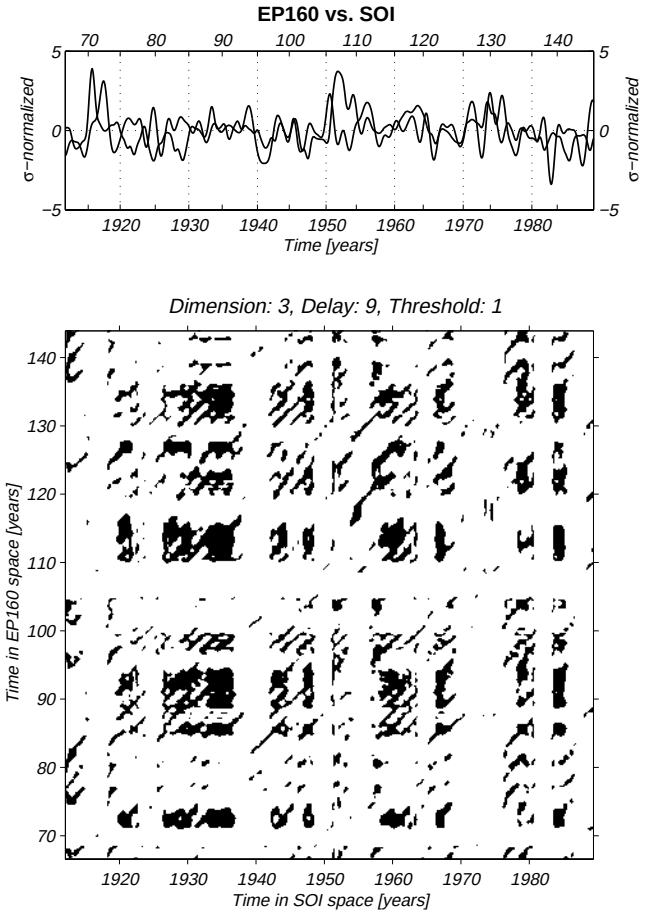

Fig. 7 Cross recurrence plot of SOI vs. the best matching section of palaeo-precipitation (EP160). Scaling as in Fig. 6. The *x*-axis shows the time along the phase space trajectory of the SOI and the *y*-axis that of EP160.

Next, the filtered rainfall data and the Southern Oscillation Index (SOI) are embedded into a phase space using $m = 3$ and $\tau = 9$. The method of nonlinear time series analysis using delay time embedding relies on a choice of good delay time and the embedding dimension. Proper values for these parameters are determined using the methods of false nearest neighbours and mutual information (Kantz and Schreiber 1997). The quantitative analysis of cross recurrence plots is then applied to pairs of time series, local precipitation records and the Southern Oscillation Index (SOI). The CRPs are computed using a fixed amount of nearest neighbours with $\varepsilon = 15\%$. Since the statistics of CRPs are sensitive to changes in the cutoff distance, we have run sensitivity tests in order to find the optimum value of ε. The value of 15 % appears to be the best choice receiving robust and precise results.

The CRPs of all pairs of time series show similar features. The significant similarities between CRPs obtained from modern (Fig. 6) and palaeo-precipitation data (Fig. 7) indicate that the red colour intensity records from the varved lake sediment do reflect rainfall in NW Argentina. First we discuss the CRP of Salta precipitation (data series SAL) vs. the Southern Oscillation Index (SOI) and the CRP of red colour intensity of varves (data series EP160) vs. SOI. The *x*-axis represents time along the phase space trajectory of the SOI, whereas the *y*-axis represents the time along the phase space trajectory of SAL or EP160, respectively. The CRP of SAL vs. SOI exhibits longer diagonal lines in two to four year intervals, which matches the same frequency band obtained by the power spectral analysis (Fig. 6). This indicates that some sequences of the phase space trajectory of the SOI recur in sequences of the phase space trajectory of SAL after relocating by the time of two to four years. Vertical white bands in the CRP represent less frequent states in SOI, such as horizontal white bands suggest for SAL. The latter occurs with intervals of more than ten years. The CRP between EP160 and SOI shows similar characteristics as the CRP described above (Fig. 7). Longer diagonal lines have spacings of about two to four years. White bands occur at time scales of more than ten years. Some linkages in both CRPs are obvious by visual inspection. Next, the quantitative analysis of the CRPs is performed in order to study statistically these relations and

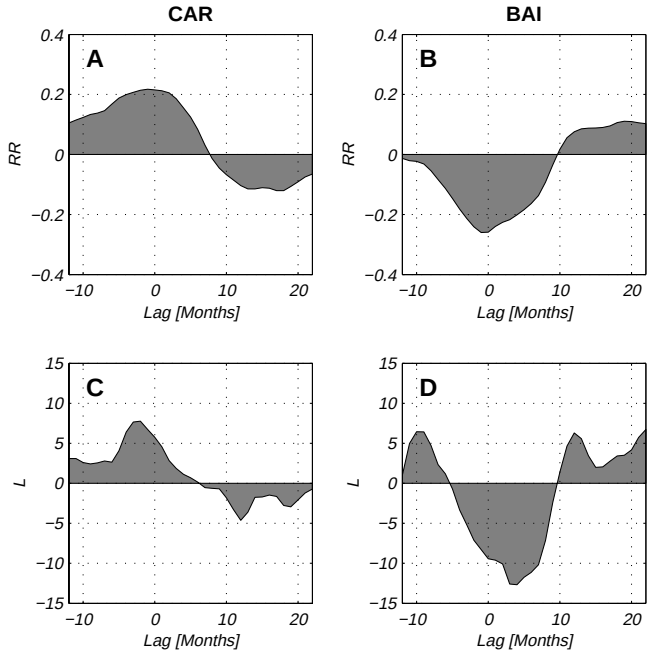

Fig. 8 *RR* and *L* measures of the cross recurrence plots between SOI and precipitation in Caracas (A, C) and Buenos Aires (B, D) with a well-established and clear ENSO influence. Extreme values reveal high similarity between the dynamics of the rainfall and the ENSO.

to allocate the predefined causality patterns to certain localities.

In order to calculate the measures of complexity *RR* and *L* between the rainfall data and SOI, we used a delay time in the range between -12 and $+22$ months, i. e. these measures are determined in a small corridor above and below the main diagonal. We are interested in the extrema and in the time lag where they occur and we get the following results for the various pairs of records. From an ensemble of $10,000$ realizations of a 5th-order AR-model we calculate the 2σ-bounds of their distributions for *RR* and *L*. The coefficients for the AR-model are adapted to the Tucuman precipitation (we also used AR-models adapted to the rainfall data of the other stations, which revealed similar results). The order of the AR-model is determined with the Akaike's Information Criterion and a criterion, which assesses whether the residues follow white noise (Schlittgen and Streitberg 1999).

The CRP measures between CAR and SOI reveal extreme positive values and between BAI and SOI extreme negative values, which reflect the strong influence of ENSO in these areas (Fig. 8). The parameter *RR* of the CRPs between TUC and SOI has small negative values, which do not exceed the 2σ-bounds, and does not show preferences for a distinct lag. The parameter *L* has also small values, but it has rather small maxima and minima at delays of -1, 4 and 8 months. These results indicate that the precipitation in Tucuman is not strongly influenced by ENSO. If there is a weak influence, the rainfall would increase during El Niño (Fig. 9 A, E). The analysis of JUY and SOI reveals clear positive values around a lag of zero and negative values after about 8 – 12 months, which suggests a significant link between Jujuy rainfall and ENSO (Fig. 9 C, G). The measures for the analysis SAL vs. SOI show smaller maxima for a delay of about zero and minima after a lag of about 8 – 12 months. We therefore infer a weaker linkage between Salta rainfall and ENSO (Fig. 9 B, F; the disrupted minima in the *L* parameter at around ten months is due to the short data length and a resulting nonstationarity in the CRP). The measures for SAL and JUY exceed the 2σ-bounds.

The 30,000 ^{14}C year old precipitation data are not simply comparable with present-day data, because there is no information available about how to synchronize the rainfall records with modern climate indices. Therefore we seek the time window in these data showing the highest coincidence in the dynamics using maximum values for *RR* and *L* as the key criterion. Although the observed coincidence is not very high, it yields the time section in the palaeo-precipitation record EP160 which can be best correlated with modern data. In our palaeo-data EP160 we find such a section represented by maximum and minima values for *RR* and *L* for delays of about zero and ten months, similar to those found for JUY and SAL (Fig. 9 D, H). The *RR* and *L* measures exceed also the 2σ-bounds.

To use the minima at lags around 8 – 12 months for climatological interpretations is difficult and might lead to erroneous conclusions, but these characteristic patterns of positive and negative interrelations can be used to compare the present-day and palaeo-data. The positive and negative interrelations have the same time delay between 10 and 12 months in the present-day and the palaeo-data.

5 Discussion

We applied the method of cross recurrence plots (CRPs) to modern and palaeo-precipitation data in order to compare the magnitude and causes of rainfall variability in the NW Argentine Andes today and during the time of enhanced landsliding at around 30,000 ^{14}C years ago. CRPs are able to look for nonlinear interrelations between two processes. The major result from this analysis is the significant similarity between the complex dynamics of modern rainfall and the palaeo-precipitation as recorded in the red colour intensity record from the lake sediments in the location El Paso. The distances between longer diagonal lines in the CRP of both records are about two to four years, the approximate time of recurrence of extreme ENSO phases today. The first implication of this result is that the red colour intensity of the sediments is indeed a good proxy for the rainfall intensity 30,000 ^{14}C ago. This result is in line with the observations of Trauth et al. (2000) suggesting an enhanced erosion of red-coloured clastic sediments during heavy rainfall events today whereas precipitation usually only reaches the elevated areas with mainly greenish low-grade metamorphic rocks exposed. This effect causes predominant greenish to buff-coloured clays deposited in the former lake basin (Trauth and Strecker 1999; Trauth et al. 2000 2003).

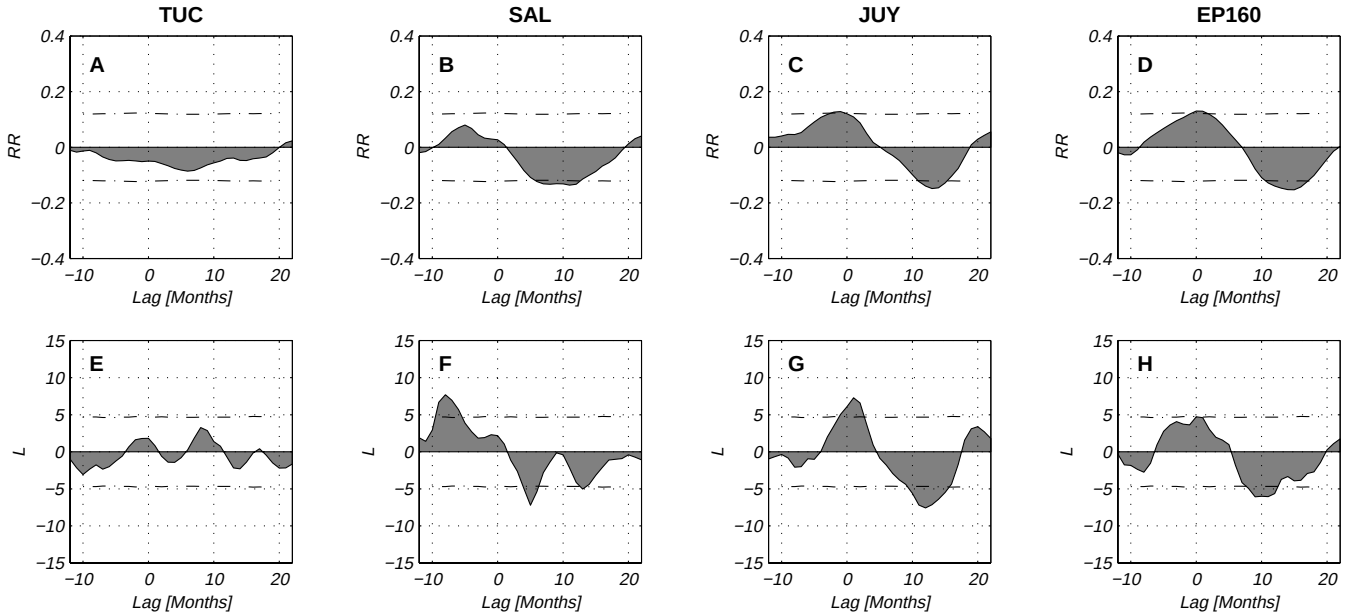

Fig. 9 *RR* and *L* measures of the cross recurrence plots between SOI and precipitation in Tucuman (A, E), Salta (B, F), Jujuy (C, G) and palaeo-precipitation (D, H). Extreme values reveal high similarity between the dynamics of the rainfall and the ENSO. The dash-dotted lines are the empirical 2σ-bounds from the distributions of an ensemble of data based on a 5th-order AR-model.

Since our analysis of modern data reveals a strong relation between local rainfall in the northern part of the study area (Jujuy) and ENSO, we interpret this similarity as an indication of a strong ENSO-like influence in the Santa Maria Basin at around 30,000 years. In contrast, there is no significant linkage between the modern rainfall in Tucuman and ENSO. This result could indicate that ENSO does not influence precipitation in the southern part of the study area or this influence is rather diffuse or changing in time.

The CRP between the SOI and the rainfall in Jujuy and Salta reveals a positive relation without any large delay, i. e. the occurrence of an El Niño at the end of a year would cause decreased rainfall in the rainy season from November to January and the occurrence of a La Niña would cause increased rainfall during this time of the year. The opposite response after a delay of 8 – 12 months is not easy to interpret, because we do not know which mechanism actually caused this linkage. The time span between the identified maxima and minima is about one year and could be explained by the fact that La Niña events often follow El Niño events. The smooth shape of the CRP measure curves are artefacts caused by low-pass filtering of the time series. The measures of CRP of Tucuman precipitation and SOI show non-significant values without any characteristic delays. The analysis of varve data reveals a significant positive relation between SOI and palaeo-precipitation at the location El Paso. Similar to the modern situation, the CRP shows a significant negative relation with SOI after a delay of about ten months. Both interrelations are rather similar to those of ENSO–JUY and ENSO–SAL.

The similarities between the time series of the modern rainfall data and the palaeo-precipitation record from the lake sediments suggests that an ENSO-like oscillation was active at around 30,000 ^{14}C years ago (roughly corresponding to 34,000 cal. years BP), which corresponds with the results of the investigation of Coccolithophores production (Beaufort et al. 2001). A younger landslide cluster in the same region at around 5000 ^{14}C (corresponding to 5800 cal. years BP) was also explained by a stronger ENSO influence at that time (Trauth et al. 2000; palaeo-ENSO evidence from Keefer et al. 1998; Sandweiss et al. 2001; Haug et al. 2001). The spacing between both landslide clusters is around 28,000 years. Although two landslide clusters do not allow to infer a systematic recurrence of such events, we believe that there is some evidence that these events correspond to the periods of a strong ENSO-like variation as reported from deep-sea sediments off-shore Peru (Oberhänsli et al. 1990), in the Indo-Pacific Ocean (Beaufort et al. 2001) and New Guinea corals (Tudhope et al. 2001). These long-term ENSO records suggest a mixed precession-glacial forcing on ENSO resulting in significant 23- and 30-kyr cyclicities, which confirms model results and recently inferred relations between ENSO variability and insolation (Clement et al. 1999; Liu et al. 2000; Rittenour et al. 2000).

In the semiarid basins of the NW Argentine Andes, the ENSO-like variation could have caused significant fluctuations in local rainfall at around 30,000 ^{14}C years similar to the modern conditions. Together with generally higher moisture levels as indicated by lake balance modeling results, this mechanism could help to explain enhanced landsliding at around 30,000 and 5,000 ^{14}C years ago in the semiarid basins of the Central Andes.

6 Conclusions

The quantitative analysis of cross recurrence plots has revealed similarities in the evolution of the phase space trajectory of climate indices and present-day and past rainfall. In comparison to the usually less variable climate during ice ages, our result suggests an enhanced impact of ENSO-like conditions on local climate in the Santa Maria Basin 30,000 ^{14}C years ago associated with a strong inter- and intraannual variability of rainfall and an intensification of moisture transport. A more variable climate due to an enhanced ENSO-like impact could have raised the risk of landsliding in this region and could help to explain enhanced landslide activity at around 30,000 ^{14}C years ago.

7 Acknowledgments

This work is part of the Collaborative Research Center 267 *Deformation Processes in the Andes* and the Priority Programme *Geomagnetic variations: Spatio-temporal structures, processes and impacts on the system Earth* supported by the German Research Foundation. We gratefully acknowledge U. Schwarz and M. Thiel for useful conversations and discussions and U. Bahr and M. Strecker for support of this work. Further we would like to thank the NOAA-CIRES Climate Diagnostics Center for providing COADS and CMAP data.

References

Aceituno P, Montecinos A (1997) Patterns of convective cloudiness in South America during austral summer from OLR pentads. In: Preprints Fifth Int. Conf. on Southern Hemisphere Meteorology and Oceanography, Pretoria, South Africa. Amer Meteor Soc, pp 328–329

Beaufort L, de Garidel-Thoron T, Mix AC, Pisias NG (2001) ENSO-like Forcing on Oceanic Primary Production During the Late Pleistocene. Science 293: 2440–2444

Bianchi AR, Yañez CE (1992) Las precipitaciones en el noroeste Argentino. Instituto Nacional de Tecnologia Agropecuaria, Estacion Experimental Agropecuaria Salta

Bookhagen B, Haselton K, Trauth MH (2001) Hydrological modelling of a Pleistocene landslide-dammed lake in the Santa Maria Basin, NW Argentina. Palaeogeogr Palaeoclimatol Palaeoecol 169: 113–127 DOI 10.1016/S0031-0182(01)00221-8

Bradley RS (1999) Paleoclimatology – Reconstructing Climates of the Quaternary. Vol 64 of International Geophysics Series. Academic Press, San Diego

Clement AC, Seager R, Cane MA (1999) Orbital controls on the El Niño/Southern Oscillation and the tropical climate. Paleoceanography 14: 441–456

Dethier DP, Reneau SL (1996) Lacustrine chronology links late Pleistocene climate change and mass movement in northern New Mexico. Geology 24: 539–542

Eckmann J-P, Kamphorst SO, Ruelle D (1987) Recurrence Plots of Dynamical Systems. Europhys Lett 5: 973–977

Elliott DF (1987) Digital Signal Processing. Academic Press, San Diego.

Garreaud R, Aceituno P (2001) Interannual rainfall variability over the South American Altiplano. J Clim 14: 2779–2789

Garreaud R, Vuille M, Clement A (in press) The climate of the Altiplano: Observed current conditions and mechanisms of past changes. Palaeogeogr Palaeoclimatol Palaeoecol DOI 10.1016/S0031-0182(03)00269-4

Garreaud RD (1999) Multi-scale analysis of the summertime precipitation over the Central Andes. Mon Weather Rev 127: 901–921

Godfrey L, Lowenstein TK, Li J, Luoand S, Ku T-L, Alonso RN, Jordan, TE (1997) Registro Continuo del Pleistocene Tardio Basado en un Testigo de Halita del Salar de Hombre Muerto, Argentina. In: VIII Congreso Geologico Chileno. Vol 1. pp 332–336

Grosjean M, Cartajena I, Messerli B (1997) Mid-Holocene Climate and Culture Change in the Atacama Desert, Northern Chile. Quaternary Res 48: 239–246 DOI 10.1006/qres.1997.1917

Haug GH, Hughen KA, Sigman DM, Peterson LC, Röhl U (2001) Southward migration of the intertropical convergence zone through the Holocene. Science 293: 1304–1308

Hermanns RL, Strecker MR (1999) Structural and lithological controls on large Quaternary rock avalanches (sturzstroms) in arid northwestern Argentina. GSA Bulletin 111: 934–948

Hoffmann JAJ (1975) Climate Atlas of South America – Maps of Mean Temperature and Precipitation. Unesco Cartographia, WMO

Kantz H, Schreiber T (1997) Nonlinear Time Series Analysis. University Press, Cambridge

Keefer DK, de France SD, Moseley ME, Richardson III JB, Satterlee DR, Day-Lewis AO (1998) Early Maritime Economy and El Niño Events at Quebrada Tacahuay, Peru. Science 281: 1833–1835

Kurths J, Herzel H (1987) An attractor in a solar time series. Physica D 25: 165–172 DOI 10.1016/0167-2789(87)90099-6

Ledru MP, Braga PIS, Soubiès F, Fournier M, Martin L, Suguio K, Turcq B (1996) The last 50,000 years in the Neotropics, Southern Brazil: evolution of vegetation and climate. Palaeogeogr Palaeoclimatol Palaeoecol 123: 239–257 DOI 10.1016/0031-0182(96)00105-8

Liu Z, Kutzbach J, Wu L (2000) Modeling climatic shift of El Niño variability in the Holocene. Geophys Res Lett 27: 2265–2268

Mandelbrot BB (1982) The fractal geometry of nature. Freeman, San Francisco

Marwan N, Kurths J (2002) Nonlinear analysis of bivariate data with cross recurrence plots. Phys Lett A 302 (5–6): 299–307 DOI 10.1016/S0375-9601(02)01170-2

Marwan N, Thiel M, Nowaczyk NR (2002) Cross Recurrence Plot Based Synchronization of Time Series. Nonlinear Proc Geoph 9 (3/4): 325–331

Nogués-Paegele J, Mo KC (1997) Alternating wet and dry conditions over South America during summer. Mon Weather Rev 125: 279–291

Oberhänsli H, Heinze P, Diester-Haass L, Wefer G (1990) Upwelling off Peru during the last 430,000 yr and its relationship to the bottom-water environment, as deduced from coarse grain-size distributions and analyses of benthic foraminifers at holes 679D, 680B, and 681B, LEG 112. In: Suess E, von Huene R (Eds.), Proceedings of the Ocean Drilling Program. Scientific Results. Vol 112. pp 369–382

Palmer TN (1999) A nonlinear dynamical perspective on climate prediction. J Clim 12: 575–591

Prohaska FJ (1976) The climate of Argentina, Paraguay and Urugay. Vol 12 of World Survey of Climatlogy. Elsevier, Amsterdam, Oxford, New York, pp 13–73

Rittenour TM, Brigham-Grette J, Mann ME (2000) El Niño Climate Teleconnections in New England During the Late Pleistocene. Science 288: 1039–1042

Ropelewski CF, Halpert MS (1987) Global and Regional Scale Precipitation Patterns Associated with the El Niño/ Southern Oscillation. Mon Weather Rev 115: 1606–162

Saltzman B (1990) Three basic problems of paleoclimate modeling: a personal perspective and review. Clim Dynam 5: 67–78

Sandweiss DH, Maasch KA, Burger RL, Richardson III JB, Rollins HB, Clement A (2001) Variation in Holocene El Niño frequencies: Climate records and cultural consequences in ancient Peru. Geology 29: 603–606

Schlittgen R, Streitberg BHJ (1999) Zeitreihenanalyse. Oldenbourg, München, Wien

Strecker MR, Marret R (1999) Kinematic evolution of fault ramps and its role in development of landslides and lakes in the northwestern Argentine Andes. Geology 27: 307–310

Takens F (1981) Detecting Strange Attractors in Turbulence. Vol 898 of Lecture Notes in Mathematics. Springer, Berlin, pp 366–381

Trauth MH, Alonso RA, Haselton K, Hermanns R, Strecker MR (2000) Climate change and mass movements in the northwest Argentine Andes. Earth Planet Sc Lett 179: 243–256 DOI 10.1016/S0012-821X(00)00127-8

Trauth MH, Bookhagen B, Mueller AB, Strecker MR (2003) Late Pleistocene Climate Change and Erosion in the Santa Maria basin, NW Argentina. J Sediment Res 73

Trauth MH, Strecker MR (1999) Formation of landslide-dammed lakes during a wet period between 40,000 and 25,000 yr B. P. in northwestern Argentina. Palaeogeogr Palaeoclimatol Palaeoecol 153: 277–287 DOI 10.1016/S0031-0182(99)00078-4

Tudhope AW, Chilcott CP, McCulloch MT, Cook ER, Chappell J, Ellam RM, Lea DW, Lough JM, Shimmield GB (2001) Variability in the El Niño Southern Oscillation Through a Glacial-Interglacial Cycle. Science 291: 1511–1517

Turcq B, Pressinotti MMN, Martin L (1997) Paleohydrology and Paleoclimate of the Past 33,000 Years at the Tamaduá River, Central Brazil. Quaternary Res 47: 284–294 DOI 10.1006/qres.1997.1880

van der Hammen T, Absy ML (1994) Amazonia during the last glacial. Palaeogeogr Palaeoclimatol Palaeoecol 109: 247–261

Vuille M (1999) Atmospheric circulation over the Bolivian Altiplano during dry and wet periods and extreme phases of the Southern Oscillation. Int J Climatol 19: 1579–1600 DOI 10.1002/(SICI)1097-0088(19991130)19:14<1579::AID-JOC441>3.0.CO;2-N

Vuille M, Bradley RS, Keimig F (2000) Interannual climate variability in the Central Andes and its relation to tropical Pacific and Atlantic forcing. J Geophys Res 105: 12447–12460

Wolf A, Swift JB, Swinney HL, Vastano JA (1985) Determining Lyapunov Exponents from a Time Series. Physica D 16: 285–317 DOI 10.1016/0167-2789(85)90011-9

Xie P, Arkin PA (1997) Global Precipitation: A 17-year monthly analysis based on gauge observations, satellite estimates, and numerical model outputs. B Am Meteorol Soc 78: 2539–2558

Zbilut JP, Giuliani A, Webber Jr., CL (1998) Detecting deterministic signals in exceptionally noisy environments using cross-recurrence quantification. Phys Lett A 246: 122–128 DOI 10.1016/S0375-9601(98)00457-5

Zhou J, Lau K-M (1998) Does a monsoon climate exist over South America? J Climate 11: 1020–1040

Appendix E

Cross Recurrence Plot Based Synchronization of Time Series

MARWAN, N., THIEL, M., NOWACZYK, N. R., Cross Recurrence Plot Based Synchronization of Time Series. Nonlinear Processes in Geophysics 9 (3/4), 2002a, 325–331.

Nonlinear Processes in Geophysics (2002) 9: 325–331

Nonlinear Processes in Geophysics

Cross recurrence plot based synchronization of time series

N. Marwan[1], **M. Thiel**[1], **and N. R. Nowaczyk**[2]

[1]Institute of Physics, University of Potsdam, Germany
[2]GeoForschungs-Zentrum Potsdam, Germany

Received: 3 September 2001 – Accepted: 25 October 2001

Abstract. The method of recurrence plots is extended to the cross recurrence plots (CRP) which, among others, enables the study of synchronization or time differences in two time series. This is emphasized in a distorted main diagonal in the cross recurrence plot, the line of synchronization (LOS). A non-parametrical fit of this LOS can be used to rescale the time axis of the two data series (whereby one of them is compressed or stretched) so that they are synchronized. An application of this method to geophysical sediment core data illustrates its suitability for real data. The rock magnetic data of two different sediment cores from the Makarov Basin can be adjusted to each other by using this method, so that they are comparable.

1 Introduction

The adjustment of data sets with various time scales occurs on many occasions, e.g. data preparation of tree rings or geophysical profiles. In geology, often a large set of geophysical data series is taken at various locations (e.g. sediment cores). That is why these data series have a different length and time scale. Before any time series analysis can be started, the data series have to be synchronized to the same time scale. Usually, this is done visually by comparing and correlating each maximum and minimum in both data sets by hand (wiggle matching), which includes the human factor of subjectiveness and is a lengthy process. An automatic and objective method for verification should be very welcome.

In the last decades some techniques for this kind of correlation and adjustment were suggested. They span graphical methods (Prell et al., 1986), inverse algorithms, e.g. using Fourier series (Martinson et al., 1982) and algorithms based on similarity of data, e.g. sequence slotting (Thompson and Clark, 1989).

However, we focus on a method based on nonlinear time series analysis. During our investigations of the method of cross recurrence plots (CRP), we have found an interesting feature. Besides the possibility of application of the recurrence quantification analysis (RQA) of Webber and Zbilut on CRPs (1994), there is a more fundamental relation between the structures in the CRP and the considered systems. This feature can be used for synchronization of data sets. Although the first steps of this method are similar to the sequence slotting method, their roots are different.

First we give an introduction to CRPs. Then we explain the relationship between the structures in the CRP and the systems and illustrate this with a simple model. Finally, we apply the CRP to geophysical data in order to synchronize various profiles and to show their practical availability. Since we focus on the synchronization feature of the CRP, we will not give a comparison between the different alignment methods.

Correspondence to: N. Marwan
(marwan@agnld.uni-potsdam.de)

2 The Recurrence Plot

Recurrence plots (RP) were firstly introduced by Eckmann et al. (1987) in order to visualize time dependent behaviour of orbits $\boldsymbol{x}_i$ in phase space. An RP represents the recurrence of the phase space trajectory to a state. The recurrence of states is a fundamental property of deterministic dynamical systems (Argyris et al., 1994; Casdagli, 1997; Kantz and Schreiber, 1997). The main step in the visualization is the calculation of the $N \times N$-matrix

$$\mathbf{R}_{i,\,j} = \Theta\big(\varepsilon - \|\boldsymbol{x}_i - \boldsymbol{x}_j\|\big), \quad i, j = 1 \ldots N, \tag{1}$$

where ε is a predefined cutoff distance, $\|\cdot\|$ is the norm (e.g. the Euclidean norm) and $\Theta(x)$ is the Heaviside function. The values *one* and *zero* in this matrix can be simply visualized by the colours black and white. Depending on the kind of application, ε can be a fixed value or it can be changed for each i in such a way that in the ball with the radius ε a predefined amount of neighbours occurs. The latter will provide a constant density of recurrence points in each column of the RP.

The recurrence plot exhibits characteristic patterns for typical dynamical behaviour (Eckmann et al., 1987; Webber Jr.

and Zbilut, 1994): A collection of single recurrence points, homogeneously and irregularly distributed over the whole plot, reveals a mainly stochastic process. Longer parallel diagonals, formed by recurrence points and with the same distance between the diagonals, are caused by periodic processes. A paling of the RP away from the main diagonal to the corners reveals a drift in the amplitude of the system. Vertical and horizontal white bands in the RP result from states which occur rarely or represent extremes. Extended horizontal and vertical black lines or areas occur if a state does not change for some time, e.g. laminar states. All these structures were formed by using the property of recurrence of states. It should be pointed out that the states are only the "same" and recur in the sense of the vicinity, which is determined by the distance ε. RPs and their quantitative analysis (RQA) became better known in the last decade (e.g. Casdagli, 1997). Their applications to a wide field of miscellaneous research show their suitability in the analysis of short and non-stationary data.

3 The Cross Recurrence Plot

Analogous to Zbilut et al. (1998), we have expanded the method of recurrence plots (RP) to the method of *cross recurrence plots*. In contrast to the conventional RP, two time series are simultaneously embedded in the same phase space. The test for closeness of each point of the first trajectory x_i $(i = 1 \dots N)$ with each point of the second trajectory y_j $(j = 1 \dots M)$ results in a $N \times M$ array

$$\mathbf{CR}_{i,j} = \Theta\big(\varepsilon - \|\boldsymbol{x}_i - \boldsymbol{y}_j\|\big). \tag{2}$$

The visualization of this is called the *cross recurrence plot*. The definition of the closeness between both trajectories can be varied as described above. Varying ε may be useful to handle systems with different amplitudes.

The CRP compares the considered systems and allows us to benchmark the similarity of states. In this paper, we focus on the bowed "*main diagonal*" in the CRP, because it is related to the frequencies and phases of the systems considered.

4 The line of synchronization in the CRP

Regarding the conventional RP, Eq. (1), one always finds a main diagonal in the plot because the (i, i)-states are identical. The RP can be considered as a special case of the CRP, Eq. (2), which usually does not have a main diagonal as the (i, i)-states are not identical.

In data analysis one is often faced with time series that are measured on varying time scales. These could be sets from borehole or core data in geophysics or tree rings in dendrochronology. Sediment cores might have undergone a number of coring disturbances such as compression or stretching. Moreover, cores from different sites with differing sedimentation rates would have different temporal resolutions. All these factors require a method of synchronization.

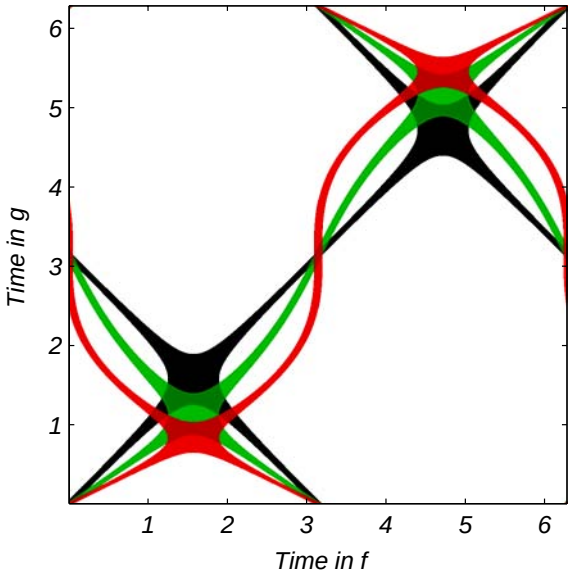

Fig. 1. Cross recurrence plots of sine functions $f(t) = \sin(\varphi t)$ and $g(t) = \sin(\varphi t + a\sin(\psi t))$, where $a = 0$ for the black CRP, $a = 0.5$ for the green CRP and $a = 1$ for the red CRP. The variation in the time domain leads to a deforming of the synchronization line.

A CRP of two corresponding time series will not contain a main diagonal. But, if the sets of data are similar, e.g. only rescaled, a more or less continuous line in the CRP that is like a distorted main diagonal can occur. This line contains information on the rescaling. We give an illustrative example. A CRP of a sine function with itself (i.e. this is the RP) contains a main diagonal (black CRP in Fig. 1). Hence, the CRPs in the Fig. 1 are computed with embeddings of dimension one; further diagonal lines from the upper left to the lower right occur. These lines typify the similarity of the phase space trajectories in positive and negative time direction.

Now we rescale the time axis of the second sine function in the following way

$$\sin(\varphi t) \longrightarrow \sin\big(\varphi t + a\sin(\psi t)\big) \tag{3}$$

We will henceforth use the notion rescaling only in the mention of the rescaling of the time scale. The rescaling of the second sine function, with different parameters φ, results in a deformation of the main diagonal (green and red CRP in Fig. 1). The distorted line contains the information on the rescaling which we will need in order to re-synchronize the two time series. Therefore, we call this distorted diagonal the *line of synchronization (LOS)*.

In the following, we present a toy function to explain the procedure. If we consider a one dimensional case without embedding, the CRP is computed with

$$\mathbf{CR}(t_1, t_2) = \Theta\big(\varepsilon - \|f(t_1) - g(t_2)\|\big). \tag{4}$$

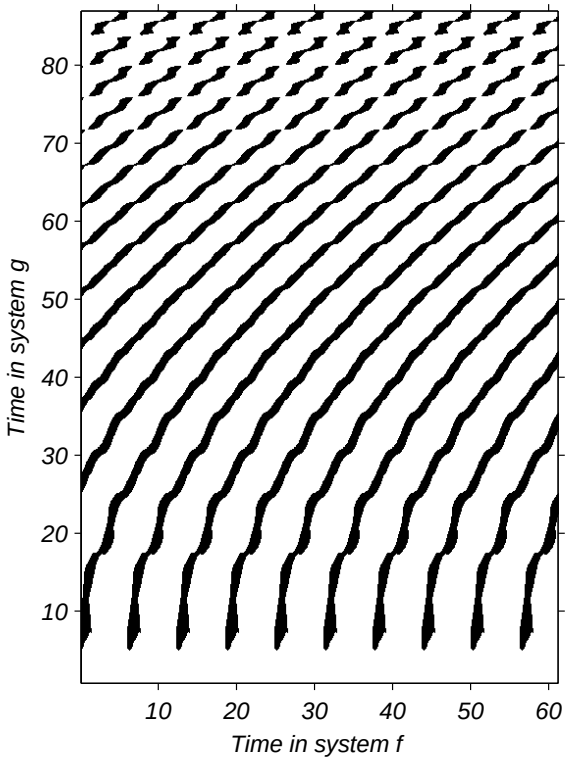

Fig. 2. Cross recurrence plots of two sine functions $f(t) = \sin(\varphi t)$ and $g(t) = \sin(\psi t^2))$ which is the basis of the determination of the rescaling function between both data series. The embedding parameters were dimension $m = 2$, delay $\tau = \pi/2$ and a varying threshold ε, in such a way that the CRP contains a constant recurrence density of 20%.

If we set $\varepsilon = 0$ to simplify the condition, Eq. (4) gives a recurrence point if

$$f(t_1) = g(t_2). \tag{5}$$

In general, this is an implicit condition that links the variable t_1 to t_2. Considering physical examples of above, it can be assumed that the time series are essentially the same – this means that $f = g$ – up to a rescaling function of time. So we can state that

$$f(t_1) = f\big(\phi(t_1)\big). \tag{6}$$

If the functions $f(\cdot)$ and $g(\cdot)$ are not identical, our method is, in general, not capable of deciding if the difference in the time series is due to different dynamics ($f(\cdot) \neq g(\cdot)$) or if it is due to simple rescaling. So the assumption that the dynamics are alike up to a rescaling in time is essential, even though, for some cases where $f \neq g$, it can be applied in the same way. If we consider the functions $f(\cdot) = a \cdot \bar{f}(\cdot) + b$ and $g(\cdot) = \bar{g}(\cdot)$, where $f(\cdot) \neq g(\cdot)$ are the observations and $\bar{f}(\cdot) = \bar{g}(\cdot)$ are the states, normalization with respect to the mean and the standard deviation allows us to use our method.

$$f(\cdot) = a \cdot \bar{f}(\cdot) + b \longrightarrow \tilde{f}(\cdot) = \frac{f(\cdot) - \langle f(\cdot)\rangle}{\sigma\,(f(\cdot))} \tag{7}$$

$$\tilde{g}(\cdot) = \frac{g(\cdot) - \langle g(\cdot)\rangle}{\sigma\,(g(\cdot))} \tag{8}$$

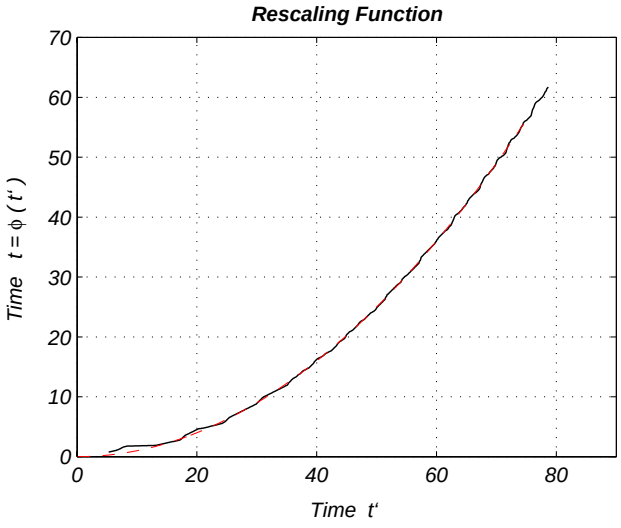

Fig. 3. The rescaling function (black) determined from the CRP in Fig. 2. This has the expected parabolic shape of the squared coherence in the time domain. In red the square function.

With $\bar{g}(\cdot) = \bar{f}(\cdot)$ the functions $\tilde{f}(\cdot)$ and $\tilde{g}(\cdot)$ are the same after the normalization. Then our method can be applied without any further modification.

In some special cases Eq. (6) can be resolved with respect to t_1. Such a case is a system of two sine functions with different frequencies

$$f(t) = \sin(\varphi \cdot t + \alpha) \tag{9}$$

$$g(t) = \sin(\psi \cdot t + \beta) \tag{10}$$

Using Eq. (5) and Eq. (6) we find

$$\sin(\varphi\, t_1 + \alpha) - \sin(\psi\, t_2 + \beta) = 0 \tag{11}$$

and one explicit solution of this equation is

$$\Rightarrow \quad t_2 = \phi(t_1) = \left(\frac{\varphi}{\psi} t_1 + \gamma\right) \tag{12}$$

with $\gamma = (\alpha - \beta)/\psi$. In this special case the slope of the main line in a cross recurrence plot represents the frequency ratio and the distance between the axes origin and the intersection of the line of synchronization with the ordinate gives the phase difference. The function $t_2 = \phi(t_1)$ (Eq. 6) is a transfer or rescaling function which allows us to rescale the second system to the first system. If the rescaling function is not linear the LOS will also be curved.

For the application, one has to determine the LOS – usually non-parametrically – and then rescale one of the time series. In the Appendix we describe a simple algorithm for estimating the LOS. Its determination will be better for higher embeddings because the vertical and cross-diagonal structures will vanish. Note that the embedding of the time series involves difficulties. The Takens Embedding Theorem holds for closed, deterministic systems without noise only. If noise is present, one needs its realization to find a reasonable embedding. For stochastic time series it does not make sense

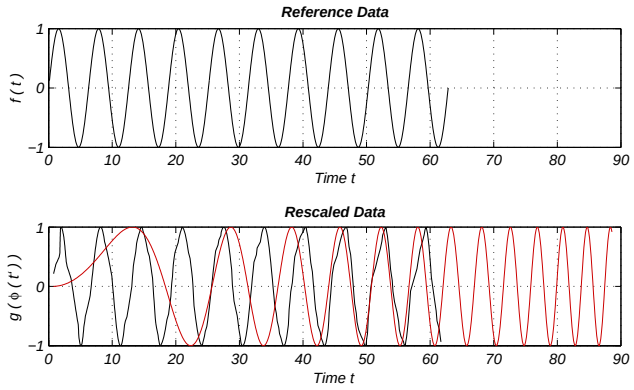

Fig. 4. Reference data series (upper panel) and rescaled data series before (red) and after (black) using the rescaling function of Fig. 3 (lower panel).

to consider a phase space and so embedding is, in general, not justified here either (Romano, to be published; Takens, 1981).

The choice of a special embedding lag could be correct for one section of the data but incorrect for another (for an example see below). This can be the case if the data is non-stationary. Furthermore, the choice of method for computing the CRP and the threshold ε will influence the quality of the estimated LOS.

The next sections will be dedicated to application.

5 Application to a simple example

First, we consider two sine functions, $f(t) = \sin(\varphi t)$ and $g(t) = \sin(\psi t^2)$, where the time scale of the second sine differs from the first by a quadratic term and the frequency $\psi = 0.01\,\varphi$. Sediment parameters are related to such kind of functions because gravity pressure increases nonlinearly with the depth. It can be assumed that both data series come from the same process and were subjected to different deposital compressions (e.g. a squared or exponential increasing of the compression). Their CRP contains a bowed LOS (Fig. 2). We have used the embedding parameters dimension $m = 2$, delay $\tau = \pi/2$ and a varying threshold ε, so that the CRP contains a constant recurrence density of 20%. Assuming that the time scale of g is not the correct scale, we denote that scale by t''. In order to determine the non-parametrical LOS, we have implemented the algorithm described in the Appendix. Although this algorithm is still not mature, we obtained reliable results (Fig. 3). The resulting rescaling function has the expected squared shape $t = \phi(t'') = 0.01\,t''^2$ (red curve in Fig. 3). Substituting the time scale t'' in the second data series $g(t'')$ by this rescaling function $t = \phi(t'')$, we get a set of synchronized data $f(t)$ and $g(t)$ with the non-parametric rescaling function $t = \phi(t'')$ (Fig. 4). The synchronized data series are approximately the same. The cause of some differences is the meandering of the LOS which itself is caused by partial weak embedding. Nevertheless, this

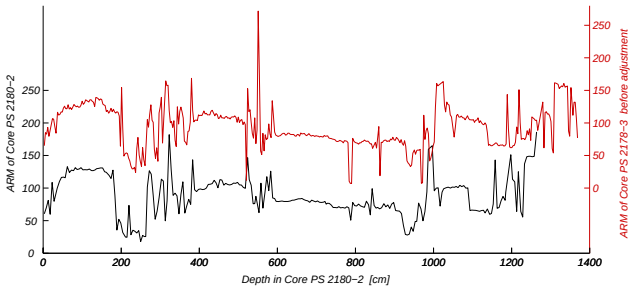

Fig. 5. ARM data of the boreholes PS 2178–3 GPC and PS 2180–2 GPC in the Central Arctic Ocean before adjustment.

can be avoided by using a more complex algorithm for estimating the LOS.

6 Application to real data

In order to continue the illustration of the working of our method we have applied it to real data from geology.

In the following, we compare the method of cross recurrence plot matching with the conventional method of visual wiggle matching (interactive adjustment). Geophysical data of two sediment cores from the Makarov Basin, central Arctic Ocean, PS 2178-3 and PS 2180–2, were analysed. The task should be to adjust the data of the PS 2178–3 data (data length $N = 436$) to the scale of the PS 2180–2 (data length $N = 251$) in order to get a depth-depth-function which allows us to synchronize both data sets (Fig. 5).

We have constructed the phase space with six normalized parameters, low field magnetic susceptibility (κ_{LF}), anhysteretic remanent magnetization (ARM), ratio of anhysteretic susceptibility to κ_{LF} (κ_{ARM}/κ_{LF}), relative palaeointensity (PJA), median destructive field of ARM (MDF_{ARM}) and inclination (INC). A comprehensive discussion of the data is given in Nowaczyk et al. (2001). The embedding was combined with the time-delayed method according to Takens (1981) in order to increase further the dimension of the phase space with the following rule: If we have n parameters a_i, the embedding with dimension m and delay τ will result in a $(m \cdot n)$-dimensional phase space:

$$\begin{aligned}\boldsymbol{x}(t) = \big(&a_1(t), \ldots, a_n(t),\\ &a_1(t+\tau), \ldots, a_n(t+\tau),\\ &a_1(t+2\tau), \ldots, a_n(t+2\tau), \ldots\\ &a_1(t+(m-1)\tau), \ldots, a_n(t+(m-1)\tau)\big) \qquad (13)\end{aligned}$$

For our investigation we have used a dimension $m = 3$ and a delay $\tau = 1$, which finally led to a phase space of dimension 18 (3×6). The recurrence criterion was $\varepsilon = 5\%$ nearest neighbours.

The resulting CRP shows a clear LOS and some clustering of black patches (Fig. 6). The latter occurs due to the plateaux in the data. The next step is to fit a non-parametric

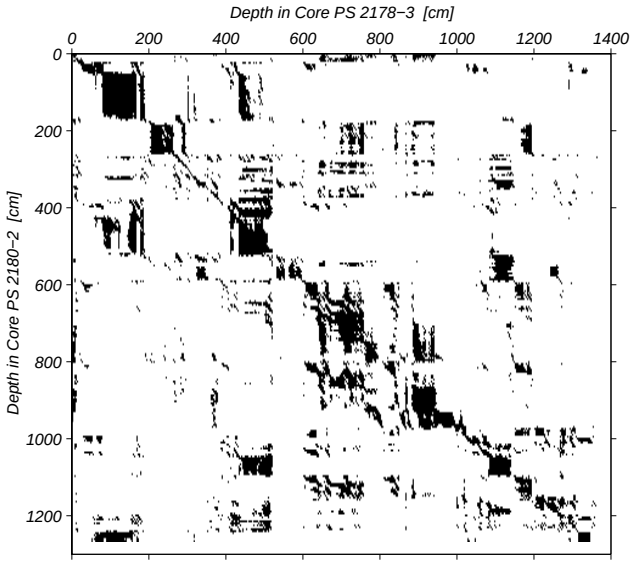

Fig. 6. Cross recurrence plot based on six normalized sediment parameters and an additional embedding dimension of $m = 3$ ($\tau = 1$, $\varepsilon = 0.05$).

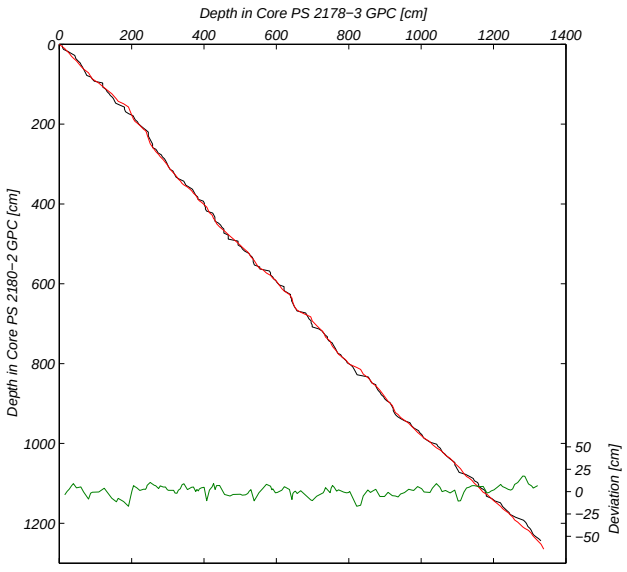

Fig. 7. Depth-depth-curves. In black, the curve gained with the CRP; in red the manually matching result. The green curve shows the deviation between both results.

function (the depth-depth-curve) to the LOS in the CRP (red curve in Fig. 6). With this function we are able to adjust the data of the PS 2178–3 core to the scale of PS 2180–2 (Fig. 8).

The determination of the depth-depth-function with the conventional method of visual wiggle matching is based on interactive and parallel searching for the same structures in the different parameters of both data sets. If the adjustment does not work in a section of the one parameter, one can use another parameter for this section which allows the multivariate adjustment of the data sets. The recognition of the same structures in the data sets requires a degree of experience. However, human eyes are usually better in the visual assessment of complex structures than a computational algorithm.

Our depth-depth-curve differs slightly from the curve which was gained by the visual wiggle matching (Fig. 7). However, despite our (still) weak algorithm used to fit the non-parametric adjustment function to the LOS, we obtained a good result of adjusted data series. If they are well adjusted, the correlation coefficient between the parameters of the adjusted data and the reference data should not vary so much. The correlation coefficients between the reference and adjusted data series is about 0.70 – 0.80, where the correlation coefficients of the interactive rescaled data varies from 0.71 – 0.87 (Table 1). The χ^2 measure of the correlation coefficients emphasizes more variation for the wiggle matching than for the CRP rescaling.

7 Discussion

Cross recurrence plots (CRP) reveal similarities in the states of the two systems. A similar trajectory evolution gives a diagonal structure in the CRP. An additional time dilatation or compression of one of these similar trajectories causes a distortion of this diagonal structure (Fig. 1). This effect is used to look into the synchronization between both systems. Synchronized systems have diagonal structures along and in the direction of the main diagonal in the CRP. Interruptions of these structures with gaps are possible because of variations in the amplitudes of both systems. However, a loss of synchronization is viewable by the distortion of this structures along the main diagonal (LOS). Fitting a non-parametric function to the LOS allows us to re-synchronize or adjust both systems on the same time scale. Although this method is based on principles from deterministic dynamics, no assumptions about the underlying systems have to be made in order for the method to work.

The first example shows the obvious relationship between the LOS and the time domains of the considered time series. The increasing frequency squared of the second harmonic function causes a parabolic LOS shape in the CRP (Fig. 2). Finally, with this LOS we are able to rescale the second function to the scale of the first harmonic function (Fig. 4). Some differences in the amplitude of the result are caused by the algorithm used in order to extract the LOS from the CRP. However, our concern is to focus on the distorted main diagonal and its relationship with the time domains.

The second example deals with real geological data and allows a comparison with the result of the conventional method of visual wiggle matching. The visual comparison of the adjusted data shows a good concordance with the reference and the wiggle matched data (Fig. 8 and 9). The depth-depth-function differs up to 20 centimeters from the depth-depth-function of the wiggle matching. The correlation coefficients between the CRP adjusted data and the reference data varies less than the correlation coefficients of the wiggle matching.

Table 1. Correlation coefficients $\varrho_{1,2}$ between adjusted data and reference data and their χ^2 deviation. The correlation of the interactive adjusted data varies more than the automatic adjusted data. The data length is $N = 170$ (wiggle matching) and $N = 250$ (CRP matching). The difference between both correlation coefficients ϱ_1 and ϱ_2 is significant at a 99% significance level when the test measure $\hat{z}$ is greater than $z_{0.01} = 2.576$

Parameter	ϱ_1, wiggle matching	ϱ_2, CRP matching	$\hat{z}$
ARM	0.8667	0.7846	6.032
MDF_{ARM}	0.8566	0.7902	4.791
κ_{LF}	0.7335	0.7826	2.661
κ_{ARM}/κ_{LF}	0.8141	0.8049	0.614
PJA	0.7142	0.6995	0.675
INC	0.7627	0.7966	1.990
χ^2	141.4	49.1	

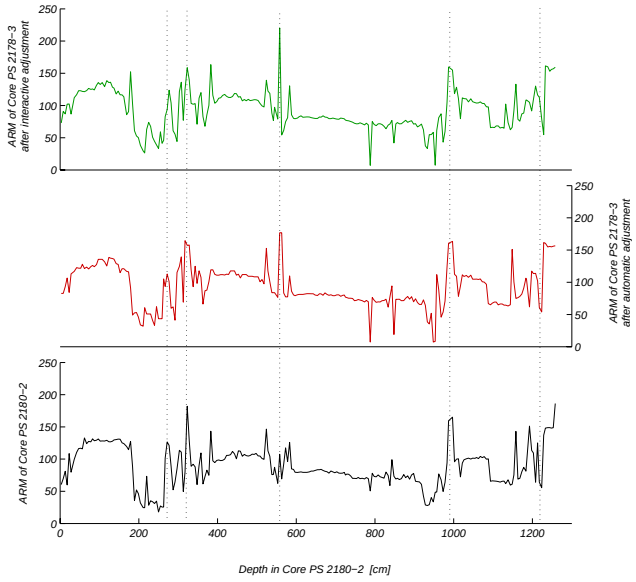

Fig. 8. ARM data after adjustment by wiggle matching (top) and by automatic adjustment using the LOS from Fig. 6. The bottom figure shows the reference data.

However, the correlation coefficients for the CRP adjusted data are smaller than these for the wiggle matched data. Although their correlation is better, it seems that the interactive method does not produce a balanced adjusting whereas the automatic matching looks for a better balanced adjusting.

These two examples exhibit the ability to work with smooth and non-smooth data whereby the result will be better for smooth data. Small fluctuations in the non-smooth data can be handled by the LOS searching algorithm. Therefore, smoothing strategies, like smoothing or parametrical fit of the LOS, are not necessary. The latter would damp one advantage of this method, that the LOS is yielded as a non-parametrical function. A future task will be the optimization of the LOS searching algorithm in order to get a clear LOS even if the data are non-smooth. Further, the influence of dynamical noise to the result will be studied. Probably, this problem may be bypassed by a suitable LOS searching algorithm too.

Our method has conspicuous similarities with the method of sequence slotting described by Thompson and Clark (1989). The first step in their method is the calculation of a distance matrix, similar to our Eq. (2), which allows the use of multivariate data sets. Thompson and Clark (1989) referred to the distance measure as dissimilarity; this is used to determine the alignment function in such a way that the sum of the dissimilarities along a path in the distance matrix is minimized. This approach is based on dynamic programming methods which were mainly developed for speech pattern recognition in the 70's (e.g. Sakoe and Chiba, 1978). In contrast, RPs were developed to visualize the phase space behaviour of dynamical systems. Therefore, a threshold was introduced to make recurrent states visible. Involvement of a fixed amount of nearest neighbours in phase space and the possibility to increase the embedding dimensions distinguish this approach from the sequence slotting method.

8 Conclusion

The cross recurrence plot (CRP) can contain information about the synchronization of data series. This is revealed by the distorted main diagonal which is called *line of synchronization (LOS)*. After isolating this LOS from the CRP one obtains a non-parametric rescaling function. With this function one can synchronize the time series. The underlying more-dimensional phase space allows us to include more than one parameter in this synchronization method as it usually appears in geological applications, e.g. core synchronization. The comparison of CRP adjusted geophysical core data with conventional visual matching shows an acceptable reliability level of the new method which can be further improved by a better method for estimating the LOS. The advantage is the automatic, objective and multivariate adjustment. Finally, this method of CRPs can open a wide range of applications as scale adjustment, phase synchronization and pattern recognition, for instance in geology, molecular biology and ecology.

Appendix: An algorithm to fit the LOS

In order to implement a recognition of the LOS we have used the following simple two-step algorithm. Denote all recurrence points by $r_{i_{\tilde{\alpha}},j_{\tilde{\beta}}}$ $(\tilde{\alpha},\tilde{\beta} = 1,2,\ldots)$ and the recurrence points lying on the LOS by r_{i_α,j_β} $(\alpha,\beta = 1,2,\ldots)$. Before the common algorithm starts, find the recurrence point r_{i_1,j_1} next to the axes origin. In the first step, the next recurrence point $r_{i_{\tilde{\alpha}},j_{\tilde{\beta}}}$, after a previous determined recurrence point r_{i_α,j_β}, is to be determined. This is carried out by a stepwise increasing of a squared $(w \times w)$ sub-matrix where the

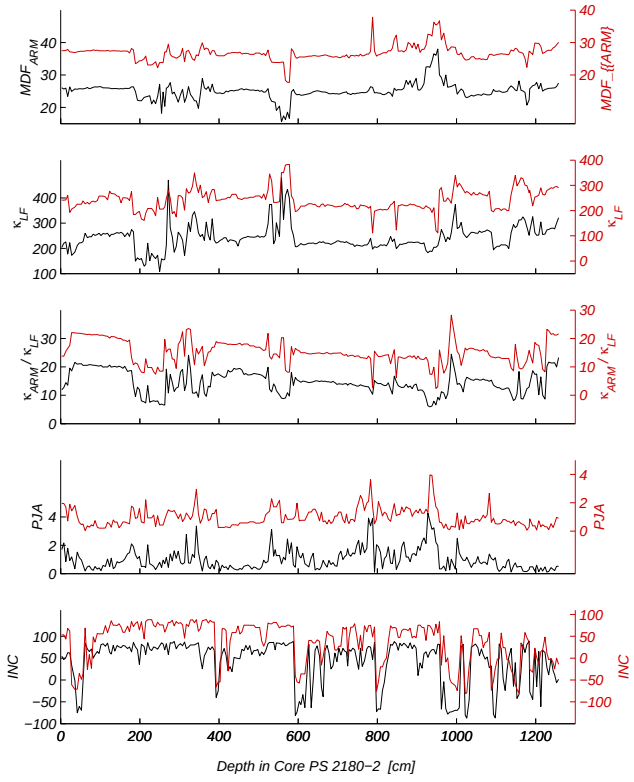

Fig. 9. The adjusted marine sediment parameters. The construction of the CRP was done with the normalized parameters. In these plots we show the parameters, which are not normalized.

previous recurrence point is at the $(1, 1)$-location. The size w of this sub-matrix increases step-wise until it meets a new recurrence point or the margin of the CRP. When the next recurrence point $r_{i_{\tilde{\alpha}}, j_{\tilde{\beta}}} = r_{i_\alpha + \delta i, j_\beta + \delta j}$ ($\delta i = w$ or $\delta j = w$) in the x-direction (y-direction) is found, the second step looks to see if there are following recurrence points in y-direction (x-direction). If this is true (e.g. there are a cluster of recurrence points) increase further the sub-matrix in y-direction (x-direction) until a predefined size $(w + d\tilde{x}) \times (w + d\tilde{y})$ ($d\tilde{x} < dx, d\tilde{y} < dy$) or until no new recurrence points are met. This further increasing of the sub-matrix is done for the both x- and y-direction. Using $d\tilde{x}, d\tilde{y}$ we compute the next recurrence point $r_{i_{\alpha+1}, j_{\beta+1}}$ by determination of the center of mass of the cluster of recurrence points with $i_{\alpha+1} = i_\alpha + (d\tilde{x} + \delta i)/2$ and $j_{\beta+1} = j_\beta + (d\tilde{y} + \delta j)/2$. The latter avoids the fact that the algorithm is driven around widespread areas of recurrence points. Instead of this, the algorithm locates the LOS within these areas. (However, the introducing two additional parameters dx and dy is a disadvantage which should be avoided in further improvements of this algorithm.) The next step is to set the recurrence point $r_{i_{\alpha+1}, j_{\beta+1}}$ to a new start point and to begin with the step one in order to find the next recurrence point. These steps are repeated until the end of the RP is reached.

We know that this algorithm is merely one of many possibilities. The following criteria should be met in order to obtain a good LOS. The number of targeted recurrence points by the LOS N_1 should converge to a maximum and the number of gaps in the LOS N_0 should converge to a minimum. An analysis with various estimated LOS confirms this requirement. The correlation between two LOS-synchronized data series arises with N_1 and with $1/N_0$ (the correlation coefficient correlates most strongly with the ratio N_1/N_0).

The algorithm for computation of the CRP and recognition of the LOS are available as Matlab programmes on http://www.agnld.uni-potsdam.de/~marwan.

Acknowledgements. The authors thank J. Kurths and U. Schwarz for continuing support and discussion. This work was supported by the special research programme 1097 of the German Science Foundation (DFG).

References

Argyris, J. H., Faust, G., and Haase, M.: An Exploration of Chaos, North Holland, Amsterdam, 1994.

Casdagli, M. C.: Recurrence plots revisited, Physica D, 108, 12–44, 1997.

Eckmann, J.-P., Kamphorst, S. O., and Ruelle, D.: Recurrence Plots of Dynamical Systems, Europhysics Letters, 5, 973–977, 1987.

Kantz, H. and Schreiber, T.: Nonlinear Time Series Analysis, University Press, Cambridge, 1997.

Martinson, D. G., Menke, W., and Stoffa, P.: An Inverse Approach to Signal Correlation, J. Geophys. Res. B6, 87, 4807–4818, 1982.

Nowaczyk, N. R., Frederichs, T. W., Kassens, H., Nørgaard-Pedersen, N., Spielhagen, R. F., Stein, R., and Weiel, D.: Sedimentation rates in the Makarov Basin, Central Arctic Ocean – A paleo- and rock magnetic approach, Paleoceanography, 2001.

Prell, W. L., Imbrie, J., Martinson, D. G., Morley, J. J., Pisias, N. G., Shackleton, N. J., and Streeter, H. F.: Graphic Correlation of Oxygen Isotope Stratigraphy Application to the Late Quaternary, Paleoceanography, 1, 137–162, 1986.

Romano, M. C.: The Dark Side of Embedding, to be published.

Sakoe, H. and Chiba, S.: Dynamic programming algorithm optimization for spoken word recognition, IEEE Trans. Acoustics, Speech, and Signal Proc., 26, 43–49, 1978.

Takens, F.: Detecting Strange Attractors in Turbulence, pp. 366–381, Springer, Berlin, 1981.

Thompson, R. and Clark, R. M.: Sequence slotting for stratigraphic correlation between cores: theory and practice, J. Paleolimnology, 2, 173–184, 1989.

Webber, Jr., C. L. and Zbilut, J. P.: Dynamical assessment of physiological systems and states using recurrence plot strategies, Journal of Applied Physiology, 76, 965–973, 1994.

Zbilut, J. P., Giuliani, A., and Webber, Jr., C. L.: Detecting deterministic signals in exceptionally noisy environments using cross-recurrence quantification, Physics Letters A, 246, 122–128, 1998.